MORPHOLOGICAL, NUCLEOTYPIC, AND GENOMIC DRIVERS OF PHYSIOLOGICAL VARIATION IN LUNGLESS SALAMANDERS: RESPIRATION AND WATER LOSS IN THE FAMILY PLETHODONTIDAE

A Dissertation

Presented to the Faculty of the Graduate School

of Cornell University

In Partial Fulfillment of the Requirements for the Degree of

Doctor of Philosophy

by

Benjamin Bradford Johnson

December 2021

MORPHOLOGICAL, NUCLEOTYPIC, AND GENOMIC DRIVERS OF PHYSIOLOGICAL VARIATION IN LUNGLESS SALAMANDERS:
RESPIRATION AND WATER LOSS IN THE FAMILY PLETHODONTIDAE

Benjamin Bradford Johnson, Ph.D.

Cornell University 2021

Physiological performance depends on the complex integration of traits across multiple levels of biological organization. Characterizing the contribution of underlying traits to variation in adaptive performance phenotypes thus offers a simplified framework to identify patterns of selection and adaptation in nature. Here, I took a trait-based approach to characterize variation in physiological performance, using metabolic and water loss physiology in lungless salamanders as a model. In the lungless salamanders (Urodela: Plethodontidae), respiratory metabolism and evaporative water loss occur through the integument, leading to clear theoretical predictions about the influence of body size, skin structure, and cell size to performance. Using a combination of morphological measurements, physiological experiments, and genomic sequencing, I found that physiological variation is well explained not only by body mass – a commonly measured trait in physiological ecology – but more so by body surface area-to-volume ratios (SA:V), which place an upper limit on transport rates of oxygen into the body. The strength of natural selection on genes encoding for metabolism was inversely related to SA:V in a small sample of species, suggesting a relationship between relative degree of oxygen limitation and selection for metabolic efficiency. Further, I found that water loss is also well explained by genome size, likely due to a nucleotypic effect of the genome in determining cell size. Genome size influences water loss in the Plethodontidae at least in part through the effects of biological

size – the interaction of both cell and body size. Though the mechanisms responsible for this effect are unknown, this work marks the first demonstration that biological size is a functional trait. Its influence over water balance physiology in the Plethodontidae suggests it is of particular ecological importance in this group, and raises the possibility that this understudied trait may be important to physiological performance in animals more broadly. Collectively, this dissertation expands upon a paradigm in physiological ecology that focuses extensively on body mass effects, revealing greater detail in the types of morphological traits that influence how physiological performance varies between individuals and evolves between species.

BIOGRAPHICAL SKETCH

Benjamin Bradford Johnson was born in Oakland, California and developed a fascination with the natural world at a young age. He quickly found a particular fondness for herpetofauna, and grew up spending much of his free time patrolling the Coast Ranges of the San Francisco East Bay in search of the local snakes and salamanders. So started a lifelong pattern of asking progressively more esoteric questions about the lives of herps. Ben pursued such questions through his undergraduate studies, receiving a B.S. in Animal Biology from the University of California, Davis in 2009. At Davis, Ben was advised by Dr. Jarrett Johnson in the lab of Dr. H. Bradley Shaffer and completed an undergraduate thesis comparing dispersal distances of native and invasive tiger salamanders (genus *Ambystoma*) in California. Following graduation, Ben worked as a field and laboratory technician in Dr. Shaffer's lab group assisting multiple projects researching the ecology and evolutionary genetics of California herpetofauna. In 2011, Ben began his doctoral studies in Ecology & Evolutionary Biology at Cornell University studying thermal biology in *Ambystoma* under Dr. Kelly Zamudio. Following a health leave, Ben returned to the department in 2016 under Drs. Jeremy Searle and Jed Sparks. Through their mentorship, Ben expanded his research interests to integrate evolutionary genomics and physiological ecology in lungless salamanders (family Plethodontidae), and defended his Ph.D. dissertation in 2021.

Dedicated to Karissa and Mateo, with love.

This work would have been impossible without her, and with him it almost was.

ACKNOWLEDGMENTS

This work is the product of invaluable support from many people and institutions. I am particularly grateful for the brilliant mentorship of my co-advisors, Jeremy Searle and Jed Sparks. Both offered me a professional home in their respective lab groups through great personal generosity, for which they deserve special thanks. Their guidance had an indelible impact on my growth as a researcher, and their tremendous skill as scientists continues to inspire. More than colleagues, both are dear friends.

I thank multiple Cornell faculty for their professional guidance at various stages. I am particularly grateful for the professional guidance of my committee members, Monica Geber and Amy McCune, both of whom challenged me to expand my thinking and hone my skills as a scientist. I also thank Kelly Zamudio, Harry Greene, and Rick Harrison, who all impacted my research; and Darlene Campbell, Michelle Smith, Chip Aquadro, and Andy Moeller, who all helped greatly with my teaching. Beyond Cornell, I thank Ryan Gregory and Maria Forzán for their helpful collaboration and insight, and David Wake for guidance and inspiration. For their technical support I owe huge thanks to Kim Sparks and Steve Bogdanowicz. Both saved me from calamity in the lab on multiple occasions. Special thanks also to John Howell and Rich Moore for their unflappable help with my demanding animal care needs, to Casey Dillman and Charles Dardia for their assistance at the Cornell University Museum of Vertebrates, to Teresa Porri for her immense help with CT scanning at the Cornell Institute of Biotechnology, and to Lynn Johnson for her invaluable assistance at the Cornell Statistical Consulting Unit. Further, I thank multiple agencies for enabling this work through generous funding: the Cornell Center for Comparative and Population Genomics seed grant, the Cornell Center for Vertebrate Genomics

priming grant, the Atkinson Center for Sustainability Sustainable Biodiversity Fund, The Society for the Study of Evolution Rosemary Grant Award, the Cornell College of Agriculture and Life Sciences Andrew R. Mellon Student Research Grant, the Cornell SUNY Diversity Fellowship, and the Ford Foundation Predoctoral Fellowship.

I thank a long list of friends and colleagues met during my time at Cornell (and apologize to whomever I've surely forgotten!). Everyone listed here deserves more accolades than a single name-drop, but a simple thank you will have to do. I'll particularly single out Sahas Barve, Chris Dalton, Nick Fletcher, Ana Longo, Tram Nguyen, and Bhavya Sridhar for their close friendship, which I value dearly. Many thanks also to Gui Becker, Rayna Bell, Gideon Bradburd, Noah Brady, Leo Campagna, Nancy Chen, Suzi Claflin, Kirsten Coe, Amelia Demery, Collin Edwards, Amy Ellison, Dave Frey, Geoff Giller, Ellie Goud, Miranda Gray, Ginny Howick, Jon Hughes, Hide Inamine, Holly Jackson, Aubrie James, Kelsey Jensen, Frida Johannesdotir, Sudan Kariuki, Henry Kunerth, Max Lambert, Ezra Lencer, Lizzie Lombardi, Nicolas Lou, Bryan Maritz, Nick Mason, Coby McDonald, Jennie Miller, Cinnamon Mittan, Morgan Mouchka, Genna Mount, Dan Petticord, Renee Petipas, Sue Pierre, Nick Polato, Laura Porturas, David Rodriguez, Katie Siriani, Trevor Sless, Fiona Soper, Amanda Stephens, Dave Toews, Allison Tracy, Jacob Tyrell, Rodrigo Vega, Marjorie Weber, Amelia Weiss, and Tom White. All are wonderful colleagues, but I consider them friends first.

Off campus, I thank my friends in music for keeping me grounded and sane: Abraham Aguilar, Frankie Aguilar, Tony Bald, Steve Henderson, Matt Occone, Jonathan Rodriguez, Santiago Ruiz, and Danny Snyder. Thanks also to Loring Barker, Chris Bastian, and Tim McKay for their enduring friendship and support. Lastly, I thank my family for their love, encouragement, and patience during my studies far from home: my parents, Brad Johnson, Mimi

Reyes-Martin, and Don Martin; my sisters, Veronica Johnson and Maritza Martin; my grandmother, Susie Zacharias; and my cousin, Lily Verduzco. I missed them all dearly during grad school, and am looking forward to renewing my family membership shortly.

Above all others, I want to thank my wife, Karissa, and our son, Mateo. Meeting Karissa and building a life together has been the great joy of my life, let alone my time in grad school. Her love, generosity of spirit, and unwavering support helped me through the highs and lows of graduate study. Wherever life leads next, I feel so lucky to share it with her. Thank you, Karissa, for everything. Finally, thank you Mateo for your tireless efforts to jeopardize the successful completion of this dissertation. This work would have been so much less without you – less stressful, to be sure, but less joyful too. I can't wait to continue exploring the world with you.

TABLE OF CONTENTS

CHAPTER ONE

GENOME SIZE INFLUENCES ADAPTIVE PLASTICITY OF WATER LOSS, BUT NOT METABOLIC RATES, IN LUNGLESS SALAMANDERS

Research in collaboration with: Jeremy B. Searle[1], Jed P. Sparks[1]

[1]Department of Ecology & Evolutionary Biology, Cornell University, Ithaca, NY, USA

Abstract

Many expressions of phenotype, such as physiological performance, integrate multiple underlying traits to function. Linking component traits to adaptive physiology thus gives insight into mechanisms of selection acting on performance. Genome size (C-value) is a trait that influences physiology in multiple taxa by exerting a nucleotypic effect, constraining cell size and cellular physiology such that whole-organism mass-specific metabolism is reduced with increasing C-value. We tested for this mechanism of C-value function acting in lungless salamanders, plus an unexplored potential mechanism of C-value effects constraining water transport across the body surface to influence cutaneous water loss rates. We found no evidence for a nucleotypic effect on metabolic rates, but we demonstrate a relationship between C-value and water loss physiology. Under warmer experimental conditions, C-value was inversely correlated with water loss and positively correlated with resistance to water loss, which demonstrated adaptive plasticity at higher temperatures. We hypothesize this pattern results from differences in cell size constraining diffusion and evaporation of water from the skin under warm conditions when cutaneous perfusion is reduced. Testing this hypothesis may confirm a previously unappreciated adaptive role for C-value variation in this group, and reveals the possibility that genome size influences physiological exchange across transport barriers more broadly.

Introduction

Natural selection operates on individual organisms by acting on all their functional phenotypes simultaneously. Because many ecologically important phenotypes – e.g., physiological performance – are themselves complex integrations of multiple underlying traits, characterizing the functional role of component traits driving performance phenotypes can offer a simplified method to identify patterns of adaptation in nature (Adler et al., 2014). To do this, we must link variation in traits to functional phenotypes of known adaptive importance. One of the most fundamental performance phenotypes is metabolic rate, the sum total of all cellular respiration within an organism. Metabolism is a critical indicator of energy turnover that limits many other biological functions (Brown et al., 2004), making the functional contributions of traits to variation in metabolism of broad ecological importance (Glazier, 2018; Uyeda et al., 2017). The most well documented such trait is body size, which covaries with metabolism across taxa (Brown et al., 2004; Gillooly et al., 2001), yet we know that variation in metabolic rate is influenced by factors beyond simply body mass (Glazier, 2005; White and Kearney, 2013). Thus, to fully understand mechanisms underlying physiological diversity will require integrating morphological and environmental variation influencing performance phenotypes to test the importance of functional diversity underlying adaptive performance in nature.

One potentially important trait influencing metabolism is cell size. Cell size correlates strongly with genome size (C-value) (Gregory, 2001a). Though the mechanism linking these traits remains unresolved, the prevailing hypothesis holds that C-value causatively determines cell volume, by extension exerting a nucleotypic effect on phenotypes related to cellular transport and differentiation rates (Gregory, 2001b). This effect on cellular physiology can scale to the level of the organism, for example C-value appears related to mass-specific metabolism in

some homeotherms (Gregory, 2002; Vinogradov, 1995) and to cellular differentiation rate (Sessions and Larson, 1987) and duration of embryonic development in amphibians (Jockusch, 1997; Litvinchuk et al., 2007). Theoretical work further suggests that C-value moderates the allometric scaling of metabolic rate across taxa, with metabolism in lineages with variable C-values demonstrating shallower allometric slopes that deviate further from isometry than in lineages without C-value diversity (Kozlowski et al., 2003). Despite these associations, it remains an open question whether variation in C-value is itself an adaptive target of selection, or represents neutral variation subject to random drift (Mueller, 2015). Given the importance of performance phenotypes in limiting many biological processes (Kearney, 2012; Pettersen et al., 2019; Riddell et al., 2018), the possibility that C-value variation influences physiology highlights a need to identify potential mechanisms by which genome size contributes to observed patterns of organismal function and diversity in nature.

The lungless salamanders (Urodela: Plethodontidae) present an excellent system in which to test for effects of genome size on organismal performance. This lineage exhibits exceptionally broad variation in C-values (~10-76 pg) (Gregory, 2016), offering substantial natural variation to test for signatures of selection on genome size. Critically, all respiratory gas and water transport in this group occurs by diffusion across the skin surface, making the structure and function of the skin strong targets of selection (Feder and Burggren, 1985). The obligately permeable and moist skin in these salamanders (Feder and Burggren, 1985; Shoemaker and Nagy, 1977) leaves individuals at high risk of desiccation, with selection favoring skin with a higher resistance to water loss (Riddell et al., 2018). Skin thickness (the diffusion path length) and composition (which determines diffusivity) influence the resistance of the integument to gas and water transport (Feder and Burggren, 1985; Lillywhite, 2006), and in this capacity C-value may

influence resistance. All else being equal, larger cells in high C-value taxa will produce thicker skins, resulting in lower transport rates (Feder and Burggren, 1985; Piiper, 1988), or will otherwise necessitate compensatory changes in skin morphology to maintain adequate transport (Lillywhite, 2006). Though resistance must remain generally low to enable cutaneous gas exchange in this group (Feder, 1983), relatively higher resistances hold clear adaptive value in reducing the risk of desiccation (Riddell and Sears, 2015; Riddell et al., 2018). The potential link between C-value and resistance to water loss in the Plethodontidae remains untested, and presents a clear test case for a potentially adaptive role of genome size variation in nature.

Here, we explore the consequences of C-value diversity on physiological performance in the lungless salamanders, testing for physical effects of C-value at the individual level which may demonstrate an adaptive role of C-value in cutaneous gas and water transport across species. We quantified body and genome size variation in eight species to test for their combined functional contributions to performance under different environmental conditions. Using a combination of linear models, comparative methods, and path analyses, our work explored the question: is C-value a functionally relevant trait in plethodontid physiology, and if so, what are the mechanisms and environmental context through which it moderates physiological performance? We hypothesized two potential mechanisms by which C-value can influence plethodontid physiological rates. First, a general nucleotypic effect of cell-specific metabolism may result in lower metabolic rates in larger C-value individuals for a given body size (Gregory, 2002). Second, C-value may moderate diffusion lengths for water evaporating out of the body, resulting in adaptive differences in resistance to water loss. By integrating morphological and environmental variation underlying critical performance phenotypes, this work takes an explicit

trait-based approach to test the importance of C-value diversity underlying adaptive performance in nature.

Materials and Methods

Species sampling and experimental design

All field, laboratory, and experimental techniques described here were approved by the Cornell University Institutional Animal Care and Use Committee (IACUC protocol 2016-0081). We collected eight species of salamanders (*Eurycea bislineata*, *E. longicauda*, *Plethodon cinereus*, *P. dunni*, *P. glutinosus*, *P. larselli*, *P. vandykei*, *P. vehiculum*) from multiple natural populations (Supplementary Table S1). *Plethodon* are direct-developing terrestrial species, and *Eurycea* are semiaquatic with a biphasic life history (aquatic larvae that metamorphose into semiaquatic adults). These species range broadly in body mass from *P. cinereus* (mean 0.71 g in our dataset) to *P. glutinosus* (mean 5.03 g), as well as substantial variation in C-value (range 22.64 – 69.3 pg). Mass and C-value are not colinear in this sample (P=0.936), allowing us to test for their interaction. We maintained animals in the laboratory at two temperatures (10°C, 15°C), housed individually in deli cups on a sponge saturated with dechlorinated water and fed crickets weekly *ad libitum*. Animals were acclimated a minimum of one week before inclusion in physiological experiments, and were measured a minimum of four days after eating or a prior trial to ensure all measurements were taken in a minimally stressed, post-absorptive state.

Flow-through system and experimental trials

We measured physiological performance using flow-through respirometry. We used a Li-Cor LI-6400XT Portable Photosynthesis System (Li-Cor Biosciences, Lincoln, NE) configured

for the 6400-89 animal respiration chamber following Li-Cor specifications and using the "Insect Rd" measurement configuration. We set the system temperature to match the ambient treatment temperature, and fully scrubbed CO_2 from the ambient inflow to set levels at 400 μmol CO_2 mol^{-1} air using a CO_2 cannister. All trials were conducted at a constant flow rate of 500 μmol air s^{-1} (715 ml min^{-1}). We set humidity treatments according to vapor pressure deficits (VPD, a measure of atmospheric water content relative to saturation). To maintain consistent VPDs we manually controlled relative humidity in real time. To do this, prior to experiments we calculated the saturation vapor pressure in kPa as

$$e_s(T) = 0.61365\frac{17.502T}{240.97+T} \quad (1),$$

where T is the Celsius treatment temperature (Buck, 1981). Using the relationship between relative humidity (RH) and $e_s(T)$:

$$RH = \frac{e_s(T)-VPD}{e_{s(T)}} * 100 \quad (2),$$

we substituted VPD ± 0.015 kPa to set upper and lower bounds on relative humidity for each temperature x VPD treatment. The appropriate VPD was maintained within these bounds by scrubbing the airflow of water vapor as needed in real time. Animals were measured within a cylindrical acrylic respiration chamber, either the Li-Cor 6400-89 chamber or custom chambers depending on animal size. All chambers had the same cross-sectional area (d = 25.4 mm).

Experimental trials consisted of repeated measurements over 30 minutes. We removed animals from their housing containers and placed each inside the respiration chamber constrained within a steel mesh tube oriented facing the incurrent airflow. This ensured all animals were immobile with the entire body surface area exposed to the airstream during steady state measurements, effectively controlling for airflow and boundary layer effects contributing to water loss rates. Immediately after placing an animal in the chamber, we set the chamber

humidity to the appropriate VPD and recorded atmospheric conditions inside the chamber every ~40 seconds, continuously monitoring the respiration rate. In all cases, respiration dropped continuously (range 5-64 min, median 13.4 min) before stabilizing at a resting rate. After 5 min of stability (determined visually), we continued the trial for an additional 25 min. We saved only stable measurements over this 30-min period for later analyses, additionally discarding all measurements that fell outside our ± 0.015 kPa boundaries. To test for environmental effects on physiological performance, we conducted four experiments per individual, factorially designed across two temperatures (10, 15°C) and two VPD treatments (0.3, 0.6 kPa). We randomized treatments with respect to temperature first and then VPD to prevent order effects and maximize randomness while avoiding repeated reacclimation between every trial.

Morphological and physiological variables

Immediately before each trial, we measured body mass to the nearest 0.01 g. We scored genome sizes per species using the animal genome size database (Gregory, 2016), calculating the median C-value for each species to account for variable estimates among studies. We used atmospheric measurements from experimental trials to estimate six physiological variables: gross metabolic rate (respiration, mg CO_2 hr^{-1}), specific metabolic rate (mg CO_2 hr^{-1} g^{-1}), gross evaporative water loss rate (EWL, mg H_2O hr^{-1}), specific evaporative water loss rate (mg H_2O hr^{-1} g^{-1}), cutaneous water loss rate (CWL, mg H_2O hr^{-1} cm^{-2}), and total resistance to water loss (*r*, s cm^{-1}). Gross respiration rates were taken directly from the LI-6400XT. We estimated gross evaporative water loss rates as

$$EWL = Trmmol \cdot M_v \cdot 0.001 \qquad (3),$$

where Trmmol is the transpiration rate (mmol H_20 s^{-1}) calculated by the LI-6400XT, M_v is the molar mass of water vapor (18 g mol^{-1}), and 0.001 is a conversion factor (mol $mmol^{-1}$). We then calculated specific EWL by dividing the organism's mass from EWL, and CWL by dividing the organism's estimated surface area from EWL, using an empirical allometric formula for the Plethodontidae from Whitford & Hutchison (Whitford and Hutchison, 1967), where surface area (cm^2) = 8.42 x mass $(g)^{0.694}$. For all downstream analyses, we calculated the mean of each physiological variable across the trial.

To test for drivers of variation in resistance to water loss (*r*), we estimated *r* by first calculating the vapor pressure (e_a) in kPa inside the respiration chamber as

$$e_a = [H_2O] \cdot 0.001p \qquad (4),$$

where $[H_2O]$ is the measured water vapor concentration (mmol H_2O mol^{-1} air), p is the air pressure (kPa), and 0.001 is a conversion factor (mol $mmol^{-1}$). We converted vapor pressures into vapor densities using

$$\rho_x = \frac{e_x}{\boldsymbol{T} \cdot R_v} \cdot 1000 \cdot 10^{-6} \qquad (5),$$

where ρ_x is either the actual (ρ_{va}) or saturated (ρ_{vs}) vapor density (g cm^{-3}), e_x is either the actual (e_a) or saturated (e_s) vapor pressure (converted from kPa to Pa), **T** is the Kelvin temperature, R_v is the gas constant for water vapor (461.52 J kg^{-1} K^{-1}), and 1000 and 10^{-6} are conversion factors (g kg^{-1}, m^3 cm^{-3}). We then calculated the vapor density gradient (ρ_v) as

$$\rho_v = \rho_{vs} - \rho_{va} \qquad (6).$$

We then calculated total resistance to water loss (s cm^{-1}) as

$$r = \frac{\rho_v}{CWL} \qquad (7).$$

Finally, we converted metabolic rate and water loss rate units prior to statistical analyses for more intuitive interpretation (respiration = mg CO_2 h^{-1}, specific respiration = mg CO_2 h^{-1} g^{-1}, EWL = mg H_2O h^{-1}, specific EWL = mg H_2O h^{-1} g^{-1}, CWL = mg H_2O h^{-1} cm^{-2}).

Linear models

We tested for the influence of environment and morphology on physiology using linear mixed effects models in R (R Core Team, 2017). We tested body mass and C-value (collectively referred to as morphological variables within our analyses) plus temperature and VPD against six physiological responses: gross and specific metabolic rate, gross and specific EWL, CWL, and *r*. For total resistance models we included mass as a covariate in all cases. Total resistance is the sum of two component resistances: the resistance of the integument itself and the boundary layer, a layer of relatively still air surrounding the animal. Because boundary layer resistances covary with body size (Gates, 1980), this approach effectively controls for boundary layer effects contributing to total resistance, and focuses on effects attributable to physiological variation in cutaneous resistance.

We followed a combination of model building and model simplification, first testing environmental and morphological variables separately to survey *a priori* any potential effects of C-value. For our environmental treatments, we tested four models for each physiological response: the interaction between temperature and VPD (Temp x VPD), both effects in tandem (Temp + VPD), and each predictor independently. All environmental models were tested across our complete dataset, which includes multiple measurements per individual across treatments. To account for multiple testing, we included individual as a random effect in all models. Because we are interested in physiological differences between morphological types, and not between species

per se, we included species as a second random effect in all models. This approach thus focuses not on the effect of phylogeny on performance or on the effect of morphological predictors through evolutionary time, rather on the physical effects of body mass, C-value, and environmental variation on organismal physiology at the individual level.

To identify environmental conditions under which C-value may be functionally relevant, we tested morphological models at four treatment levels: across the complete dataset, at each temperature, at each VPD, and within each treatment (Temp x VPD) combination. Across the full dataset, we tested each response against morphological predictors while controlling for treatment combination, plus random effects for species and individual. Models tested at each temperature or VPD included random effects for species and individual while controlling for VPD or temperature, respectively. When tested within treatment combinations, models used only a random effect for species. For each response-subset combination, we compared four models: the interaction between body size and genome size (Mass x C-value), both in tandem (Mass + C-value), and each independently.

For each response variable, we constructed a more complex full dataset model incorporating all significant predictors from our morphological and environmental models, plus random effects. We selected a final model for each response by removing nonsignificant effects from these larger models through stepwise model simplification. These final models are presented in Table 2, with the complete table of all tested models and model results in Supplemental Table S2. We tested a total of 216 morphological and 24 environmental models before constructing final models. We assessed each model's support by calculating the corrected Akaike information criterion (AICc) of each and comparing values among nested models (Table S2).

Phylogenetic generalized least squares regressions

While our linear models account for environmental and individual-level variation contributing to trends in physiological performance, this approach cannot account for phylogenetic history in contributing to performance. To control for phylogenetic nonindependence among species and analyze our performance data in a comparative framework, we conducted phylogenetic generalized least squares (PGLS) regressions. We used DNA sequences from previously published studies (Fisher-Reid and Wiens, 2011; Newman et al., 2016) to construct a multilocus phylogeny of 60 plethodontid species, plus two outgroup species of *Amphiuma*. A similar phylogeny for 55 of these species was previously published by Newman et al. (2016). We used all sequences used by Newman et al., plus homologous sequences for *P. dunni*, *P. larselli*, and *E. longicauda*. Because *E. bislineata* was used as an outgroup by Newman et al. but is a focal taxon in this study, we included sequences from *Amphiuma means* and *A. tridactylum* as new outgroups. All sequences were downloaded from GenBank (Clark et al., 2016), aligned using MAFFT v7 (Katoh and Standley, 2013), and concatenated for a final alignment of 4,078 nucleotides over six nuclear loci: BDNF (707 bp), GAPD (664 bp), ILF3 (281 bp), MLC2A (253 bp), POMC (481 bp), RAG1 (1,467 bp), and RHO (225 bp). A complete list of sequences is available in Supplemental Table S10. We assembled our phylogeny in a Bayesian framework using MrBayes v3.2.7 (Ronquist et al., 2012), employing the same sequence partitions, models of nucleotide evolution, and software settings used previously by Newman et al. (2016) and Fisher-Reid & Wiens (2011). We conducted two runs of 1 million generations using four chains sampled every 1000 generations. After discarding the first 100,000 samples as burn-in, we assessed convergence in Tracer v1.7.1 (Rambaut et al., 2018) by ensuring effective sample sizes were above 200 before accepting the consensus tree.

For PGLS analyses, we trimmed taxa from the consensus tree to produce a phylogeny of just our eight focal species. We calculated mean predictor and response values for each species across our entire dataset and at each experimental subset, using subset-specific trait values for each model. In all cases, we included a covariance structure based on Brownian evolution across the trimmed phylogeny and fitted models by maximizing the log-likelihood. For morphological models, we used C-value estimates as in our linear models, and mean body mass for each species from our experimental measurements. Because PGLS analyses allow only one measurement per species (Garamszegi, 2014), this approach cannot make within-species comparisons between our experimental treatments. Thus, for environmental models, we substituted experimental treatments with climate profiles generated for each species by randomly sampling geographic coordinates within each species distribution and extracting environmental data from the sample. We extracted mean annual temperature (BIO1) from WorldClim (http://www.worldclim.org; Fick and Hijmans, 2017) and aridity index (AI) from CGIAR-CSI (http://www.cgiar-csi.org; Zomer et al., 2008), extracting one sample per 400 km^2 (range 39 [*P. larselli*] – 4722 [*P. cinereus*]), and used the mean of extracted values for each species in our model dataset. All geospatial processing was conducted in the R packages 'raster' (Hijmans, 2017) and 'sp' (Bivand et al., 2013) using a 30 arc-second (~1 km^2) spatial resolution.

Using our phylogeny, we conducted PGLS regressions in R using 'ape' v5.0 (Paradis and Schliep, 2018). We constructed PGLS models equivalent to each of our morphological linear models, substituting experimental temperature and VPD treatments with species-level climate profiles for BIO1 and AI. While our linear models test direct environmental effects on individual-level variation in performance, these PGLS models test for the contribution of the natural home environment to each species' performance, as well as evolutionary associations

between morphological variables and physiological responses. As above, we constructed final models across the complete dataset with all significant morphological and environmental effects, reaching a final model through a last round of model simplification. We tested 216 morphological and 24 environmental models before constructing final models, evaluating model support by AICc comparison.

Variance analysis

We constructed further linear mixed models to test for effects of C-value diversity on the relationship between body size and gross metabolic rates. Species in the genus *Plethodon* vary substantially in genome size, in contrast with minimal C-value diversity in *Eurycea* (Gregory, 2016). To test if these differences result in different allometric scaling of metabolism among genera (Kozlowski et al., 2003), we modeled metabolic rate as a function of the interaction between mass and genus using the R package 'lme4' (Bates et al., 2015). We tested models across our entire data set, and at each temperature and VPD, using species and individual as random variables in all models. Because our linear models found no interaction between temperature and VPD (see Results), we did not test individual treatment combinations.

We tested for differences between genera in both the slope and variance around the slope ("weights = varIdent(form = ~ log(mass) | genus)"). To test for differences in allometric scaling among genera, we compared model slopes between genera using the 'emtrends' function in the R package 'emmeans' (Lenth, 2018). To test if C-value diversity contributes significant variance to the relationship between mass and metabolism, we constructed a second model per data subset without genus-specific variances, and compared each model pair using likelihood ratio tests. We assessed parameter significance of each by correcting for the false discovery rate within each

response variable (five model pairs each). Though the theoretical model tested here (Kozlowski et al., 2003) applies specifically to metabolic rate, shared physical constraints on gas and water transport in plethodontid salamanders and the collinearity of these two responses in our dataset ($p < 2E^{-16}$) make it reasonable to expect a similar effect of C-value on water loss rates. Thus, we investigated the allometry of water loss by repeating the same analyses on allometric scaling and variance using EWL as a response.

Path analyses

We conducted path analyses to quantify mediation effects among our morphological and physiological variables. These models tested three responses: gross, specific, and cutaneous water loss rate. We tested each response under each VPD and temperature treatment, and across our complete dataset. In each case, models had the same general structure: mass had a direct path to the response variable and a path mediated through total resistance. C-value was also mediated through the resistance parameter but lacked a direct path to the response. While similar in concept to our linear models testing physical links between morphology and water loss rates, these path models explicitly address the mechanisms underlying these relationships. This path structure tests the hypothesis that C-value may influence resistance to water loss through its impact on skin morphology, and quantifies the relative contributions of both mass and C-value as predictors of water loss rates, both directly and as mediated by resistance.

We log-transformed all variables, testing a total of 15 path models across all responses and treatments. All models were constructed and analyzed in the R package 'lavaan' (Rosseel, 2012) using a maximum likelihood estimator with robust standard errors. We assessed the significance of path parameters using a Bonferroni correction for each response (five models

each). Because lavaan only provides significance estimates to three decimal points, we manually assigned all estimates of 0.000 a value of 0.00049 (the largest value that rounds down to 0.000) before *p*-value correction to provide a maximally conservative estimate of significance. Full descriptions of all models can be found in Table S6. For each response, we compared the total effects of mass and C-value between temperature and VPD treatments (Table S7), again with modified *p*-values and Bonferroni corrections between treatment combinations (two comparisons). Because all path predictors and responses are at a log scale, we interpreted model slopes in terms of percent change (Yang, 2012).

Thermal ratio

To investigate temperature effects evident in our linear models (see Results), we compared *r* values between 10°C and 15°C using a t-test across all individuals and for each species. Because the different life histories of our focal taxa (terrestrial *Plethodon* vs. semiaquatic *Eurycea*) are likely to influence their physiological resistance to water loss, we also compared *r* thermal dependency for each genus. We quantified the temperature dependence of *r* using the thermal ratio (R_{10}) for *r* following Bennett (1984). This metric quantifies the degree of change in a response with changing temperature, where $R_{10}>1$ is a positive thermal dependence, $R_{10}<1$ is a negative dependence, and $R_{10}=1$ indicates no effect of temperature. We calculated one R_{10} per group, using group mean *r* values at 10°C and 15°C. We then used PGLS to test for an effect of C-value on temperature dependence by regressing C-value and R_{10} while controlling for mass (Table S9). We ran models across the full dataset, and at each VPD. To test for a signature of adaptive functionality of C-value, we ran two PGLS models per subset: one assuming Brownian motion (BM, random drift), and another assuming an Ornstein-Uhlenbeck

evolutionary model (OU, adaptive evolution), and compared each model pair using a likelihood ratio test.

Results

Linear models

In our environmental models, temperature and VPD significantly predicted all physiological responses in tandem, but without an interaction effect between them (Supplementary Table S2). Among our morphological models, when tested across the entire dataset, body mass was the best supported predictor for all responses. Mass best predicted gross and specific respiration across all treatments (Fig. 1), and best predicted the majority of water loss models (gross and specific EWL, CWL), with occasional exceptions. C-value showed no significant effect on metabolism, nor on gross or specific water loss across the full dataset, however it predicted CWL and total resistance to water loss at 15°C (Fig. 1). For both these responses, C-value alone was the best supported model when tested at either VPD combination at 15°C, but tested across both VPD treatments we found equivocal evidence for an interaction between C-value and mass, as C-value and Mass * C-value were statistically indistinguishable by AICc. When compared to our separate environmental and morphological models (Supplementary Table S3), final models were the best supported model for all responses (Table 1). All top models except total resistance included mass, temperature, and VPD as predictors. For *r*, the best supported model included the interaction between mass and C-value plus temperature and VPD.

Phylogenetic generalized least squares regressions

Body mass was the best supported morphological predictor for all PGLS models when tested across the complete data set (Supplementary Table S4). Similar to our linear models, we also found evidence for an effect of C-value on CWL and *r* at 15°C (Fig. 2). For gross and specific EWL at 15°C, the best supported model was either Mass + C-value in tandem or Mass alone, however this was indistinguishable from Mass + C-value and occasionally Mass * C-value. For *r* at 15°C, C-value alone was best supported. For environmental models, mean annual temperature was the best supported predictor for all responses except specific respiration, which was best predicted by aridity index. Final models were variable among responses (Supplementary Table S5). When compared to morphological and environmental models, final models were either the best supported or indistinguishable from the best supported model for all responses except gross metabolic rate, which was best predicted by mass alone (Table 1).

Variance analysis

We found no difference in scaling coefficients for metabolism between *Plethodon* and *Eurycea*, regardless of data subset (P=0.429 – 0.870) (Supplementary Table S6, Fig. S1). Gross water loss also scaled equivalently between genera (P=0.265 – 0.731). Variance around the slope was consistently higher in the diverse C-value genus *Plethodon* for all metabolism models (mean ratio: 1.241/1), but only one of five water loss models (mean ratio: 0.989/1). Following a *p*-value correction, none of these differences were significant for either metabolic rate (P=0.100 – 0.731) or water loss (P=0.675 – 0.813).

Path analyses

C-value had a positive effect on total resistance in all path models (Supplementary Table S7). Across our full dataset, this amounted to a 0.11% increase in *r* per 1% increase in C-value (P=0.025). The significance of this effect varied across treatments; C-value consistently predicted total resistance across the full dataset (P=0.025), but never at 10°C (P=1) or 0.3 kPa (P=0.175). Mass had a positive effect on *r* in all cases (0.14% across the full dataset), consistent with covariation between mass and boundary layer resistance. For all responses, this influence was significant across our complete dataset (P=0.002), but when divided among treatments was only significant at 10°C and never at 15°C.

C-value had a negative effect on all water loss responses (mean = -0.15%) (Fig. 3), but significance of this effect was highly variable across treatments. C-value predicted each response at 15°C and 0.6 kPa, but never at 10°C or 0.3 kPa. This effect remained significant across the complete dataset for all responses (P=0.025). The total (direct + indirect) effect of mass was positive on gross water loss rates (0.55%) and negative on specific (-0.45%) and cutaneous rates (-0.15%) (Fig. 3b). This effect was consistently significant across the complete dataset ($p <$ 0.003), but was not significant for CWL at 15°C. For all water loss responses, neither mass nor C-value showed significant differences in total effect when compared between temperatures (P=0.064 – 0.074) or VPD treatments (P=1) (Supplementary Table S8).

Thermal ratio

Total resistance values increased with temperature ($R_{10} > 1$) for all species except *P. glutinosus* (Table 2, Fig. 4a). Across the complete dataset, *r* was significantly different between temperature treatments (t = 3.95, P=0.0001), but this trend was driven by patterns in *Plethodon*.

When split by genus, *r* was significantly different between temperatures in all subsets for *Plethodon*, but never for *Eurycea*. All *Plethodon* except *P. glutinosus* showed a significant difference in at least one VPD subset, but this trend held across the full dataset for only three species (*P. cinereus*, *P. larselli*, *P. vandykei*). Our PGLS models found an effect of C-value on R_{10} (Fig. 4b; Supplementary Table S9) across the full dataset using an Ornstein-Uhlenbeck covariance structure, however this model was not distinguishable from Brownian motion.

Discussion

Organisms are highly integrated biological units, and the functional interactions that underlie their performance are extremely complex. In this study, we tested for a role of genome size contributing to physiological performance in lungless salamanders, for which we find support under specific conditions. While we found no relationship between C-value and metabolic rates or any effect of C-value variation on physiological allometry, our data do demonstrate that larger genomes are associated with reduced water loss in lungless salamanders exposed to warmer temperatures – a potentially adaptive function of genome size that has not previously been reported. Though identifying a consistent model for this relationship was challenging, our results repeatedly demonstrated that C-value – in some capacity, whether interacting with mass, in tandem with mass, or acting alone – exerts an effect on water loss physiology at 15°C. Discerning a mechanism for this effect requires a careful accounting of our analyses and synthesis with established theory and empirical evidence.

Any effects of genome size on physiology are clearly secondary to the influence of body size. Consistent with a robust literature documenting the importance of body mass to metabolic rates (Brown et al., 2004; Gillooly et al., 2001) and water loss (Peters, 1986; Spight, 1968) across

taxa, mass best predicted all physiological responses in all linear and PGLS models across our full dataset, and consistently exerted a greater total effect than C-value in our path models. Unsurprisingly, the influence of body mass in plethodontid physiological performance is clear. How genome size moderates this effect is more complicated to assess. C-value appears to play no role in moderating physiological allometry in these taxa (Supplementary Fig. S1, Table S6), as both variance and allometric slopes for gross respiration and water loss were statistically equivalent between *Plethodon* and *Eurycea* despite their differences in C-value diversity. We found no effect of genome size on metabolic rates either, as models containing C-value had universally low support across linear and PGLS models. This result is consistent with previous studies demonstrating no relationship between genome size and metabolism in salamanders specifically (Gregory, 2003; Licht and Lowcock, 1991) and contributes to an emerging consensus that these traits are unrelated across vertebrates generally (Gardner et al., 2020; Uyeda et al., 2017), and suggests that C-value does not exert a nucleotypic effect on metabolism in this lineage as we hypothesized.

In contrast to metabolism, water loss physiology appears to be influenced by C-value in this group. Gross and specific EWL, CWL, and *r* all showed support for an effect of C-value at 15°C, however in all cases our linear models lacked a clear best model. Multiple models containing C-value were nonetheless better supported than models for mass alone, suggesting a functional role of C-value in driving water loss rates under warm conditions. Despite this, only our top linear model for *r* had a C-value parameter, and our top PGLS models all lacked C-value. Together, these results imply a potentially subtle functional role of C-value that is not universal across physiological responses, environmental conditions, or phylogeny. Instead, larger C-values may play a role specific to moderating water loss that: 1) acts specifically via resistance to water

transport and 2) is environment-dependent with greatest effect under warmer conditions. This inference is supported by both our linear and PGLS models at 15°C. Though our path models also found a significant *r*-mediated effect of C-value on all water loss phenotypes across the full dataset, since all three model sets agreed in identifying an effect at 15°C, we tentatively infer that larger C-values help reduce water loss specifically at higher temperatures.

Our analyses raise the possibility that C-value variation plays a functional, component role in plastic increases in *r* at high temperatures. Resistance increased with temperature in our experimental trials (Fig. 4a), coincident with decreases in all our water loss responses, a pattern indicative of plasticity in *r* across temperature. Given the selective strength of desiccation risk in plethodontids (Baken et al., 2020; Feder, 1983) and the ecological importance of minimizing water loss (Feder, 1983; Riddell et al., 2018), this result suggests plasticity in *r* is adaptive at higher temperatures (Ghalambor et al., 2007). The significant mediation of C-value in our path models at 15°C thus implies that genome size mechanistically influences increased resistance to water loss under warmer conditions. Our analyses cannot address the specific mechanism underlying this relationship, but the biophysics of resistance indicates one possibility. Total resistance is the sum of two component resistances in series: the resistance of the integument to water transport (r_i), and that of the boundary layer surrounding the animal (r_b). r_i is a biophysical and physiological property dependent upon skin structure and composition, and r_b is a physical property dependent on environmental conditions (largely air flow), body mass, shape, and orientation to air flow (Gates, 1980). Thus, any strictly physiological (non-behavioral) control of resistance will by necessity be mediated through the cutaneous (r_i) component of *r*. Because we constrained our study organisms to prevent behavioral adjustment of r_b, after controlling for differences in body mass, measured variation in *r* can be attributed to differences in cutaneous

resistance. Our path models demonstrate a significant relationship between *r* and C-value, therefore suggesting a mechanistic link between them within plethodontid skin.

Recent work has revealed the importance of temperature-induced adaptive plasticity in r_i in plethodontids (Riddell et al., 2018; Riddell et al., 2019), but how C-value influences this phenotype has until now been unexplored. The apparent mechanism for plastic resistance is by regulating cutaneous perfusion, in which vasoconstriction and the eventual breakdown of skin capillaries shunts blood away from the body surface to minimize water loss to the external environment as both temperature (Riddell et al., 2019) and dehydration severity increase (Brown, 1972). The effects of C-value we observed at our higher experimental temperature thus raise the possibility that C-value is only functionally relevant in less-perfused skin. Thus, we hypothesize that under stressfully warm conditions, as capillaries recede from or vasoconstrict in the integument, skin composed of larger cells may provide a defense of last resort against further rapid desiccation.

Theoretical and empirical work in amphibians support our hypothesis. Theory predicts thicker skins to reduce mass transfer rates across the integument (Piiper, 1988), while denser capillary networks are empirically associated with higher transport rates (Malvin, 1988). Capillary recruitment influences "effective" skin thickness, as vasoconstriction in the dermis increases the distance between the body surface and the nearest perfused capillaries exchanging material with the environment (Lillywhite, 2006). Thus, under normal skin perfusion, high water content in the capillaries of the skin should promote relatively high rates of water loss through the integument (Burggren and Vitalis, 2005). Under these high fluxes, C-value variation between species may produce negligible differences in their capacity to resist water loss. However, as cutaneous capillaries constrict to increase the skin's effective thickness, flux rates will depend

more upon the diffusion of water from skin cells themselves. Under these conditions, larger cells with higher C-values may more effectively limit water transport through the integument before evaporation from the body surface, either due to their lower diffusion rates (Goniakowska, 1973) or their effect on skin composition (Lillywhite, 2006). Skin thickness (the depth of the dermal layer) *per se* therefore may not underlie transport rates as we originally hypothesized, rather water loss may be constrained by an interaction between effective skin thickness and cell size in tissues between peripheral capillaries and the body surface. While C-value is clearly not the primary driver of variation in water loss rates, we hypothesize this mechanism may play a role in reducing marginal evaporative loss for terrestrial plethodontid salamanders under stressful conditions.

Other factors besides effective skin thickness may contribute to observed water loss patterns. Water evaporating from the body surface may be lost after diffusing through skin cells, or from cutaneous glandular mucous secretions produced to avoid loss from the epidermis itself (Lillywhite and Maderson, 1988). Studies of variation in mucous secretion in salamanders are lacking, but in frogs mucous is predominantly secreted by species that bask in direct sunlight (Lillywhite and Licht, 1975). Given that lungless salamanders are restricted to moist microhabitats away from direct sun (Feder, 1983), mucous secretion is unlikely to be a meaningful contributor to water loss rates in our sample. Alternatively, lower water loss rates may result from higher lipid concentrations within, or secreted onto, the integument. Lipid secretions can enormously improve resistance to water loss, but also reduce cutaneous gas exchange (Lillywhite, 2006). Strict reliance on cutaneous respiration in the Plethodontidae thus makes lipid secretion another unlikely strategy for managing water loss. Variation in skin lipid content may contribute to variation in r, but the strength of this relationship is, to our knowledge,

unexplored in this group. While we cannot rule out this possible mechanism, it is unclear how lipid content would plastically increase *r* at higher temperatures, or in species with larger C-values. Covariation between genome size and lipid content in the skin could still produce our observed results, as could differences in skin diffusing capacity if C-value influences cell packing and other structural changes under desiccation. However, without having quantified these traits and without a strong literature in this family, the effects of these or other unmeasured potential covariates with C-value remain speculative. As it stands and given our data, our best hypothesis holds that, whatever the mechanism, observed plasticity in *r* is underlain by variation in genome size itself.

Selection on C-value for resistance to water loss is likely to be strongest in terrestrial environments. C-value correlates with cellular differentiation rate (Sessions and Larson, 1987) and development time (Jockusch, 1997; Litvinchuk et al., 2007) in salamanders, with strong selection in biphasic, semiaquatic species, for whom ephemeral habitats favor fast development and associated small C-values to metamorphose before habitats become dry (Lertzman-Lepofsky et al., 2019). This timing constraint is absent in direct-developing terrestrial species, in which selection instead acts to minimize the risk of desiccation under exposure to air, making an association between C-value and *r* more likely in this group. We found this pattern in our R_{10} data, where the terrestrial genus *Plethodon* consistently showed adaptive increases in *r* with temperature ($R_{10} > 1$ for five of six species), but biphasic *Eurycea* showed none (Table 2). In terrestrial taxa, selection for this plasticity should be strongest where desiccation risk is greatest, placing tighter constraints on C-value evolution in drier climates. Intriguingly, the contribution of random drift to variation in plethodontid genome size is most evident in the Neotropics (Itgen et al., 2019), an environment defined by selective release from desiccation risk (Baken et al.,

2020). Thus, selection on genome size is likely stronger in temperate species more prone to evaporative water loss.

Our results collectively support a new and specific potential context for C-value function. That is, larger genomes appear to increase resistance to water loss in temperate terrestrial lungless salamanders exposed to increased temperature. While this physical effect of C-value is clear in our data, its adaptive functionality is less so. Future tests of this putative function will need to quantify both *r* and the extent and depth of capillarization and lipid deposits in the skin, compared between species with adequate variation in genome size across a greater thermal breadth to better characterize reaction norms for effective skin thickness and *r*. The thermal dependence of *r* in our dataset is modest (per-species mean R_{10} = 1.41), and our path analyses found no distinction between effects of C-value across temperatures, though only marginally so (P=0.064 – 0.070). Similarly, we did find an effect of C-value on R_{10} (Fig. 4b) under our full dataset OU model (P=0.042, Supplementary Table S9), but were unable to distinguish this model from Brownian motion. Alongside our occasional difficulty in selecting top models using AIC, these consistently subtle results suggest some of our analyses may be missing a clearer pattern of temperature-dependent plasticity due to lack of power, either through small sample size, species sampling, measurement error, or experimental design. By only sampling two temperatures, we cannot conclude whether *r* increases linearly or by some other function with increasing temperature, such as a sudden increase in resistance above a certain temperature threshold. Tests across a wider range of temperatures will increase power to identify temperature effects, and will ultimately reveal the overall thermal reaction norm of resistance to water loss, helping us identify conditions under which physiological performance is most adaptive. Measuring potential covariates of C-value may increase power further and would clarify the

mechanism through which genome size influences performance. These issues underscore the need to further test for mechanisms of C-value influencing water loss and desiccation risk in the Plethodontidae. Indeed, C-value may affect analogous physiological performance phenotypes by constraining transport rates across exchange surfaces in other taxa, potentially revealing a previously unappreciated functional consequence of genome size variation. By identifying this research avenue, this study presents a template for integrating data on morphological, physiological, and environmental variation underlying an important performance phenotype that will help quantify the role of functional diversity underlying adaptive plasticity in nature.

Acknowledgments

We thank Reed Ojala-Barbour, Marc Hayes, and Jarrett Johnson for assistance in the field and Kim Sparks for technical assistance with experiments. We also thank Lynn Johnson and Stephen Parry of the Cornell University Statistical Consulting Unit for invaluable assistance with linear and path models, respectively. Thanks also to Eric Riddell and two anonymous reviewers, whose comments greatly improved earlier drafts of this manuscript.

REFERENCES

Adler, P. B., Salguero-Gómez, R., Compagnoni, A., Hsu, J. S., Ray-Mukherjee, J., Mbeau-Ache, C. and Franco, M. (2014). Functional traits explain variation in plant life history strategies. *Proc. Natl. Acad. Sci. U. S. A.* 111, 740–745.

Baken, E. K., Mellenthin, L. E. and Adams, D. C. (2020). Macroevolution of desiccation-related morphology in plethodontid salamanders as inferred from a novel surface area to volume ratio estimation approach. *Evolution* 74, 476–486.

Bates, D., Maechler, M., Bolker, B. and Walker, S. (2015). Fitting linear mixed-effects models using lme4. *J. Stat. Softw.* 67, 1–48.

Bennett, A. F. (1984). Thermal dependence of muscle function. *Am. J. Physiol.* 247, R217–R229.

Bivand, R. S., Pebesma, E. and Gomez-Rubio, V. (2013). *Applied spatial data analysis with R*. 2nd ed. New York, NY, USA: Springer.

Brown, A. (1972). Responses to problems of water and electrolyte balance by salamanders (Genus *Aneides*) from different habitats. PhD thesis, University of California, Berkeley, CA.

Brown, J. H., Gillooly, J. F., Allen, A. P., Savage, V. M. and West, G. B. (2004). Toward a metabolic theory of ecology. *Ecology* 85, 1771–1789.

Buck, A. L. (1981). New equations for computing vapor pressure and enhancement factor. *J. Appl. Meteorol.* 20, 1527–1532.

Burggren, W. W. and Vitalis, T. Z. (2005). The interplay of cutaneous water loss, gas exchange and blood flow in the toad, *Bufo woodhousei*: adaptations in a terrestrially adapted amphibian. *J. Exp. Biol.* 208, 105–112.

Clark, K., Karsch-Mizrachi, I., Lipman, D. J., Ostell, J. and Sayers, E. W. (2016). Genbank. *Nucleic Acids Res.* 4, D67–D72.

Feder, M. E. (1983). Integrating the ecology and physiology of plethodontid salamanders. *Herpetologica* 39, 291–310.

Feder, M. E. and Burggren, W. W. (1985). Cutaneous gas exchange in vertebrates: design, patterns, control and implications. *Biol. Rev. Camb. Philos. Soc.* 60, 1–45.

Fick, S. E. and Hijmans, R. J. (2017). WorldClim 2: new 1-km spatial resolution climate surfaces for global land areas. *Int. J. Climatol.* 37, 4301–4315.

Fisher-Reid, M. C. and Wiens, J. J. (2011). What are the consequences of combining nuclear and mitochondrial data for phylogenetic analysis? Lessons from *Plethodon* salamanders and 13 other vertebrate clades. *BMC Evol. Biol.* 11, 300.

Garamszegi, L. Z. ed. (2014). *Modern Phylogenetic Comparative Methods and Their Application in Evolutionary Biology*. Berlin: Springer.

Gardner, J. D., Laurin, M. and Organ, C. L. (2020). The relationship between genome size and metabolic rate in extant vertebrates. *Philos. Trans. R. Soc. B Biol. Sci.* 375, 20190146.

Gates, D. M. (1980). *Biophysical Ecology*. New York, NY, USA: Springer-Verlag.

Ghalambor, C. K., McKay, J. K., Carroll, S. P. and Reznick, D. N. (2007). Adaptive versus non-adaptive phenotypic plasticity and the potential for contemporary adaptation in new environments. *Funct. Ecol.* 21, 394–407.

Gillooly, J. F., Brown, J. H. and West, G. B. (2001). Effects of size and temperature on metabolic rate. *Science* 293, 2248–2252.

Glazier, D. S. (2005). Beyond the "3/4-power law": variation in the intra- and interspecific scaling of metabolic rate in animals. *Biol. Rev. Camb. Philos. Soc.* 80, 611–62.

Glazier, D. S. (2018). Rediscovering and reviving old observations and explanations of metabolic scaling in living systems. *Systems* 6, 4.

Goniakowska, L. (1973). Metabolism, resistance to hypotonic solutions, and ultrastructure of erythrocytes of five amphibian species. *Acta Biol. Cracoviensia, Ser. Zool.* 16, 114–134.

Gregory, T. R. (2001a). The bigger the C-value, the larger the cell: genome size and red blood cell size in vertebrates. *Blood Cells, Mol. Dis.* 27, 830–843.

Gregory, T. R. (2001b). Coincidence, coevolution, or causation? DNA content, cell size, and the C-value enigma. *Biol. Rev.* 76, 65–101.

Gregory, T. (2002). A bird's-eye view of the C-value enigma: genome size, cell size, and metabolic rate in the class Aves. *Evolution* 56, 121–130.

Gregory, T. R. (2003). Variation across amphibian species in the size of the nuclear genome supports a pluralistic, hierarchical approach to the C-value enigma. *Biol. J. Linn. Soc.* 79, 329–339.

Gregory, T. R. (2016). Animal Genome Size Database. *http://www.genomesize.com*.

Hijmans, R. J. (2017). raster: Geographic data analysis and modeling. R package version 2.6-7.

Itgen, M. W., Prsa, P., Janza, R., Skubic, L., Townsend, J. H., Kladnik, A., Mali, L. B. and Sessions, S. K. (2019). Genome size diversification in Central American Bolitoglossine salamanders (Caudata; Plethodontidae). *Copeia* 107, 560–566.

Jockusch, E. L. (1997). An evolutionary correlate of genome size change in plethodontid salamanders. *Proc. R. Soc. London B* 264, 597–604.

Katoh, K. and Standley, D. M. (2013). MAFFT multiple sequence alignment software version 7: Improvements in performance and usability. *Mol. Biol. Evol.* 30, 772–780.

Kearney, M. (2012). Metabolic theory, life history and the distribution of a terrestrial ectotherm. *Funct. Ecol.* 26, 167–179.

Kozlowski, J., Konarzewski, M. and Gawelczyk, A. T. (2003). Cell size as a link between noncoding DNA and metabolic rate scaling. *Proc. Natl. Acad. Sci. USA.* 100, 14080–14085.

Lenth, R. (2018). emmeans: estimated marginal means, aka least-squares means. R package version 1.1.

Lertzman-Lepofsky, G., Mooers, A. Ø. and Greenberg, D. A. (2019). Ecological constraints associated with genome size across salamander lineages. *Proc. R. Soc. B* 286, 20191780.

Licht, L. E. and Lowcock, L. A. (1991). Genome size and metabolic rate in salamanders. *Comp. Biochem. Physiol. Part B* 100, 83–92.

Lillywhite, H. B. (2006). Water relations of tetrapod integument. *J. Exp. Biol.* 209, 202–226.

Lillywhite, H. B. and Licht, P. (1975). A comparative study of integumentary mucous secretions in amphibians. *Comp. Biochem. Physiol.* 51A, 937–941.

Lillywhite, H. B. and Maderson, P. F. A. (1988). The structure and permeability of integument. *Am. Zool.* 28, 945–962.

Litvinchuk, S. N., Rosanov, J. M. and Borkin, L. J. (2007). Correlations of geographic distribution and temperature of embryonic development with the nuclear DNA content in the Salamandridae. *Genome* 50, 333–342.

Malvin, G. M. (1988). Microvascular regulation of cutaneous gas exchange in amphibians. *Am. Zool.* 28, 999–1007.

Mueller, R. L. (2015). Genome biology and the evolution of cell-size diversity. *Cold Spring Harb. Perspect. Biol.* 7, a019125.

Newman, C. E., Gregory, T. R. and Austin, C. C. (2016). The dynamic evolutionary history of genome size in North American woodland salamanders. *Genome* 8, 1–8.

Paradis, E. and Schliep, K. (2018). ape 5.0: an environment for modern phylogenetics and evolutionary analyses in R. *Bioinformatics* 35, 526–528.

Peters, R. H. (1986). *The Ecological Implications of Body Size*. New York, NY, USA: Cambridge University Press.

Pettersen, A. K., White, C. R., Bryson-Richardson, R. J. and Marshall, D. J. (2019). Linking life-history theory and metabolic theory explains the offspring size - temperature relationship. *Ecol. Lett.* 22, 518–526.

Piiper, J. (1988). Models for cutaneous gas exchange and transport. *Am. Zool.* 28, 963–972.

R Core Team (2017). R: A language for statistical computing.

Rambaut, A., Drummond, A. J., Xie, D., Baele, G. and Suchard, M. A. (2018). Posterior summarization in Bayesian phylogenetics using Tracer 1.7. *Syst. Biol.* 67, 901–904.

Riddell, E. A. and Sears, M. W. (2015). Geographic variation of resistance to water loss within two species of lungless salamanders: implications for activity. *Ecosphere* 6, 1–16.

Riddell, E. A., Odom, J. P., Damm, J. D. and Sears, M. W. (2018). Plasticity reveals hidden resistance to extinction under climate change in the global hotspot of salamander diversity. *Sci. Adv.* 4, eaar5471.

Riddell, E. A., Roback, E. Y., Wells, C. E., Zamudio, K. R. and Sears, M. W. (2019). Thermal cues drive plasticity of desiccation resistance in montane salamanders with implications for climate change. *Nat. Commun.* 10, 4091.

Ronquist, F., Teslenko, M., Van Der Mark, P., Ayres, D. L., Darling, A., Höhna, S., Larget, B., Liu, L., Suchard, M. A. and Huelsenbeck, J. P. (2012). Mrbayes 3.2: Efficient bayesian phylogenetic inference and model choice across a large model space. *Syst. Biol.* 61, 539–542.

Rosseel, Y. (2012). lavaan: an R package for structural equation modeling. *J. Stat. Softw.* 48, 1–36.

Sessions, S. K. and Larson, A. (1987). Developmental correlates of genome size in plethodontid salamanders and their implications for genome evolution. *Evolution* 41, 1239–1251.

Shoemaker, V. H. and Nagy, K. A. (1977). Osmoregulation in amphibians and reptiles. *Annu. Rev. Physiol.* 39, 449–471.

Spight, T. M. (1968). The water economy of salamanders: evaporative water loss. *Physiol. Zool.* 41, 195–203.

Uyeda, J. C., Pennell, M. W., Miller, E. T., Maia, R. and Mcclain, C. R. (2017). The evolution of energetic scaling across the vertebrate tree of life. *Am. Nat.* 190, 185–199.

Vinogradov, A. E. (1995). Nucleotypic effect in homeotherms: body-mass-corrected basal metabolic rate of mammals is related to genome size. *Evolution* 49, 1249–1259.

White, C. R. and Kearney, M. R. (2013). Determinants of inter-specific variation in basal metabolic rate. *J. Comp. Physiol. B* 183, 1–26.

Whitford, W. G. and Hutchison, V. H. (1967). Body size and metabolic rate in salamanders. *Physiol. Zool.* 40, 127–133.

Yang, J. (2012). Interpreting coefficients in regression with log-transformed variables. *Cornell Univ. Stat. Consult. Unit News Arch.* 83.

Zomer, R. J., Trabucco, A., Bossio, D. A. and Verchot, L. V (2008). Climate change mitigation: A spatial analysis of global land suitability for clean development mechanism afforestation and reforestation. *Agric. Ecosyst. Environ.* 126, 67–80.

Table 1. Top supported linear and PGLS models for seven physiological response variables. Entries in parentheses were statistically indistinguishable from the top model by AICc comparison.

Response	Model type	Best model	df	Log likelihood	AICc
gross respiration	linear	Mass + Temp + VPD	7	-97.40	227.0
specific respiration	linear	Mass + Temp + VPD	7	-97.74	227.6
gross water loss	linear	Mass + Temp + VPD	7	-27.25	90.7
specific water loss	linear	Mass + Temp + VPD	7	-27.54	91.4
cutaneous water loss	linear	Mass + Temp + VPD	7	-27.31	90.9
total resistance	linear	Mass * C-value + Temp + VPD	9	-24.97	100.6
gross respiration	PGLS	Mass	3	-0.29	12.58
specific respiration	PGLS	AI	3	1.34	9.33
gross water loss	PGLS	Mass (Mass + Temp)	3	10.07	-8.14
specific water loss	PGLS	Mass (Mass + Temp)	3	10.01	-8.02
cutaneous water loss	PGLS	Mass	3	10.06	-8.12
total resistance	PGLS	Mass	3	9.84	-7.69

Note: PGLS = phylogenetic generalized least squares, Temp = temperature, VPD = vapor pressure deficit, AI = aridity index, df = degrees of freedom, AICc = corrected Akaike information criterion

Table 2. Temperature dependency of total resistance to water loss. R_{10} values are calculated by taxon group and subset by VPD treatment, with significant differences in resistance assessed by t-tests between 10° and 15°C.

	Full dataset			0.3 kPa			0.6 kPa		
Species	**R_{10}**	***t*-value**	***p*-value**	**R_{10}**	***t*-value**	***p*-value**	**R_{10}**	***t*-value**	***p*-value**
all	1.33	3.95	0.000	1.39	3.22	0.002	1.28	3.58	0.000
all *Eurycea*	1.37	1.85	0.069	1.48	1.68	0.106	1.21	1.62	0.114
all *Plethodon*	1.32	3.52	0.000	1.38	2.80	0.006	1.29	3.34	0.001
E. bislineata	1.42	1.70	0.097	1.55	1.56	0.135	1.23	1.44	0.163
E. longicauda	1.29	0.82	0.426	1.34	0.64	0.556	1.22	0.93	0.381
P. cinereus	1.67	3.65	0.001	1.70	2.42	0.022	1.68	4.10	0.000
P. dunni	1.37	1.67	0.104	1.84	2.37	0.037	1.06	0.20	0.843
P. glutinosus	0.75	-1.53	0.132	0.66	-1.51	0.144	0.88	-0.75	0.463
P. larselli	1.69	2.85	0.008	1.91	2.33	0.038	1.49	2.19	0.042
P. vandykei	1.66	3.09	0.003	1.86	2.91	0.008	1.49	2.77	0.009
P. vehiculum	1.41	1.73	0.092	1.34	0.98	0.341	1.51	2.27	0.034

Note: R_{10} = thermal ratio, VPD = vapor pressure deficit

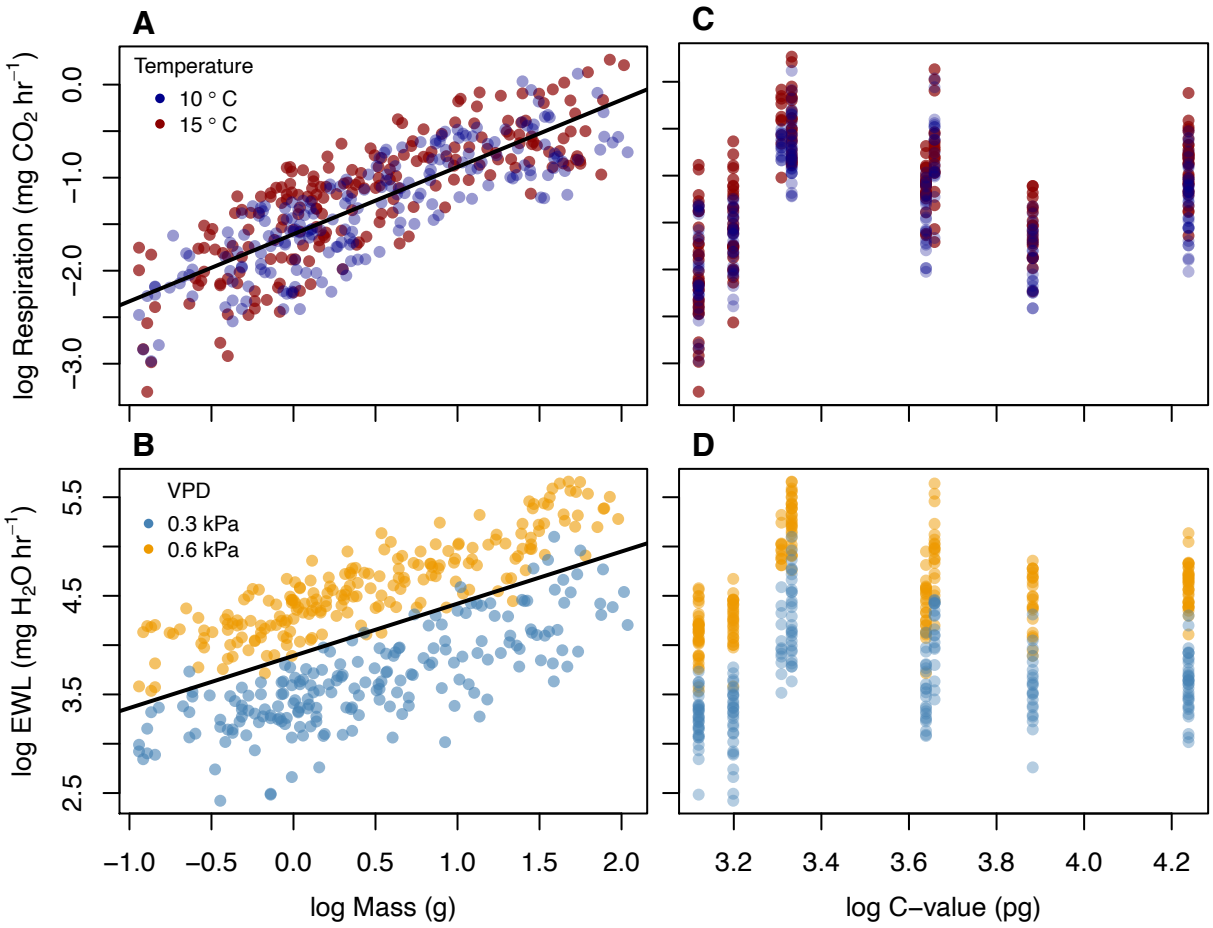

Figure 1. Effects of body mass and genome size on gross physiological rates of 126 individuals from eight species of plethodontid salamanders, tested across all experimental conditions. Mass predicts metabolic rate (**a**), and evaporative water loss (**b**), but C-value predicts neither metabolism (**c**) nor evaporative water loss (EWL) (**d**). Trend lines are best fits to the data to represent significant effects across the complete dataset (P<0.001 for both respiration, EWL). Metabolic data are colored by temperature treatment, and water loss data are colored by vapor pressure deficit (VPD) to illustrate environmental effects on physiological responses.

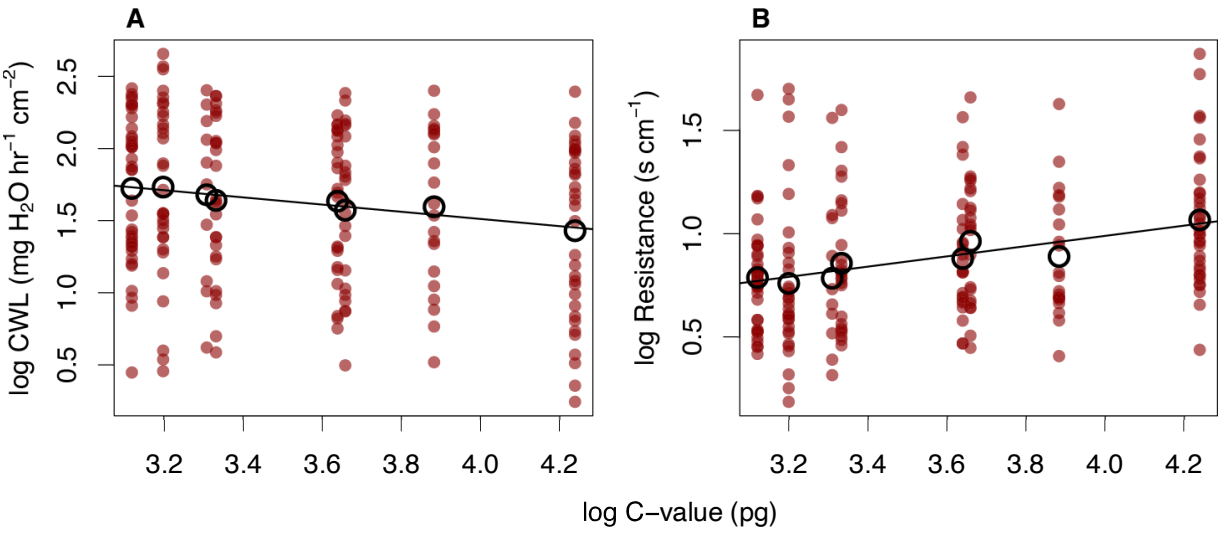

Figure 2. Effects of genome size on cutaneous water loss (CWL) (A) and total resistance to water loss (B) across VPD treatments at 15°C. Red points reflect individual measurements (*n*=126 individuals) used in linear models (*P*<0.001 for CWL and *r*) and open circles are species means (*n*=8 species) used in PGLS regressions (CWL: *P*=0.0012, *r*: *P*=0.0048). Trend lines are a best fit to the individual data.

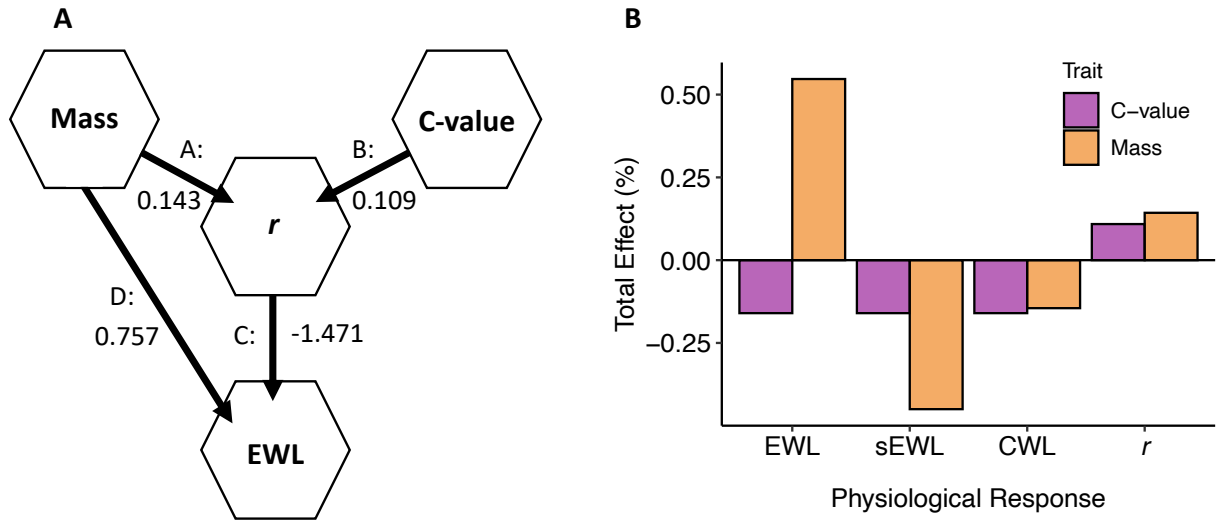

Figure 3. Path model structure and total path effects of mass and C-value, tested across our complete dataset. All path models follow the same structure, presented here with example results for gross evaporative water loss (EWL) (**A**). Mass and C-value both have effects on EWL mediated by total resistance (*r*). Path D is the direct effect of mass, A*C is the indirect effect of mass, B*C is the indirect (total) effect of C-value, (A*C)+D is the total effect of mass. These total effects are represented in (**B**) for all water loss responses: gross evaporative water loss (EWL), specific EWL (sEWL), and cutaneous water loss (CWL), plus direct effects on total resistance (*r*). Effect sizes reflect % change with corresponding 1% change in the predictor.

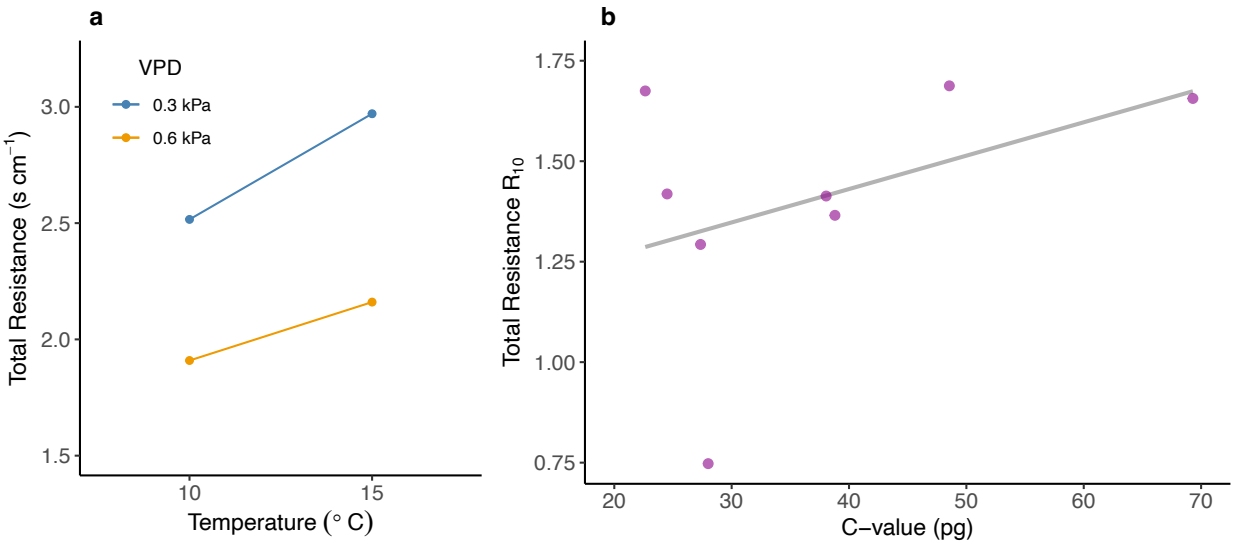

Figure 4. Temperature-dependence of resistance to water loss. Resistance increases with temperature (P<0.001) when testing all eight species together (n=126 individuals) (**a**), and thermal ratios (R_{10}) for *r* are predicted by C-value using PGLS regression (**b**). The trendline is a best fit to the data to represent a significant effect across the complete dataset using an OU model (P=0.042).

CHAPTER TWO

NOVEL ALLOMETRIC ESTIMATORS IMPROVE ESTIMATION ACCURACY OF BODY SURFACE AREA, VOLUME, AND SURFACE AREA-TO-VOLUME RATIO IN LUNGLESS SALAMANDERS (URODELA: PLETHODONTIDAE)

Research in collaboration with: Jeremy B. Searle[1], Jed P. Sparks[1]

[1]Department of Ecology & Evolutionary Biology, Cornell University, Ithaca, NY, USA

Abstract

Body surface area and volume are both physiologically important traits in amphibians, as their ratio constrains transport rates for water and respiratory gases across the skin. This is especially true in the lungless salamanders (Urodela: Plethodontidae), whose lungless morphology restricts nearly all gas and water transport to the body surface. Due to methodological difficulties of measuring surface area and volume, estimation techniques are the most convenient way to produce usable phenotype scores. To this end, we used high resolution CT scans of three plethodontid species varying in body size and shape to produce allometric regression models to estimate body surface area (SA), volume, and surface area-to-volume ratios (SA:V). We compared our model estimates to empirical measurements and established estimation methods employed in the Plethodontidae using linear models and Deming regressions. We found our model estimates are both accurate and generalizable across temperate plethodontid species. This method significantly improves SA estimation accuracy when compared to published allometric models. Our models are also significantly more accurate than SA or volume estimates following geometric measurements, although SA:V estimates are comparable between these techniques for most body sizes. We discuss the relative utility of different estimation methods for future research questions.

Introduction

The body surface is a critically important phenotype, acting as both a protective barrier and a site of energy and mass exchange between organisms and the external environment (Feder and Burggren 1985). In amphibians, a permeable skin makes the body surface central to water uptake and loss, as well as the transport of respiratory gases into and out of the body (Toledo and Jared 1993; Hutchison et al. 1968). This is especially true in the lungless salamanders (family Plethodontidae), whose lungless morphology ensures that effectively all respiratory gases (and body water) are transferred across the body surface (Spight 1968; Whitford and Hutchison 1965).

In terrestrial plethodontid salamanders, respiratory gas transport is predominantly limited by its diffusion through the skin (Piiper et al. 1976; Feder et al. 1988), meaning the total body surface area (SA) constrains gross transport and metabolic rates (Beckenbach 1975). More specifically, the strength of the constraint on physiology depends on the ratio of SA to body volume (SA:V), as larger organisms have a smaller SA relative to volume than small organisms due to differences in the allometric scaling of these traits (Okie 2013). This constraint keeps larger salamanders close to their aerobic capacity, with a relatively limited supply of oxygen to tissues beyond what is needed for baseline metabolism (Beckenbach 1975; Feder 1988). The functional consequences of this constraint are profound, as it accounts for the generally low metabolic rates and physiologically conservative life histories common in this group (Feder 1983). Further, constraint on respiratory metabolism presents a tradeoff with cutaneous water transport, as a high SA:V simultaneously increases both O_2 absorption into the body and water loss out the body (Riddell et al. 2018a). Desiccation strongly alters activity (Feder and Londos 1984) and can rapidly kill plethodontids, especially smaller individuals (Littleford et al. 1947), suggesting strong selection to minimize water loss. Plastic control of water loss can provide

protection against desiccation to a degree (Riddell et al. 2018b), but even given such physiological adaptations, the consequences of morphological constraint remain visible across the Plethodontidae, as SA:V values are generally lower in species found in drier, cooler (temperate) climates (Baken et al. 2020).

The functional importance of SA and SA:V in lungless salamanders makes clear the need for accurate, easy-to-reproduce estimates of these phenotypes. While body volume can be relatively easily measured through volume displacement, such measurements using graduated cylinders (e.g., Riddell et al. 2017; Baken et al. 2020) are limited in their precision. Further, SA is a complex trait that is much more difficult to quantify. Previous empirical methods for measuring SA in salamanders include wrapping individuals in aluminum foil (Ultsch 1973), shadow tracing (Beckenbach 1975), tracing skin peeled from preserved specimens (Whitford and Hutchison 1967), and 3D scans (Baken et al. 2020). The labor involved in these techniques demonstrates that SA is a particularly inconvenient phenotype to measure. To avoid this difficulty, plethodontid SA values are most often produced through more convenient estimation methods. Two such methods have been validated by empirical measurements, one validated by skin tracings using allometric regressions (Whitford and Hutchison 1967), and the other validated by 3D scans using geometric calculations using linear body measurements (Baken et al. 2020). While the allometric method of Whitford and Hutchison (1967) has been widely employed in plethodontid physiology for its easy implementation (e.g., Houck and Bellis 1972; Feder 1976; Peterman et al. 2013; Riddell et al. 2017), the geometric approach of Baken et al. (2020) presents a recent improvement that is far more sensitive to inter- and intra-specific variation in body shape, but is more time-consuming.

The goal of this study is to contrast established and new methods for estimating SA, volume, and SA:V (hereafter "body dimensions") in order to identify the relative advantages and disadvantages of each method for future physiological research. While focusing here on the Plethodontidae, these methodologies could also be applied in other vertebrate systems where estimates of body dimensions are needed. Here, we present novel allometric estimates for plethodontid SA, volume, and SA:V validated by high resolution CT scans and compare our estimates with previously published methods using linear models and Deming regressions. In evaluating our method in comparison with others, we assess whether different methods may suit particular research questions better than others.

Materials and Methods

Rationale

The original impetus for this work was to evaluate the performance of the allometric estimates for SA established by Whitford and Hutchison (1967). Whitford and Hutchison (1967) presented two allometric models for estimating SA, one specific to the Plethodontidae and the other general to all salamanders. They found these models to be statistically equivalent, and both have been applied to plethodontids in subsequent studies. However, these models may not be appropriate in all cases because they were trained on data exclusively from large-bodied salamanders (*Ambystoma maculatum, Salamandra salamandra, Plethodon glutinosus, Gyrinophilus porphyriticus, Pseudotriton ruber, Desmognathus quadramaculatus*, and *Taricha granulosa*), raising the possibility that they do not adequately describe variation in smaller or thinner taxa. Also, because most individuals used to train these models were of adult size, the models are unlikely to accurately describe variation due to ontogeny. Further, there may be

considerable error associated with Whitford and Hutchison's (1967) empirical validation of SA, in which they peeled skin from preserved specimens and traced removed pieces. Stretching (due to pulling) and shrinking (due to desiccation) of skin could make this method problematic. For these reasons, we compared Whitford and Hutchison's (1967) estimators to more reliable empirical measurements and tested the applicability of Whitford and Hutchison's (1967) models to plethodontid species with more variable body types than those originally tested, using new SA estimators for comparison.

A novel method for estimating SA and SA:V was recently presented by Baken et al. (2020), in which individual salamanders are modeled as a set of geometric volumes whose dimensions are estimated using 11 linear body measurements. This approach offers substantial benefits over the allometric approach in that it faithfully captures individual-level variation in body shape – not just mass – contributing to SA, volume, and SA:V. Baken et al. (2020) validated a subset of their estimates against Lidar 3D scans of measured specimens (Erica Baken, personal communication). Model comparisons using the Akaike Information Criterion indicated that the Baken et al. (2020) technique better predicted SA:V than the combination of Whitford and Hutchison's (1967) estimates and volume displacement measurements (Baken et al. 2020). This could represent a better fit of the model slope and/or improved residual error by Baken et al. (2020), however no direct regression between the two metrics was made, so it is unclear how similarly they behave in terms of model slopes when estimating SA:V across body size.

If the Baken et al. (2020) approach in fact better estimates a model slope for SA:V, this technique would represent an improvement upon Whitford and Hutchison (1967) for all applications. However, if Baken et al. (2020) better captures residual error but slopes are equivalent between the two, the increased effort required by Baken et al. (2020), at least for

some applications, may represent negligible improvement in model accuracy over the Whitford and Hutchison (1967) method. Further, while the Baken et al. (2020) approach is well suited to comparisons of body dimensions between preserved specimens, these measurements are difficult to obtain accurately from living salamanders without anesthesia, complicating their application to studies on live organisms. With these issues in mind, we wanted to directly compare body dimension estimates produced following Baken et al. (2020) with allometric estimates and empirical measurements to identify situations where one estimation method is more appropriate than the other.

CT scans and body dimensions

To obtain accurate measurements of body volume and surface area, we employed high resolution X-ray computed tomography (CT) scanning of museum specimens from the Cornell University Museum of Vertebrates (CUMV) (Table S1, Supplemental Material, available online). All scans were conducted using a Bruker Skyscan 1276 micro-CT scanner at the Cornell University Biotechnology Resource Center imaging facility. We scanned 14-18 individuals each from three species (*E. longicauda*, *P. cinereus*, *P. glutinosus*), selected to represent the breadth of size and shape variation in temperate terrestrial Plethodontidae, from small and thin (*P. cinereus*) to large and bulky (*P. glutinosus*), to highly elongate (*E. longicauda*). For each species, we scanned complete museum specimens with no evidence of damage or destructive sampling (no breaks or incisions in the body surface) and with no evidence of previous tail autotomy. We selected individual specimens spanning a broad range of body sizes (*E. longicauda* 0.229 – 3.02 g, *P. cinereus* 0.035–1.483 g, *P. glutinosus* 0.109–7.386 g) in order to sample across all developmental stages for accurate estimates of allometry (see below). We stained all specimens

following Metscher (2009), using a 1% I_2 solution in 99% USP grade isopropanol for 2–3 days prior to scanning. We substituted ethanol (recommended by Metscher 2009) with isopropanol to match the solution specimens were stored in. Because all specimens were originally stored in 50% isopropanol, we transferred specimens into sequentially higher concentrations (50% to 70% to 90% to 99%) for one week at each concentration before the final staining step. This strategy avoided possible specimen damage due to rapid desiccation after an abrupt transition to high-concentration isopropanol. Stained specimens were scanned in batches of 3-8 individuals at a resolution of either 20 or 40 μm $pixel^{-1}$, depending on body size.

We measured SA and volume of all specimen CT scans using Avizo Lite v9.7.0 (Thermo Fisher Scientific, Waltham, MA). The batched museum specimens were physically separated with foam during scanning for easier segmentation. We manually segmented the batched CT data in Avizo by thresholding for brightness, meaning bright, high-density specimens could be easily segmented from the remaining scanned volume using the magic wand tool, enabling more straightforward analysis of individual specimens. After segmentation, we selected the entire body volume of each individual as a region of interest (ROI). We manually filled low-density regions within the body (empty cavities in the gut and mouth) to include within the ROI, and manually removed erroneously assigned pixels from the ROI (identification tags and pixelated noise extending beyond the body surface). We then estimated SA (mm^2) and volume (mm^3) of the ROI using Avizo's basic 3D label analysis. We estimated SA:V (mm^2 mm^{-3}) by dividing CT-measured SA and volume values for each individual.

Allometry

To model covariance of whole-organism morphology with body mass, we estimated the allometry of SA, volume, and SA:V for each of our scanned species. We measured the mass of scanned specimens to the nearest 0.001 g, and regressed the log of body mass against the log of CT-measured SA, volume, and SA:V using ordinary least squares in R (v4.0.0, R Core Team 2020). In these and all downstream log transformations, we used the natural log. For each body dimension, we conducted one regression for each species, plus one general model using all individuals from our CT dataset. We then produced two new sets of body dimension estimates for each specimen using specific and general model outputs.

Published estimation methods

To compare our estimates of body dimensions to other published methods, we created a second set of estimates using linear measurements and geometric calculations following Baken et al. (2020) for the same specimens used in CT scans. We measured 11 relevant linear body dimensions to the nearest 0.01 mm using calipers, and estimated SA (mm^2), volume (mm^3), and SA:V ($mm^2\ mm^{-3}$) using the "SAtoV.Function" R script published by Baken et al. (2020). We also estimated the SA of each specimen using the allometric models of Whitford and Hutchison (1967). We used both the Whitford and Hutchison (1967) model specific to the Plethodontidae, where SA (cm^2) = $0.983 \cdot \text{mass (g)}^{0.614}$, and the model general to all salamanders ($SA = 8.42 \cdot \text{mass}^{0.694}$). For downstream comparisons, we converted these estimates to mm^2.

Method performance

To characterize the accuracy of different methods for estimating body dimensions, we used Deming regressions to compare estimates to CT-measured values. This method is a total least squares regression that accounts for observation error in both predictor and response variables, commonly employed in methods comparisons (Linnet 1993). We assessed seven estimators for surface area: our general allometric model, our three species-specific allometric models, the general and Plethodontidae-specific allometric models of Whitford and Hutchison (1967), and the geometric estimates of Baken et al. (2020). Because Whitford and Hutchison (1967) only estimated SA, for volume and SA:V, we assessed only the remaining five estimates. For all general (not species-specific) methods, we evaluated the accuracy of the estimator across our complete specimen dataset, and subset by species. We conducted 41 regressions in total. For each, we calculated confidence intervals around the slope and intercept of the regression starting with an α significance level of 0.05. We used Bonferroni corrections on α grouped by each combination of method and body dimension evaluated. That is, we corrected by the number of instances at which a given method was used to estimate a given body dimension (usually four: once for each species-specific regression and once across the complete dataset, resulting in $\alpha = 0.0125$ to produce 98.75% confidence intervals). Using these α corrections, we defined an accurate estimator as one whose confidence intervals bounded a slope of one and intercept of zero, indicating statistically indistinguishable estimators and measurements. Finally, we calculated the estimation error of different methods when applied across the complete dataset. We defined error as the relative error: the ratio of the absolute error of an estimate to its corresponding empirical measurement (e.g., [CT-measured SA – allometry-estimated SA] / CT-measured SA), which we multiplied by 100 to present as a percentage. We calculated estimation

errors for the Whitford and Hutchison (1967) Urodele model, all Baken et al. (2020) estimates, and our general allometric models. For each method, we tested if estimation error varies with body size using linear regressions between mass and error.

Method comparisons

To compare method performance in estimating body dimensions, we used a combination of Deming regressions and linear models. To determine if allometry of each dimension is species-specific, we fit random slope linear models to our CT dataset. We regressed SA, volume, and SA:V with the interaction between mass and species (after log transformations), then compared each species' regression slope using the 'emtrends' function in the 'emmeans' R package (v1.5.3, Lenth 2018). For each body dimension, we compared our allometric and Baken et al. (2020) estimates using a Deming regression. We also compared both types of estimates for SA to our Whitford and Hutchison (1967) allometric estimates using Deming regressions. First, we used a Deming regression to compare our fitted values of the general and plethodontid-specific Whitford and Hutchison (1967) models, ensuring that 95% confidence intervals around model slopes were overlapping to confirm their statistical equivalency in our dataset. Because these models were statistically equivalent, we continued with the general Urodele model in further Deming comparisons with our allometric and Baken et al. (2020) estimates.

We compared our allometric estimates to our Baken et al. (2020) estimates using three subsets of our dataset. Our data span a broader range of body size (0.035–7.386 g) compared to Baken et al. (2020) (0.216–5.899 g), meaning our measurements may capture variation in the scaling of SA:V not examined by Baken et al. (2020) in validating their method, thus making comparisons between methods problematic at more extreme body sizes. For this reason, we

compared estimates using Deming regressions on both our full dataset (n = 46 specimens), and only those falling within the mass range explored by Baken et al. (2020) (0.22 g =< mass =< 5.90 g, n = 38). We followed this comparison with another excluding only smaller specimens (mass >= 0.22 g, n = 40).

To quantify the effects of different estimation methods on downstream physiological estimates, we compared our allometric estimates to Whitford and Hutchison (1967) estimates used to calculate cutaneous water loss rates (CWL) and total resistance to water loss (r) in live plethodontid salamanders. We used the dataset of Johnson et al. (2021), which comprises multiple physiological experiments measuring 126 individuals (409 total observations) from eight plethodontid species (*Plethodon cinereus*, *P. dunni*, *P. glutinosus*, *P. larselli*, *P. vandykei*, *P. vehiculum*, *Eurycea bislineata*, and *E. longicauda*). We used body mass and gross evaporative water loss measurements from Johnson et al (2021) to recalculate CWL and r (two physiological variables whose estimation requires a SA parameter) as outlined in their study. We used the same units for r (s cm^{-1}) as Johnson et al. (2021) and converted CWL to mg H_2O hr^{-1} mm^{-2} for consistency with SA units used in this study. We calculated each response twice, using either estimates for SA produced with the Whitford and Hutchison (1967) Urodele model, or estimates produced with our general SA model. We compared final CWL and r estimates using Deming regressions.

Results

We successfully produced 46 high fidelity 3D models of museum specimens from CT scans and used these to produce parameters for allometric regressions (Table 1). In all cases, our species-specific models showed a Deming regression slope equivalent to m = 1 and intercept

equivalent to $b = 0$ when compared with empirical measurements, consistent with our definition of an accurate estimator (Table S2, Supplemental Material, available online). Our general allometric models (trained on all species pooled together) accurately predicted SA and SA:V, but not volume when tested across all species (Fig. 1), as the model slope was statistically equivalent to $m = 1$, but the intercept was not equivalent to $b = 0$ ($m = 0.94$, 98.75% CI = 0.84–1.00, $b =$ 66.58, 98.75% CI = 5.65–171.96). Estimation error was low for our three general models, with a mean relative error of 0.3%, 0.5%, and 0.3% for SA, volume, and SA:V models, respectively. This error did not covary with body mass (Fig. S1, Supplemental Material, available online). When applied to individual species, general models were variable in their accuracy (Table S2).

Neither the Whitford and Hutchison (1967) allometric estimates nor the Baken et al. (2020) geometric estimates accurately predicted body dimensions in any case we examined (Table S2; Figs. S2 & S3, Supplemental Material, available online), due to high estimation error. The Whitford and Hutchison (1967) Urodele model demonstrated a mean relative error of 31.5%, with no covariation with body mass (Fig. S4, Supplemental Material, available online). Baken et al. (2020) estimates for SA, volume, and SA:V deviated from empirical measurements by a mean of 33.7%, 26.5%, and 9.2%, respectively. Volume and SA:V estimates did not covary with body mass, but error for SA estimates was inversely related with mass (Fig. S5, Supplemental Material, available online).

We found no differences in allometric slopes between species for either SA ($P = 0.061$–0.947) or SA:V ($P = 0.753$–0.996) when compared using our random slope linear models (Fig. 2). Only *P. cinereus* and *P. glutinosus* differed in the allometry of volume ($P = 0.007$; Table S3, Supplemental Material, available online). Using Deming regressions, our general model estimates for SA differed from Whitford and Hutchison's (1967) estimates (CI = 0.702–0.709),

and our SA, volume, and SA:V estimates differed from Baken et al. (2020) in all cases when compared across the full dataset (Fig. 3; Table S4, Supplemental Material, available online). However, when compared across our two data subsets (0.22 g =< mass =< 5.90 g and mass >= 0.22 g), our estimates for SA:V were statistically equivalent with Baken et al. (2020) (Fig. S3D). We found no statistical difference in SA estimates between Whitford and Hutchison (1967) and Baken et al. (2020) (Table S4). Per Deming regressions, estimates of CWL and *r* were significantly different when calculated using either Whitford and Hutchison (1967) or our general SA estimators (Fig. 4; Table S5, Supplemental Material, available online).

Discussion

Obligate cutaneous transport has profound consequences on respiratory physiology and water balance in plethodontid salamanders, and is constrained by the dimensions of the body surface. In this study, we produced accurate measurements of body surface area, volume, and SA:V to inform new allometric estimators for these important traits and to assess the accuracy of established estimation methods. Here, we characterize the utility of our estimates and contrast our method with those of Whitford and Hutchison (1967) and Baken et al. (2020) to outline their respective strengths for future research questions in plethodontid physiology.

Novel allometric estimates

Our allometric models demonstrate a tight relationship between body mass and body dimensions, with minimal variance even when pooled among species (general SA, volume, & SA:V R^2 = 0.991, 0.995, & 0.960, respectively) (Fig. 1). Our species-specific models accurately estimated body dimensions in all cases, therefore we interpret our allometric models as accurate

and useful predictors of body dimensions in these target species. Our general models, however, occasionally failed to accurately predict body dimensions when applied to individual species (Table S2). Following a Deming regression, general estimates inaccurately fit the data for SA in *P. cinereus*, volume in *P. cinereus* and *E. longicauda*, and SA:V in *E. longicauda*. Deviation between these estimates and empirical measurements range from small (mean relative error = 0.6% for *P. cinereus* volume) to modest (4.2% *P. cinereus* SA, 8.6% *E. longicauda* volume, 9.6% *E. longicauda* SA:V), raising the prospect that some interspecific differences in the allometry of body dimensions could be functionally consequential. We compared allometric slopes between species to investigate this possibility, but found no differences in the scaling of SA or SA:V (Table S3). This shared allometry of SA is consistent with Whitford and Hutchison (1967), even despite broader apparent differences in gestalt body types (small vs. large vs. elongate) in our dataset. The only significant interspecific difference in our dataset was in volume allometry between *P. cinereus* and *P. glutinosus*. The difference in slope between these species is subtle (Table 1), and the significance of this comparison is likely attributable to the extremely low residual variance in our allometric models (volume $R^2 > 0.99$ for each species). Together, these results suggest that differences between species in the allometry of body dimensions do exist, but are small in magnitude and largely restricted to the most extreme comparisons. That is, very large and very small species do show some differences in allometry, but rates of change in body dimensions with size are otherwise largely consistent and conserved across most temperate plethodontids. For this reason, in future studies employing allometry-based estimates of SA, volume, and SA:V in temperate taxa, species-specific models are not necessary and a general model for temperate Plethodontidae should suffice. Further research in

Neotropical plethodontids, which vary more broadly in both body size and shape, is necessary to determine if these generalities hold across the entire Plethodontidae.

Previous allometric estimation methods

We found Whitford and Hutchison's (1967) allometric models to systematically underestimate SA (Fig. 3, Table S2). As previously reported by Whitford and Hutchison (1967), their models for the Plethodontidae and all Urodeles were statistically equivalent. Per Deming regressions, neither accurately estimated SA, with a mean relative difference from empirical measurements of 25.2% and 31.5% for the plethodontid and Urodele models, respectively (Fig. S4). Estimation error for the Urodele model decreased slightly with body mass, but this trend was not significant, and estimates remained erroneous across all body sizes (Fig. S2). These results suggest the empirical method (skin peeling and tracing) used to validate the established Whitford and Hutchison (1967) models is biased and inaccurate, and/or the dataset used to train their models is too biased to be generalizable to all Plethodontidae or salamanders more broadly. While relative differences in SA compared using the Whitford and Hutchison (1967) method are still valid, the absolute SA estimates produced using this method are flawed. Accordingly, we found the Whitford and Hutchison (1967) Urodele model to be substantially less accurate and statistically distinct from our general SA model (Fig. 3A), which can result in biased estimates of physiological rates (Fig. 4). We therefore recommend that future studies employing allometric techniques to estimate SA in plethodontid salamanders use our general SA model instead of either Whitford and Hutchison (1967) model.

Previous geometric estimation methods

The geometric estimates of Baken et al. (2020) systematically underestimated all body dimensions (Fig. S3, Table S2). Geometric estimates for SA, volume, and SA:V differed significantly from empirical measurements by a mean relative difference of 33.7%, 26.5%, and 9.2%, respectively. These estimates were significantly different from all our allometric estimates when compared across the entire dataset (Fig. 3B, 3C; Table S4), and we found Baken et al. (2020) and Whitford and Hutchison (1967) estimates for SA to be statistically equivalent. When compared across a subset of our data including a narrower range of body size, our estimates still differed from Baken et al. (2020) estimates for SA and volume, however SA:V estimates were equivalent. This improved performance appears to be due to variable estimation error across body sizes. Baken et al. (2020) estimates particularly underestimate SA, and this bias is most pronounced in small individuals (Fig. S5A). SA estimates following Baken et al. (2020) ignore both limbs and surface details such as costal grooves, whose scaling with body size likely accounts for higher measurement error in small individuals (Erica Baken, personal communication). While this method inaccurately estimates SA and volume independently, it offers accurate estimates of SA:V — the phenotype for which this method was developed — for salamanders larger than 0.22 g. As such, we suggest the Baken et al. (2020) method is a reliable option for estimating SA:V in most cases, excluding extremely small animals.

Relevance of estimation methods to future studies

The allometric approach presented here and geometric approach presented by Baken et al. (2020) offer two useful methods for estimating body dimensions in plethodontid salamanders, each with its own strengths and weaknesses. Critically, the Baken et al. (2020) method provides

accurate estimates of SA:V — though not SA or volume individually — and our allometric equations offer accurate estimates for all three traits. Perhaps the most appealing benefit of the allometric approach is its ease of implementation. To calculate body dimensions, this method requires only a body mass measurement, which is easily obtained from both living organisms and preserved specimens. In contrast, the multiple linear measurements needed for Baken et al. (2020) estimates require substantially more effort to obtain, and are difficult to measure on living, moving salamanders without considerable measurement error. Where the Baken et al. (2020) method excels, however, is in capturing natural, individual-level variation in SA:V estimates independent of body mass. This variance is highly useful when statistically investigating the relationship between SA:V and other phenotypes including physiology, behavior, and other morphological traits. However, this variance is lost through allometric estimation, in which the estimates are deterministically a function of body mass. As a result, allometric body dimension estimates perfectly correlate with mass at a log scale and behave statistically equivalently to mass when investigating the relationship between either trait and other phenotypes.

The tradeoffs inherent in different estimation methods means each may be better suited to specific research needs. When accurate estimates of body dimensions are a top priority, we suggest future research use our allometric equations, whose accuracy is validated by high fidelity empirical measurements. This approach will best apply when estimating cutaneous (SA-specific) transport rates during respiration or desiccation (e.g., Spotila 1972, Ultsch 1974), or when SA estimates are required as a part of physiological or biophysical calculations, such as when estimating cutaneous resistances (e.g., Riddell et al. 2017). Given the bias that inaccurate models can introduce into these types of estimates (e.g., Fig. 4), the need for accurate allometric

estimators is clear. For studies more focused on comparative morphology, such as the evolution of body dimensions or their correlation with other variables, we recommend researchers use the Baken et al. (2020) method for its superior accommodation of natural variance in these phenotypes. To our knowledge, Baken et al. (2020) is itself the only such study to pursue this goal to date, though similar types of questions previously focused on body mass (e.g., Adams and Church 2011) could be easily revisited and reassessed by examining other body dimensions. Though absolute SA and volume estimates produced with this method will be biased, comparisons between them will remain valid and reliably capture natural variation in these traits.

Body dimensions including surface area, volume, and SA:V are physiologically and ecologically important traits that need not be prohibitively difficult to estimate and study. By producing reliable estimates presented and contrasted here, future studies will be equipped to pursue compelling research questions in plethodontid physiological ecology and evolution. Indeed, we encourage future efforts to produce accurate allometric estimators of body dimensions in other amphibian taxa. Even in anurans and caudates with lungs, transport across the body surface is an important physiological process (Whitford and Hutchison 1965; Hutchison et al. 1968), making body dimensions ecologically important traits across taxa. Given the reliability of CT scans in measuring these dimensions, and the wide availability of museum specimens to measure, new estimators should be relatively easy to produce in any number of target groups. Developing both allometric and geometric estimators of body dimensions in other taxa will thus expand the methodological toolkit available to amphibian researchers to greatly facilitate future hypothesis testing in the morphology and physiology of the Amphibia.

Acknowledgments

We thank E. Baken for helpful discussions on estimation techniques. We also thank C. Dillman and C. Dardia of the Cornell University Museum of Vertebrates for specimen loans and permissions, T. Porri of the Cornell BRC Imaging Core Facility for assistance with CT scans, A. Voehl for help with scan processing, L. Johnson of the Cornell Statistical Consulting Unit for assistance with linear models and analyses, and two anonymous reviewers for helpful comments that improved the quality of the manuscript. This work was funded by a Herpetologists' League EE Williams Award in Physiology to BBJ. The Skyscan 1276 micro-CT used in this study was purchased using an NIH OSIP S10 Instrumentation Grant to the Cornell Institute of Biotechnology (NIH S10OD025049). The authors have no conflicts of interest to declare.

REFERENCES

Adams, D.C., and J.O. Church. 2011. The evolution of large-scale body size clines in *Plethodon* salamanders: Evidence of heat-balance or species-specific artifact? Ecography 34:1067–1075. DOI: https://doi.org/10.1111/j.1600-0587.2011.06911.x

Baken, E.K., L.E. Mellenthin, and D.C. Adams. 2020. Macroevolution of desiccation-related morphology in plethodontid salamanders as inferred from a novel surface area to volume ratio estimation approach. Evolution 74:476–486. DOI: https://doi.org/10.1111/evo.13898

Beckenbach, A.T. 1975. Influences of body size and temperature on the critical oxygen tension of some plethodontid salamanders. Physiological Zoology 48:338–347.

Feder, M.E. 1976. Lunglessness, body size, and metabolic rate in salamanders. Physiological Zoology 49:398–406.

Feder, M.E. 1983. Integrating the ecology and physiology of plethodontid salamanders. Herpetologica 39:291–310.

Feder, M.E. 1988. Exercising with and without lungs II: Experimental elimination of pulmonary and buccopharyngeal gas exchange in individual salamanders (*Ambystoma tigrinum*). Journal of Experimental Biology 138:487–497.

Feder, M.E., and W.W. Burggren. 1985. Cutaneous gas exchange in vertebrates: Design, patterns, control and implications. Biological Reviews of the Cambridge Philosophical Society 60:1–45. DOI: https://doi.org/10.1111/j.1469-185X.1985.tb00416.x

Feder, M.E., R.J. Full, and J. Piiper. 1988. Elimination kinetics of acetylene and Freon 22 in resting and active lungless salamanders. Respiration Physiology 72:229–240.

Feder, M.E., and P.L. Londos. 1984. Hydric constraints upon foraging in a terrestrial salamander, *Desmognathus ochrophaeus* (Amphibia: Plethodontidae). Oecologia 64:413–418.

Houck, M.A., and E.D. Bellis. 1972. Comparative tolerance to desiccation in the salamanders *Desmognathus f . fuscus* and *Desmognathus o. ochrophaeus*. Journal of Herpetology 6:209–215.

Hutchison, V.H., W.G. Whitford, and M. Kohl. 1968. Relation of body size and surface area to gas exchange in anurans. Physiological Zoology 41:65–85.

Johnson, B.B., J.B. Searle, and J.P. Sparks. 2021. Genome size influences adaptive plasticity of water loss, but not metabolic rates, in lungless salamanders. Journal of Experimental Biology 224:jeb242196. DOI: https://doi.org/10.1242/jeb.242196

Lenth, R. 2018. emmeans: Estimated marginal means, aka least-squares means. R package version 1.1.

Linnet, K. 1993. Evaluation of regression procedures for methods comparison studies. Clinical Chemistry 39:424–432.

Littleford, R.A., W.F. Keller, and N.E. Phillips. 1947. Studies on the vital limits of water loss in the Plethodont salamanders. Ecology 28:440–447.

Metscher, B.D. 2009. MicroCT for comparative morphology: simple staining methods allow high-contrast 3D imaging of diverse non-mineralized animal tissues. BMC Physiology 9. DOI: https://doi.org/10.1186/1472-6793-9-11

Okie, J.G. 2013. General models for the spectra of surface area scaling strategies of cells and organisms: fractality, geometric dissimilitude, and internalization. The American Naturalist 181:421–439. DOI: https://doi.org/10.1086/669150

Peterman, W.E., J.L. Locke, and R.D. Semlitsch. 2013. Spatial and temporal patterns of water loss in heterogeneous landscapes: Using plaster models as amphibian analogues. Canadian Journal of Zoology 91:135–140.

Piiper, J., R.N. Gatz, and E.C. Crawford Jr. 1976. Gas transport characteristics in an exclusively skin-breathing salamander, *Desmognathus fuscus* (Plethodontidae). Pp. 339–356 in Respiration of Amphibious Vertebrates (G.M. Hughes, ed.). Academic Press.

R Core Team. 2020. R: A language and environment for statistical computing.

Riddell, E.A., E.K. Apanovitch, J.P. Odom, and M.W. Sears. 2017. Physical calculations of resistance to water loss improve predictions of species range models. Ecological Monographs 87:21–33. DOI: https://doi.org/10.1002/ecm.1240

Riddell, E.A., J. Mcphail, J.D. Damm, and M.W. Sears. 2018a. Trade-offs between water loss and gas exchange influence habitat suitability of a woodland salamander. Functional Ecology 32:916–925. DOI: https://doi.org/10.1111/1365-2435.13030

Riddell, E.A., J.P. Odom, J.D. Damm, and M.W. Sears. 2018b. Plasticity reveals hidden resistance to extinction under climate change in the global hotspot of salamander diversity. Science Advances 4:eaar5471.

Spight, T.M. 1968. The water economy of salamanders: evaporative water loss. Physiological Zoology 41:195–203.

Spotila, J.R. 1972. Role of temperature and water in the ecology of lungless salamanders. Ecological Monographs 42:95–125.

Toledo, R.C., and C. Jared. 1993. Cutaneous adaptations to water balance in amphibians. Comparative Biochemistry & Physiology 105A:593–608.

Ultsch, G.R. 1973. A theoretical and experimental investigation of the relationships between metabolic rate, body size, and oxygen exchange capacity. Respiration Physiology 18:143–160.

Ultsch, G.R. 1974. Gas exchange and metabolism in the Sirenidae (Amphibia: Caudata) I. Oxygen consumption of submerged sirenids as a function of body size and respiratory surface area. Comparative Biochemistrty & Physiology Part A Physiol. 47:485–498.

Whitford, W.G., and V.H. Hutchison. 1965. Gas exchange in salamanders. Physiological Zoology 38:228–242.

Whitford, W.G., and V.H. Hutchison. 1967. Body size and metabolic rate in salamanders. Physiological Zoology 40:127–133.

Table 1. General and species-specific allometric models for plethodontid surface area (mm^2), volume (mm^3) and SA:V (mm^2 mm^{-3}) obtained from 46 individuals of three plethodontid species. Estimates for body dimensions can be calculated using these models and measured body mass (g).

Species	***n***	**Surface area (mm^2)**	**Volume (mm^3)**	**SA:V (mm^2 mm^{-3})**
All	46	log SA = 7.115 + 0.678 * log mass	log vol = 6.924 + 1.018 * log mass	log SA:V = 0.192 - 0.341 * log mass
E. longicauda	14	log SA = 7.136 + 0.674 * log mass	log vol = 6.843 + 1.014 * log mass	log SA:V = 0.293 - 0.340 * log mass
P. cinereus	18	log SA = 7.033 + 0.631 * log mass	log vol = 6.879 + 0.973 * log mass	log SA:V = 0.154 - 0.342 * log mass
P. glutinosus	14	log SA = 7.142 + 0.682 * log mass	log vol = 6.997 + 1.036 * log mass	log SA:V = 0.145 - 0.354 * log mass

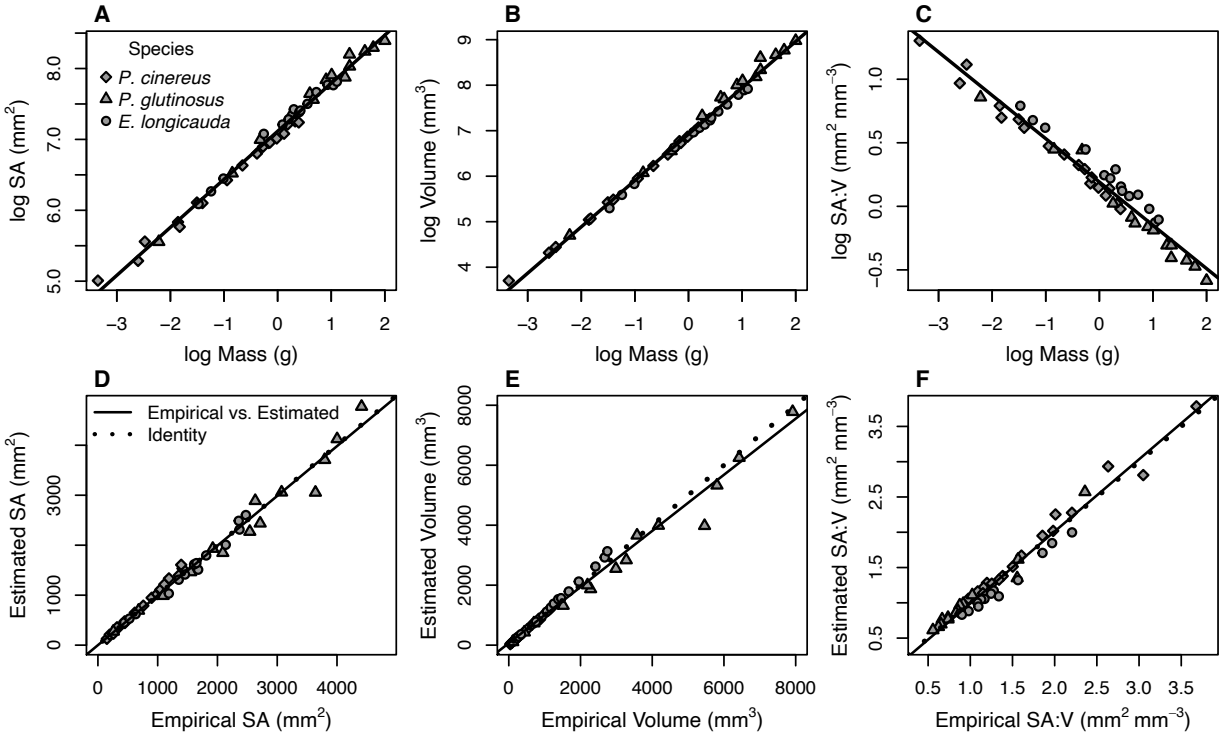

Figure 1. Performance of allometric estimates of body dimensions for three species of plethodontid salamanders. General regressions for SA (A), volume (B), and SA:V (C) showed minimal variance across pooled species. Comparisons of these general model estimates with empirical measurements (D-F) generated a 1:1 slope for all three dimensions. Intercepts were equivalent to zero for SA (E) and SA:V (F). The intercept for volume (E) was statistically distinct from zero but remained highly similar.

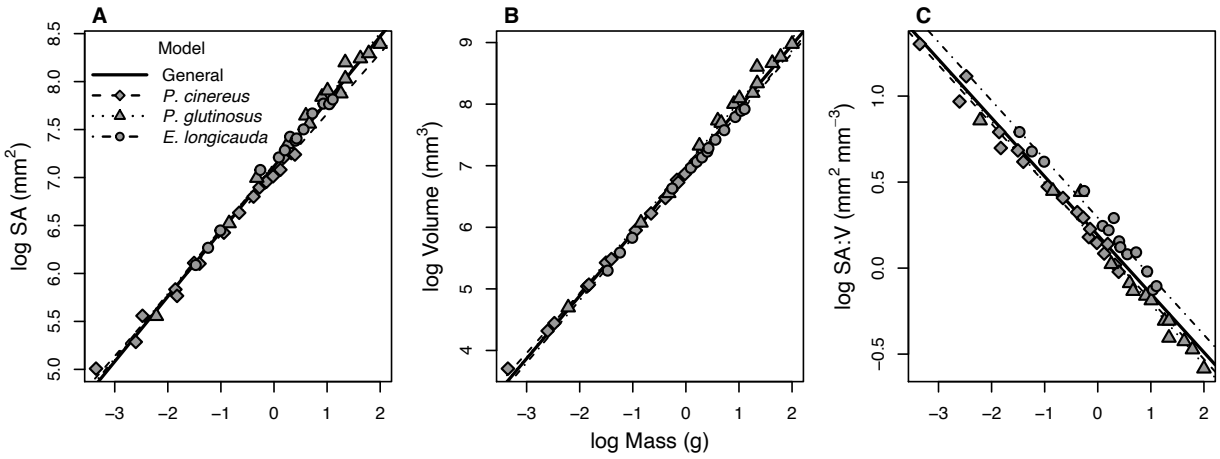

Figure 2. Comparisons between three allometric models fit for individual plethodontid salamander species. Species-specific model plus general model slopes for SA (A), volume (B), and SA:V (C) were highly similar. All species-specific slopes were statistically equivalent for SA and SA:V. Although *P. cinereus* and *P. glutinosus* slopes differed statistically for volume, they remained highly similar and all other volume comparisons were statistically equivalent.

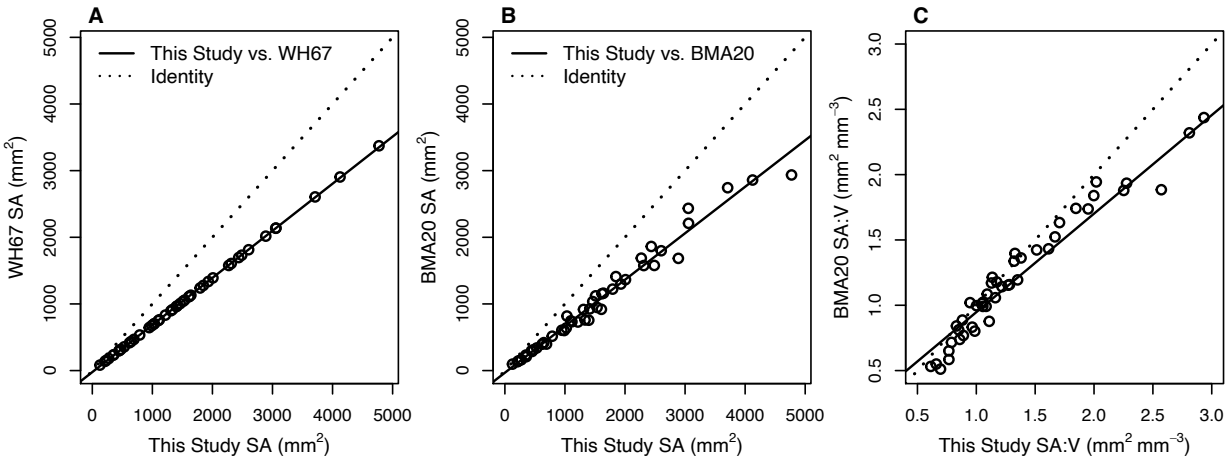

Figure 3. Comparisons between body dimension estimates for plethodontid salamanders obtained in this study and estimates from Whitford and Hutchison (1967) ("WH67") and Baken et al. (2020) ("BMA20"). SA estimates following Whitford and Hutchison (1967) (A) were smaller than our estimates, as were SA estimates following Baken et al. (2020) (B). SA:V estimates following Baken et al. (2020) were lower than our estimates for smaller (high SA:V) individuals (C), but were statistically comparable for body masses greater than 0.22 g (SA:V < 1.99).

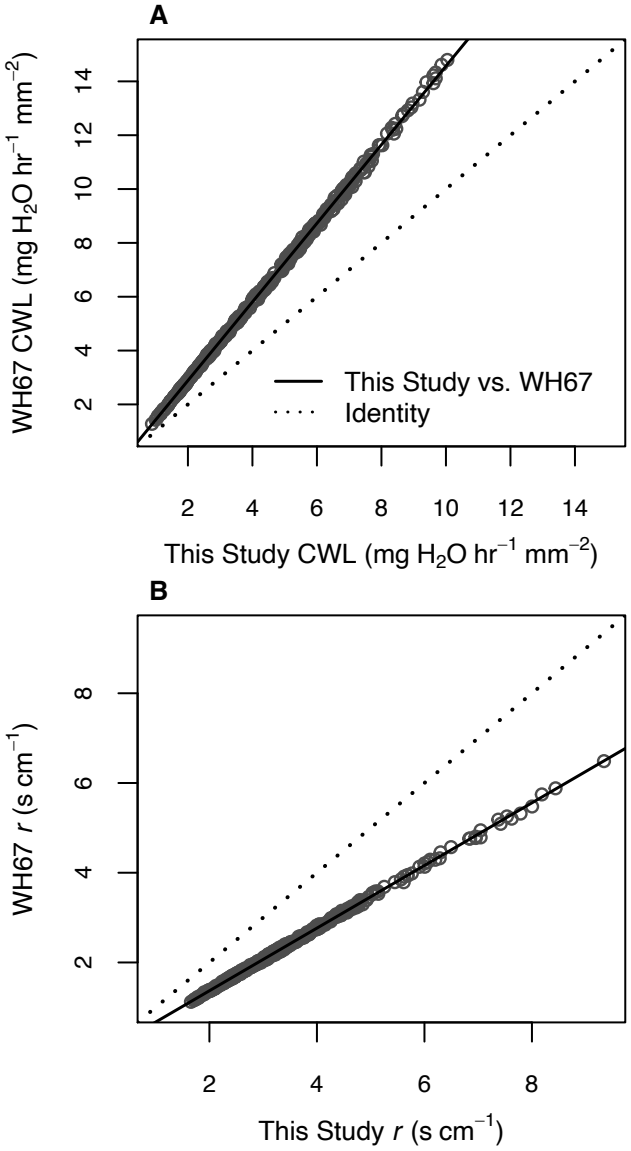

Figure 4. Comparisons between estimates of cutaneous water loss (CWL) (A) and total resistance to water loss (*r*) (B) from physiological experiments on plethodontid salamanders using SA estimates following Whitford and Hutchison (1967) ("WH67") or this study. Incorrectly estimated SA can lead to biased estimates of physiological rates, including overestimation of CWL (A) and underestimation of *r* (B).

CHAPTER THREE

BIOLOGICAL SIZE AS A PREDICTOR OF PHYSIOLOGICAL PERFORMANCE AND EVOLUTION: EVIDENCE FROM LUNGLESS SALAMANDERS

Research in collaboration with: T. Ryan Gregory[1], Jeremy B. Searle[2¶], and Jed P. Sparks[2¶]

[1]Department of Integrative Biology, University of Guelph, Guelph, ON N1G 2W1, Canada

[2]Department of Ecology & Evolutionary Biology, Cornell University, Ithaca, NY 14850, USA

[¶]Contributed equally

Abstract

Biological size is an integrative but little-studied phenotype conceptualized as the interaction between body size and cell size[1]. Correlations between genome size and cell size mean that genome size variation ultimately determines biological size such that larger genomes make organisms biologically smaller at a given body size. Though some studies have hypothesized that biological size is relevant to structural complexity and physiological performance in animals[1–3], no work has tested such hypotheses. We formally defined biological size as the ratio of body volume to mean cell volume of an individual, and estimated two proxy biological size indices (BSIs) to conduct the first formal tests of the relationship between biological size and animal physiology using eight species of Nearctic lungless salamanders. Whether defined as the ratio of body mass to genome size (BSI_1: g pg^{-1}) or body length to the square root of genome size (BSI_2: cm $pg^{-0.5}$), both proxies predicted metabolic and water loss rates at the individual level, and across species for some phenotypes. Critically, BSI_2 better predicted water loss physiology than did body mass, a widely appreciated phenotype in ecological physiology. Our findings suggest that for some phenotypes in some species, biological size may be a more relevant predictor of physiological performance than either body size or genome size alone. This result highlights a need to survey the taxa, physical sizes, and phenotypes to which biological size is most functionally relevant to better understand its prevalence and mechanisms in organizing organismal form and function.

Results and Discussion

Organismal function depends on the integration of traits across multiple levels of biological organization. In the Metazoa, this includes complex interactions between traits from the cellular to the organismal level, as cells both coordinate and contribute individually to overall organismal performance[4]. Individual cell function is strongly determined by a fundamental phenotype – cell size. A given cell's size determines its surface area-to-volume ratio, which influences the transport of energy and materials across the cell membrane[5]. While the effects of cell size on cellular physiology are clear, we understand little about how cell size variation influences whole-organism physiological performance, or its potential downstream effects on fitness and adaptation[6].

In animals, how cell size influences gross performance depends on variation in another fundamental trait – body size – which dictates the absolute energy requirements of the individual[7]. A given body size limits how many cells of a given size can fit within the available space of the body, such that differences in cell size can profoundly impact the development and structural complexity of tissues and organs[8], and may alter the physiological performance of the individual as cellular physiology changes with cell size. This interaction between cell size and body size is the foundation of a more conceptually elusive trait – biological size[1]. Here, we formalize the definition of biological size – an understudied but re-emerging concept in biodiversity research – as the ratio of body volume to mean cell volume. We introduce novel metrics to quantify biological size and present the first formal test of its functional relevance to animal physiology using eight species of Nearctic lungless salamanders (Urodela: Plethodontidae) as a model. Using linear and evolutionary regressions, we demonstrate that biological size is a functionally consequential trait underlying organismal performance and its

evolution in our focal species. Specifically, biological size strongly predicts water loss physiology in this group, both at the individual and species level. While the mechanisms underlying this relationship are unknown, this work suggests biological size may be relevant to performance phenotypes in taxa beyond our focal species, highlighting a need to study the contribution of biological size to the evolution of organismal morphology and performance.

Biological size: conceptual background

The concept of biological size was introduced by Hanken and Wake[1], who noted that the influence of cell size on animal metabolism and development complicates comparisons of the effects of body size when species differ in cell size. Literature on biological size is extremely limited[1–3], but by various descriptions, biological size is proportional to body (or physical) size and inversely proportional to cell size. That is, organisms of a given physical size have a smaller biological size when they have relatively larger cells. Strong (and likely causative[9]) covariation between cell size and genome size (C-value) across eukaryotes[10] means it is genome size that ultimately determines the biological size of animals of a given physical size[2]. C-value has a known impact on organismal physiology including developmental[11–13] and metabolic rates[14] in animals and photosynthetic metabolism in plants[15,16], and its influence on morphology has been considered alongside body size variation in amphibians[3,11,17] and insects[18]. Despite investigations into the biological consequences of extremely small bodies[1,18] and extremely large genomes[6,10,19], exceedingly little research has focused explicitly on the effects of biological size on organismal performance and evolution.

Descriptions of biological size remain largely conceptual, and the mechanisms by which biological size influences organismal physiology are unexplored. Though Hanken and Wake[1] did

not specify the relationship between biological size and metabolism, the implication is that variation in cell-level physiology can scale to influence performance at the level of the whole organism. Small cells have smaller mass-specific metabolic rates than larger cells[20], presumably due at least in part to limits on transport rates imposed by surface area-to-volume ratios (SA:V)[5]. Theory predicts cell size variation to influence the allometry of metabolic rates across taxa[21], and this pattern has been observed empirically in ants[22], birds[23], and geckos[24]. Whether this relationship is due simply to cellular SA:V is unclear, and may involve variation in other factors including cell density[25], organellar interactions[26], and cell membrane composition[27], among others. Whatever its underlying mechanism(s), biological size as a trait captures the interaction between genome-, cell-, and body size effects on whole-organism morphology and physiology. In some taxa, biological size may be a more appropriate measure than physical size when considering the phenotypic consequences of genome size evolution[2], yet beyond its relevance to the evolution of miniaturized body plans[1,2] the functional consequences of variation in biological size are almost entirely unexplored. Authors have speculated about the potential importance of this trait to metabolic physiology[1,2], but this relationship remains untested until now.

New definitions of biological size

We estimated biological size in the lungless salamanders, an excellent system in which to test for its functional consequences. Genome size varies widely in the Plethodontidae[28], and is known to influence morphological complexity[17], development[12,13], and water loss physiology[29] in this group. Body mass and C-value are not colinear in our sample (p=0.936), enabling us to test for their integrated effect via biological size. Here we establish novel biological size indices (BSI) to quantify biological size and test its relationship with metabolic and water loss

physiology in this group. Integrating the multiple descriptions of biological size in the literature, we formally define it as the ratio of body volume to mean cell volume of an individual organism (μm^3 μm^{-3}). Because body volume is difficult to estimate in most taxa, and because estimates of cell volume are less common than genome size, we estimated a novel proxy BSI, defined as the ratio of body mass and C-value (BSI_1 ; g pg^{-1}), using body mass measurements and analysis of blood smears taken from lungless salamanders used in the study of Johnson et al.[29]. We also measured the pre-existing BSI proxy introduced by Decena-Segarra et al.[2] (BSI_2; mm $pg^{-0.5}$), which approximates the number of cells that can be aligned along the body length of an individual (based on the square root of the nuclear area based in genome size estimation). In this way we are able to compare two distinct proxies for biological size. Using our proxy, biological size varies by an order of magnitude across our eight species of salamander (BSI_1: 0.014-0.317 g pg^{-1}), with a larger coefficient of variation (CV = 0.903) than either mass (0.778) or genome size (0.349), suggesting ample natural variation necessary to test for the functional consequences of biological size. Our proxy well approximates BSI_2 at the log scale (log-log R^2=0.809), offering substantially increased variation over the previously-described metric (BSI_2: 5.384-14.632 mm $pg^{-0.5}$; CV = 0.251). Mass correlated more strongly with volume in our focal taxa (r = 0.999) than did snout-vent length (r = 0.924), suggesting BSI_1 offers a more faithful proxy for true biological size in our sample.

Biological size predicts physiological performance

Prior work indicates that biological size evolves adaptively in neotropical lungless salamanders, with evolutionary regressions between body size and cell size suggestive of selection for an optimal cell size at a given physical size[2]. While the target of selection in this

relationship remains unclear, it highlights the potential that biological size is functionally relevant to a number of morphological, developmental, and physiological traits in the Plethodontidae. We tested the hypothesis that biological size predicts metabolic and water loss physiology in eight Nearctic plethodontids by running linear mixed models and evolutionary regressions between each of the two BSI proxies and six physiological response variables measured by Johnson et al.[29]: gross respiratory metabolic rate (or respiration: Resp; mg CO_2 h^{-1}), specific metabolic rate (sResp; mg CO_2 h^{-1} g^{-1}), gross evaporative water loss rate (EWL; mg H_2O h^{-1}), specific water loss (sEWL; mg H_2O h^{-1} g^{-1}), cutaneous water loss (CWL; mg H_2O h^{-1} mm^{-2}), and total resistance to water loss (r, s cm^{-1}). We additionally conducted evolutionary regressions between body mass and the BSI proxies, using residuals from these regressions – a metric of deviation from an evolutionarily "expected" biological size – as predictors in linear regressions. Lastly, we regressed all responses against body mass to compare model performance against BSIs.

Both BSI proxies significantly predicted all physiological responses across our full dataset (BSI_1 $P < 0.001$; BSI_2 $P = <0.001$-0.011) (Fig. 1), as did body mass ($P < 0.001$). Residual variation from expected BSI_1 similarly predicted all responses ($P = <0.001$-0.001), however residuals for BSI_2 predicted only gross respiration ($P = 0.005$) and EWL ($P = 0.006$) (Table S1). These results suggest substantial functional relevance of biological size to whole-organism physiology. That is, cell and body size contribute jointly to multiple whole-organism performance phenotypes across species of different physical size. Though we cannot determine a mechanism by which biological size affects physiological performance from our dataset, the consistent relationship between both BSI proxies and physiology suggests that some form of influence does exist. While the effects of genome size variation have been explored before, this

result marks the first formal demonstration that the interaction between cell size and body size – biological size *per se* – has functional consequences at the individual level.

Predictive power of BSI

In salamanders, genome size variation (independent of its interaction with body mass) consistently predicts phenotypes associated with development[12,13,30] but not respiratory metabolism,[29,31] and the morphological consequences of cell size variation are most apparent in miniaturized species.[1,17] Accordingly, we hypothesized that the effect strength of biological size on physiology is likely to vary with physical size and that this strength varies between physiological responses. To test these hypotheses, we divided our dataset into five subsets based on body mass. We calculated 20% quantiles for body mass across our dataset and regressed all six physiological responses against our BSIs and mass in each quantile subset. For each predictor, we estimated predictive accuracy as mean squared error (MSE, the squared difference between observed data and model predictions), interpreting higher predictive accuracy as reflective of stronger effective control over the response. Similarly, we estimated predictive power as semi-partial R^2 (pR^2, the proportion of variation in the response explained by the predictor)[32], with greater power reflective of stronger control over the response. Lastly, we estimated effect size as beta weights (standardized regression coefficients demonstrating the effect size in standard deviations enacted on the response by the predictor), with larger values indicative of greater functional control over the response. To characterize a holistic, overall effect of biological size on physiology, we pooled each support metric for all responses. To test whether biological size better predicts overall physiology at a given physical size range, these pooled support values were compared between quantiles using estimated marginal means. For

each individual response, we regressed support metrics across quantiles, testing for a sloped change in support with increasing body size. To test whether biological size better predicts any individual response, we compared individual support metrics among responses at each quantile using estimated marginal means.

BSI_2 was the best predictor of water loss physiology across the full dataset (Fig. 1D-F). Specifically, all water loss rates (EWL, sEWL, and CWL) were best explained by BSI_2 per MSE estimates (mean MSE = 2.695), however resistance to water loss was best explained by mass (MSE = 0.917) (Table S1). Metabolic physiology did not share a consistent best predictor, with gross respiration best predicted by residuals for BSI_2 (MSE = 1.485) and specific respiration by BSI_1 (MSE = 2.301). Residuals for BSI_1 best explained variance in all responses (pR^2 = 0.279-0.448) except for gross respiration, which was best explained by mass (pR^2 = 0.638). BSI_1 residuals also produced the largest effect size in all physiological responses ($|\beta|$ = 0.831-2.752). Within quantiles, some predictors occasionally differed in their overall predictive power, but we found no apparent general trend across body sizes (Table S3). When comparing between mass quantiles, all predictors performed holistically equally well across quantiles according to MSE (pairwise P = 0.834-1.000; Fig. 2A), pR^2 (P = 0.463-1.000; Fig. 2B), and beta weights (P = 0.529-1.000) (Table S4). When analyzing responses individually, BSI_2 and residuals for both proxies better predicted EWL at lower body sizes, whereas mass improved prediction of EWL with increasing body size (Fig. 3A). Mass also better predicted sEWL at larger quantiles, as did BSI_2 (Fig. 3B). No other predictors showed any change in MSE (P = 0.070-0.835), pR^2 (P = 0.203-0.966), or beta weights (P = 0.141-0.966) across quantiles (Table S5).

Relevance of biological size to physiology

Biological size is a compelling and integrative concept that elegantly links variation across levels of biological organization to variation in organismal form and function. However, despite testable hypotheses about its relevance to animal morphology and physiology[1–3], biological size has received minimal direct attention in biodiversity research. Here, we offer the first formal tests of this phenotype's relation to physiological performance in a defined group of vertebrates, and our results make clear that biological size can strongly influence multiple organismal performance phenotypes. Whatever the mechanism, biological size demonstrates a clear relationship with each of our measured physiological variables, including a greater influence than body mass over a subset of responses in individuals and taxa of different physical size. This result casts new light upon an extensive literature that has focused broadly on the physiological consequences of body size variation (e.g.[33–35]), and a smaller literature on the physiological consequences of genome size diversity (e.g.[16,36]). Physical size (measured as body mass) is a commonly investigated predictor in biodiversity research that demonstrates clear covariation with a broad range of physiological responses (e.g.[33,34,37,38]). However, we found that neither body mass nor any measure of BSI is the best predictor of all responses (Table S3), suggesting that no one trait is a universally best predictor of organismal physiology. Rather, for some phenotypes in some taxa, the functional consequences of body size may be significantly modulated by variation in genome size (e.g.[29]), making their interactive effect via biological size a more functionally relevant predictor.

The clearest effect of biological size in our sample is on water loss. Specifically, we demonstrate that biological size (when defined as BSI_2; cm $pg^{-0.5}$) consistently predicts water loss rates better than body mass in lungless salamanders (Fig. 3; Table S1). BSI_2 repeatedly best

predicted EWL and sEWL across the full dataset and within subsets of body mass, and best predicted CWL in all cases but the largest quantile. In contrast, the remaining responses showed no clear trend, with inconsistent best predictors of model accuracy, physiological variance, and effect sizes across quantiles (Table S1). The generally high BSI_2 model performance for water loss is consistent with our hypothesis that biological size influences different physiological phenotypes to varying degrees, and suggests a stronger relationship with water loss physiology than respiratory physiology in our focal species. Selection on respiratory metabolism appears to be generally low in the Plethodontidae[39,40], whereas water balance is fundamental to lungless salamander activity[41,42] and selection to avoid desiccation is high[43,44]. Though the mechanistic role biological size plays in these selective processes is unknown, our results raise the possibility that biological size is an important driver of water loss physiology in this group. Previous work has found correlations between genome size and water loss in lungless salamanders[29], as well as with aquatic life-histories in this group[45]. Our results contribute to an emerging pattern that genome size variation is linked with water relations in some Plethodontidae, and may be mediated, at least in part, through biological size.

Our hypothesis that biological size should be most functionally relevant at small physical sizes was supported only by evaporative water loss data. BSI_2 and residuals for both BSIs all progressively improved their prediction of EWL from larger to smaller mass quantiles, whereas the performance of mass improved with increasing body size (Fig. 3A). No other responses (including pooled holistic performance) showed changes in their prediction across mass except for sEWL, which demonstrated conflicting results. Similar to gross EWL, mass best predicted sEWL at larger quantiles, however BSI_2 predictions also improved at larger quantiles (Fig. 3B). This discrepancy may reflect true differences in how biological size influences whole-organism

versus mass-specific water transport rates, for example larger genomes covary negatively with specific metabolic rates in some taxa[23,46]. Alternatively, a recent hypothesis by Glazier[47] posits that the strength of correlation between genome size and body size should be lower in larger organisms (whose physical size depends primarily on variation in cell count) than smaller organisms (whose physical size is more greatly influenced by cell size). By extension, the relative contribution of genome- and cell size to the overall effect of biological size may plausibly vary with physical size such that a given change in genome size could have minimal impact on the gross physiology of large organisms, but still influence physiological process at, for example, a per-gram level. Whether gross and specific physiological rates are impacted differently by biological size is a fascinating possibility, but is unconfirmed by most tests in our dataset. However, the consistently poor signal in our quantile comparisons is likely due to methodological effects. Particularly, our small sample size of six responses means that pairwise comparisons between predictors will have limited power to detect differences in their overall, holistic effects. Similarly, dividing our dataset into five subsets by body size also reduces our power to detect differences in predictive power between mass quantiles. These issues could be overcome in future experiments by sampling more taxa from a broader range of physical and biological sizes. With adequate taxonomic and phenotypic sampling, tests of biological size's effect on gross and specific physiological rates merits further attention.

In spite of sampling issues, the consistently high predictive power of biological size in water loss models suggests a strong influence over water loss physiology. We hypothesized that strong effects of BSI on a given physiological phenotype should result in greater stabilizing selection on the response across taxa, which should be evident as significant evolutionary correlations between variables. To test for such associations between biological size and

physiology across phylogeny, we conducted evolutionary regressions between BSIs or mass and all physiological responses. BSI_1 correlated with gross respiration ($P = 0.016$), EWL ($P = 0.001$), and sEWL ($P = 0.016$) (Fig. 1D-1F), whereas BSI_2 correlated only with EWL ($P = 0.022$) (Table S2). BSI_1 thus supports our hypothesis, however BSI_2 only partly so. Furthermore, BSI_1 also correlated with respiration rate despite its more modest predictive power at the individual level (Table S1), and mass correlated with most responses. These results may indicate that the relationship between predictive power and selection is not as clear as we hypothesized, or that the individual-level physical effects of biological size simply manifest in different selective pressures on different phenotypes when comparing among taxa. Regardless, our results demonstrate that for a number of physiological phenotypes biological size has functional consequences both at the individual level and for the evolution of organismal performance. BSI_2 itself evolves adaptively in neotropical lungless salamanders[2]. Further study would elucidate whether its evolution reflects adaptation to maintain particular physiological or morphological variation within proscribed bounds.

Our results confirm prior hypotheses about the functional relevance of biological size to organismal physiology. Specifically, biological size strongly predicts water loss physiology in lungless salamanders – a suite of critically important phenotypes in this group. This result, alongside the variation and effect sizes well explained by biological size in other phenotypes, make clear the potential that biological size could similarly underlie variation and adaptation in other physiological and morphological traits in multiple taxa. As such, future investigations of size effects in the biology of multicellular organisms should consider the joint effects of body and cell size as integrated through biological size. Taxonomic surveys of biological size will expand our understanding of its evolutionary history, and associational studies will reveal the

physical sizes and physiological, morphological, and life history phenotypes that are influenced by biological size. This research avenue will lay the groundwork for explicit hypothesis testing and experimental work to reveal the mechanisms by which this fundamental and integrative phenotype influences organismal form and function.

Detailed Methods

Species sampling

All animal procedures were approved by the Cornell University Institutional Animal Care and Use Committee (protocol # 2016-0081). Detailed experimental methods are described in[29]. Briefly, we collected 18 *Eurycea bislineata*, 7 *Eurycea longicauda*, 24 *Plethodon cinereus*, 12 *Plethodon dunni*, 20 *Plethodon glutinosus*, 12 *Plethodon larselli*, 19 *Plethodon vandykei*, and 14 *Plethodon vehiculum* from natural populations. We selected these species based on both their broad range in both physical size and genome size (using the median published genome size from the animal genome size database, www.genomesize.org), which do not covary in this sample ($P = 0.936$), making this an excellent model group in which to study biological size variation.

Experimental design

Animals were acclimated at either 10° or 15°C for a minimum of one week prior to inclusion in experimental trials, and were measured a minimum of four days after eating or a prior trial to ensure measurements were taken in a minimally-stressed, post-absorptive state. We conducted physiological experiments under a 2x2 factorial design testing temperature (10° and 15°C) x humidity (0.3 and 0.6 kPa vapor pressure deficit) effects on physiological performance.

Individuals were measured once at each treatment combination, requiring one week of acclimation when changed between temperatures. Due to occasional technical limitations and premature deaths in the laboratory, not all individuals were measured across all four treatments.

We measured physiological performance using flow-through respirometry. We used a Li-Cor LI-6400XT Portable Photosynthesis System (Li-Cor Biosciences, Lincoln, NE, USA), configured for the 6400-89 animal respiration chamber and using the 'Insect Rd' measurement configuration. We set the system temperature according to the experimental treatment, and maintained the treatment humidity within ± 0.015 kPa using Drierite scrubbers. Once the metabolic rate of the animal inside the measurement chamber reached a steady state, we measured CO_2 and H_2O content inside the chamber at ~40s intervals for 30min. We used these concentrations to calculate the gross metabolic rate (mg CO_2 h^{-1}), specific metabolic rate (mg CO_2 h^{-1} g^{-1}), gross evaporative water loss rate (mg H_2O h^{-1}), specific evaporative water loss rate (mg H_2O h^{-1} g^{-1}), cutaneous water loss rate (mg H_2O h^{-1} cm^{-2}), and total resistance to water loss (s cm^{-1}) at each measurement. For each response, we calculated the mean across 30min for use in downstream data analysis. For mass-specific responses, we measured body mass to the nearest 0.01g immediately prior to each experiment. We estimated surface area for CWL and resistance estimates following[48].

Genome and cell size estimates

Following experiments, we euthanized 57 individuals in a 3 g L^{-1} buffered solution of tricaine methanesulfonate (MS-222). Immediately following euthanasia, we clipped the end of the tail from each salamander and directly applied the severed ends of the tail to a glass microscope slide for a blood sample, which was smeared using a glass cover slip angled to avoid

cell shearing. We estimated genome sizes using Feulgen densitometry on stained blood smears following[49], using *Ambystoma jeffersonianum*, *Oncorhynchus mykiss*, and *Gallus gallus* as internal standards.

Biological size definition and estimators

We contrasted all previous descriptions of biological size[1–3], identifying their conceptual overlap to formalize its definition and develop new metrics for quantifying this phenotype. Given the interrelatedness of body size[1–3], body "space"[2], genome size[1,2], cell size[1–3], and cell number[2] in conceptualizing biological size, multiple different metrics are likely to adequately characterize its variation. We propose that the most biologically meaningful definition of biological size is the ratio of an individual organism's body volume to its mean cell volume. When using equivalent units for both cell and body volumes, this index yields a unitless "size" value that increases with body size and decreases with cell size, or otherwise yields a volume estimate to intuitively represent biological size (μm^3 μm^{-3}).

Given the difficulties of measuring both body and cell volume in most taxa, proxy metrics will likely be needed for most studies of biological size. Body mass is easily and widely measured, and covaries strongly with body volume[50], making mass an excellent proxy for volume. Similarly, the strong correlation between genome size and cell volume[51] and the prevalence of C-value estimates in the literature[28] make C-value another useful proxy in estimating biological size. To compare these proxies with true biological size, we estimated a proxy body size index (BSI) using the ratio of our body mass measurements taken prior to physiological experiments and our densitometric C-value estimates (BSI_1; g pg^{-1}). Similar to true biological size, consistent units used in this metric produce a unitless size value, or otherwise

result in an intuitive mass estimate to represent biological size. Finally, we compared our metric to that introduced by Decena-Segarra et al.[2] (BSI_2; mm $pg^{-0.5}$). This proxy substitutes snout-vent length (SVL) for volume in estimating body size, and employs a square root transformation of C-value to reflect the use of a linear proxy for body size, as the square root of the C-value should be proportional to the square root of the nuclear area measured from cells stained for Feulgen densitometry (Sean Rovito, personal communication). Such a transformation therefore approximates biological size as the number of cells that could be counted along the SVL measurement.

Datasets

We used two subsets of our physiological dataset to test the effects of biological size. First, we constructed a dataset of all individuals with new C-value and cell size estimates produced by Feulgen densitometry (small dataset: 57 individuals, 211 experimental trials). Second, we took our mean C-value estimate for each species and applied this mean to all individuals with physiological data (full dataset: 127 individuals, 409 experimental trials). Lastly, we calculated the per-species mean of all measured variables from our full dataset to use in evolutionary analyses (phylogenetic dataset: 8 species). The smaller dataset more accurately captures individual-level variation in biological size contributing to physiology, while the larger improves power with increased sample size. Because the vast majority of studies on the effects of genome size employ a species-level mean C-value estimate, use of this larger dataset is more reflective of common research practices.

Physical effects of biological size: linear models

We used our physiology and Feulgen densitometry measurements to test the effects of biological size on whole-organism physiology. We tested the relationship between biological size and physiological performance using linear mixed-effects models in R[52]. We modeled each of our physiological response variables as a function of biological size (the predictor variable) plus temperature and humidity (environmental variables). All models included a random effect for individual to account for repeated measurements across environmental treatments, and a random effect for species. Because we are interested in differences between morphological types and not between species *per se*, this parameter effectively controls for interspecific variance not attributable to biological size. For each response, we tested each BSI proxy individually following the same model structure. Because biological size encompasses variation in both physical and cell size, its explanatory power for physiology may be greater than that of mass alone. To compare BSI- and mass-related effects on physiology, we tested models using mass as the predictor following the same model structure as above. In all cases, we natural log-transformed all predictor and response variables.

Evolutionary effects of biological size: phylogenetic comparative methods

We conducted evolutionary regressions to test for effects of biological size on physiological performance across evolutionary history. While our linear models test for physical effects of biological size influencing physiology in individuals, they cannot account for phylogenetic history contributing to performance. To correct for this phylogenetic nonindependence, we used an eight-taxon phylogeny produced by[29] to fit Ornstein-Uhlenbeck (OU) models following[53] in the R package 'slouch' v2.1.4[54]. These regressions meet our

assumption of a potentially functional (adaptive) effect of biological size by modeling each response evolving toward an adaptive optimum that is determined by the predictor variable[53]. From our phylogenetic dataset, we regressed six physiological responses against each of our BSI metrics and mass, incorporating variances in both predictor and response variables to account for estimation error underlying species mean estimates. To test for model significance, we compared evolutionary models to a second set of null, intercept-only models lacking predictors. These models estimate the effect of phylogeny alone on the response variable, thus differences between full and intercept-only models are attributable to the effects of the predictor on the response. We tested the hypothesis that a given predictor underlies adaptation to the response by comparing model pairs using likelihood ratio tests and assessed model significance after correcting for multiple hypothesis tests using the false discovery rate (FDR) correction of[32] across all regressions using the R package 'qvalue' v2.20.0.

Effects of extreme biological size: residual models

We used a combination of evolutionary and linear models to test for effects of variation in biological size on individual-level physiological performance. Because biological size covaries with body size (physical size is in the numerator in true biological size and both BSI proxies), regressions between either predictor and a given response will be qualitatively similar. To account for this relationship, we constructed evolutionary models as above, regressing each BSI proxy against body mass (following log transformations). We then fit these models to our full dataset to predict BSIs for all individuals based on body mass. We estimated residuals from these regressions by subtracting model predictions from our BSI proxy estimates for each individual. We then used these regression residuals as predictors of physiological performance in

linear mixed models. These evolutionary regressions represent the evolutionarily "expected" biological size for a given physical size in our species sample, thus these residuals reflect the degree to which a given individual's biological size deviates from evolutionary expectations given its physical size. Modeling physiological responses as predicted by these residuals therefore tests the effect of this deviation on physiological performance. This approach subtly differs from our linear models testing the effects of absolute biological size, instead testing whether more vs. less extreme cases of biological size predict performance in our sample.

Explanatory strength of biological size

To characterize the phenotypic consequences of variation in biological size, we estimated regression coefficients and the proportion of variance in physiological performance that was explained by each BSI metric. To do this, we calculated semi-partial R^2 coefficients (pR^2) for the predictor parameter in each of our linear models[32]. This method accounts for covariance between the predictor and other model parameters in order to accurately estimate the proportion of variance in the response explained uniquely by the predictor of interest. We estimated pR^2 and beta weights (standardized regression coefficients) in the R package 'partR2' v0.9.1[32] using 500 bootstraps per pR^2 estimate. We further estimated the mean-squared error (MSE) of all models to characterize the quality of each predictor as an estimator for physiological performance. To test for differences in the explanatory strength of each predictor, we compared MSE, pR^2, and beta coefficients between predictor categories and compared estimated marginal means in the R package 'emmeans' v1.6.2[55], using a significance value of α=0.05 after a Tukey correction for multiple hypothesis tests. Here, we interpret these metrics as reflective of the strength of physical constraint exerted by each predictor over a given response, with lower MSE scores, larger pR^2

values, and larger magnitude beta weights reflective of stronger effective control over the response.

Physical size effects: mass quantiles

Because the functional importance of biological size may vary among groups, we repeated all analyses across data subsets binned by physical size. We took 20% quantiles of body mass from the full dataset and repeated analyses of all linear models across each quantile for a total of 180 models tested across all predictors, responses, and subsets. We employed an FDR correction[32] across all models to assess model significance at α=0.05 and test the hypothesis that a given variable predicts physiological performance across a given data subset. To test if different predictors outperform others at different physical sizes, we compared predictor performance across each mass quantile using estimated marginal means[55] (EMM), comparing EMMs for model MSE scores, pR^2, and beta weights between all quantile pairs. To test if each predictor performs better overall at different body sizes, we compared each predictor's set of MSE scores, pR^2, or beta weights for all responses between each pair of quantiles. By pooling all responses in this approach, these comparisons test for differences in the holistic performance of a given predictor with changing physical size. To test for body mass effects on each predictor-response combination individually, we regressed individual support metrics over the numerical vector of mass quantiles, testing for a regression slope different from m=0 as reflective of changing predictive power (and changing functional constraint) of the predictor with changes in physical size.

REFERENCES

1. Hanken, J., and Wake, D.B. (1993). Miniaturization of body size: Organismal consequences and evolutionary significance. Annu. Rev. Ecol. Syst. *24*, 501–519.

2. Decena-Segarra, L.P., Bizjak-Mali, L., Kladnik, A., Sessions, S.K., and Rovito, S.M. (2020). Miniaturization, genome size, and biological size in a diverse clade of salamanders. Am. Nat. *196*, 649–661.

3. Yeh, J. (2002). The effect of miniaturized body size on skeletal morphology in frogs. Evolution *56*, 628–641.

4. Niklas, K.J., and Newman, S.A. eds. (2016). Multicellularity: Origins and evolution (The MIT Press).

5. Okie, J.G. (2013). General models for the spectra of surface area scaling strategies of cells and organisms: Fractality, geometric dissimilitude, and internalization. Am. Nat. *181*, 421–439.

6. Levy, D.L., and Heald, R. (2016). Biological scaling problems and solutions in amphibians. Cold Spring Harb. Perspect. Biol. *8*, a019166.

7. West, G.B., Brown, J.H., and Enquist, B.J. (1997). A general model for the origin of allometric scaling laws in biology. Science *276*, 122–126.

8. Gregory, T.R. (2002). Genome size and developmental complexity. Genetica *115*, 131–146.

9. Gregory, T.R. (2001). Coincidence, coevolution, or causation? DNA content, cell size, and the C-value enigma. Biol. Rev. *76*, 65–101.

10. Elliott, T.A., and Gregory, T.R. (2015). What's in a genome? The C-value enigma and the evolution of eukaryotic genome content. Philos. Trans. R. Soc. B Biol. Sci. *370*, 20140331.

11. Womack, M.C., Metz, M.J., and Hoke, K.L. (2019). Larger genomes linked to slower development and loss of late-developing traits. Am. Nat. *194*, 854–864.

12. Sessions, S.K., and Larson, A. (1987). Developmental correlates of genome size in plethodontid salamanders and their implications for genome evolution. Evolution *41*, 1239–1251.

13. Jockusch, E.L. (1997). An evolutionary correlate of genome size change in plethodontid salamanders. Proc. R. Soc. London B *264*, 597–604.

14. Vinogradov, A.E. (1997). Nucleotypic effect in homeotherms: Body-mass independent resting metabolic rate of passerine birds is related to genome size. Evolution *51*, 220–225.

15. Roddy, A.B., Théroux-Rancourt, G., Abbo, T., Benedetti, J.W., Brodersen, C.R., Castro, M., Castro, S., Gilbride, A.B., Jensen, B., Jiang, G., et al. (2020). The scaling of genome size and cell size limits maximum rates of photosynthesis with implications for ecological strategies. Int. J. Plant Sci. *181*, 75–87.

16. Théroux-Rancourt, G., Roddy, A.B., Earles, J.M., Gilbert, M.E., Zwieniecki, M.A., Boyce, C.K., Tholen, D., McElrone, A.J., Simonin, K.A., and Brodersen, C.R. (2021). Maximum CO_2 diffusion inside leaves is limited by the scaling of cell size and genome size. Proc. R. Soc. B *288*, 20203145.

17. Roth, G., Blanke, J., and Wake, D.B. (1994). Cell size predicts morphological complexity in the brains of frogs and salamanders. Proc. Natl. Acad. Sci. U. S. A. *91*, 4796–4800.

18. Polilov, A.A. (2015). Small is beautiful: Features of the smallest insects and limits to miniaturization. Annu. Rev. Entomol. *60*, 103–121.

19. Dufresne, F., and Jeffery, N. (2011). A guided tour of large genome size in animals: What we know and where we are heading. Chrom. Res. *19*, 925–938.

20. Goniakowska, L. (1973). Metabolism, resistance to hypotonic solutions, and ultrastructure of erythrocytes of five amphibian species. Acta Biol. Cracoviensia, Ser. Zool. *16*, 114–134.

21. Kozłowski, J., Konarzewski, M., Gawelczyk, A.T., Kozlowski, J., Konarzewski, M., and Gawelczyk, A.T. (2003). Cell size as a link between noncoding DNA and metabolic rate scaling. Proc. Natl. Acad. Sci. U. S. A. *100*, 14080–14085.

22. Chown, S.L., Marais, E., Terblanche, J.S., Klok, C.J., Lighton, J.R.B., and Blackburn, T.M. (2007). Scaling of insect metabolic rate is inconsistent with the nutrient supply network model. Funct. Ecol. *21*, 282–290.

23. Gregory, T. (2002). A bird's-eye view of the C-value enigma: Genome size, cell size, and metabolic rate in the class Aves. Evolution *56*, 121–130.

24. Starostová, Z., Kubicka, L., Konarzewski, M., Kozłowski, J., Kratochvíl, L., Kubička, L., Konarzewski, M., Kozłowski, J., and Kratochvíl, L. (2009). Cell size but not genome size affects scaling of metabolic rate in eyelid geckos. Am. Nat. *174*, E100–E105.

25. Dill, K.A., Ghosh, K., and Schmit, J.D. (2011). Physical limits of cells and proteomes. Proc. Natl. Acad. Sci. U. S. A. *108*, 17876–17882.

26. Gordaliza-Alaguero, I., Cantó, C., and Zorzano, A. (2019). Metabolic implications of organelle-mitochondria communication. EMBO Rep. *20*, e47928.

27. Kai, L., and Kaldenhoff, R. (2014). A refined model of water and CO_2 membrane diffusion: Contribution of sterols and proteins. Sci. Rep. *4*, 6665.

28. Gregory, T.R. (2016). Animal Genome Size Database. http://www.genomesize.com.

29. Johnson, B.B., Searle, J.B., and Sparks, J.P. (2021). Genome size influences adaptive plasticity of water loss, but not metabolic rates, in lungless salamanders. J. Exp. Biol. *224*, jeb242196.

30. Litvinchuk, S.N., Rosanov, J.M., and Borkin, L.J. (2007). Correlations of geographic distribution and temperature of embryonic development with the nuclear DNA content in the Salamandridae. Genome *50*, 333–342.

31. Licht, L.E., and Lowcock, L.A. (1991). Genome size and metabolic rate in salamanders. Comp. Biochem. Physiol. Part B *100*, 83–92.

32. Stoffel, M.A., Nakagawa, S., and Schielzeth, H. (2021). partR2 : Partitioning R^2 in generalized linear mixed models. PeerJ *9*, e11414.

33. Gillooly, J.F., Brown, J.H., and West, G.B. (2001). Effects of size and temperature on metabolic rate. Science *293*, 2248–2252.

34. Peralta-Maraver, I., and Rezende, E.L. (2021). Heat tolerance in ectotherms scales predictably with body size. Nat. Clim. Change *11*, 58–63.

35. Peters, R.H. (1986). The ecological implications of body size (Cambridge University Press).

36. Gardner, J.D., Laurin, M., and Organ, C.L. (2020). The relationship between genome size and metabolic rate in extant vertebrates. Philos. Trans. R. Soc. B Biol. Sci. *375*, 20190146.

37. Callier, V., and Nijhout, H.F. (2011). Control of body size by oxygen supply reveals size-dependent and size-independent mechanisms of molting and metamorphosis. Proc. Natl. Acad. Sci. U. S. A. *108*, 14664–14669.

38. Ruhs, E.C., Martin, L.B., Downs, C.J., and Ruhs, E.C. (2020). The impacts of body mass on immune cell concentrations in birds. Proc. R. Soc. B *287*, 20200655.

39. Chong, R.A., and Mueller, R.L. (2013). Low metabolic rates in salamanders are correlated with weak selective constraints on mitochondrial genes. Evolution *67*, 894–899.

40. Kakehashi, R., and Kurabayashi, A. (2021). Patterns of natural selection on mitochondrial protein-coding genes in lungless salamanders: relaxed purifying selection and presence of positively selected codon sites in the family Plethodontidae. Int. J. Genomics *2021*, 6671300.

41. Spight, T.M. (1968). The water economy of salamanders: Evaporative water loss. Physiol. Zool. *41*, 195–203.

42. Riddell, E.A., and Sears, M.W. (2015). Geographic variation of resistance to water loss within two species of lungless salamanders: implications for activity. Ecosphere *6*, 1–16.

43. Littleford, R.A., Keller, W.F., and Phillips, N.E. (1947). Studies on the vital limits of water loss in the Plethodont salamanders. Ecology *28*, 440–447.

44. Baken, E.K., Mellenthin, L.E., and Adams, D.C. (2020). Macroevolution of desiccation-related morphology in plethodontid salamanders as inferred from a novel surface area to volume ratio estimation approach. Evolution *74*, 476–486.

45. Lertzman-Lepofsky, G., Mooers, A.Ø., and Greenberg, D.A. (2019). Ecological constraints associated with genome size across salamander lineages. Proc. R. Soc. B *286*, 20191780.

46. Gregory, T.R. (2003). Variation across amphibian species in the size of the nuclear genome supports a pluralistic, hierarchical approach to the C-value enigma. Biol. J. Linn. Soc. *79*, 329–339.

47. Glazier, D.S. (2021). Genome size covaries more positively with propagule size than adult size: new insights into an old problem. Biology *10*, 270.

48. Whitford, W.G., and Hutchison, V.H. (1967). Body size and metabolic rate in salamanders. Physiol. Zool. *40*, 127–133.

49. Hardie, D.C., Gregory, T.R., and Hebert, P.D.N. (2002). From pixels to picograms: A beginners' guide to genome quantification by Feulgen image analysis densitometry. J. Histochem. Cytochem. *50*, 735–749.

50. Johnson, B.B., Searle, J.B., and Sparks, J.P. (2021). Novel allometric estimators improve estimation accuracy of body surface area, volume, and surface area-to-volume ratio in lungless salamanders (Urodela: Plethodontidae). Herpetologica *77*, 219–226.

51. Gregory, T.R. (2001). The bigger the C-value, the larger the cell: Genome size and red blood cell size in vertebrates. Blood Cells, Mol. Dis. *27*, 830–843.

52. R Core Team (2020). R: A language and environment for statistical computing.

53. Hansen, T.F., Pienaar, J., and Orzack, S.H. (2008). A comparative method for studying adaptation to a randomly evolving environment. Evolution *62*, 1965–1977.

54. Kopperud, B.T., Pienaar, J., Voje, K.L., Orzack, S.H., and Hansen, T.F. (2020). slouch: Stochastic linear Ornstein-Uhlenbeck comparative hypotheses.

55. Lenth, R. (2018). emmeans: Estimated marginal means, aka least-squares means. R package version 1.1.

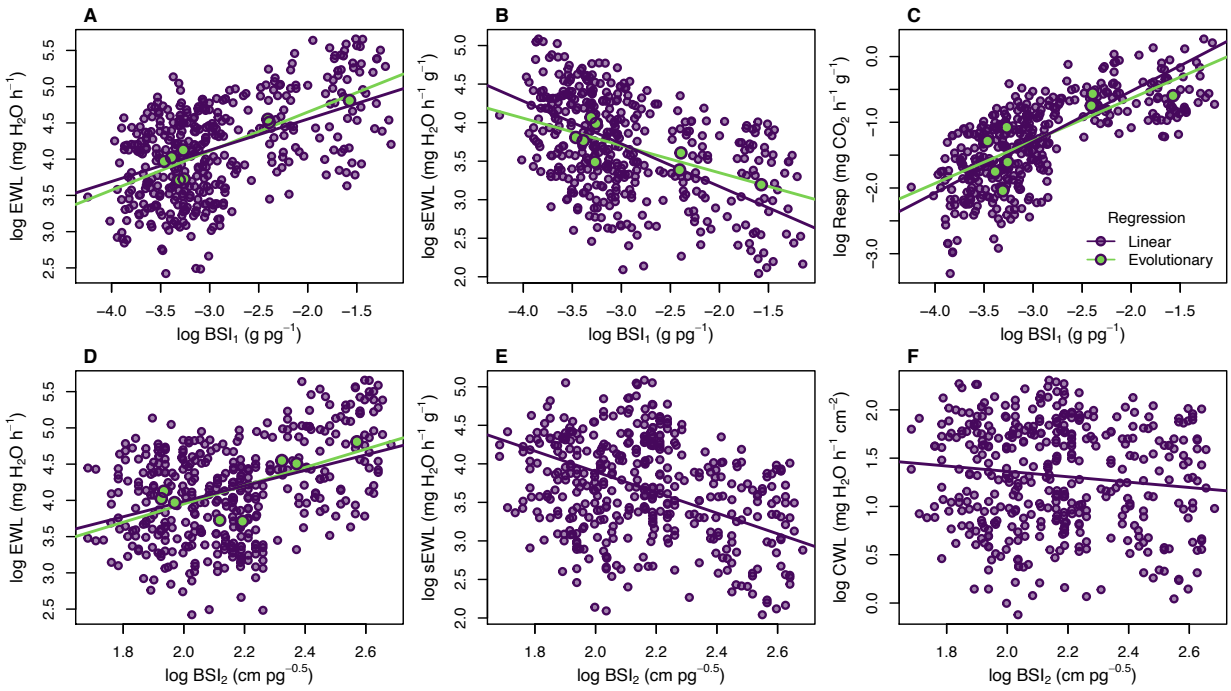

Figure 1. Correlations between proxy biological size indices (BSI) and selected physiological responses using linear regressions across all individuals, and evolutionary regressions across all species in this study. Purple points represent individual physiological measurements, and green points represent species-level means. Significant correlations are represented with fitted model slopes. BSI_1 predicts gross evaporative water loss (EWL; A) and specific water loss rates (sEWL; B) and gross metabolic rates (Resp; C) across individuals and evolutionary history, suggesting functional constraint of these traits at the individual level that influences adaptive evolution of these phenotypes. BSI_2 is the best predictor of EWL (D), sEWL (E), and cutaneous water loss (CWL; F), predicting all three responses at the individual level with lowest mean squared errors when compared to other predictors. BSI_2 only predicts EWL across phylogeny (D).

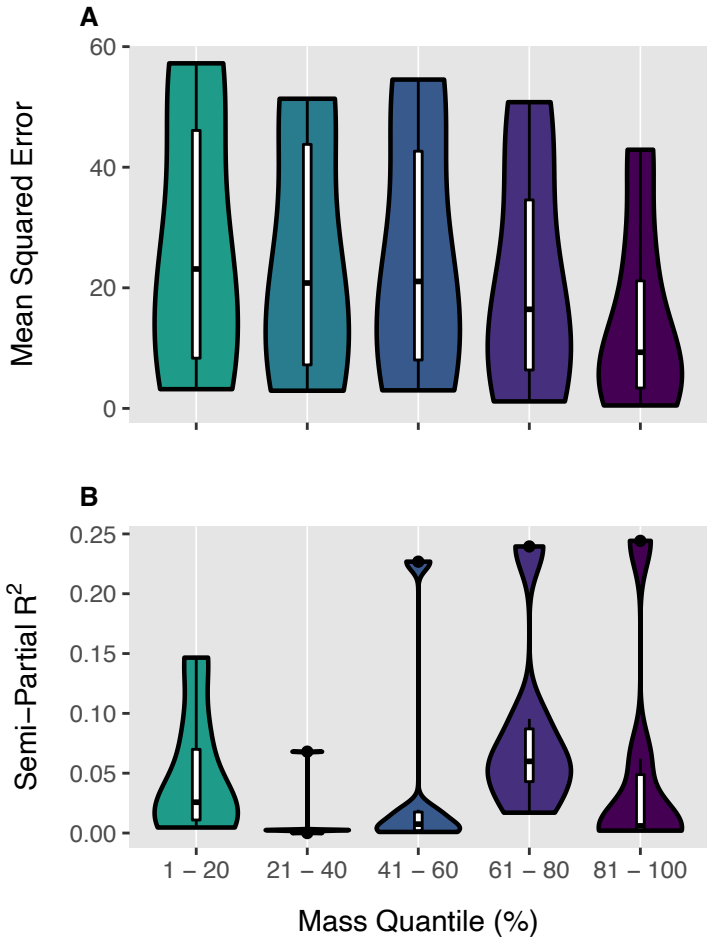

Figure 2. Holistic performance of biological size (BSI_1) across quantiles for body mass. Violin plots represent the distribution of scores for the predictive performance of BSI_1 for all physiological responses, with box plots inset to show means and quartiles. BSI_1 shows no trend in overall predictive power according to mean squared errors (A), or in overall variation explained according to semi-partial R^2 (B).

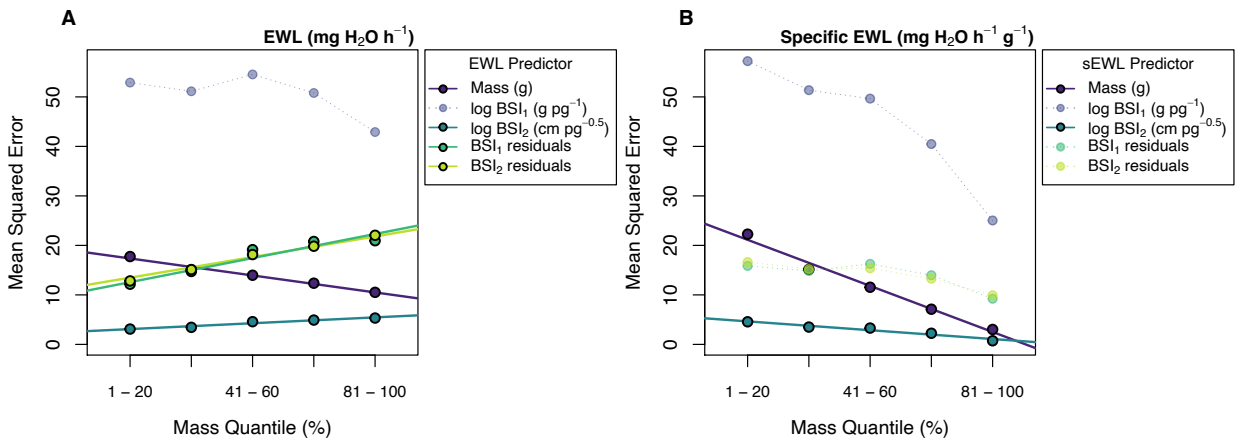

Figure 3. Comparisons of individual predictor performances for gross evaporative water loss (EWL; A) and specific water loss (sEWL; B) across quantiles for body mass. Solid lines through bold circles represent significant trends across mass quantiles, while dashed lines though opaque circles are nonsignificant. BSI_2 consistently best predicts both responses with lowest mean squared errors among predictors. BSI_2 and two residual metrics best predict EWL at smaller body sizes, whereas mass best predicts EWL at larger sizes (A). Both mass and BSI_2 best predict sEWL at larger physical sizes (B).

CHAPTER FOUR

VARIABLE TARGETS OF SELECTION SUGGEST MULTIPLE MECHANISMS FOR ADAPTATION OF METABOLIC PHYSIOLOGY IN LUNGLESS SALAMANDERS

Research in collaboration with: Steven M. Bogdanowicz[1], Maria D. Forzán[2], Avery J. Voehl[1], Jed P. Sparks[1], and Jeremy B. Searle[1]

[1]Department of Ecology & Evolutionary Biology, Cornell University, Ithaca, NY 14850, USA

[2]Department of Veterinary Biomedical Sciences, College of Veterinary Medicine, Long Island University, Brookville, NY 11548, USA

Abstract

Adaptive organismal function requires the coordination of interacting genes and traits. Oxidative phosphorylation (OXPHOS), the central energy-producing step in respiratory metabolism, is conducted by interacting protein subunits encoded in both the nuclear and the mitochondrial genomes of animals. Because the mitochondrion is prone to accumulation of mutations, selection to maintain metabolic function must rely on purifying selection to remove deleterious mutations in mitochondrial OXPHOS genes, or on compensatory mutations in nuclear OXPHOS loci to accommodate mitochondrial mutations. To test hypotheses about mechanisms of selection underlying variation in metabolic physiology, we estimated the strength of selection on mitochondrial and nuclear OXPHOS loci in a group of lungless salamanders. Lungless respiration in this group establishes clear physical constraints on metabolic performance that may limit energetic efficiency, thereby dictating the selective strength necessary to maintain function. Using a combination of phylogenetic regressions and codon models, we found evidence of relaxed selection on metabolic loci in species under lower physical constraint, and a combination of purifying selection and adaptive sequence evolution in species under stronger physical constraint. Lax selection on mitochondrial genomes and positive selection on the nuclear genome are consistent with compensatory coevolution of nuclear OXPHOS loci in some taxa, but variability in the strength and genomic targets of selection between species suggest that mechanisms of physiological adaptation are highly taxon-specific in this group.

Introduction

Coordinated interactions among genes are critical to the evolution of complex phenotypes (Gros et al. 2009). Most cellular processes are carried out by interacting traits, whose activity must be integrated for organisms to function, survive, and reproduce. This functional integration of traits manifests as organismal performance – emergent whole-organism phenotypes central to fitness and adaptation in nature (Calow 1987; Kearney et al. 2021). Because natural selection acts on the integrated function of individual traits, maintaining organismal performance requires coordinated interactions between the genomic loci that encode these traits (Gros et al. 2009), highlighting the functional importance of epistasis underlying performance phenotypes.

One of the most fundamental performance phenotypes is metabolic rate – the sum total of all cellular respiration within an organism. Aerobic respiratory metabolism is a critical indicator of energy turnover whose end product, adenosine triphosphate (ATP), is used to fuel countless cellular functions. In eukaryotes, the bulk of metabolic ATP is produced in mitochondria during oxidative phosphorylation (OXPHOS), in which redox reactions pump protons across respiratory chain proteins in the mitochondrial membrane to fuel ATP synthase. Crucially, the multiple polypeptide subunits that comprise these protein complexes are encoded by two separate genomes: 13 by the mitochondrial and approximately 78 by the nuclear genome (McKenzie et al. 2007). The need to maintain OXPHOS function should theoretically result in strong negative selection on most new mutations in the mitochondrial genome (mtDNA) (Hill 2020). However, the dual genomic architecture of OXPHOS function can alternatively shield against deleterious mtDNA mutations via coadaptation of interacting mtDNA and nuclear OXPHOS loci (mtOX and nuOX, respectively) (Rand et al. 2004). Specifically, functional integration of these loci means that deleterious mutations in mtOX loci select for compensatory mutations in nuOX genes to

maintain function (Hill 2020), evident as elevated substitution rates in nuOX genes relative to background, non-OXPHOS loci (Havird et al. 2015; Barreto et al. 2018)

Coding and (or) regulatory variation in OXPHOS loci may arise between taxa when differences in morphology and physiology incur shifts in the strength of selection between groups (Evans and Bernatchez 2012; Chong and Mueller 2013). Specifically, variation in morphological structures can enact varying influence on physiological function by means of immutable biophysical processes. Whereas one morphological trait value (or combination of trait values) may promote optimal physiological performance, progressively greater deviations from this value will negatively influence performance, resulting in reduced fitness (Kempes et al. 2019), and stronger selection to improve performance. For example, at the organismal level, body mass dictates gross energetic demands, resulting in strong covariation between mass and metabolism in all organisms (Gillooly et al. 2001). More specifically, rates of oxygen diffusion into the body to fuel OXPHOS are closely tied to the diffusing capacity of the respiratory surface, as dictated by the size and thickness of the respiratory surface available for oxygen consumption (Gillooly et al. 2016). This constraint suggests that, by limiting metabolic performance, properties of the respiratory surface itself may dictate the OXPHOS efficiency needed to meet physiological demand, and thus may influence the strength of selection or epistatic coordination between mtOX and nuOX loci necessary to maintain metabolic function.

The lungless salamanders (Urodela: Plethodontidae) present an excellent system in which to test for functional constraints on metabolic performance and mitonuclear epistasis. Lacking lungs, salamanders in this family transport nearly all respiratory gases across the body surface in order to fuel metabolism (Feder and Burggren 1985). Theory predicts cutaneous diffusion limits oxygen transport to tissues in the Plethodontidae (Burggren and Moalli 1984; Feder and

Burggren 1985, 1992), meaning skin structure likely constrains metabolic performance directly. Specifically, the thickness of the integument dictates the path length for diffusive transfer of gases in and out the body (Feder and Burggren 1985), potentially limiting metabolic rates beyond a certain thickness. Further, a smaller body surface area (SA) relative to body volume (V) reduces the amount of cutaneous respiratory surface available to supply oxygen to tissues. Assuming unchanging shape, increases in body volume are accompanied by an increase in SA to the two-thirds power, as V increases cubically and SA quadratically ($SA \propto V^{2/3}$) (Okie 2013). This relationship determines the surface area-to-volume ratio (SA:V), leaving larger organisms with a proportionally smaller SA:V ratio relative to smaller organisms. As such, larger salamanders with smaller SA:V ratios experience a reduced respiratory capacity (the ability to supply oxygen to tissues) due to a limited diffusing capacity of the skin (the diffusive conductance rate of gas across the integument) (Feder 1988).

Here, we characterize the relationships between natural selection and physical constraints on metabolic performance in lungless salamanders. Stronger limitations on respiratory gas transport in thicker-skinned and larger organisms should be reflected by stronger selection on metabolic performance and the epistatic interactions that drive it (Hill 2020). Accordingly, we tested five hypotheses: (H_1) smaller SA:V ratios require greater metabolic efficiency to maintain organismal function; (H_2) stronger functional constraints on physiology result in greater purifying selection on OXPHOS loci to maintain this more efficient metabolic performance; (H_3) stricter purifying selection on OXPHOS loci reduces metabolic rates to increase energetic efficiency; (H_4) stronger constraints result in elevated compensatory mutations in nuOX loci to maintain function; and (H_5) compensatory coadaptation between mtDNA and nuclear genomes reduces metabolic rates. H_3 and H_5 can be considered alternative hypotheses of

the relationship between selection and metabolism, both of which have been investigated in other diverse taxa. H_2 and H_4 offer alternative hypotheses of the relationship between physiological constraint and natural selection, which to our knowledge is unexplored in the literature. To test these hypotheses, we quantified morphological and biophysical constraints, including SA:V, skin thicknesses and diffusing capacities in eight species of different size to link variation in whole-organism metabolic performance to coding variation and mitonuclear coadaptation. By combining these physiological and genomic approaches, we provide evidence that species under stricter physical constraint experience stronger selection on metabolic performance.

Methods

Species sampling and experimental design

All procedures described here were approved by the Cornell University Institutional Animal Care and Use Committee (IACUC protocol # 2016-0081). Detailed field and experimental methods are outlined in Johnson et al. (2021a), and detailed laboratory and analytical methods are in the Supporting Information. Briefly, we collected eight species of lungless salamanders (*Eurycea bislineata*, *E. longicauda*, *Plethodon cinereus*, *P. dunni*, *P. glutinosus*, *P. larselli*, *P. vandykei*, and *P. vehiculum*) from multiple natural populations (Table S1). These species vary broadly in both body size (0.39g - 7.67g) and C-value (19.17pg – 49.77pg). These variables do not covary in our sample ($P = 0.936$), allowing us to test for their interactive influence on physiological performance and constraint. We measured mass prior to experimental trials and estimated C-value from red blood cells (Johnson et al. unpublished data). Individuals were acclimated under two treatment temperatures (low = 10°C, high = 15°C) for experimental trials in a fully factorial 2x2 experimental design crossing temperature and

humidity treatments (measured as vapor pressure deficit (VPD); low = 0.6 kPa, high = 0.3 kPa). Individual physiological rates were measured under all four treatment combinations using flow-through respirometry. Here, we focus on two of six physiological variables measured by Johnson et al. (2021a): gross respiratory metabolic rate (respiration; mg CO_2 h^{-1}) and mass-specific metabolic rate (mg CO_2 h^{-1} g^{-1}). Here, we interpreted gross rates as indicative of overall energetic demands of the organism and specific rates as indicative of energetic efficiency, with lower rates reflective of more efficient physiological performance.

Physiological constraint

To test for effects of physiological constraint on the strength of selection, we estimated six phenotypes likely to impose physical constraints on respiratory metabolism: surface area-to-volume ratio (mm^2 mm^{-3}), biological size (g pg^{-1}), epidermal thickness (μm), total skin thickness (μm), and the diffusing capacities of the epidermis and total integument to CO_2 (nmol CO_2 h^{-1} $torr^{-1}$). Here we define these trait values as indicative of relative physical constraint, whereas their relationship with metabolism reflects their effective, or functional constraint. Specifically, while no phenotypes measured here represent a true constraint, or a physical limit to organismal function, we defined constraint as the relative proximity of a given trait score to the that limit. Though the absolute SA:V, skin thickness, or diffusing capacity that limits performance is unknown for a given individual, it is clear that progressively larger SA:V ratios, thinner integuments, and greater diffusing capacities all increase respiratory capacity, cutaneous transport rates, and gross transport rates, respectively (Feder and Burggren 1985; Feder 1988). As such, smaller SA:V ratios, thicker skins, and lower diffusing capacities all reflect physical (or biophysical) properties that reduce metabolic performance, enacting a stronger relative constraint

on physiology, and smaller biological size values reflect a greater contribution of cell size to physical constraint relative to body size. Using this framework, we hypothesized that stronger physical constraints should result in stricter functional constraint, defined as the effective control of the physical constraint over the response variable. Specifically, we define greater predictive power, effect size, and variation in metabolism explained by a predictor as indicative of a stronger effective constraint.

First, we estimated surface area-to-volume ratios using allometric estimates for body surface area and volume following Johnson et al. (2021b) to characterize whole-organism constraint on cutaneous transport rates. Second, we estimated biological size as the ratio of body mass to genome size (g pg^{-1}) following Johnson et al. (unpublished data). This metric has been shown to influence metabolic rates across our eight taxa (Johnson et al. unpublished data). To estimate constraints imposed by the structure of the integument, we measured the total thickness of the skin and the thickness of the epidermis. The epidermis is underlain by dermal capillaries (Lillywhite and Maderson 1988), meaning the thickness of epidermis is the primary diffusive distance traveled for gas exchange with the environment. Variation in this diffusion path length therefore constrains diffusion rates and dictates the conductance of the integument to gas transport in and out of the body, potentially influencing whole-individual physiology more broadly (Feder and Burggren 1985; Lillywhite and Maderson 1988). When cutaneous capillaries are constricted (such as under desiccating conditions; e.g. Riddell et al., 2019), exchanged gases must diffuse across the entire thickness of the integument, whose multilayered structure is more variable and complex than the epidermis. Therefore, under some conditions, variation in total thickness (the diffusion path length) and composition (which determines diffusivity) may constrain respiration rates. We measured cutaneous thicknesses using linear measurements of

stained histological sections in QuPath v0.2.3 (Bankhead et al. 2017), taking multiple measurements along the body surface to generate mean thickness estimates for each species (Supporting Information). Lastly, we estimated diffusing capacities of the skin (D_{CO2}) following the morphometric approach of Piiper et al. (1976). To calculate D_{CO2}, we modeled the diffusion path length using our mean skin thickness estimates and modeled functional respiratory surface area using allometric estimates based on published measurements of cutaneous capillary densities (Czopek 1961). We applied unit conversions to interpret estimates as the molar quantity of CO_2 diffused across the path length (either skin or epidermis) per hour per torr of CO_2 partial pressure gradient between capillaries and air surrounding the body (nmol CO_2 h^{-1} $torr^{-1}$) (Supporting Information).

Linear regressions: functional constraints

We regressed gross and specific respiration rates against our six morphological traits to characterize their relationship with metabolic physiology. To compare the predictive power of different traits, we modeled covariance between respiration rates and each trait individually using linear mixed models in R (R Core Team 2020). We natural log transformed all morphological and physiological variables, and included temperature and humidity as covariates to control for environmental effects on metabolism, as well as random effects for individuals and species. An individual random effect corrects for repeated measurements in the experiments of Johnson et al. (2021a), while a species random effect corrects for differences among species not attributable to the predictor of interest, employed because we are not interested in differences among species *per se*, rather among representatives of different morphological types. We tested for model significance following a false discovery rate (FDR) correction across all regressions

following Storey et al. (2002), then compared estimates of effective constraint among significant models.

For all linear models, we used three estimates to determine effective constraint. (1) We estimated mean squared errors (MSE) – the mean squared difference between model predictions and observed data – as a metric for predictive power of each constraint variable, with high predictive power reflective of stronger effective control over the response. (2) We estimated standardized regression coefficients (beta weights) to infer effect sizes of each predictor on the response, with a larger beta weight indicative of greater functional control. (3) We estimated the semi-partial R^2 (pR^2) of the constraint variable – the proportion of the variation in the response that is attributable to the predictor – with larger pR^2 values reflective of stronger functional constraint. We estimated MSE manually in R and estimated beta weights and pR^2 using 500 bootstrap replicates in the R package 'partR2' v0.9.1 (Stoffel et al. 2021).

Phylogenetic regressions: evolution of constraint

We conducted phylogenetic generalized least squares regressions (PGLS) to test for evolutionary correlations between morphology and metabolic rates. We calculated means for each of our six constraint phenotypes (Table S1) and gross and specific metabolic rates, and regressed metabolism against each constraint metric after natural log transformations of all variables, using a phylogeny of our eight experimental species (Johnson et al. 2021a). To test the hypothesis that relative constraint causatively predicts performance, we used a covariance structure based on the Ornstein-Uhlenbeck (OU) model (reflecting trait evolution in the response toward an adaptive optimum determined by the predictor). While our linear models test for the influence of morphology on physiological performance at the individual level, these PGLS

models test the hypothesis that variation in relative physical constraints allows adaptive evolution of performance toward each species' respective adaptive optimum (Cooper et al. 2016). We tested for model significance following an FDR correction across all regressions, then compared effective constraint among significant models. Here, we interpreted effective evolutionary constraint as the estimated model parameter α, which describes the strength of the selective pull toward the adaptive optimum. We further estimated MSEs and manually calculated total R^2 for each regression following Paradis (2012) to estimate the proportion of interspecific variation in the each response explained by each predictor.

mtDNA libraries and mtOX alignments

Following physiological experiments, we extracted whole genomic DNA from preserved tissues and amplified mitochondrial genomes in two large fragments using PCR (Supporting Information). PCR samples were prepared for sequencing and pooled onto an Illumina MiSeq sequencer (Illumina Inc., San Diego, CA, USA) using single-end, 150 bp reads. We trimmed Illumina adapter sequences and low quality reads using Trimmomatic v0.39 (Bolger et al. 2014) before assembling mitogenomes de novo using SPAdes v3.14.1 (Bankevich et al. 2012). Assemblies were cleaned following Douglass et al. (2019) by visualizing coverage depth versus length of all contigs and filtering reads that fell below assembly-specific quality thresholds. We removed contaminant sequences following a blastn search against the NCBI nonredundant (nr/nt) nucleotide database, keeping only reads whose highest bit score matched a vertebrate mitochondrial sequence. Final assemblies were annotated using the MITOS2 web server (Donath et al. 2019). We extracted all protein-coding sequences from assemblies and grouped sequences

by OXPHOS locus. Each mtOX group was aligned using MAFFT v7.453 (Katoh and Standley 2013) and poorly aligned positions were removed using Gblocks v0.91b (Castresana 2000).

RNA sequencing and transcriptome assembly

To test for selection on the nuclear genome associated with physiological performance, we assembled nuclear transcriptomes for three focal species (*P. cinereus*, *P. glutinosus*, and *P. vandykei*) (Supporting Information). We selected these three species as representative of morphological and nucleotypic extremes: *P. cinereus* is small-bodied (mean 0.73 g in our sample), whereas *P. glutinosus* is much larger (mean 5.12 g), but both have comparable genome sizes (19.17 and 24.21 pg, respectively). *P. vandykei* is intermediate in size (mean 1.99 g), but with an exceptionally large genome (49.77 pg) (Johnson et al., unpublished data). In combination, these taxa should enable us to identify selective regimes associated with constraints on body and genome size. RNA was extracted from 10 RNALater-preserved tissues from each species and RNA libraries prepared for 2x150 bp paired-end sequencing on an Illumina Novaseq sequencer. Illumina adapters and low quality reads were trimmed using fastp v0.20.0 (Chen et al. 2018) and all unpaired reads were discarded before assembling one *de novo* transcriptome per individual using Trinity v2.8.4 (Grabherr et al. 2013) with default parameters. We identified long open reading frames (ORFs) in our transcriptome assemblies using TransDecoder v5.4.0 and removed contaminant (non-chordate) sequences from our transcriptomes following a blastp query against the nr/nt database using Diamond v2.0.7 (Buchfink et al. 2021).

Orthologous loci and functional groups

We identified groups of orthologous sequences shared between our individual assemblies using Orthofinder v2.5.2 (Emms and Kelly 2019) (Supporting Information). To test hypotheses about evolution across interacting mitonuclear loci, we divided orthogroups into three functional groups: 1) loci with known function in oxidative phosphorylation ("nuOX"), 2) loci whose mitochondrial proteins are not involved in OXPHOS ("mitochondrially-targeted proteins" or "MTPs"), and 3) loci with no known mitochondrial function or interaction ("background loci"). We assigned orthogroups to their respective categories by comparing each to the MitoCarta v3.0 *Mus musculus* mitochondrial proteome (Rath et al. 2021) using blastp, using blast hits to categorize sequences as either nuOX or MTP loci. Sequences without blast hits were classified as background loci.

We saved a random sample of 1000 MTP and 1000 background orthogroups represented by all sequenced individuals, and the complete set of 146 nuOX orthogroups that were fully represented. We additionally retained 52 nuOX orthogroups represented by at least five individuals per species. Orthogroups were aligned using MAFFT, and alignments were converted to DNA format using PAL2NAL v14 (Suyama et al. 2006), with poorly aligned positions eliminated from alignments using Gblocks.

Selection on functional groups

We employed codon models to characterize rates and patterns of molecular evolution across orthogroups with respect to metabolic function (Supporting Information). We fit models to each orthogroup alignment using the program CODEML implemented in PAML v4.9 (Yang 2007). At each locus, CODEML compares the number of nonsynonymous (d_N) and synonymous

(d_S) nucleotide substitutions, taking their ratio (d_N/d_S) to estimate the parameter ω. This parameter serves as a measure of selection intensity, with $\omega > 1$ indicative of positive selection, $\omega < 1$ indicative of purifying selection, and $\omega = 1$ reflective of neutrality. For general comparisons, we separated our orthogroup alignments by species and used the one-ratio model M0 (Goldman and Yang 1994) in CODEML to produce a single estimate of ω per species per locus. While a homogeneous ω is unlikely across all nucleotide sites of a coding sequence (Yang and Nielsen 2002), this approach helps us approximate relative differences in selection pressure among loci from different species and functional types. We ran each model twice to ensure consistency of model estimates, keeping the model run with the higher likelihood score from each pair of consistent runs. We removed all runs with extreme ω estimates ($\omega > 20$), suggesting poor convergence of the model run.

Because distributions of ω estimates were non-normal, we used Mann-Whitney tests to make pairwise comparisons of ω among groups. We made comparisons using subsets of two datasets: (1) all transcriptome-derived orthogroups for our three focal species plus mitochondrial sequences for these three, and (2) mitochondrial sequences only for all eight plethodontid species. In the first dataset, we tested for differences in ω across five axes of comparison: (1) between all functional types (background vs nuOX vs MTP vs mtOX loci) across all three species, (2) between all functional types within each species individually, (3) between species for a given functional type, (4) between OXPHOS complexes for all loci (both nuclear and mitochondrial) associated with the OXPHOS pathway, and (5) between OXPHOS complexes using only nuclear OXPHOS loci. We focused particularly on comparisons with OXPHOS complex II. This is the only complex with no subunits encoded in the mitochondrial genome (Signes and Fernandez-Vizarra 2018), meaning compensatory evolution in the nuclear genome

should result in higher ω values in loci for all other OXPHOS complexes relative to complex II. In our second dataset we compared (1) between OXPHOS complexes across all species and (2) between species across all mtOX loci. Finally, we assessed the significance of comparisons following an FDR correction across all 87 pairwise tests.

Mitonuclear coadaptation

We tested for signatures of compensatory coevolution in the nuclear genome by comparing kernel densities and summary statistics between model M0 ω estimates for genomic functional types. Compensatory evolution of nuclear OXPHOS genes should be evident as elevated evolutionary rates in nuOX loci (Hill 2020), resulting in a low overlap in the distributions of ω for mtOX and nuOX loci relative to mtOX and background loci. For each of our three focal species, we used the empirical distribution of whole-locus ω estimates for each functional category to estimate kernel densities for each functional group. We compared all functional groups within a species using the R package 'overlapping' v1.6 (Pastore 2018) to estimate a percent overlap in kernel density. We additionally compared median ω estimates among functional groups. Here, we interpret a greater difference between median mtOX and nuOX loci relative to mtOX and background loci as evidence of epistatic compensatory evolution in the nuclear genome.

Selection across phylogeny

We tested explicit phylogenetic hypotheses using codon models in CODEML to test for heterogeneity in the strength of natural selection between species (Supporting Information). Using an individual-level phylogeny of three species, these 12 phylogenetic hypotheses ($H_{P1\text{-}P12}$)

reflect four potential evolutionary scenarios for each of our three species: (1) episodic positive selection on the branch leading to each species ($H_{P1\text{-}P3}$), (2) long-term positive selection across the entire clade (comprised of all individuals) for each species ($H_{P4\text{-}P6}$), (3) episodic changes in selection (not necessarily positive selection) on the branch leading to each species ($H_{P7\text{-}P9}$), and (4) extended changes in selection across each species clade ($H_{P9\text{-}P12}$). This suite of hypotheses tests for evidence of molecular adaptation associated with the respective physiological constraints of each species: large body size in *P. glutinosus*, small body size in *P. cinereus*, and large genome size in *P. vandykei*. To test these hypotheses, we used likelihood ratio tests between nested pairs of models. We tested for episodic positive selection using constrained and unconstrained versions of branch-site model A (Zhang et al. 2005), and for extended shifts in positive selection by comparing clade model C (Bielawski and Yang 2004) to the "relaxed" form of sites model 2a (Weadick and Chang 2012). We tested for episodic changes in selection intensity by comparing branch-site model B (Yang and Nielsen 2002) to sites model 3 (Yang et al. 2000), and for extended shifts in selection intensity by comparing clade model D (Bielawski and Yang 2004) to sites model 3 (Yang et al. 2000). We ran all models twice, keeping only fully converged, higher-likelihood runs from consistent pairs. From this final set of models, for each evolutionary hypothesis (H_{P1}-H_{P12}) we corrected for multiple tests across all tested loci with an FDR correction across all loci.

Functional annotation

We annotated loci under selection with gene ontology (GO) terms using Blast2GO v1.5.1 (Götz et al. 2008). All orthogroup sequences were queried against the Uniref90 database using a blastx search in Diamond, returning 50 target sequences per search with an e-value cutoff of $1e^{-}$

[10]. We queried our entire collection of tested loci across all orthogroups and functional categories, plus one query of only significantly selected loci for each of the 12 hypothesis tests run in CODEML. We tested for overrepresentation of GO categories under each hypothesis using Fisher exact tests in topGO v3.14 (Alexa and Rahnenfuhrer 2020) using the 'weight01' algorithm with a significance threshold of α=0.05. To characterize heterogeneity in selection strength on GO categories between species, we took the ratio of ω estimates between foreground clades (the clade undergoing the selective shift) and background clades (experiencing no shift under the model) for each phylogenetic hypothesis, focusing explicitly on GO terms related to metabolism, energetics, and growth.

Phylogenetic regressions: selection and epistasis

We conducted PGLS regressions to test for evolutionary correlations between physiological constraint, mitonuclear epistasis, and selection strength. For each species in our eight-species dataset, we calculated means for locus-wide ω estimates across all mtOX loci. We regressed ω as the response against each of our six physical constraint metrics, testing the hypothesis that stronger physical constraints on metabolic physiology result in stronger purifying selection on mtOX genes. We natural log transformed of all variables and used the phylogeny of Johnson et al. (2021a) and OU covariance structure in all regressions, and tested for model significance following an FDR correction across all regressions.

For our three focal species, we tested for further correlations between constraint and selection in the nuclear genome, and between constraint and the strength of mitonuclear epistasis. We trimmed our phylogeny to three taxa and used untransformed variables due to low sample size in these comparisons, again using an OU covariance structure in all cases. Similar to

the mitochondrial regressions above, median ω estimates from each nuclear functional type were regressed against species-mean morphological traits, testing the hypothesis that stronger physical constraints result in stronger selection on nuclear OXPHOS loci relative to background loci. To test for evolutionary correlations with epistasis, we also regressed the difference in median ω between each pair of functional types and the overlap in kernel density of each pair of functional types against each morphological trait, testing the hypothesis that stronger constraints on physiology should result in stronger epistasis between mitochondrial and nuclear OXPHOS loci.

Results

All morphological traits except skin thickness predicted gross metabolic rates (Fig. 1), and specific metabolism was predicted by all but skin and epidermal thickness at the individual level (Fig. 2). Surface area-to-volume ratios showed the overall strongest effect on metabolic rates (Table S2), as SA:V had the greatest effect size and explained the most variance in both gross and specific metabolism, and best predicted gross rates. Specific rates were best predicted by biological size, though SA:V also performed well with a comparable MSE. All traits but diffusing capacities predicted gross respiration across phylogeny, but none predicted specific rates (Fig. 1, Fig. 2; Table S3). SA:V again best predicted gross metabolism and explained the most variation among species.

Comparing among eight species, Mann-Whitney tests identified the strongest purifying selection across mtOX loci in *P. larselli*, with significant differences from *P. cinereus, P. vandykei, E. bislineata,* and *E. longicauda* (P = 0.04-0.031; Fig. 3; Table S4). No other pairwise comparisons were significant, including comparisons with *P. vandykei*, which showed the weakest median purifying selection. mtDNA loci coding for different OXPHOS complexes

showed no differences in selection strength pooled across eight species. However, among nuOX loci from three species, complex IV was under weaker purifying selection than either complexes III or V. Complex II did not differ from any other complexes (P = 0.524-0.893). Selection strength on mtOX loci did not predict either gross nor specific metabolic rates in eight species, and selection on nuOX predicted neither across three species (Table S5). No morphological traits predicted selection strength on the mitochondrial genome across eight species (Fig. 4; Table S6), nor on any nuclear functional groups in three species (Table S7).

In our three-species genomic sample, mtOX loci had the lowest median ω in each species, but did not differ statistically from nuclear functional types in any (P = 0.659-0.893), or when pooled across all three (Fig. 3D). MTPs, however, demonstrated stronger purifying selection than nuclear background loci in each species, a trend that was significant in *P. vandykei* and across the three species together (Fig. 3D). When comparing between species, all three nuclear functional types were under strongest selection in *P. glutinosus* (Table S4). Selection was equivalent in MTP and nuOX loci between *P. cinereus* and *P. vandykei*, but purifying selection on background loci differed between all three species, with the highest ω in *P. cinereus*. Differences in median ω were generally low in all comparisons between functional groups (Table S8). Similarly, overlap in the empirical distributions of ω were generally high, with >50% overlap in all distributions when pooled across all three species. Neither of these epistasis metrics was predicted by any constraint phenotype for any pair of functional types (Fig. 4D-G; Table S9).

Codon models run on nuclear functional groups (Table S10) produced consistently short branch lengths among species, frequently resulting in extreme ω values (> 20), suggesting difficulty in producing accurate d_N/d_S estimates. Excluding extreme estimates produced a modest

sample of 14 gene ontology categories with reliable estimates of selection (Table 1). *P. cinereus* showed relaxed selection strength relative to *P. glutinosus* and *P. vandykei* in all metabolism-related GO terms except for fatty acid biosynthesis. *P. glutinosus* demonstrated stronger purifying selection than others in all terms related to OXPHOS, with relatively relaxed terms for organismal growth and mitochondrial ribosome binding. *P. vandykei* demonstrated relative relaxation of terms associated with OXPHOS, and constraint on loci associated with the mitochondrial large ribosomal subunit and cellular responses to hypoxia.

Discussion

Interactions between mitochondrial and nuclear-encoded proteins are integral to the proper function of oxidative phosphorylation in eukaryotes. Due to its asexual inheritance without recombination, theory predicts deleterious mutations to accumulate in the mitochondrial genome (Muller 1964), necessitating either purifying selection to remove these variants, or compensatory coevolution of the nuclear genome to accommodate them (Hill 2020). Here, we tested hypotheses that physical constraints on metabolic physiology, by limiting gas transport rates, predict either purifying selection on mtDNA loci or compensatory evolution in nuclear loci needed to meet energetic requirements. We find mixed support for these hypotheses in lungless salamanders. While we could not demonstrate any relationships between constraints and mitonuclear coevolution using locus-wide estimates of selection on different functional groups, our more detailed codon models confirm that metabolic loci in both the nuclear and mitochondrial genomes do experience selection heterogeneously among species with different functional constraints, consistent with our hypothesis that variation in constraints on physiology can result in differences in selection on performance. Though these results do not definitively

implicate mitonuclear interactions underlying physiological performance in our sample, positive selection on a subset of codon sites in nuOX loci in two of our three species (*P. cinereus* and *P. vandykei*) is strongly reflective of compensatory evolution for generally relaxed mtOX selection we observed using locus-wide estimates (Hill 2020). Not all species displayed this pattern, however, suggesting that multiple modes of selection may act in combination to maintain variation in metabolic performance in temperate Plethodontidae. This observed variation in selection experienced by different species opens multiple new hypotheses about mechanisms of selection acting on lungless salamander physiology. Though this result may represent general differences in the overall selective environment experienced by each species, it could also reflect varying selection to overcome divergent functional constraints on respiration. This open possibility is consistent with our hypothesis relating constraint and selection, however these alternatives must be investigated to confirm the targets of selection underlying physiological diversity in lungless salamanders.

Our results confirm multiple, but not all, biophysical predictions about functional constraints on metabolism in lungless salamanders. SA:V, biological size, epidermal thickness, and epidermal and cutaneous diffusing capacities all covaried with gross metabolic rates, and all but thicknesses predicted mass-specific rates. Together, these results suggest that morphological traits interact to determine metabolic performance in this group, both at the level of the whole organism and at mass-specific scales. Whole-organism factors appear to dominate these effects. SA:V best predicted gross metabolism and well predicted mass-specific metabolism, with lower specific respiration in low SA:V individuals consistent with our hypothesis (H_1) that stricter constraint necessitates greater metabolic efficiency (Fig. 2A). Biological size best predicted specific metabolism, suggesting a cell-size influence on metabolism operating at a per-gram

scale that differs among individuals of different body size. However, the mechanisms underlying this relationship are unknown and merit investigation (Johnson et al. unpublished data). Intriguingly, our codon models identified positive selection acting on loci associated with organismal cell number in all three species. This effect was strongest in *P. cinereus*, the biologically smallest species in our sample (Table 1), suggesting that larger effects of cell size on performance may be associated with increased rates of molecular adaption. While epidermal thickness predicted gross respiration, the positive covariation between these traits (Fig. 1D) contradicts the hypothesis that thicker skins impose greater restrictions on gas transport (H_1). Rather, the lack of relationship between epidermal thickness and specific metabolism (Fig. 2C) suggests that the physical constraint imposed by thickness of the respiratory surface does not necessitate greater energetic efficiency and is therefore not functionally limiting in lungless salamanders. As such, the positive correlation with gross metabolic rate is likely incidental to thickness' covariation with body mass in our sample ($p < 0.001$). Diffusing capacities of the epidermis and total integument both predicted gross and specific physiology (Fig. 1E, 2D), but again these trends appear to be due to effects of body size. Diffusing capacities include both a parameter for respiratory barrier thickness and functional surface area (which correlates with total body surface area), and surface area accounts for much more variation in epidermal diffusing capacity ($R^2 = 0.810$) than does epidermal thickness ($R^2 = 0.156$). Together these results suggest that respiratory diffusive transport in the Plethodontidae is limited by the amount of surface available for transport (as dictated by SA:V), not by the transport rate across the respiratory surface (as dictated by skin thicknesses). Once in the body, cell size effects (mediated through biological size) influence energy turnover at a per-gram scale. If any physical constraints

influence how selection acts on physiological performance, we hypothesize these two to be the most likely candidates worth pursuing in future expanded studies.

While this combination of morphological traits strongly predicts metabolic performance across individuals, PGLS regressions found no association between morphology and mass-specific metabolism over evolutionary time (Fig. 2). Gross metabolic rates demonstrated evolutionary correlations with multiple traits, suggesting that selection favors changes in gross respiration in response to changes in morphology (an assumption of the OU model structure) (Hansen et al. 2008). However, it is unclear why gross rates covary with relative constraint and specific rates do not, as mass-specific physiology is more reflective of metabolic efficiency. This result may suggest our hypothesis that increased physical constraints induce increased energetic efficiency (H_1) does not apply at evolutionary timescales, but expanded taxonomic sampling is needed to confirm this possibility.

Codon models, but not PGLS regressions, suggest an association between relative morphological constraints and selection strength across phylogeny. Using PGLS models, no morphological traits predicted selection on mtDNA loci (Fig. 4D,4E), nor on any nuclear functional groups (Table S7). These results reject our hypothesis (H_2) that stronger physical constraints result in increased selection on OXPHOS genes. However, we caution that our regressions in nuclear functional groups are limited by small taxonomic sampling, and are further handicapped by low phylogenetic signal, as suggested by short branch lengths in our CODEML analyses. We chose our three focal species as examples of structural extremes in *Plethodon*. *P. cinereus* and *P. glutinosus* are particularly small and large-bodied (with extreme SA:V) (University of California 2021), respectively, while *P. vandykei* has the largest genome size (contributing to biological size) in the genus (Gregory 2016). Consistently poor phylogenetic

signal in these taxa suggests that substantial body and cell size variation has arisen in *Plethodon* despite modest overall genomic divergence. As such, we could not identify a relationship between selection and performance or selection and morphology among these extreme examples, however expanded taxonomic sampling is needed to clarify trends more broadly across the Plethodontidae. PGLS regressions did not detect an evolutionary relationship between selection and performance in our eight-species mtDNA sample, although apparent trends in locus-wide mtOX selection may contribute to poor signal in these results. Specifically, pairwise Mann-Whitney tests identified some interspecific differences in selection, with median ω across all loci notably falling into two categories: strict purifying selection ($\omega \approx 0$ for *P. dunni*, *P. glutinosus*, *P. larselli*, and *P. vehiculum*) and relaxed selection ($\omega > 0.07$ for *P. cinereus*, *P. vandykei*, *E. bislineata*, and *E. longicauda*), though relaxed outliers do occur in the former group (Fig. 3A,3B). It is not immediately clear why mitochondrial selective regimes differ qualitatively between these two groups, but this effective binary distribution of mtOX ω across species may contribute to a lack of signal in our PGLS regressions. Our codon models, however, remain consistent with hypothesis H_2. *P. glutinosus*, our largest species under strictest SA:V limitation, demonstrated both the lowest specific metabolic rate of eight species and greatest selective constraint of three on nuclear loci associated with OXPHOS (Table 1) as the only species showing purifying selection on loci associated with the electron transport chain and the respirasome (OXPHOS supercomplexes) more generally. Positive selection on OXPHOS complex IV, however, suggests that a combination of purifying and positive selection acting concurrently on different metabolic loci contribute to the adaptation of physiological performance at large body size.

This relationship between selection and metabolism in our focal species aligns with other studies linking selection with energetic requirements. Selection on OXPHOS loci covaries with proxies for energy demand such as mode of locomotion or dispersal distance in diverse taxa including birds, mammals, fishes, and molluscs (Shen et al. 2009; Sun et al. 2011, 2017). Salamanders demonstrate lower ω in 10 of 13 mtOX loci than do frogs, presumably due to generally lower metabolic rates in the Caudata (Chong and Mueller 2013). The predominant hypothesis for these data posits that low specific metabolic rates such as in salamanders relax selection on metabolic loci, with lower energetic requirements allowing for greater mutational drift in OXPHOS genes. Though our locus-wide estimates of selection showed no such pattern, our codon models demonstrating stronger purifying selection in larger, more energy-demanding species and relaxed selection in smaller groups (Table 1) are consistent with this hypothesis, though wider taxonomic sampling is needed to confirm wider patterns in the Plethodontidae.

Codon models partially support our hypothesis (H_3) that stronger selection increases metabolic efficiency. Purifying selection in *P. glutinosus* and lax selection on *P. cinereus* best exemplify this relationship. However, positive selection on some loci in *P. glutinosus* also suggests alternative mechanisms for maintaining metabolic function. PGLS regressions could not confirm a relationship between selection and physiology, but comparisons among functional groups offer some insights. Purifying selection was consistently stronger on mtOX loci than any nuclear loci regardless of functional category. Though Mann-Whitney tests did not assign statistical significance to these differences, in some cases this may be due to the small number of mtOX loci included in these comparisons. For example, MTP and background loci were determined statistically distinct in *P. vandykei* despite a smaller difference in ω than between mtOX and background loci. Nuclear functional groups showed much more variable patterns of

selection relative to others, and purifying selection was generally stronger (mean mtOX ω_0 = 0.025, nuclear ω_0 = 0.094) and more extensive across mtOX loci than nuclear loci in codon models (mean proportion of mtOX sites under purifying selection = 0.732; nuclear mean = 0.672), suggesting that negative selection is consistently stronger on the mitochondrial than the nuclear genome in these species. This pattern is clear in diverse organisms spanning corals, insects, nematodes, birds, mammals, and select fungi and plants (Nabholz et al. 2012; Popadin et al. 2012; Havird and Sloan 2016), though not universal (with notable exceptions in most plants (Havird and Sloan 2016) and bivalves (Piccinini et al. 2021)). Our results thus contribute to accumulating evidence of generally stronger selection on the mitochondrion than the nucleus in vertebrates. Where these salamanders differ, however, is in the degree of this relative strength. Across measured tetrapod species (including *Xenopus* and multiple non-avian reptiles, birds, primates, rodents, Cetartiodactyls, and carnivorans), the ratio of mtOX ω / nuOX ω averages 0.221 (range 0.037-0.560) (Havird and Sloan 2016), meaning that on average, nonsynonymous mutations are maintained in vertebrate mitochondrial genomes at ~22% the rate of those in nuclear genomes, or mtDNA nonsynonymous mutations are removed at ~5x (or 500%) the rate of nuclear nonsynonymous mutations. Strikingly, the mean ratio in our sample of three congeners (0.748, range 0.549-1.00) indicates that mtDNA mutations are only ~34% more likely to be removed on average than nuclear mutations in *Plethodon*. Estimates for teleost fishes are much more comparable to our estimates (mean 0.543, range 0.342-0.636), but still show stronger selection on mtDNA than that observed in our sample. These results indicate that relative strength of selection between mitochondrial and nuclear genomes is exceptionally lax in the Plethodontidae compared to measured vertebrates. This result is consistent with the pattern of weak absolute selection strength in salamanders relative to frogs attributed to energetic

requirements (Chong and Mueller 2013). Further, a recent analysis within salamanders found selection is particularly relaxed in direct-developing Plethodontidae (including *Plethodon*) (Kakehashi and Kurabayashi 2021), with this elevated ω also hypothesized to relate to energetics. Whether such weak selection is due to lungless physiology *per se* remains unresolved, but is most clear in direct-developing taxa relative to species that metamorphose from aquatic larvae, with mtOX ω relaxed in those whose development avoids the high energetic cost of metamorphosis (Reagan and Verrell 1991; Kakehashi and Kurabayashi 2021). We did not find a similar pattern of interspecific variation in ω, likely due to our limited taxonomic sampling between direct-developing *Plethodon* and biphasic *Eurycea*. Still, consistent trends across studies linking selection to energetic demands suggest a substantial role of life history underlying selection on the mitochondrial genome at large taxonomic scales. We tested an alternative hypothesis (H_3) that physical constraints on energetic turnover predict selection strength and found evidence at a subset of metabolic loci. Expanded taxonomic sampling to test this hypothesis will reveal if our result is generalizable to the Plethodontidae, and future comparative analyses using mixed models will clarify the relative contribution of life history and morphological constraints selection on physiological performance.

Relatively weak selection on mtOX loci observed in our species suggests a potential need for compensatory evolution of nuOX loci to maintain metabolic function (Hill 2020). We found no evidence of relaxed or positive selection in the nuclear genome using PGLS regressions and locus-wide comparisons among functional groups, however our codon models demonstrate elevated evolutionary rates in the nuclear genome in all three focal species (Table 1), consistent with the hypothesis of nuclear compensation in lungless salamanders (H_4). However, we found no relationship between mitonuclear epistasis (as median difference or percent overlap in

distributions of ω between genomes) and metabolic rates, rejecting the hypothesis that mitonuclear interactions predict physiological performance (H_5). Nuclear compensation has been observed in taxa including angiosperms, insects, crustaceans, birds, and mammals (Barreto and Burton 2013; Adrion et al. 2015; Havird et al. 2015), producing coevolutionary patterns in OXPHOS loci (our focus here) and mitochondrial ribosomes, which are themselves encoded by two genomes with component RNAs encoded in the mitochondrion and protein subunits encoded in the nucleus. *P. vandykei* showed no elevated ω in nuclear loci associated with the mitochondrial large ribosome, suggesting compensatory evolution is restricted to OXPHOS loci in this species. In contrast, *P. glutinosus* largely showed strict selective constraint on OXPHOS loci (with the exception of complex IV), but showed strong purifying selection on mitochondrial ribosome binding relative to other species. These results suggest different species may employ different mechanisms of nuclear compensation to maintain physiological function in the lungless salamanders. Expanded taxonomic sampling will help characterize variation in the genomic targets of selection and the strength of selection acting on them. Whether this heterogeneity covaries at broader taxonomic scales with functional constraints on physiology is an intriguing possibility to explore in future studies.

Our results point to potentially complex patterns of selection and mitonuclear coevolution underlying metabolic physiology in the Plethodontidae. Specifically, our codon models indicate that selection strength on mitochondrial and nuclear OXPHOS loci varies alongside metabolic rates and functional constraints on metabolism, with multiple targets and modes of selection operating on physiological performance both between and within species. Despite low taxonomic sampling and low phylogenetic signal, we took advantage of our large sample of genomic loci to test hypotheses of molecular evolution across taxa (H_{P1}-H_{P24}). Most clearly, these hypothesis

tests indicate that selection strength in *P. cinereus*, our smallest species under weakest SA:V constraint, is particularly lax in gene ontology categories related to respiration (GO:0022900, GO:0042773, GO:0070469; H_{P10}) and regulation of metabolism (GO:0019222; H_{P10}). In contrast, *P. glutinosus* demonstrates strict selective constraint on GOs associated with biosynthesis (GO:0006633; H_{P5}), electron transport during OXPHOS (GO:0042773; H_{P11}), and the OXPHOS supercomplexes of the respirasome (GO:0070469; H_{P11}), with positive selection restricted to complex IV and ribosome binding (GO:0045277, GO:0097177; H_{P5}). *P. vandykei* showed different patterns of selection still, with positive selection on OXPHOS function (GO:0042773, GO:0070469; H_{P12}) but constraint on mitochondrial ribosome function (GO:0005762; H_{P6}).

The specific physiological mechanisms underlying these selective patterns require investigation, but together these results suggest in general terms that reduced physical constraints on metabolic physiology can indeed allow for reduced selective constraints on metabolic genes in lungless salamanders. While small-bodied *P. cinereus* appears to have escaped strict selection on metabolic efficiency, selection on the much larger *P. glutinosus* has been characterized by a combination both adaptive sequence evolution and strict purifying selection on OXPHOS, whereas medium-sized *P. vandykei* demonstrates relaxed selection on OXPHOS loci at a rate intermediate between the other two species. The fact that both *P. cinereus* and *P. vandykei* both demonstrate elevated evolutionary rates relative to each other (GO:0042773, GO: 0070469; Table 1), suggests that positive selection is acting on different loci and even different codon sites in these species, and that mechanisms of physiological adaptation are highly taxon-specific in this group. Selective constraint on responses to hypoxia in this species (GO:0071456; H_{P9}) may represent selective pressure due to increased hypoxic stress in *P. vandykei*, though it is unclear why an intermediate body size or large genome in this species could underlie this relationship.

Another possibility is in the different life history of *P. vandykei*, which is intimately associated with running streams (Brodie 1970). Regular contact with water could make cutaneous respiration much less efficient, as oxygen diffuses much more slowly through water than air. This may present an occasional but severe constraint on transport rates specific to this species in our sample, and could have resulted in selection on loci to accommodate this specific constraint.

To definitively link patterns of selection to metabolic performance will require a combination of expanded taxonomic and experimental investigations. Here, we focused on coding sequence variation in OXPHOS loci, however selection on gene expression and other mitochondrial loci could also contribute to observed variation in physiology. Expression can govern rates of molecular evolution, with highly expressed loci subject to stronger evolutionary constraint (Adrion et al. 2015), meaning relative expression of mtDNA and nuclear OXPHOS genes could be one target or even the primary target of selection underlying metabolic physiology in lungless salamanders. Further, mtDNA ribosomes and the molecules that synthesize them (mitochondrial transfer RNAs and nuclear-encoded aminoacyl tRNA synthetase proteins) both show particularly clear signals of compensatory evolution in some taxa, both at the coding and the expression level (Sloan et al. 2013; Adrion et al. 2015; Barreto et al. 2018), thus it remains possible that mitonuclear coadaptation of ribosomal sequences underlies adaptation of physiological performance in our sample. Some mitonuclear effects interact with temperature to determine metabolic rates (Arnqvist et al. 2010), meaning selection may only act on physiology within a particular temperature range, thus tests for evolutionary relationships between selection and physiology will need to measure performance across multiple temperatures. Quantifying the fitness effects of variation in metabolism and identifying adaptive combinations of interacting mitonuclear loci (Dowling et al. 2007) will also greatly improve

future studies linking physiology and selection. With these issues in mind, future studies in lungless salamanders can expand upon the general patterns of selection identified here to successfully link physiology, functional constraint, and selection across genomes to patterns of adaptive performance in nature.

REFERENCES

Adrion, J. R., P. S. White, and K. L. Montooth. 2015. The roles of compensatory evolution and constraint in aminoacyl tRNA synthetase evolution. Mol. Biol. Evol. 33:152–161.

Alexa, A., and J. Rahnenfuhrer. 2020. topGO: Enrichment analysis for gene ontology.

Arnqvist, G., D. K. Dowling, P. Eady, L. Gay, T. Tregenza, M. Tuda, and D. J. Hosken. 2010. Genetic architecture of metabolic rate: environment specific epistasis between mitochondrial and nuclear genes in an insect. Evolution 64:3354–3363.

Bankevich, A., S. Nurk, D. Antipov, A. A. Gurevich, M. Dvorkin, A. S. Kulikov, V. M. Lesin, S. I. Nikolenko, S. Pham, A. D. Prjibelski, A. V Pyshkin, A. V Sirotkin, N. Vyahhi, G. Tesler, M. A. Alekseyev, and P. A. Pevzner. 2012. SPAdes: A new genome assembly algorithm and its applications to single-cell sequencing. J. Comput. Biol. 19:455–477.

Bankhead, P., M. B. Loughrey, J. A. Fernández, Y. Dombrowski, D. G. McArt, P. D. Dunne, S. McQuaid, R. T. Gray, L. J. Murray, H. G. Coleman, J. A. James, M. Salto-Tellez, and P. W. Hamilton. 2017. QuPath: Open source software for digital pathology image analysis. Sci. Rep. 7:16878.

Barreto, F. S., and R. S. Burton. 2013. Evidence for compensatory evolution of ribosomal proteins in response to rapid divergence of mitochondrial rRNA. Mol. Biol. Evol. 30:310–314.

Barreto, F. S., E. T. Watson, T. G. Lima, C. S. Willett, S. Edmands, W. Li, and R. S. Burton. 2018. Genomic signatures of mitonuclear coevolution across populations of *Tigriopus californicus*. Nat. Ecol. Evol. 2:1250–1257.

Bielawski, J. P., and Z. Yang. 2004. A maximum likelihood method for detecting functional divergence at individual codon sites, with application to gene family evolution. J. Mol. Evol. 59:121–132.

Bolger, A. M., M. Lohse, and B. Usade. 2014. Trimmomatic: A flexible trimmer for Illumina sequence data. Bioinformatics 30:2114–2120.

Brodie, E. D., Jr. 1970. Western salamanders of the genus *Plethodon*: Systematics and geographic variation. Herpetologica 26:468–516.

Buchfink, B., K. Reuter, and H. Drost. 2021. Sensitive protein alignments at tree-of-life scale using DIAMOND. Nat. Methods 18:366–368.

Burggren, W. W., and R. Moalli. 1984. "Active" regulation of cutaneous gas exchange by capillary recruitment in amphibians: experimental evidence and a revised model for skin respiration. Respir. Physiol. 55:379–392.

Calow, P. 1987. Towards a definition of functional ecology. Funct. Ecol. 1:57–61.

Castresana, J. 2000. Selection of conserved blocks from multiple alignments for their use in phylogenetic analysis. Mol. Biol. Evol. 17:540–552.

Chen, S., Y. Zhou, Y. Chen, and J. Gu. 2018. fastp: an ultra-fast all-in-one FASTQ preprocessor. Bioinformatics 34:i884–i890.

Chong, R. A., and R. L. Mueller. 2013. Low metabolic rates in salamanders are correlated with weak selective constraints on mitochondrial genes. Evolution 67:894–899.

Cooper, N., G. H. Thomas, C. Venditti, A. Meade, and R. P. Freckleton. 2016. A cautionary note on the use of Ornstein Uhlenbeck models in macroevolutionary studies. Biol. J. Linn. Soc. 118:64–77.

Czopek, J. 1961. Vascularization of respiratory surfaces in some Plethodontidae. Zool. Pol. 11:131–148.

Donath, A., F. Juhling, M. Al-Arab, S. H. Bernhart, F. Reinhardt, P. F. Stadler, M. Middendorf, and M. Bernt. 2019. Improved annotation of protein-coding genes boundaries in metazoan mitochondrial genomes. Nucleic Acids Res. 47:10543–10552.

Douglass, A. P., C. E. O'Brien, B. Offei, A. Y. Coughlan, R. A. Ortiz-Merino, G. Butler, K. P. Byrne, and K. H. Wolfe. 2019. Coverage-versus-length plots, a simple quality control step for de novo yeast genome sequence assemblies. G3 Genes|Genomes|Genetics 9:879–887.

Dowling, D. K., U. Friberg, F. Hailer, and G. Arnqvist. 2007. Intergenomic epistasis for fitness: Within-population interactions between cytoplasmic and nuclear genes in *Drosophila melanogaster*. Genetics 175:235–244.

Emms, D. M., and S. Kelly. 2019. OrthoFinder: Phylogenetic orthology inference for comparative genomics. Genome Biol. 20:1–14.

Evans, M. L., and L. Bernatchez. 2012. Oxidative phosphorylation gene transcription in whitefish species pairs reveals patterns of parallel and nonparallel physiological divergence. J. Evol. Biol. 25:1823–1834.

Feder, M. E. 1988. Exercising with and without lungs II: Experimental elimination of pulmonary and buccopharyngeal gas exchange in individual salamanders (*Ambystoma tigrinum*). J. Exp. Biol. 138:487–497.

Feder, M. E., and W. W. Burggren. 1985. Cutaneous gas exchange in vertebrates: Design, patterns, control and implications. Biol. Rev. Camb. Philos. Soc. 60:1–45.

Feder, M. E., and W. W. Burggren (eds). 1992. Environmental physiology of the amphibians. University of Chicago Press, Chicago, IL.

Gillooly, J. F., J. H. Brown, and G. B. West. 2001. Effects of size and temperature on metabolic rate. Science 293:2248–2252.

Gillooly, J. F., J. P. Gomez, E. V Mavrodiev, Y. Rong, and E. S. Mclamore. 2016. Body mass scaling of passive oxygen diffusion in endotherms and ectotherms. Proc. Natl. Acad. Sci. U. S. A. 113:5340–5345.

Goldman, N., and Z. Yang. 1994. A codon-based model of nucleotide substitution for protein-coding DNA sequences. Mol. Biol. Evol. 11:725–736.

Götz, S., J. M. García-Gómez, J. Terol, T. D. Williams, S. H. Nagaraj, M. J. Nueda, M. Robles, M. Talón, J. Dopazo, and A. Conesa. 2008. High-throughput functional annotation and data mining with the Blast2GO suite. Nucleic Acids Res. 36:3420–3435.

Grabherr, M. G., B. J. Haas, M. Yassour, J. Z. Levin, D. A. Thompson, I. Amit, X. Adiconis, L. Fan, R. Raychowdhury, Q. Zeng, Z. Chen, E. Mauceli, N. Hacohen, A. Gnirke, N. Rhind, F. di Palma, B. W. Birren, C. Nusbaum, K. Lidbland-Toh, N. Friedman, and A. Regev. 2013. Trinity: Reconstructing a full-length transcriptome without a genome from RNA-Seq data. Nat. Biotechnol. 29:644–652.

Gregory, T. R. 2016. Animal Genome Size Database.

Gros, P. A., H. Le Nagard, and O. Tenaillon. 2009. The evolution of epistasis and its links with genetic robustness, complexity and drift in a phenotypic model of adaptation. Genetics 182:277–293.

Hansen, T. F., J. Pienaar, and S. H. Orzack. 2008. A comparative method for studying adaptation to a randomly evolving environment. Evolution 62:1965–1977.

Havird, J. C., and D. B. Sloan. 2016. The roles of mutation, selection, and expression in determining relative rates of evolution in mitochondrial versus nuclear genomes. Mol. Biol. Evol. 33:3042–3053.

Havird, J. C., N. S. Whitehill, C. D. Snow, and D. B. Sloan. 2015. Conservative and compensatory evolution in oxidative phosphorylation complexes of angiosperms with highly divergent rates of mitochondrial genome evolution. Evolution 69:3069–3081.

Hill, G. E. 2020. Mitonuclear compensatory coevolution. Trends Genet. 36:403–414.

Johnson, B. B., T. R. Gregory, J. B. Searle, and J. P. Sparks. n.d. Biological size as a predictor of physiological performance and adaptation: Evidence from lungless salamanders. Unpubl. data.

Johnson, B. B., J. B. Searle, and J. P. Sparks. 2021a. Genome size influences adaptive plasticity of water loss, but not metabolic rates, in lungless salamanders. J. Exp. Biol. 224:jeb242196.

Johnson, B. B., J. B. Searle, and J. P. Sparks. 2021b. Novel allometric estimators improve estimation accuracy of body surface area, volume, and surface area-to-volume ratio in lungless salamanders (Urodela: Plethodontidae). Herpetologica 77:219–226.

Kakehashi, R., and A. Kurabayashi. 2021. Patterns of natural selection on mitochondrial protein-coding genes in lungless salamanders: Relaxed purifying selection and presence of positively selected codon sites in the family Plethodontidae. Int. J. Genomics 2021:6671300.

Katoh, K., and D. M. Standley. 2013. MAFFT multiple sequence alignment software version 7: Improvements in performance and usability. Mol. Biol. Evol. 30:772–780.

Kearney, M. R., M. Jusup, M. A. McGeoch, S. A. L. M. Kooijman, and S. L. Chown. 2021. Where do functional traits come from? The role of theory and models. Funct. Ecol. 35:1385–1396.

Kempes, C. P., M. A. R. Koehl, and G. B. West. 2019. The scales that limit: The physical boundaries of evolution. Front. Ecol. Evol. 7:242.

Lillywhite, H. B., and P. F. A. Maderson. 1988. The structure and permeability of integument. Am. Zool. 28:945–962.

McKenzie, M., M. Lazarou, D. R. Thorburn, and M. T. Ryan. 2007. Analysis of mitochondrial subunit assembly into respiratory chain complexes using Blue Native polyacrylamide gel electrophoresis. Anal. Biochem. 364:128–137.

Muller, H. J. 1964. The relation of recombination to mutational advance. Mutat. Res. 1:2–9.

Nabholz, B., H. Ellegren, and J. B. W. Wolf. 2012. High levels of gene expression explain the strong evolutionary constraint of mitochondrial protein-coding genes. Mol. Biol. Evol. 30:272–284.

Okie, J. G. 2013. General models for the spectra of surface area scaling strategies of cells and organisms: Fractality, geometric dissimilitude, and internalization. Am. Nat. 181:421–439.

Paradis, E. 2012. Analysis of phylogenetics and evolution with R. 2nd ed. Springer, New York, NY, USA.

Pastore, M. 2018. Overlapping: A R package for estimating overlapping in empirical distributions. J. Open Source Softw. 3:1023.

Piccinini, G., M. Iannello, G. Puccio, F. Plazzi, J. C. Havird, and F. Ghiselli. 2021. Mitonuclear coevolution, but not nuclear compensation, drives evolution of OXPHOS complexes in bivalves. Mol. Biol. Evol. 38:2597–2614.

Piiper, J., R. N. Gatz, and E. C. Crawford Jr. 1976. Gas transport characteristics in an exclusively skin-breathing salamander, *Desmognathus fuscus* (Plethodontidae). Pp. 339–356 *in* G. M. Hughes, ed. Respiration of Amphibious Vertebrates. Academic Press.

Popadin, K. Y., S. I. Nikolaev, T. Junier, M. Baranova, and S. E. Antonarakis. 2012. Purifying selection in mammalian mitochondrial protein-coding genes is highly effective and congruent with evolution of nuclear genes. Mol. Biol. Evol. 30:347–355.

R Core Team. 2020. R: A language and environment for statistical computing.

Rand, D. M., R. A. Haney, and A. J. Fry. 2004. Cytonuclear coevolution: The genomics of cooperation. Trends Ecol. Evol. 19:645–653.

Rath, S., R. Sharma, R. Gupta, T. Ast, C. Chan, T. J. Durham, R. P. Goodman, Z. Grabarek, M. E. Haas, W. H. W. Hung, P. R. Joshi, A. A. Jourdain, S. H. Kim, A. V Kotrys, S. S. Lam, J. G. McCoy, J. D. Meisel, M. Miranda, A. Panda, A. Patgiri, R. Rogers, S. Sadre, H. Shah, O. S. Skinner, T.-L. To, M. A. Walker, H. Wang, P. S. Ward, J. Wengrod, C.-C. Yuan, S. E. Calvo, and V. K. Mootha. 2021. MitoCarta3.0: An updated mitochondrial proteome now with sub-organelle localization and pathway annotations. Nucleic Acids Res. 49:D1541–D1547.

Reagan, N. L., and P. A. Verrell. 1991. The evolution of plethodontid salamanders: Did terrestrial mating facilitate lunglessness? Am. Nat. 138:1307–1313.

Riddell, E. A., E. Y. Roback, C. E. Wells, K. R. Zamudio, and M. W. Sears. 2019. Thermal cues drive plasticity of desiccation resistance in montane salamanders with implications for climate change. Nat. Commun. 10:4091.

Shen, Y.-Y., P. Shi, Y.-B. Sun, and Y.-P. Zhang. 2009. Relaxation of selective constraints on avian mitochondrial DNA following the degeneration of flight ability. Genome Res. 19:1760–1765.

Signes, A., and E. Fernandez-Vizarra. 2018. Assembly of mammalian oxidative phosphorylation complexes I – V and supercomplexes. Essays Biochem. 62:255–270.

Sloan, D. B., D. A. Triant, M. Wu, and D. R. Taylor. 2013. Cytonuclear interactions and relaxed selection accelerate sequence evolution in organelle ribosomes. Mol. Biol. Evol. 31:673–682.

Stoffel, M. A., S. Nakagawa, and H. Schielzeth. 2021. partR2 : Partitioning R2 in generalized linear mixed models. PeerJ 9:e11414.

Storey, J. D. 2002. A direct approach to false discovery rates. J. R. Stat. Soc. B 64:479–498.

Sun, S., Q. Li, L. Kong, and H. Yu. 2017. Limited locomotive ability relaxed selective constraints on molluscs mitochondrial genomes. Sci. Rep. 7:10628.

Sun, Y.-B., Y.-Y. Shen, D. M. Irwin, and Y.-P. Zhang. 2011. Evaluating the roles of energetic functional constraints on teleost mitochondrial-encoded protein evolution. Mol. Biol. Evol. 28:39–44.

Suyama, M., D. Torrents, and P. Bork. 2006. PAL2NAL: Robust conversion of protein sequence alignments into the corresponding codon alignments. Nucleic Acids Res. 34:W609–W612.

University of California, Berkeley. 2021. AmphibiaWeb. https://amphibiaweb.org/.

Weadick, C. J., and B. S. W. Chang. 2012. An improved likelihood ratio test for detecting site-specific functional divergence among clades of protein-coding genes. Mol. Biol. Evol. 29:1297–1300.

Yang, Z. 2007. PAML 4 : Phylogenetic Analysis by Maximum Likelihood. Mol. Biol. Evol. 24:1586–1591.

Yang, Z., and R. Nielsen. 2002. Codon-substitution models for detecting molecular adaptation at individual sites along specific lineages. Mol. Biol. Evol. 19:908–917.

Yang, Z., R. Nielsen, N. Goldman, and A.-M. K. Pedersen. 2000. Codon-substitution models for heterogeneous selection pressure at amino acid sites. Genetics 155:431–449.

Zhang, J., R. Nielsen, and Z. Yang. 2005. Evaluation of an improved branch-site likelihood method for detecting positive selection at the molecular level. Mol. Biol. Evol. 22:2472–2479.

Table 1. Enriched gene ontology (GO) terms under selection in three species of lungless salamander. For each enriched GO term per species, median ω represents the median selection strength on all loci annotated with the term. The ratio ω_{FG} / ω_{BG} represents the relative selection strength across GO-annotated loci in the foreground (FG) species relative to the other two background (BG) species.

		P. cinereus		***P. glutinosus***		***P. vandykei***	
GO term	**GO annotation**	**median ω**	**ω_{FG} / ω_{BG}**	**median ω**	**ω_{FG} / ω_{BG}**	**median ω**	**ω_{FG} / ω_{BG}**
GO:0005762	mitochondrial large ribosomal subunit	-	-	-	-	0.483	0.034
GO:0006633	fatty acid biosynthetic process	0.707	0.180	0.039	0.057	-	-
GO:0010510	regulation of acetyl-CoA biosynthetic process	5.321	7.809	-	-	-	-
GO:0019222	regulation of metabolic process	2.236	14.583	-	-	-	-
GO:0022900	electron transport chain	3.879	34.988	-	-	-	-
GO:0034599	cellular response to oxidative stress	3.079	1.577	-	-	-	-
GO:0035264	multicellular organism growth	-	-	10.453	1.249	-	-
GO:0042594	response to starvation	3.309	11.918	-	-	-	-
GO:0042773	ATP synthesis coupled electron transport	3.879	41.915	0.037	0.117	4.224	46.816
GO:0045277	respiratory chain complex IV	-	-	3.223	0.160	-	-
GO:0048872	homeostasis of number of cells	12.169	7.381		-	-	-
GO:0070469	respirasome	6.082	123.062	0.037	0.117	3.985	35.050
GO:0071456	cellular response to hypoxia	-	-	-	-	0.806	0.766
GO:0097177	mitochondrial ribosome binding	-	-	12.064	4.261	-	-

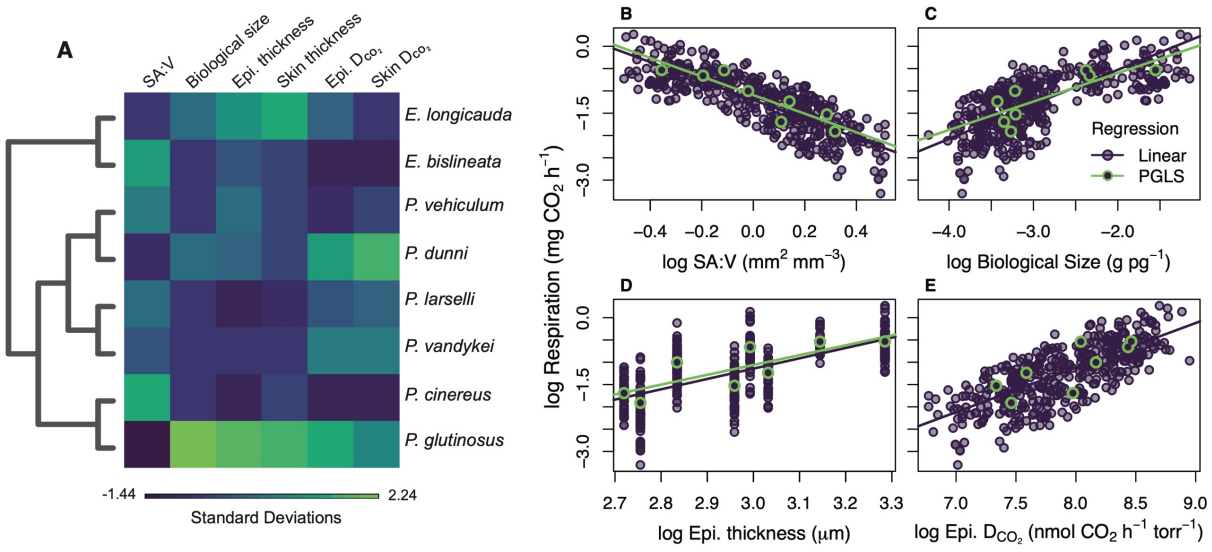

Figure 1. Relationships between physical constraints and gross metabolic rates (respiration) in eight species of lungless salamander. (A) Standardized phenotype scores visualizing variation of surface area-to-volume ratios (SA:V), biological size, epidermis thickness, skin thickness, epidermal diffusing capacity for CO_2 (D_{CO2}), and total skin D_{CO2} across phylogeny. (B) SA:V covaries negatively gross respiration across individuals (purple points) and species (green points) using linear and phylogenetic least squares (PGLS) regressions, respectively. (C) Biological size positively covaries with gross metabolism at both individual and species scales, as does thickness of the epidermis (D). (E) Epidermal D_{CO2} covaries with gross metabolism at the individual level, but not across evolutionary history. Significant regressions are represented with fitted model slopes.

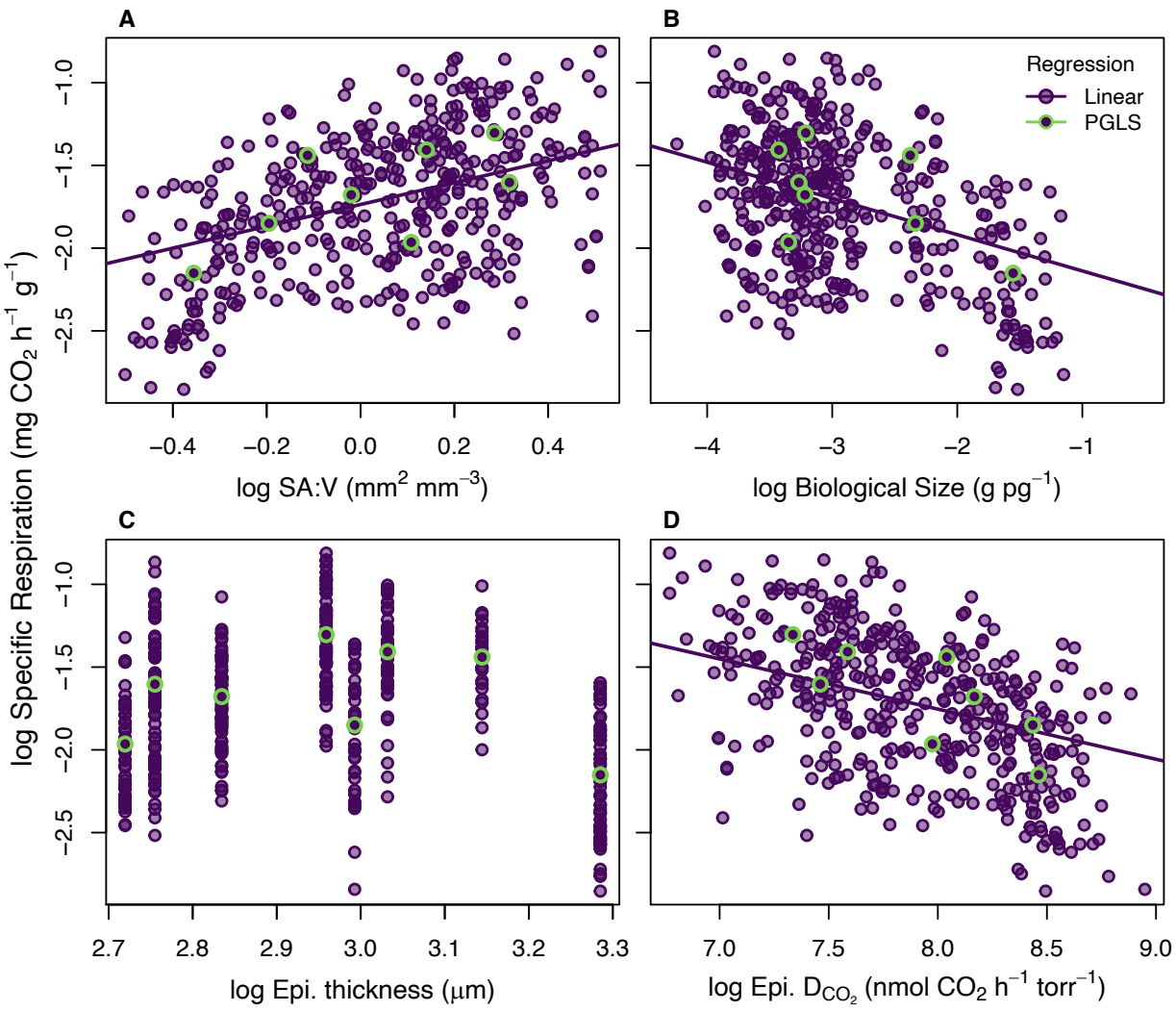

Figure 2. Regressions between physical constraints and mass-specific metabolic rate (respiration) in eight species of lungless salamander. (A) Surface area-to-volume ratio (SA:V) and (B) biological size both covary with individual-level specific metabolism (purple points). (C) Epidermal thickness does not covary with specific respiration, but epidermal diffusing capacity for CO_2 (D_{CO2}) does covary (D). No constraints covary with specific metabolism across evolutionary history (green points). Significant regressions are represented with fitted model slopes.

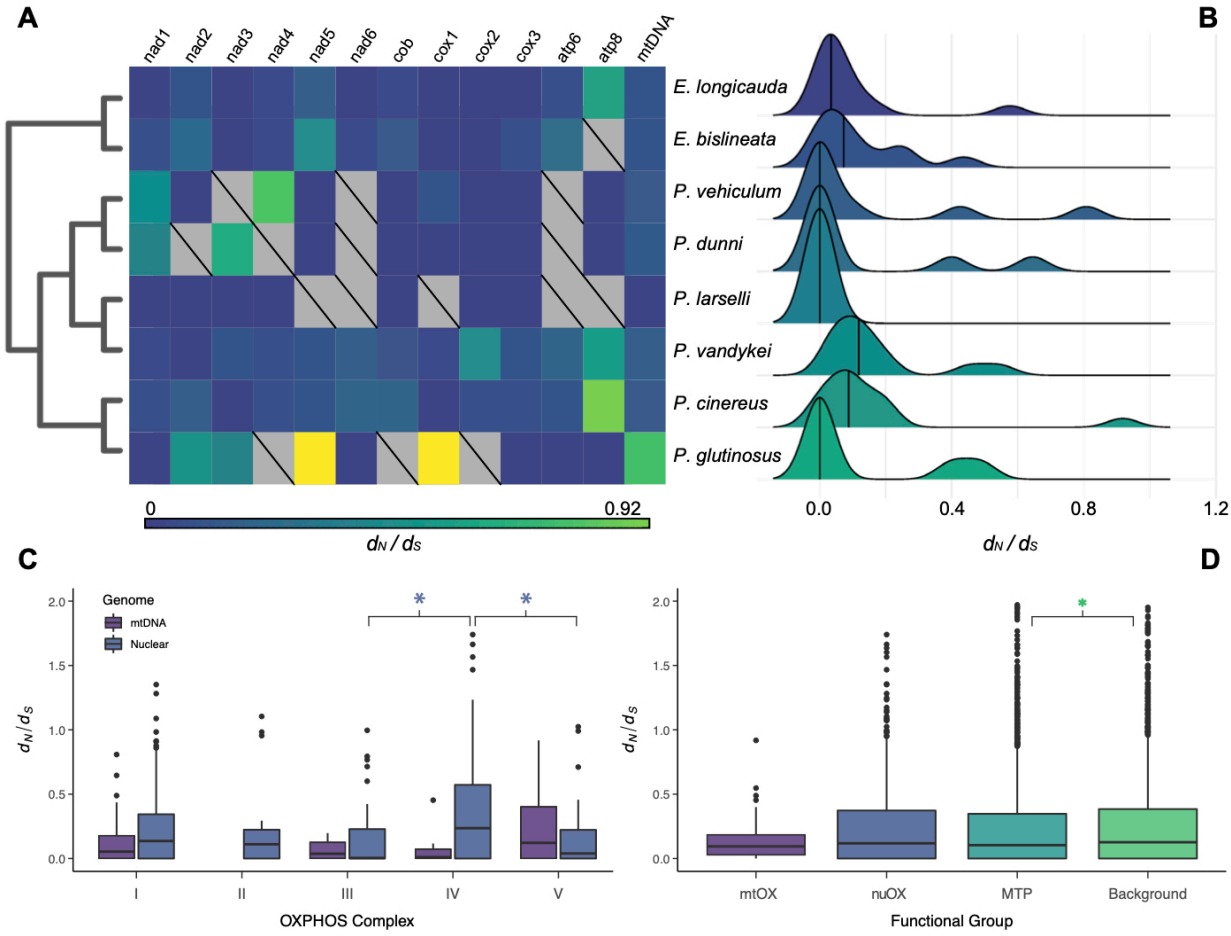

Figure 3. Strength of selection (d_N/d_S) across lungless salamander species and functional categories of genomic loci. (A) Selection strength on 12 of 13 mitochondrial OXPHOS (mtOX) loci, plus mean estimates across loci (mtDNA) for eight species. d_N/d_S values >1 are colored in yellow, and missing data are colored gray. (B) Empirical distributions of selection strength across all loci for each species, with outliers (>1.2) removed. Note that colors do not correspond to selection strength as visualized in panel A. (C) Selection strength on mitochondrial and nuclear-encoded loci organized by their function within oxidative phosphorylation (OXPHOS) complexes. Significant differences between complexes are noted with an asterisk. (D) Selection strength on mtOX loci and nuclear functional groups in three species. Significant differences are noted with an asterisk.

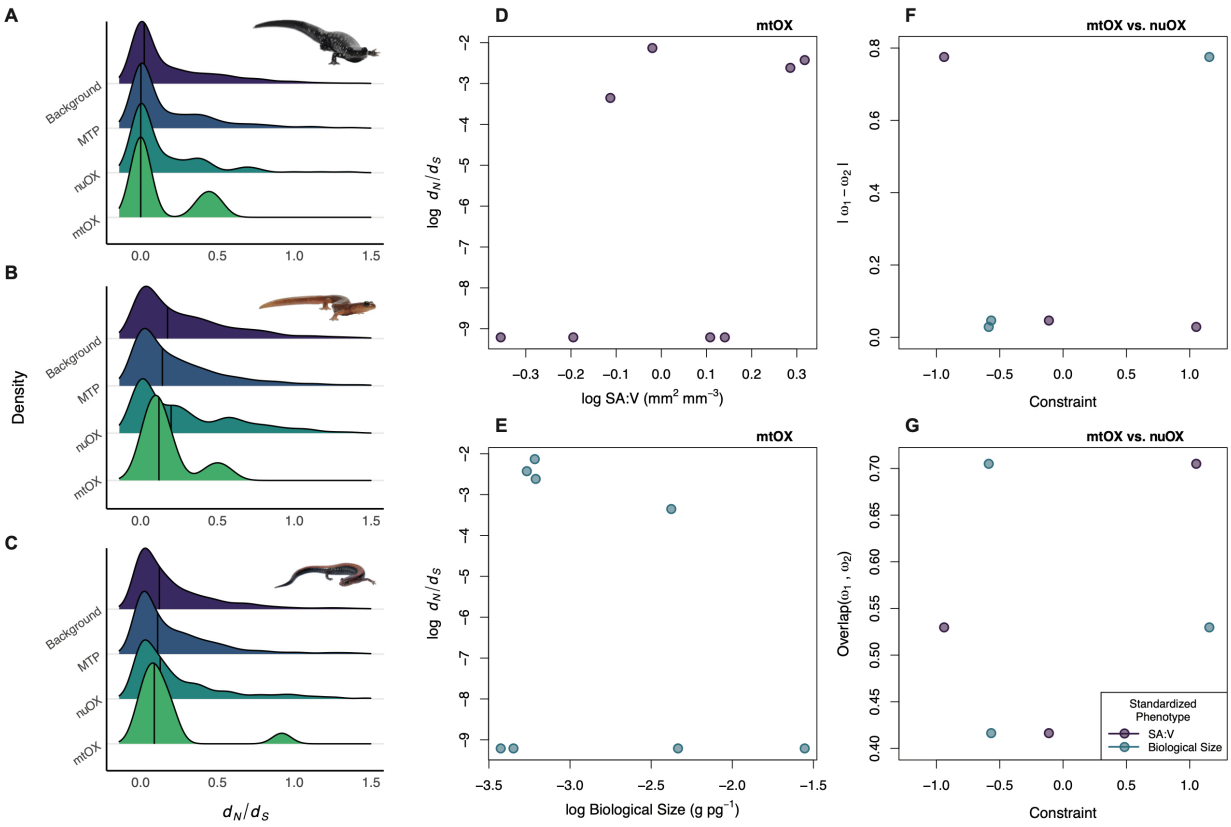

Figure 4. Species-specific selection strength (d_N/d_S) on functional categories and evolutionary regressions between physical constraints and natural selection. (A-C) Empirical distributions of locus-wide selection strength in *P. glutinosus* (A), *P. vandykei* (B), and *P. cinereus* (C). (D) Surface area-to-volume ratio (SA:V) does not covary with selection on mitochondrial OXPHOS (mtOX) loci following a phylogenetic least squares regression, nor does biological size (E). (F) Neither constraint phenotype covaries with mitonuclear epistasis, defined as the absolute difference in selection strength (ω) between mtOX and nuclear OXPHOS (nuOX) loci. (G) Neither phenotype covaries with mitonuclear epistasis, defined as the overlap in empirical distributions of ω on mtOX and nuOX loci. Phenotypes in F-G are presented as standardized values for visualization together.

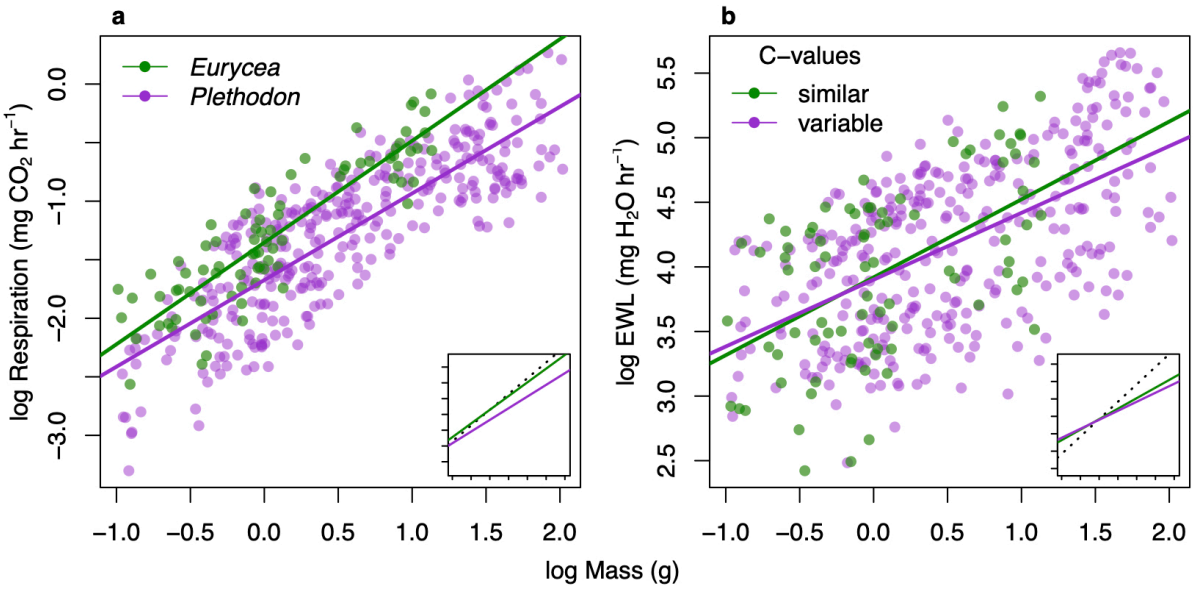

Figure S1. Lineage-specific allometric scaling and variance of gross physiological responses with body mass, tested across the complete dataset. Slopes and variances are statistically indistinguishable between *Plethodon* (purple) and *Eurycea* (green) for both metabolic rate (respiration) (**a**) and evaporative water loss (EWL) (**b**) despite differences in C-value diversity between groups. Inset graphs present the same data to illustrate deviations from isometry (slope = 1) using the same intercept as *Eurycea*.

Table S1. Species sampling and body size and C-value diversity of individuals measured in this study. C-value estimates are the median value obtained for each species from the animal genome size database (Gregory, 2016). Mass estimates are the mean of individual body mass measurements taken at the beginning of physiological trials.

Species	**N**	**Mass (g)**	**C-value (pg)**
Eurycea bislineata	18	0.79	24.50
Eurycea longicauda	7	2.46	27.35
Plethodon cinereus	24	0.71	22.64
Plethodon dunni	12	3.41	38.80
Plethodon glutinosus	20	5.03	28.00
Plethodon larselli	12	1.32	48.55
Plethodon vandykei	19	1.97	69.30
Plethodon vehiculum	14	1.21	38.05

Table S2. Model comparisons for all tested linear models. Comparisons are made for morphological and environmental models within each data subset. Nested models are listed in order of statistical support by ΔAICc, with each set of compared models separated by a solid line. Entries in bold represent statistically significant parameters ($p < 0.05$).

Model Type	Dataset	Response	Predictor	df	Log likelihood	AICc	ΔAICc
morphological	full data	Resp	**Mass**	8	-97.28	232.73	0
morphological	full data	Resp	Mass + C-value	9	-97.2	235.66	2.93
morphological	full data	Resp	Mass * C-value	10	-97.17	239.9	6.48
morphological	full data	Resp	C-value	8	-155.01	341.62	108.89
morphological	full data	sResp	**Mass**	8	-97.63	233.41	0
morphological	full data	sResp	Mass + C-value	9	-97.56	236.35	2.93
morphological	full data	sResp	Mass * C-value	10	-97.53	240.56	7.15
morphological	full data	sResp	C-value	8	-109.46	252.96	19.55
morphological	full data	EWL	**Mass**	8	-27.24	96.95	0
morphological	full data	EWL	Mass + C-value	9	-24.13	99.53	2.57
morphological	full data	EWL	Mass * C-value	10	-22.21	101.24	4.29
morphological	full data	EWL	C-value	8	-73.76	181.15	84.2
morphological	full data	sEWL	**Mass**	8	-27.52	97.61	0
morphological	full data	sEWL	Mass + C-value	9	-24.68	100.55	2.94
morphological	full data	sEWL	Mass * C-value	10	-22.71	102.23	4.62
morphological	full data	sEWL	C-value	8	-89.98	214.78	117.17
morphological	full data	CWL	**Mass**	8	-27.3	97.15	0
morphological	full data	CWL	Mass + C-value	9	-24.37	99.97	2.82
morphological	full data	CWL	Mass * C-value	10	-22.43	101.67	4.52
morphological	full data	CWL	C-value	8	-42.75	125.13	27.98
morphological	full data	*r*	**Mass**	8	-30.29	103.11	0
morphological	full data	*r*	Mass + C-value	9	-27.28	105.71	2.6
morphological	full data	*r*	**Mass * C-value**	10	-24.89	106.68	3.57
morphological	full data	*r*	C-value	8	-44.36	128.27	25.16
morphological	10 C	Resp	**Mass**	6	-20.2	64.8	0
morphological	10 C	Resp	Mass + C-value	7	-19.84	67.3	2.5
morphological	10 C	Resp	Mass * C-value	8	-19.47	70.69	5.89
morphological	10 C	Resp	C-value	6	-70.71	159.63	94.83
morphological	10 C	sResp	**Mass**	6	-19.8	64.01	0

morphological	10 C	sResp	Mass + C-value	7	-19.46	66.51	2.51
morphological	10 C	sResp	Mass * C-value	8	-19.14	69.98	5.97
morphological	10 C	sResp	C-value	6	-25.89	72.65	8.64
morphological	10 C	EWL	**Mass**	6	14.02	1.33	0
morphological	10 C	EWL	Mass + C-value	7	14.32	6.94	5.61
morphological	10 C	EWL	Mass * C-value	8	14.42	11.53	10.2
morphological	10 C	EWL	C-value	6	-14.97	50.32	49
morphological	10 C	sEWL	**Mass**	6	14.33	0.7	0
morphological	10 C	sEWL	Mass + C-value	7	14.58	6.38	5.68
morphological	10 C	sEWL	Mass * C-value	8	14.69	10.96	10.26
morphological	10 C	sEWL	C-value	6	-35.48	91.53	90.83
morphological	10 C	CWL	**Mass**	6	14.44	0.51	0
morphological	10 C	CWL	Mass + C-value	7	14.69	6.2	5.68
morphological	10 C	CWL	Mass * C-value	8	14.8	10.78	10.27
morphological	10 C	CWL	C-value	6	-3.61	31.32	30.8
morphological	10 C	*r*	**Mass**	6	15.48	-1.62	0
morphological	10 C	*r*	Mass + C-value	7	15.93	3.87	5.48
morphological	10 C	*r*	Mass * C-value	8	16.15	8.32	9.94
morphological	10 C	*r*	C-value	6	-2.44	28.94	30.56
morphological	15 C	Resp	**Mass**	6	-62.57	148.7	0
morphological	15 C	Resp	Mass + C-value	7	-62.57	151.64	2.94
morphological	15 C	Resp	Mass * C-value	8	-61.28	152.7	4
morphological	15 C	Resp	C-value	6	-97.99	213.81	65.11
morphological	15 C	sResp	**Mass**	6	-62.86	149.27	0
morphological	15 C	sResp	Mass + C-value	7	-62.86	152.2	2.93
morphological	15 C	sResp	Mass * C-value	8	-61.54	153.19	3.92
morphological	15 C	sResp	C-value	6	-68.47	156.92	7.65
morphological	15 C	EWL	**Mass * C-value**	8	-18.37	76.77	0
morphological	15 C	EWL	**Mass + C-value**	7	-21.55	78.11	1.33
morphological	15 C	EWL	**Mass**	6	-26.91	80.13	3.36
morphological	15 C	EWL	C-value	6	-62.76	144.12	67.34
morphological	15 C	sEWL	**Mass * C-value**	8	-19.14	78.29	0
morphological	15 C	sEWL	**Mass + C-value**	7	-22.37	79.7	1.42
morphological	15 C	sEWL	**Mass**	6	-27.54	81.48	3.2
morphological	15 C	sEWL	C-value	6	-56.6	134.51	56.22
morphological	15 C	CWL	**C-value**	6	-24.82	76.99	0
morphological	15 C	CWL	**Mass * C-value**	8	-18.86	77.74	0.75
morphological	15 C	CWL	**Mass + C-value**	7	-22.06	79.11	2.13
morphological	15 C	CWL	**Mass**	6	-27.31	80.99	4.01

morphological	15 C	*r*	**C-value**	6	-27.15	81.61	0
morphological	15 C	*r*	**Mass * C-value**	8	-21.78	83.43	1.81
morphological	15 C	*r*	**Mass + C-value**	7	-25.07	85	3.39
morphological	15 C	*r*	**Mass**	6	-30.43	87.34	5.72
morphological	0.3 kPa	Resp	**Mass**	6	-63.88	151.36	0
morphological	0.3 kPa	Resp	Mass + C-value	7	-63.82	154.38	3.02
morphological	0.3 kPa	Resp	Mass * C-value	8	-63.8	158.18	6.81
morphological	0.3 kPa	Resp	C-value	6	-109.32	236	84.63
morphological	0.3 kPa	sResp	**Mass**	6	-64.12	151.83	0
morphological	0.3 kPa	sResp	Mass + C-value	7	-64.07	154.85	3.02
morphological	0.3 kPa	sResp	Mass * C-value	8	-64.04	158.64	6.81
morphological	0.3 kPa	sResp	C-value	6	-69.4	158.94	7.11
morphological	0.3 kPa	EWL	**Mass**	6	-43.88	114.64	0
morphological	0.3 kPa	EWL	Mass + C-value	7	-42	117.75	3.11
morphological	0.3 kPa	EWL	Mass * C-value	8	-41.27	120.97	6.32
morphological	0.3 kPa	EWL	C-value	6	-67.35	153.86	39.22
morphological	0.3 kPa	sEWL	**Mass**	6	-44.31	115.51	0
morphological	0.3 kPa	sEWL	Mass + C-value	7	-42.65	118.92	3.41
morphological	0.3 kPa	sEWL	Mass * C-value	8	-41.9	122.14	6.63
morphological	0.3 kPa	sEWL	C-value	6	-81.04	182.17	66.66
morphological	0.3 kPa	CWL	**Mass**	6	-44.1	115.09	0
morphological	0.3 kPa	CWL	Mass + C-value	7	-42.37	118.41	3.32
morphological	0.3 kPa	CWL	Mass * C-value	8	-41.62	121.62	6.53
morphological	0.3 kPa	CWL	C-value	6	-52.84	130.02	14.93
morphological	0.3 kPa	*r*	**Mass**	6	-47.06	121	0
morphological	0.3 kPa	*r*	Mass + C-value	7	-45.37	124.28	3.29
morphological	0.3 kPa	*r*	Mass * C-value	8	-44.52	127.25	6.25
morphological	0.3 kPa	*r*	C-value	6	-54.35	133.04	12.04
morphological	0.6 kPa	Resp	**Mass**	6	-45.23	114.47	0
morphological	0.6 kPa	Resp	Mass + C-value	7	-45.1	117.35	2.88
morphological	0.6 kPa	Resp	Mass * C-value	8	-45.03	121.24	6.77
morphological	0.6 kPa	Resp	C-value	6	-93.57	204.86	90.4
morphological	0.6 kPa	sResp	**Mass**	6	-45.23	114.44	0
morphological	0.6 kPa	sResp	Mass + C-value	7	-45.11	117.32	2.88
morphological	0.6 kPa	sResp	Mass * C-value	8	-45.03	121.18	6.75
morphological	0.6 kPa	sResp	C-value	6	-54.33	128.83	14.39
morphological	0.6 kPa	EWL	**Mass**	6	27.51	-26.22	0
morphological	0.6 kPa	EWL	Mass + C-value	7	30.5	-23.97	2.25
morphological	0.6 kPa	EWL	Mass * C-value	8	32.32	-22.14	4.07

morphological	0.6 kPa	EWL	C-value	6	-17.44	54.59	80.81
morphological	0.6 kPa	sEWL	**Mass**	6	28.14	-27.32	0
morphological	0.6 kPa	sEWL	Mass + C-value	7	30.95	-24.85	2.46
morphological	0.6 kPa	sEWL	Mass * C-value	8	32.79	-23.09	4.22
morphological	0.6 kPa	sEWL	C-value	6	-26.29	73.41	100.73
morphological	0.6 kPa	CWL	**Mass**	6	28.03	-27.13	0
morphological	0.6 kPa	CWL	Mass + C-value	7	30.9	-24.74	2.39
morphological	0.6 kPa	CWL	Mass * C-value	8	32.71	-22.92	4.21
morphological	0.6 kPa	CWL	C-value	6	16.28	-6.91	20.22
morphological	0.6 kPa	*r*	**Mass**	6	30.57	-32.34	0
morphological	0.6 kPa	*r*	Mass + C-value	7	33.48	-29.9	2.44
morphological	0.6 kPa	*r*	**Mass * C-value**	8	35.72	-28.73	3.61
morphological	0.6 kPa	*r*	C-value	6	19.23	-12.9	19.44
morphological	10 C x 0.3 kPa	Resp	**Mass**	4	-21.26	57.09	0
morphological	10 C x 0.3 kPa	Resp	Mass + C-value	5	-20.88	59.35	2.26
morphological	10 C x 0.3 kPa	Resp	Mass * C-value	6	-20.53	62.42	5.32
morphological	10 C x 0.3 kPa	Resp	C-value	4	-58.15	125.42	68.32
morphological	10 C x 0.3 kPa	sResp	**Mass**	4	-21.39	57.33	0
morphological	10 C x 0.3 kPa	sResp	C-value	4	-23.94	59.32	1.99
morphological	10 C x 0.3 kPa	sResp	Mass + C-value	5	-21.02	59.62	2.29
morphological	10 C x 0.3 kPa	sResp	Mass * C-value	6	-20.69	62.71	5.38
morphological	10 C x 0.3 kPa	EWL	**Mass**	4	-9.18	36.26	0
morphological	10 C x 0.3 kPa	EWL	Mass + C-value	5	-9.14	41.2	4.95
morphological	10 C x 0.3 kPa	EWL	Mass * C-value	6	-9.05	45.04	8.78
morphological	10 C x 0.3 kPa	EWL	C-value	4	-28.33	67.69	31.44
morphological	10 C x 0.3 kPa	sEWL	**Mass**	4	-9.37	36.58	0
morphological	10 C x 0.3 kPa	sEWL	Mass + C-value	5	-9.36	41.51	4.93
morphological	10 C x 0.3 kPa	sEWL	Mass * C-value	6	-9.27	45.35	8.77
morphological	10 C x 0.3 kPa	sEWL	C-value	4	-40.03	91.1	54.52
morphological	10 C x 0.3 kPa	CWL	**Mass**	4	-9.2	36.29	0
morphological	10 C x 0.3 kPa	CWL	Mass + C-value	5	-9.18	41.24	4.95
morphological	10 C x 0.3 kPa	CWL	Mass * C-value	6	-9.1	45.08	8.79
morphological	10 C x 0.3 kPa	CWL	C-value	4	-19.28	52.61	16.31
morphological	10 C x 0.3 kPa	*r*	**Mass**	4	-8.39	34.83	0
morphological	10 C x 0.3 kPa	*r*	Mass + C-value	5	-8.33	39.87	5.04
morphological	10 C x 0.3 kPa	*r*	Mass * C-value	6	-8.3	43.88	9.04
morphological	10 C x 0.3 kPa	*r*	C-value	4	-18.46	50.99	16.16
morphological	10 C x 0.6 kPa	Resp	**Mass**	4	-7.62	30.41	0
morphological	10 C x 0.6 kPa	Resp	Mass + C-value	5	-7.35	33.26	2.85

morphological	10 C x 0.6 kPa	Resp	Mass * C-value	6	-7.07	36.5	6.08
morphological	10 C x 0.6 kPa	Resp	C-value	4	-42.66	94.48	64.07
morphological	10 C x 0.6 kPa	sResp	**Mass**	4	-7.21	29.56	0
morphological	10 C x 0.6 kPa	sResp	Mass + C-value	5	-6.95	32.39	2.83
morphological	10 C x 0.6 kPa	sResp	Mass * C-value	6	-6.69	35.69	6.13
morphological	10 C x 0.6 kPa	sResp	C-value	4	-13.41	38.76	9.2
morphological	10 C x 0.6 kPa	EWL	**Mass**	4	23.95	-27.94	0
morphological	10 C x 0.6 kPa	EWL	Mass + C-value	5	24.35	-22.34	5.6
morphological	10 C x 0.6 kPa	EWL	Mass * C-value	6	25.23	-19.19	8.75
morphological	10 C x 0.6 kPa	EWL	C-value	4	-2	15.06	43
morphological	10 C x 0.6 kPa	sEWL	**Mass**	4	25.22	-30.42	0
morphological	10 C x 0.6 kPa	sEWL	Mass + C-value	5	25.59	-24.74	5.68
morphological	10 C x 0.6 kPa	sEWL	Mass * C-value	6	26.49	-21.62	8.8
morphological	10 C x 0.6 kPa	sEWL	C-value	4	-20.83	52.81	83.23
morphological	10 C x 0.6 kPa	CWL	**Mass**	4	24.84	-29.67	0
morphological	10 C x 0.6 kPa	CWL	Mass + C-value	5	25.21	-24	5.67
morphological	10 C x 0.6 kPa	CWL	Mass * C-value	6	26.09	-20.84	8.83
morphological	10 C x 0.6 kPa	CWL	C-value	4	7.14	0.43	30.1
morphological	10 C x 0.6 kPa	*r*	**Mass**	4	25.68	-31.32	0
morphological	10 C x 0.6 kPa	*r*	Mass + C-value	5	26.31	-26.15	5.17
morphological	10 C x 0.6 kPa	*r*	Mass * C-value	6	27.51	-23.58	7.74
morphological	10 C x 0.6 kPa	*r*	C-value	4	8.36	-2.06	29.26
morphological	15 C x 0.3 kPa	Resp	**Mass**	4	-35.37	85.23	0
morphological	15 C x 0.3 kPa	Resp	Mass + C-value	5	-35.33	88.19	2.95
morphological	15 C x 0.3 kPa	Resp	Mass * C-value	6	-34.31	89.42	4.18
morphological	15 C x 0.3 kPa	Resp	C-value	4	-62.13	133.35	48.11
morphological	15 C x 0.3 kPa	sResp	**Mass**	4	-35.51	85.48	0
morphological	15 C x 0.3 kPa	sResp	C-value	4	-38.03	87.57	2.09
morphological	15 C x 0.3 kPa	sResp	Mass + C-value	5	-35.46	88.41	2.93
morphological	15 C x 0.3 kPa	sResp	Mass * C-value	6	-34.43	89.62	4.14
morphological	15 C x 0.3 kPa	EWL	**Mass + C-value**	5	-27.12	77.32	0
morphological	15 C x 0.3 kPa	EWL	Mass * C-value	6	-25.23	77.58	0.26
morphological	15 C x 0.3 kPa	EWL	**Mass**	4	-31.04	78.58	1.27
morphological	15 C x 0.3 kPa	EWL	C-value	4	-46.27	102.51	25.2
morphological	15 C x 0.3 kPa	sEWL	**Mass + C-value**	5	-27.39	77.85	0
morphological	15 C x 0.3 kPa	sEWL	Mass * C-value	6	-25.49	78.09	0.23
morphological	15 C x 0.3 kPa	sEWL	**Mass**	4	-31.15	78.87	1.02
morphological	15 C x 0.3 kPa	sEWL	C-value	4	-46.53	105.56	27.71
morphological	15 C x 0.3 kPa	CWL	**C-value**	4	-28.46	73.44	0

morphological	15 C x 0.3 kPa	CWL	Mass + C-value	5	-27.3	77.68	4.24
morphological	15 C x 0.3 kPa	CWL	Mass * C-value	6	-25.4	77.91	4.48
morphological	15 C x 0.3 kPa	CWL	Mass	4	-31.11	78.77	5.34
morphological	15 C x 0.3 kPa	*r*	**C-value**	4	-30.82	78.07	0
morphological	15 C x 0.3 kPa	*r*	Mass + C-value	5	-30.17	83.23	5.16
morphological	15 C x 0.3 kPa	*r*	Mass * C-value	6	-28.33	83.52	5.46
morphological	15 C x 0.3 kPa	*r*	Mass	4	-33.85	84.41	6.34
morphological	15 C x 0.6 kPa	Resp	**Mass**	4	-36.89	88.2	0
morphological	15 C x 0.6 kPa	Resp	Mass + C-value	5	-36.85	90.99	2.79
morphological	15 C x 0.6 kPa	Resp	Mass * C-value	6	-36.11	92.78	4.57
morphological	15 C x 0.6 kPa	Resp	C-value	4	-64.08	137.28	49.07
morphological	15 C x 0.6 kPa	sResp	**Mass**	4	-36.99	88.41	0
morphological	15 C x 0.6 kPa	sResp	Mass + C-value	5	-36.96	91.2	2.8
morphological	15 C x 0.6 kPa	sResp	Mass * C-value	6	-36.22	92.96	4.56
morphological	15 C x 0.6 kPa	sResp	C-value	4	-41.52	94.11	5.7
morphological	15 C x 0.6 kPa	EWL	**Mass + C-value**	5	14.8	-3.96	0
morphological	15 C x 0.6 kPa	EWL	**Mass**	4	10.72	-3.54	0.42
morphological	15 C x 0.6 kPa	EWL	Mass * C-value	6	16.07	-1.59	2.37
morphological	15 C x 0.6 kPa	EWL	C-value	4	-27.12	64.19	68.15
morphological	15 C x 0.6 kPa	sEWL	**Mass + C-value**	5	14.12	-2.6	0
morphological	15 C x 0.6 kPa	sEWL	**Mass**	4	10.23	-2.44	0.16
morphological	15 C x 0.6 kPa	sEWL	Mass * C-value	6	15.42	-0.29	2.32
morphological	15 C x 0.6 kPa	sEWL	C-value	4	-13.82	40.05	42.65
morphological	15 C x 0.6 kPa	CWL	**C-value**	4	12.46	-6.78	0
morphological	15 C x 0.6 kPa	CWL	Mass + C-value	5	14.41	-3.16	3.62
morphological	15 C x 0.6 kPa	CWL	**Mass**	4	10.44	-2.9	3.88
morphological	15 C x 0.6 kPa	CWL	Mass * C-value	6	15.69	-0.8	5.98
morphological	15 C x 0.6 kPa	*r*	**C-value**	4	14.13	-10.1	0
morphological	15 C x 0.6 kPa	*r*	Mass + C-value	5	16.06	-6.36	3.73
morphological	15 C x 0.6 kPa	*r*	**Mass**	4	12.16	-6.23	3.86
morphological	15 C x 0.6 kPa	*r*	Mass * C-value	6	17.53	-4.31	5.79
environmental	full data	Resp	**Temp + VPD**	6	-155.48	335.2	0
environmental	full data	Resp	Temp * VPD	7	-155.07	340.4	5.21
environmental	full data	Resp	**Temp**	5	-167.99	352.7	17.55
environmental	full data	Resp	**VPD**	5	-181.24	379.3	44.07
environmental	full data	sResp	**Temp + VPD**	6	-109.71	244.8	0
environmental	full data	sResp	Temp * VPD	7	-109.66	250.7	5.85
environmental	full data	sResp	**VPD**	5	-118.37	254.8	9.85
environmental	full data	sResp	**Temp**	5	-123.67	265.4	24.59

environmental	full data	EWL	**Temp + VPD**	6	-73.8	173	0
environmental	full data	EWL	Temp * VPD	7	-73.78	179.1	6.17
environmental	full data	EWL	**VPD**	5	-81.36	180.5	7.51
environmental	full data	EWL	Temp	5	-347.82	711.9	538.93
environmental	full data	sEWL	**Temp + VPD**	6	-90.61	207	0
environmental	full data	sEWL	Temp * VPD	7	-90.5	213	6
environmental	full data	sEWL	**VPD**	5	-114.32	246.8	39.41
environmental	full data	sEWL	**Temp**	5	-359.69	736.1	531.97
environmental	full data	CWL	**Temp + VPD**	6	-44.52	117	0
environmental	full data	CWL	Temp * VPD	7	-44.48	123.2	6.17
environmental	full data	CWL	**VPD**	5	-63.04	146.4	29.34
environmental	full data	CWL	**Temp**	5	-335.22	689.2	574.07
environmental	full data	*r*	**Temp + VPD**	6	-46.2	120.3	0
environmental	full data	*r*	Temp * VPD	7	-46.07	126.3	5.97
environmental	full data	*r*	**VPD**	5	-63.33	147	26.47
environmental	full data	*r*	**Temp**	5	-95.48	211	95.49

Note: Temp = temperature, VPD = vapor pressure deficit, df = degrees of freedom, AICc = corrected Akaike information criterion, Resp = gross respiration, sResp = specific respiration, EWL = gross evaporative water loss, sEWL = specific evaporative water loss, CWL = cutaneous water loss, *r* = total resistance

Table S3. Model comparisons for all full-dataset linear models. Comparisons are made between morphological and environmental models, and final joint models assembled from both. Nested models are listed in order of statistical support by ΔAICc, with each set of compared models separated by a solid line. Entries in bold represent statistically significant parameters ($p < 0.05$).

Model type	Dataset	Response	Predictor	df	Log likelihood	AICc	ΔAICc
final	full data	Resp	**Mass + Temp + VPD**	7	-97.4	227	0
morphological	full data	Resp	**Mass**	8	-97.28	232.73	5.78
morphological	full data	Resp	Mass + C-value	9	-97.2	235.66	8.71
morphological	full data	Resp	Mass * C-value	10	-97.17	239.9	12.94
environmental	full data	Resp	**Temp + VPD**	6	-155.48	335.2	108.23
environmental	full data	Resp	Temp * VPD	7	-155.07	340.4	113.43
morphological	full data	Resp	C-value	8	-155.01	341.62	114.67
environmental	full data	Resp	**Temp**	5	-167.99	352.7	125.78
environmental	full data	Resp	**VPD**	5	-181.24	379.3	152.3
final	full data	sResp	**Mass + Temp + VPD**	7	-97.74	227.6	0
morphological	full data	sResp	**Mass**	8	-97.63	233.41	5.79
morphological	full data	sResp	Mass + C-value	9	-97.56	236.35	8.72
morphological	full data	sResp	Mass * C-value	10	-97.53	240.56	12.94
environmental	full data	sResp	**Temp + VPD**	6	-109.71	244.8	17.21
environmental	full data	sResp	Temp * VPD	7	-109.66	250.7	23.07
morphological	full data	sResp	C-value	8	-109.46	252.96	25.34
environmental	full data	sResp	**VPD**	5	-118.37	254.8	27.16
environmental	full data	sResp	**Temp**	5	-123.67	265.4	37.73
final	full data	EWL	**Mass + Temp + VPD**	7	-27.25	90.7	0
morphological	full data	EWL	**Mass**	8	-27.24	96.95	6.26
morphological	full data	EWL	Mass + C-value	9	-24.13	99.53	8.83
morphological	full data	EWL	Mass * C-value	10	-22.21	101.24	10.55
environmental	full data	EWL	**Temp + VPD**	6	-73.8	173	82.28
environmental	full data	EWL	Temp * VPD	7	-73.78	179.1	88.45
environmental	full data	EWL	**VPD**	5	-81.36	180.5	89.79
morphological	full data	EWL	C-value	8	-73.76	181.15	90.45
environmental	full data	EWL	Temp	5	-347.82	711.9	621.21
final	full data	sEWL	**Mass + Temp + VPD**	7	-27.54	91.4	0

morphological	full data	sEWL	**Mass**	8	-27.52	97.61	6.25
morphological	full data	sEWL	Mass + C-value	9	-24.68	100.55	9.18
morphological	full data	sEWL	Mass * C-value	10	-22.71	102.23	10.87
environmental	full data	sEWL	**Temp + VPD**	6	-90.61	207	115.69
environmental	full data	sEWL	Temp * VPD	7	-90.5	213	121.67
morphological	full data	sEWL	C-value	8	-89.98	214.78	123.42
environmental	full data	sEWL	**VPD**	5	-114.32	246.8	155.47
environmental	full data	sEWL	**Temp**	5	-359.69	736.1	644.73
final	full data	CWL	**Mass + Temp + VPD**	7	-27.31	90.9	0
morphological	full data	CWL	**Mass**	8	-27.3	97.15	6.25
morphological	full data	CWL	Mass + C-value	9	-24.37	99.97	9.07
morphological	full data	CWL	Mass * C-value	10	-22.43	101.67	10.77
environmental	full data	CWL	**Temp + VPD**	6	-44.52	117	26.1
environmental	full data	CWL	Temp * VPD	7	-44.48	123.2	32.27
morphological	full data	CWL	C-value	8	-42.75	125.13	34.23
environmental	full data	CWL	**VPD**	5	-63.04	146.4	55.5
environmental	full data	CWL	**Temp**	5	-335.22	689.2	598.29
final	full data	*r*	**Mass * C-value + Temp + VPD**	9	-24.97	100.6	0
morphological	full data	*r*	**Mass**	8	-30.29	103.11	2.51
morphological	full data	*r*	Mass + C-value	9	-27.28	105.71	5.11
morphological	full data	*r*	**Mass * C-value**	10	-24.89	106.68	6.08
environmental	full data	*r*	**Temp + VPD**	6	-46.2	120.3	19.69
environmental	full data	*r*	Temp * VPD	7	-46.07	126.3	25.65
morphological	full data	*r*	C-value	8	-44.36	128.27	27.67
environmental	full data	*r*	**VPD**	5	-63.33	147	46.36
environmental	full data	*r*	**Temp**	5	-95.48	211	110.38

Note: Temp = temperature, VPD = vapor pressure deficit, AI = aridity index, df = degrees of freedom, AICc = corrected Akaike information criterion, Resp = gross respiration, sResp = specific respiration, EWL = gross evaporative water loss, sEWL = specific evaporative water loss, CWL = cutaneous water loss, *r* = total resistance

Table S4. Model comparisons for all tested phylogenetic least squares models. Comparisons are made for morphological and environmental models within each data subset. Nested models are listed in order of statistical support by ΔAICc, with each set of compared models separated by a solid line. Entries in bold represent statistically significant parameters ($p < 0.05$).

Model type	Dataset	Response	Predictor	df	Log likelihood	AICc	ΔAICc
morphological	full data	Resp	**Mass**	3	-0.29	12.58	0
morphological	full data	Resp	Mass + C-value	4	-0.28	21.89	9.31
morphological	full data	Resp	C-value	3	-8.56	29.13	16.55
morphological	full data	Resp	Mass * C-value	5	-0.25	40.5	27.92
morphological	full data	sResp	Mass	3	-0.36	12.72	0
morphological	full data	sResp	C-value	3	-2.48	16.96	4.23
morphological	full data	sResp	Mass + C-value	4	-0.35	22.03	9.3
morphological	full data	sResp	Mass * C-value	5	-0.32	40.65	27.92
morphological	full data	EWL	**Mass**	3	10.07	-8.14	0
morphological	full data	EWL	Mass + C-value	4	12.03	-2.73	5.41
morphological	full data	EWL	Mass * C-value	5	13.14	13.73	21.86
morphological	full data	EWL	C-value	3	-6.15	24.3	32.44
morphological	full data	sEWL	**Mass**	3	10.01	-8.02	0
morphological	full data	sEWL	Mass + C-value	4	11.77	-2.21	5.81
morphological	full data	sEWL	Mass * C-value	5	12.88	14.24	22.26
morphological	full data	sEWL	C-value	3	-3.11	18.22	26.24
morphological	full data	CWL	**Mass**	3	10.06	-8.12	0
morphological	full data	CWL	Mass + C-value	4	11.89	-2.44	5.68
morphological	full data	CWL	C-value	3	6.93	-1.86	6.26
morphological	full data	CWL	Mass * C-value	5	13.01	13.99	22.11
morphological	full data	*r*	**Mass**	3	9.84	-7.69	0
morphological	full data	*r*	C-value	3	6.8	-1.61	6.08
morphological	full data	*r*	Mass + C-value	4	11.43	-1.53	6.16
morphological	full data	*r*	Mass * C-value	5	12.96	14.08	21.76
morphological	10 C	Resp	**Mass**	3	-0.83	13.67	0
morphological	10 C	Resp	Mass + C-value	4	-0.82	22.98	9.31
morphological	10 C	Resp	C-value	3	-8.51	29.01	15.34
morphological	10 C	Resp	Mass * C-value	5	-0.52	41.04	27.37
morphological	10 C	sResp	Mass	3	-0.91	13.81	0

morphological	10 C	sResp	C-value	3	-2.93	17.87	4.05
morphological	10 C	sResp	Mass + C-value	4	-0.9	23.13	9.31
morphological	10 C	sResp	Mass * C-value	5	-0.6	41.2	27.39
morphological	10 C	EWL	**Mass**	3	8.32	-4.64	0
morphological	10 C	EWL	Mass + C-value	4	8.55	4.24	8.88
morphological	10 C	EWL	C-value	3	-5.03	22.07	26.71
morphological	10 C	EWL	Mass * C-value	5	8.73	22.54	27.18
morphological	10 C	sEWL	**Mass**	3	8.33	-4.67	0
morphological	10 C	sEWL	Mass + C-value	4	8.54	4.26	8.93
morphological	10 C	sEWL	C-value	3	-4.6	21.2	25.87
morphological	10 C	sEWL	Mass * C-value	5	8.72	22.56	27.22
morphological	10 C	CWL	**Mass**	3	8.38	-4.75	0
morphological	10 C	CWL	Mass + C-value	4	8.58	4.17	8.92
morphological	10 C	CWL	C-value	3	2.51	6.97	11.72
morphological	10 C	CWL	Mass * C-value	5	8.77	22.46	27.21
morphological	10 C	*r*	**Mass**	3	8.98	-5.96	0
morphological	10 C	*r*	Mass + C-value	4	9.23	2.88	8.84
morphological	10 C	*r*	C-value	3	2.5	6.99	12.95
morphological	10 C	*r*	Mass * C-value	5	9.41	21.18	27.14
morphological	15 C	Resp	**Mass**	3	-0.75	13.49	0
morphological	15 C	Resp	Mass + C-value	4	-0.65	22.62	9.13
morphological	15 C	Resp	C-value	3	-8.89	29.78	16.29
morphological	15 C	Resp	Mass * C-value	5	-0.57	41.14	27.65
morphological	15 C	sResp	Mass	3	-0.81	13.62	0
morphological	15 C	sResp	C-value	3	-2.51	17.02	3.4
morphological	15 C	sResp	Mass + C-value	4	-0.7	22.73	9.12
morphological	15 C	sResp	Mass * C-value	5	-0.62	41.23	27.62
morphological	15 C	EWL	**Mass + C-value**	4	16.95	-12.57	0
morphological	15 C	EWL	**Mass * C-value**	5	24.21	-8.42	4.15
morphological	15 C	EWL	**Mass**	3	8.93	-5.86	6.71
morphological	15 C	EWL	C-value	3	-7.16	26.32	38.89
morphological	15 C	sEWL	**Mass + C-value**	4	16.42	-11.5	0
morphological	15 C	sEWL	**Mass * C-value**	5	23.75	-7.49	4.01
morphological	15 C	sEWL	**Mass**	3	9.04	-6.07	5.42
morphological	15 C	sEWL	C-value	3	-1.63	15.26	26.76
morphological	15 C	CWL	**C-value**	3	14.68	-17.37	0
morphological	15 C	CWL	Mass + C-value	4	16.61	-11.88	5.49
morphological	15 C	CWL	**Mass * C-value**	5	24.07	-8.14	9.23
morphological	15 C	CWL	Mass	3	9.01	-6.03	11.34

morphological	15 C	*r*	**C-value**	3	13.23	-14.45	0
morphological	15 C	*r*	Mass + C-value	4	13.94	-6.54	7.91
morphological	15 C	*r*	Mass	3	8.61	-5.23	9.22
morphological	15 C	*r*	**Mass * C-value**	5	21.75	-3.51	10.94
morphological	0.3 kPa	Resp	**Mass**	3	-0.83	13.66	0
morphological	0.3 kPa	Resp	Mass + C-value	4	-0.82	22.97	9.31
morphological	0.3 kPa	Resp	C-value	3	-8.74	29.47	15.81
morphological	0.3 kPa	Resp	Mass * C-value	5	-0.75	41.5	27.84
morphological	0.3 kPa	sResp	Mass	3	-0.88	13.75	0
morphological	0.3 kPa	sResp	C-value	3	-2.61	17.22	3.46
morphological	0.3 kPa	sResp	Mass + C-value	4	-0.86	23.06	9.3
morphological	0.3 kPa	sResp	Mass * C-value	5	-0.8	41.6	27.85
morphological	0.3 kPa	EWL	**Mass**	3	7.8	-3.59	0
morphological	0.3 kPa	EWL	Mass + C-value	4	9.35	2.63	6.22
morphological	0.3 kPa	EWL	Mass * C-value	5	10.19	19.61	23.21
morphological	0.3 kPa	EWL	C-value	3	-6.05	24.11	27.7
morphological	0.3 kPa	sEWL	**Mass**	3	7.68	-3.37	0
morphological	0.3 kPa	sEWL	Mass + C-value	4	9.08	3.18	6.55
morphological	0.3 kPa	sEWL	C-value	3	-3.33	18.66	22.03
morphological	0.3 kPa	sEWL	Mass * C-value	5	9.91	20.18	23.55
morphological	0.3 kPa	CWL	**Mass**	3	7.75	-3.5	0
morphological	0.3 kPa	CWL	C-value	3	5.59	0.82	4.31
morphological	0.3 kPa	CWL	Mass + C-value	4	9.19	2.95	6.45
morphological	0.3 kPa	CWL	Mass * C-value	5	10.04	19.93	23.42
morphological	0.3 kPa	*r*	**Mass**	3	7.25	-2.5	0
morphological	0.3 kPa	*r*	C-value	3	5.36	1.27	3.77
morphological	0.3 kPa	*r*	Mass + C-value	4	8.41	4.52	7.01
morphological	0.3 kPa	*r*	Mass * C-value	5	9.21	21.58	20.3
morphological	0.6 kPa	Resp	**Mass**	3	0.17	11.67	0
morphological	0.6 kPa	Resp	Mass + C-value	4	0.18	20.98	9.31
morphological	0.6 kPa	Resp	C-value	3	-8.39	28.78	17.12
morphological	0.6 kPa	Resp	Mass * C-value	5	0.18	39.64	27.97
morphological	0.6 kPa	sResp	Mass	3	0.06	11.88	0
morphological	0.6 kPa	sResp	C-value	3	-2.46	16.92	5.04
morphological	0.6 kPa	sResp	Mass + C-value	4	0.07	21.18	9.31
morphological	0.6 kPa	sResp	Mass * C-value	5	0.08	39.84	27.97
morphological	0.6 kPa	EWL	**Mass**	3	12.2	-12.4	0
morphological	0.6 kPa	EWL	Mass + C-value	4	14.04	-6.75	5.65
morphological	0.6 kPa	EWL	Mass * C-value	5	16.1	7.81	20.21

morphological	0.6 kPa	EWL	C-value	3	-6.21	24.41	36.81
morphological	0.6 kPa	sEWL	**Mass**	3	12.28	-12.55	0
morphological	0.6 kPa	sEWL	Mass + C-value	4	13.96	-6.6	5.96
morphological	0.6 kPa	sEWL	Mass * C-value	5	16.13	7.73	20.28
morphological	0.6 kPa	sEWL	C-value	3	-3.03	18.05	30.61
morphological	0.6 kPa	CWL	**Mass**	3	12.28	-12.55	0
morphological	0.6 kPa	CWL	Mass + C-value	4	14.01	-6.68	5.87
morphological	0.6 kPa	CWL	C-value	3	7.64	-3.28	9.27
morphological	0.6 kPa	CWL	Mass * C-value	5	16.15	7.7	20.25
morphological	0.6 kPa	*r*	**Mass**	3	11.61	-11.22	0
morphological	0.6 kPa	*r*	Mass + C-value	4	13.13	-4.92	6.3
morphological	0.6 kPa	*r*	C-value	3	7.44	-2.88	8.33
morphological	0.6 kPa	*r*	Mass * C-value	5	15.62	8.76	19.98
morphological	10 C x 0.3 kPa	Resp	**Mass**	3	-1.95	15.91	0
morphological	10 C x 0.3 kPa	Resp	Mass + C-value	4	-1.93	25.2	9.29
morphological	10 C x 0.3 kPa	Resp	C-value	3	-8.65	29.3	13.4
morphological	10 C x 0.3 kPa	Resp	Mass * C-value	5	-1.53	43.07	27.16
morphological	10 C x 0.3 kPa	sResp	Mass	3	-1.96	15.93	0
morphological	10 C x 0.3 kPa	sResp	C-value	3	-3.64	19.27	3.34
morphological	10 C x 0.3 kPa	sResp	Mass + C-value	4	-1.95	25.22	9.3
morphological	10 C x 0.3 kPa	sResp	Mass * C-value	5	-1.56	43.11	27.19
morphological	10 C x 0.3 kPa	EWL	**Mass**	3	5.37	1.27	0
morphological	10 C x 0.3 kPa	EWL	Mass + C-value	4	5.44	10.45	9.18
morphological	10 C x 0.3 kPa	EWL	C-value	3	-4.98	21.97	20.7
morphological	10 C x 0.3 kPa	EWL	Mass * C-value	5	5.44	29.12	27.85
morphological	10 C x 0.3 kPa	sEWL	**Mass**	3	5.29	1.41	0
morphological	10 C x 0.3 kPa	sEWL	Mass + C-value	4	5.36	10.62	9.21
morphological	10 C x 0.3 kPa	sEWL	C-value	3	-4.97	21.95	20.53
morphological	10 C x 0.3 kPa	sEWL	Mass * C-value	5	5.36	29.28	27.87
morphological	10 C x 0.3 kPa	CWL	**Mass**	3	5.37	1.26	0
morphological	10 C x 0.3 kPa	CWL	C-value	3	1.22	9.57	8.3
morphological	10 C x 0.3 kPa	CWL	Mass + C-value	4	5.43	10.47	9.2
morphological	10 C x 0.3 kPa	CWL	Mass * C-value	5	5.44	29.13	27.87
morphological	10 C x 0.3 kPa	*r*	**Mass**	3	5.73	0.54	0
morphological	10 C x 0.3 kPa	*r*	C-value	3	1.18	9.63	9.09
morphological	10 C x 0.3 kPa	*r*	Mass + C-value	4	5.82	9.7	9.16
morphological	10 C x 0.3 kPa	*r*	Mass * C-value	5	5.82	28.35	27.81
morphological	10 C x 0.6 kPa	Resp	**Mass**	3	-0.18	12.35	0
morphological	10 C x 0.6 kPa	Resp	Mass + C-value	4	-0.17	21.68	9.33

morphological	10 C x 0.6 kPa	Resp	C-value	3	-8.44	28.87	16.52
morphological	10 C x 0.6 kPa	Resp	Mass * C-value	5	-0.01	40.03	27.68
morphological	10 C x 0.6 kPa	sResp	Mass	3	-0.34	12.68	0
morphological	10 C x 0.6 kPa	sResp	C-value	3	-2.61	17.22	4.54
morphological	10 C x 0.6 kPa	sResp	Mass + C-value	4	-0.34	22.01	9.33
morphological	10 C x 0.6 kPa	sResp	Mass * C-value	5	-0.18	40.37	27.69
morphological	10 C x 0.6 kPa	EWL	**Mass**	3	10.84	-9.69	0
morphological	10 C x 0.6 kPa	EWL	Mass + C-value	4	11.08	-0.83	8.86
morphological	10 C x 0.6 kPa	EWL	Mass * C-value	5	12.01	15.99	25.68
morphological	10 C x 0.6 kPa	EWL	C-value	3	-5.1	22.19	31.88
morphological	10 C x 0.6 kPa	sEWL	**Mass**	3	10.85	-9.71	0
morphological	10 C x 0.6 kPa	sEWL	Mass + C-value	4	11.07	-0.81	8.9
morphological	10 C x 0.6 kPa	sEWL	Mass * C-value	5	11.96	16.08	25.79
morphological	10 C x 0.6 kPa	sEWL	C-value	3	-4.44	20.87	30.58
morphological	10 C x 0.6 kPa	CWL	**Mass**	3	10.86	-9.72	0
morphological	10 C x 0.6 kPa	CWL	Mass + C-value	4	11.08	-0.83	8.89
morphological	10 C x 0.6 kPa	CWL	C-value	3	3.2	5.6	15.32
morphological	10 C x 0.6 kPa	CWL	Mass * C-value	5	11.98	16.03	25.75
morphological	10 C x 0.6 kPa	*r*	**Mass**	3	10.57	-9.14	0
morphological	10 C x 0.6 kPa	*r*	Mass + C-value	4	10.89	-0.46	8.68
morphological	10 C x 0.6 kPa	*r*	C-value	3	3.13	5.74	14.87
morphological	10 C x 0.6 kPa	*r*	Mass * C-value	5	12.14	15.71	24.85
morphological	15 C x 0.3 kPa	Resp	**Mass**	3	-1.51	15.02	0
morphological	15 C x 0.3 kPa	Resp	Mass + C-value	4	-1.36	24.05	9.03
morphological	15 C x 0.3 kPa	Resp	C-value	3	-9.12	30.24	15.22
morphological	15 C x 0.3 kPa	Resp	Mass * C-value	5	-1.29	42.58	27.56
morphological	15 C x 0.3 kPa	sResp	Mass	3	-1.56	15.12	0
morphological	15 C x 0.3 kPa	sResp	C-value	3	-2.76	17.53	2.4
morphological	15 C x 0.3 kPa	sResp	Mass + C-value	4	-1.4	24.14	9.02
morphological	15 C x 0.3 kPa	sResp	Mass * C-value	5	-1.33	42.67	27.54
morphological	15 C x 0.3 kPa	EWL	**Mass + C-value**	4	11.2	-1.06	0
morphological	15 C x 0.3 kPa	EWL	**Mass**	3	5.95	0.09	1.15
morphological	15 C x 0.3 kPa	EWL	**Mass * C-value**	5	19.92	0.17	1.23
morphological	15 C x 0.3 kPa	EWL	C-value	3	-7.15	26.29	27.35
morphological	15 C x 0.3 kPa	sEWL	**Mass + C-value**	4	10.96	-0.6	0
morphological	15 C x 0.3 kPa	sEWL	**Mass**	3	6	0.01	0.6
morphological	15 C x 0.3 kPa	sEWL	**Mass * C-value**	5	19.11	1.78	2.38
morphological	15 C x 0.3 kPa	sEWL	C-value	3	-1.75	15.51	16.1
morphological	15 C x 0.3 kPa	CWL	**C-value**	3	10.42	-8.84	0

morphological	15 C x 0.3 kPa	CWL	Mass + C-value	4	11.03	-0.73	8.11
morphological	15 C x 0.3 kPa	CWL	Mass	3	5.98	0.04	8.88
morphological	15 C x 0.3 kPa	CWL	**Mass * C-value**	5	19.44	1.11	9.96
morphological	15 C x 0.3 kPa	*r*	**C-value**	3	10.44	-8.89	0
morphological	15 C x 0.3 kPa	*r*	Mass	3	6.09	-0.18	8.7
morphological	15 C x 0.3 kPa	*r*	Mass + C-value	4	10.6	0.14	9.03
morphological	15 C x 0.3 kPa	*r*	**Mass * C-value**	5	19.71	0.58	9.47
morphological	15 C x 0.6 kPa	Resp	**Mass**	3	-0.31	12.61	0
morphological	15 C x 0.6 kPa	Resp	Mass + C-value	4	-0.26	21.84	9.23
morphological	15 C x 0.6 kPa	Resp	C-value	3	-8.71	29.43	16.81
morphological	15 C x 0.6 kPa	Resp	Mass * C-value	5	-0.15	40.31	27.7
morphological	15 C x 0.6 kPa	sResp	Mass	3	-0.37	12.73	0
morphological	15 C x 0.6 kPa	sResp	C-value	3	-2.54	17.08	4.35
morphological	15 C x 0.6 kPa	sResp	Mass + C-value	4	-0.31	21.95	9.22
morphological	15 C x 0.6 kPa	sResp	Mass * C-value	5	-0.19	40.38	27.65
morphological	15 C x 0.6 kPa	EWL	**Mass**	3	10.07	-8.13	0
morphological	15 C x 0.6 kPa	EWL	**Mass + C-value**	4	14.18	-7.02	1.11
morphological	15 C x 0.6 kPa	EWL	Mass * C-value	5	15.09	9.83	17.96
morphological	15 C x 0.6 kPa	EWL	C-value	3	-7.14	26.29	34.42
morphological	15 C x 0.6 kPa	sEWL	**Mass**	3	10.31	-8.63	0
morphological	15 C x 0.6 kPa	sEWL	**Mass + C-value**	4	14.31	-7.28	1.35
morphological	15 C x 0.6 kPa	sEWL	Mass * C-value	5	15.56	8.87	17.5
morphological	15 C x 0.6 kPa	sEWL	C-value	3	-1.85	15.7	24.33
morphological	15 C x 0.6 kPa	CWL	**C-value**	3	12.62	-13.24	0
morphological	15 C x 0.6 kPa	CWL	Mass	3	10.26	-8.53	4.71
morphological	15 C x 0.6 kPa	CWL	Mass + C-value	4	14.32	-7.3	5.94
morphological	15 C x 0.6 kPa	CWL	Mass * C-value	5	15.46	9.08	22.32
morphological	15 C x 0.6 kPa	*r*	**C-value**	3	12.82	-13.64	0
morphological	15 C x 0.6 kPa	*r*	Mass	3	10.39	-8.79	4.85
morphological	15 C x 0.6 kPa	*r*	Mass + C-value	4	14.31	-7.29	6.35
morphological	15 C x 0.6 kPa	*r*	Mass * C-value	5	16.05	7.89	21.53
environmental	full data	Resp	**Temp**	3	-1.59	15.19	0
environmental	full data	Resp	**Temp + AI**	4	2.16	17.01	1.82
environmental	full data	Resp	AI	3	-7.35	26.7	11.51
environmental	full data	Resp	Temp * AI	5	2.21	35.58	20.39
environmental	full data	sResp	**AI**	3	1.34	9.33	0
environmental	full data	sResp	Temp	3	-1.09	14.18	4.85
environmental	full data	sResp	Temp + AI	4	1.63	18.07	8.74
environmental	full data	sResp	Temp * AI	5	2.14	35.72	26.39

environmental	full data	EWL	**Temp**	3	5.08	1.84	0
environmental	full data	EWL	Temp + AI	4	5.13	11.08	9.24
environmental	full data	EWL	**AI**	3	-2.03	16.07	14.23
environmental	full data	EWL	Temp * AI	5	5.13	29.74	27.9
environmental	full data	sEWL	**Temp**	3	2.34	7.32	0
environmental	full data	sEWL	AI	3	-1.59	15.17	7.85
environmental	full data	sEWL	Temp + AI	4	2.65	16.04	8.71
environmental	full data	sEWL	Temp * AI	5	2.92	34.17	26.84
environmental	full data	CWL	Temp	3	7.49	-2.98	0
environmental	full data	CWL	AI	3	5.82	0.35	3.33
environmental	full data	CWL	Temp + AI	4	8.2	4.93	7.91
environmental	full data	CWL	Temp * AI	5	8.69	22.63	25.6
environmental	full data	*r*	Temp	3	7.47	-2.93	0
environmental	full data	*r*	AI	3	5.61	0.79	3.72
environmental	full data	*r*	Temp + AI	4	8.87	3.6	6.53
environmental	full data	*r*	Temp * AI	5	9.24	21.53	24.46

Note: Temp = mean annual temperature, AI = aridity index, df = degrees of freedom, AICc = corrected Akaike information criterion, Resp = gross respiration, sResp = specific respiration, EWL = gross evaporative water loss, sEWL = specific evaporative water loss, CWL = cutaneous water loss, *r* = total resistance

Table S5. Model comparisons for all full-dataset PGLS models. Comparisons are made between morphological and environmental models, and final joint models assembled from both. Nested models are listed in order of statistical support by ΔAICc, with each set of compared models separated by a solid line. Entries in bold represent statistically significant parameters ($p < 0.05$).

Model type	Dataset	Response	Predictor	df	Log likelihood	AICc	ΔAICc
morphological	full data	Resp	**Mass**	3	-0.29	12.58	0
environmental	full data	Resp	**Temp**	3	-1.59	15.19	2.61
environmental	full data	Resp	**Temp + AI**	4	2.16	17.01	4.43
final	full data	Resp	**Temp + AI**	4	2.16	17.01	4.43
morphological	full data	Resp	Mass + C-value	4	-0.28	21.89	9.31
environmental	full data	Resp	AI	3	-7.35	26.7	14.13
morphological	full data	Resp	C-value	3	-8.56	29.13	16.55
environmental	full data	Resp	Temp * AI	5	2.21	35.58	23
morphological	full data	Resp	Mass * C-value	5	-0.25	40.5	27.92
environmental	full data	sResp	**AI**	3	1.34	9.33	0
final	full data	sResp	**AI**	3	1.34	9.33	0
morphological	full data	sResp	Mass	3	-0.36	12.72	3.4
environmental	full data	sResp	Temp	3	-1.09	14.18	4.85
morphological	full data	sResp	C-value	3	-2.48	16.96	7.63
environmental	full data	sResp	Temp + AI	4	1.63	18.07	8.74
morphological	full data	sResp	Mass + C-value	4	-0.35	22.03	12.7
environmental	full data	sResp	Temp * AI	5	2.14	35.72	26.39
morphological	full data	sResp	Mass * C-value	5	-0.32	40.65	31.32
morphological	full data	EWL	**Mass**	3	10.07	-8.14	0
final	full data	EWL	**Mass + Temp**	4	13.81	-6.29	1.84
morphological	full data	EWL	Mass + C-value	4	12.03	-2.73	5.41
environmental	full data	EWL	**Temp**	3	5.08	1.84	9.98
environmental	full data	EWL	Temp + AI	4	5.13	11.08	19.22
morphological	full data	EWL	Mass * C-value	5	13.14	13.73	21.86
environmental	full data	EWL	**AI**	3	-2.03	16.07	24.2
morphological	full data	EWL	C-value	3	-6.15	24.3	32.44
environmental	full data	EWL	Temp * AI	5	5.13	29.74	37.88
morphological	full data	sEWL	**Mass**	3	10.01	-8.02	0
final	full data	sEWL	**Mass + Temp**	4	13.74	-6.15	1.88

morphological	full data	sEWL	Mass + C-value	4	11.77	-2.21	5.81
environmental	full data	sEWL	**Temp**	3	2.34	7.32	15.35
morphological	full data	sEWL	Mass * C-value	5	12.88	14.24	22.26
environmental	full data	sEWL	AI	3	-1.59	15.17	23.19
environmental	full data	sEWL	Temp + AI	4	2.65	16.04	24.06
morphological	full data	sEWL	C-value	3	-3.11	18.22	26.24
environmental	full data	sEWL	Temp * AI	5	2.92	34.17	42.19
morphological	full data	CWL	**Mass**	3	10.06	-8.12	0
final	full data	CWL	**Mass**	3	10.06	-8.12	0
environmental	full data	CWL	Temp	3	7.49	-2.98	5.15
morphological	full data	CWL	Mass + C-value	4	11.89	-2.44	5.68
morphological	full data	CWL	C-value	3	6.93	-1.86	6.26
environmental	full data	CWL	AI	3	5.82	0.35	8.48
environmental	full data	CWL	Temp + AI	4	8.2	4.93	13.06
morphological	full data	CWL	Mass * C-value	5	13.01	13.99	22.11
environmental	full data	CWL	Temp * AI	5	8.69	22.63	30.75
morphological	full data	*r*	**Mass**	3	9.84	-7.69	0
final	full data	*r*	**Mass**	3	9.84	-7.69	0
environmental	full data	*r*	Temp	3	7.47	-2.93	4.76
morphological	full data	*r*	C-value	3	6.8	-1.61	6.08
morphological	full data	*r*	Mass + C-value	4	11.43	-1.53	6.16
environmental	full data	*r*	AI	3	5.61	0.79	8.47
environmental	full data	*r*	Temp + AI	4	8.87	3.6	11.29
morphological	full data	*r*	Mass * C-value	5	12.96	14.08	21.76
environmental	full data	*r*	Temp * AI	5	9.24	21.53	29.21

Note: Temp = mean annual temperature, AI = aridity index, df = degrees of freedom, AICc = corrected Akaike information criterion, Resp = gross respiration, sResp = specific respiration, EWL = gross evaporative water loss, sEWL = specific evaporative water loss, CWL = cutaneous water loss, *r* = total resistance

SUPPLEMENTAL MATERIALS – CHAPTER TWO

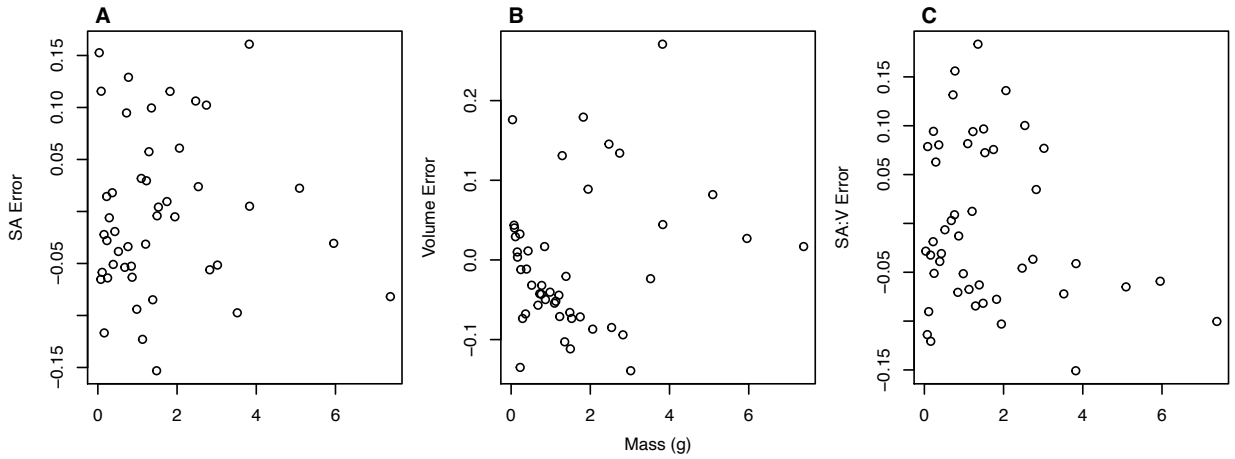

Figure S1. Estimation error of our general allometric models for surface area (A), volume (B), and SA:V (B). Estimation error is defined as the relative error ([empirical measurement - allometric estimate] / empirical measurement). Error is generally low for all models and does not covary with body mass, demonstrating that models are consistently reliable across body sizes.

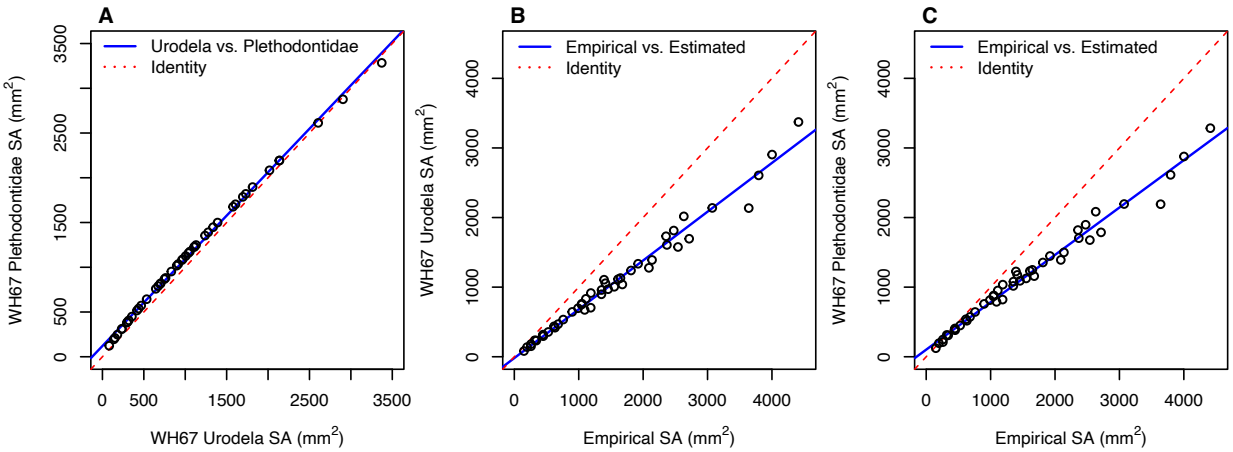

Figure S2. Performance of allometric estimators for SA following Whitford and Hutchison (1967) ("WH67"). WH67 models for the Plethodontidae and for all Urodeles are statistically equivalent (A), and both models systematically underestimate SA (B,C).

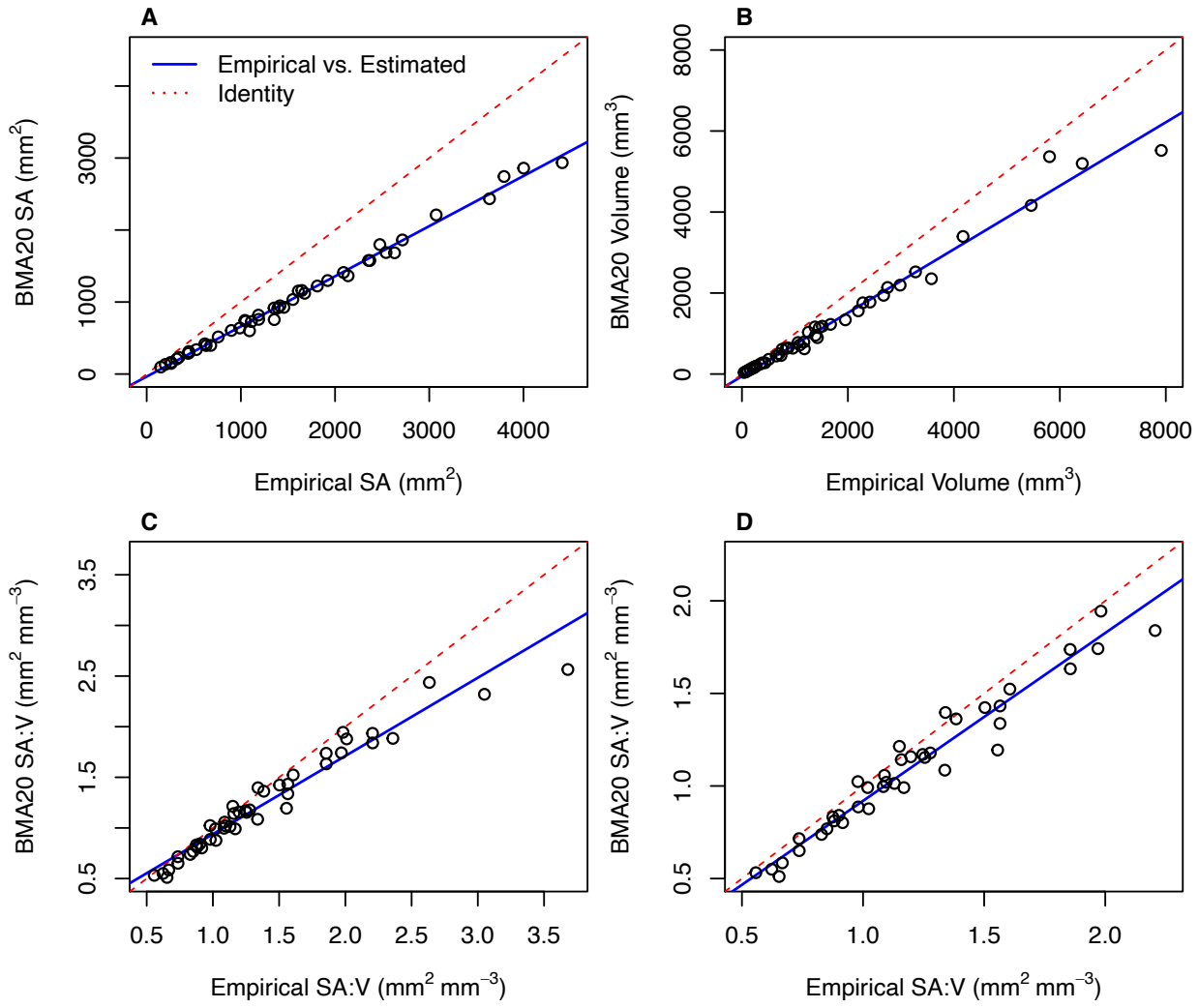

Figure S3. Performance of geometric estimators for SA, volume, and SA:V following Baken et al. (2020) ("BMA20"). This method systematically underestimates SA (A) and volume (B) individually. SA:V estimates differ from empirical measurements when tested across our complete dataset (C), largely driven by estimation bias in smaller (higher SA:V) individuals. For individuals with mass greater than 0.22 g, BMA20 estimates of SA:V are statistically indistinguishable from empirical measurements (D).

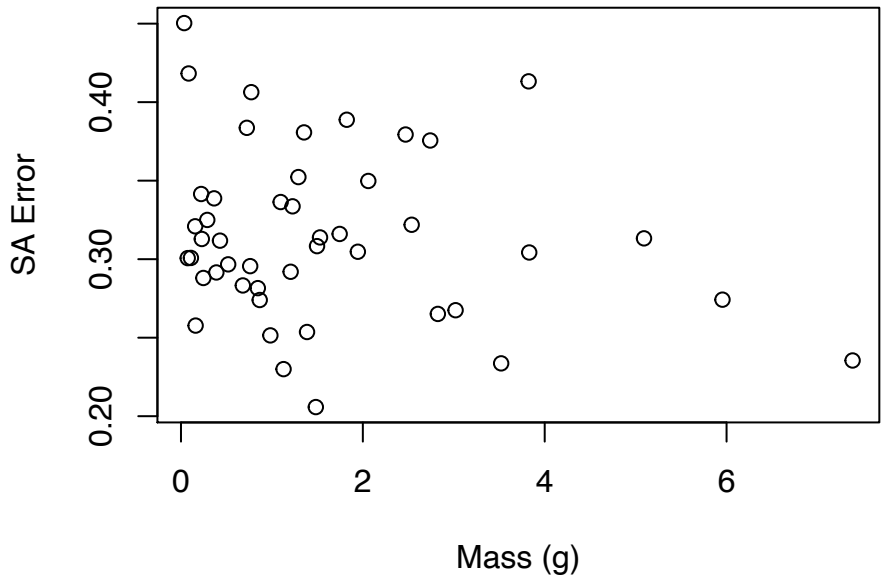

Figure S4. Estimation error of allometric estimates for surface area using the Whitford and Hutchison (1967) Urodele model ("WH67"). Estimation error is defined as the relative error ([empirical measurement – WH67 estimate] / empirical measurement). Error is generally high and does not covary with body mass, demonstrating consistently poor model fit across body sizes.

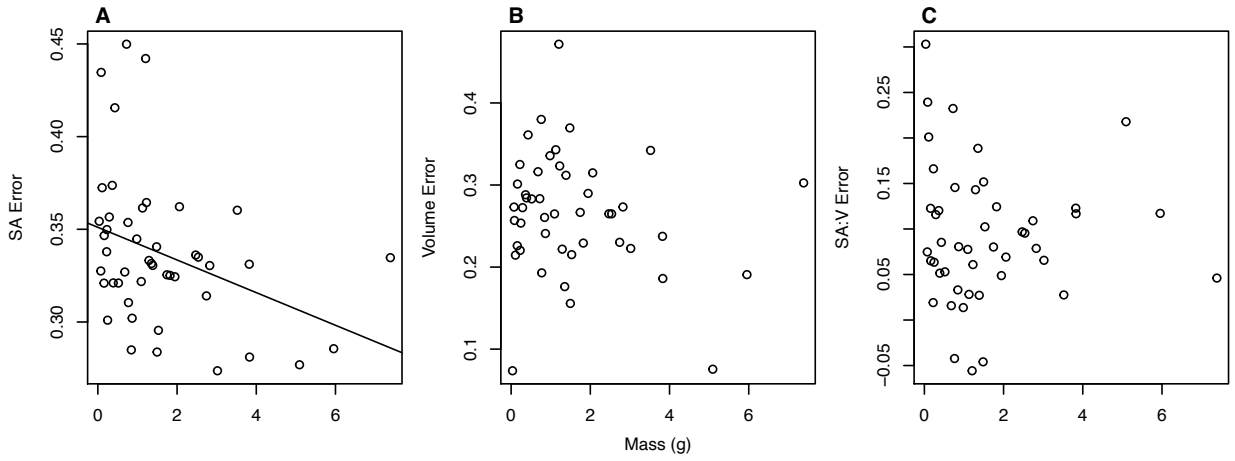

Figure S5. Estimation error using geometric estimates of surface area (A), volume (B), and SA:V (C) following Baken et al. (2020) ("BMA20"). Estimation error is defined as the relative error ([empirical measurement – BMA20 estimate] / empirical measurement). Error is highest when estimating surface area (A), with a significant bias toward higher error in small-bodied individuals, as represented by a significant regression line between mass and error. The magnitude of error is progressively lower for estimates of volume (B) and SA:V (C), with no bias across body size. In combination with Deming regressions (Fig. S3), these results demonstrate that BMA20 estimates of SA:V are reliable for body sizes > 0.22g.

Table S1. Specimen numbers and body mass of all specimens used for CT scans, Baken et al. (2020) linear measurements, and allometric regressions.

CUMV Specimen	Species	Mass (g)
3826	*P. cinereus*	0.035
3825	*P. cinereus*	0.074
5504b	*P. cinereus*	0.084
3782	*P. cinereus*	0.156
4064d	*P. cinereus*	0.161
5109p	*P. cinereus*	0.222
5105	*P. cinereus*	0.246
5103a	*P. cinereus*	0.389
5111i	*P. cinereus*	0.519
3504b	*P. cinereus*	0.680
3816c	*P. cinereus*	0.761
3504a	*P. cinereus*	0.845
3888b	*P. cinereus*	0.866
3816i	*P. cinereus*	0.983
5113f	*P. cinereus*	1.128
3816f	*P. cinereus*	1.206
(no ID)	*P. cinereus*	1.386
(no ID)	*P. cinereus*	1.483
5126	*P. glutinosus*	0.109
4522c	*P. glutinosus*	0.429
5015j	*P. glutinosus*	0.724
5015e	*P. glutinosus*	1.291
4246a	*P. glutinosus*	1.823
5015d	*P. glutinosus*	1.945
9587	*P. glutinosus*	2.470
6198c	*P. glutinosus*	2.741
4522h	*P. glutinosus*	3.521

4522b	*P. glutinosus*	3.823
9588	*P. glutinosus*	3.830
9589	*P. glutinosus*	5.092
12599	*P. glutinosus*	5.955
5126	*P. glutinosus*	7.386
2962a	*E. longicauda*	0.229
5196c	*E. longicauda*	0.289
5200a	*E. longicauda*	0.364
4248b	*E. longicauda*	0.773
5188b	*E. longicauda*	1.096
5191c	*E. longicauda*	1.227
4196	*E. longicauda*	1.353
3060a	*E. longicauda*	1.496
5338	*E. longicauda*	1.529
5197g	*E. longicauda*	1.745
5571a	*E. longicauda*	2.060
6206c	*E. longicauda*	2.537
5191d	*E. longicauda*	2.825
5190	*E. longicauda*	3.020

Table S2. Method performance for novel allometric models, plus allometric models of Whitford and Hutchison (1967) ("WH67") and geometric measurements of Baken et al. (2020) ("BMA20"). For this study we tested specific models for each of our three target species, plus a general model including all species. Whitford and Hutchison (1967) models are those developed for the family Plethodontidae and for all salamanders. Each general method was tested on each target species individually, plus all three together. Model parameters and (100 · [1- α]) % confidence intervals are results from a Deming regression of each dataset's empirical values (the independent variable) against each method's estimated values (the dependent variable). Accurate estimators are defined as those whose regression fit includes m = 1 and b = 0 within 95% confidence intervals.

Method	Trait	Model	Species	α	Slope (m)	Lower m CI	Upper m CI	Intercept (b)	Lower b CI	Upper b CI
this study	SA	general	all	0.0125	0.995	0.892	1.063	0.175	-78.531	112.275
this study	SA	general	*P. cinereus*	0.0125	1.115	1.057	1.178	-38.695	-87.053	-3.802
this study	SA	general	*P. glutinosus*	0.0125	1.031	0.860	1.153	-139.327	-486.911	136.230
this study	SA	general	*E. longicauda*	0.0125	1.031	0.929	1.182	-73.322	-349.333	36.736
this study	SA	*P. cinereus*	*P. cinereus*	0.0167	0.989	0.932	1.036	6.270	-27.144	42.783
this study	SA	*P. glutinosus*	*P. glutinosus*	0.0167	1.070	0.916	1.219	-157.066	-635.803	97.894
this study	SA	*E. longicauda*	*E. longicauda*	0.0167	1.046	0.951	1.166	-67.206	-307.565	39.128
this study	Volume	general	all	0.0125	0.936	0.843	1.002	66.584	5.650	171.962
this study	Volume	general	*P. cinereus*	0.0125	1.051	1.024	1.072	-10.863	-21.766	-1.795
this study	Volume	general	*P. glutinosus*	0.0125	0.952	0.771	1.021	-125.113	-477.318	208.461
this study	Volume	general	*E. longicauda*	0.0125	1.114	1.079	1.161	-32.700	-102.298	-0.275
this study	Volume	*P. cinereus*	*P. cinereus*	0.0167	0.983	0.960	1.003	7.380	-0.099	20.312
this study	Volume	*P. glutinosus*	*P. glutinosus*	0.0167	1.064	0.871	1.150	-189.094	-648.674	137.412
this study	Volume	*E. longicauda*	*E. longicauda*	0.0167	1.022	0.992	1.063	-25.812	-93.649	6.218

this study	SA:V	general	all	0.0125	1.022	0.911	1.121	-0.033	-0.159	0.101
this study	SA:V	general	*P. cinereus*	0.0125	1.016	0.865	1.175	0.030	-0.210	0.232
this study	SA:V	general	*P. glutinosus*	0.0125	1.037	0.711	1.105	0.013	-0.058	0.275
this study	SA:V	general	*E. longicauda*	0.0125	0.914	0.695	0.988	-0.015	-0.140	0.226
this study	SA:V	*P. cinereus*	*P. cinereus*	0.0167	0.987	0.854	1.144	0.019	-0.196	0.194
this study	SA:V	*P. glutinosus*	*P. glutinosus*	0.0167	1.039	0.706	1.110	-0.038	-0.111	0.233
this study	SA:V	*E. longicauda*	*E. longicauda*	0.0167	1.014	0.791	1.087	-0.018	-0.131	0.225
WH67	SA	Plethodontidae	all	0.0125	0.681	0.625	0.722	101.940	55.335	168.779
WH67	SA	Plethodontidae	*P. cinereus*	0.0125	0.827	0.785	0.869	19.039	-12.957	46.657
WH67	SA	Plethodontidae	*P. glutinosus*	0.0125	0.689	0.596	0.755	40.915	-150.980	210.788
WH67	SA	Plethodontidae	*E. longicauda*	0.0125	0.721	0.669	0.802	40.193	-99.251	103.644
WH67	SA	Urodela	all	0.0125	0.701	0.631	0.752	-18.888	-76.371	56.387
WH67	SA	Urodela	*P. cinereus*	0.0125	0.772	0.726	0.814	-35.874	-66.317	-9.579
WH67	SA	Urodela	*P. glutinosus*	0.0125	0.728	0.607	0.838	-118.061	-442.812	79.630
WH67	SA	Urodela	*E. longicauda*	0.0125	0.723	0.648	0.821	-68.116	-248.005	14.954
BMA20	SA	NA	all	0.0125	0.697	0.669	0.723	-35.668	-73.895	-2.902
BMA20	SA	NA	*P. cinereus*	0.0125	0.646	0.579	0.700	8.799	-17.766	45.585
BMA20	SA	NA	*P. glutinosus*	0.0125	0.714	0.671	0.775	-89.411	-236.547	-5.048
BMA20	SA	NA	*E. longicauda*	0.0125	0.695	0.645	0.751	-29.816	-117.408	40.963
BMA20	vol	NA	all	0.0125	0.784	0.709	0.887	-55.315	-173.596	22.963
BMA20	vol	NA	*P. cinereus*	0.0125	0.638	0.564	0.704	18.950	-0.041	44.451
BMA20	vol	NA	*P. glutinosus*	0.0125	0.790	0.697	0.951	-65.791	-481.649	136.943
BMA20	vol	NA	*E. longicauda*	0.0125	0.743	0.693	0.793	11.171	-46.737	70.947
BMA20	SA:V	NA	all	0.0125	0.772	0.665	0.929	0.167	-0.012	0.303
BMA20	SA:V	NA	*P. cinereus*	0.0125	0.659	0.548	0.906	0.431	0.083	0.647
BMA20	SA:V	NA	*P. glutinosus*	0.0125	0.778	0.666	0.968	0.087	-0.069	0.184
BMA20	SA:V	NA	*E. longicauda*	0.0125	0.808	0.724	0.877	0.103	0.006	0.193

Table S3. Comparisons of species-specific allometric slopes for SA, volume, and SA:V.

Trait	Species 1	Slope 1	Species 2	Slope 2	*t* ratio	*P* value
Surface area	*P. cinereus*	0.631	*P. glutinosus*	0.682	-2.349	0.0605
Surface area	*P. cinereus*	0.631	*E. longicauda*	0.674	-1.591	0.2614
Surface area	*P. glutinosus*	0.682	*E. longicauda*	0.674	0.315	0.9469
Volume	*P. cinereus*	0.973	*P. glutinosus*	1.036	-3.234	0.0068
Volume	*P. cinereus*	0.973	*E. longicauda*	1.014	-1.700	0.2176
Volume	*P. glutinosus*	1.036	*E. longicauda*	1.014	0.905	0.6404
SA:V	*P. cinereus*	-0.342	*P. glutinosus*	-0.354	0.703	0.7629
SA:V	*P. cinereus*	-0.342	*E. longicauda*	-0.340	-0.081	0.9963
SA:V	*P. glutinosus*	-0.354	*E. longicauda*	-0.340	-0.631	0.8039

Table S4. Comparisons between estimation methods using Deming regressions. Model parameters are given for regressions with Method 1 as the independent variable and Method 2 as the dependent variable. Comparisons are made either across our entire dataset (Mass Range = "all"), or using only specimens larger than the minimum size analyzed by Baken et al. (2020) (Mass Range = "BMA20"), or individuals of mass at least 0.22 g.

Trait	Method 1	Method 2	Mass Range	Slope (*m*)	Lower *m* CI	Upper *m* CI	Intercept (*b*)	Lower *b* CI	Upper *b* CI
Surface area	WH67 Urodela	WH67 Plethodontidae	all	0.971	0.951	1.006	120.388	93.500	143.473
Surface area	This study	WH67 Urodela	all	0.707	0.702	0.709	-22.599	-27.681	-17.143
Surface area	WH67 Urodela	BMA20	all	0.993	0.917	1.087	-17.105	-91.919	45.433
Surface area	This study	BMA20	all	0.698	0.646	0.762	-32.373	-108.568	24.448
Volume	This study	BMA20	all	0.836	0.728	0.979	-107.497	-276.334	-1.392
SA:V	This study	BMA20	all	0.754	0.658	0.925	0.193	-0.003	0.322
Surface area	This study	BMA20	BMA20	0.745	0.659	0.800	-99.687	-178.494	-3.541
Volume	This study	BMA20	BMA20	0.933	0.723	1.040	-258.411	-425.654	-21.290
SA:V	This study	BMA20	BMA20	0.982	0.909	1.076	-0.057	-0.164	0.046
Surface area	This study	BMA20	>= 0.22 g	0.701	0.640	0.773	-40.668	-147.408	43.519
Volume	This study	BMA20	>= 0.22 g	0.845	0.727	1.001	-140.443	-360.796	-3.476
SA:V	This study	BMA20	>= 0.22 g	0.988	0.921	1.070	-0.065	-0.155	0.026

Table S5. Comparisons between estimations of SA-dependent physiological responses, calculated using SA estimates from either Whitford and Hutchison (1967) or this study.

Response	SA Estimator 1	SA Estimator 2	Slope (*m*)	Lower *m* CI	Upper *m* CI	Intercept (*b*)	Lower *b* CI	Upper *b* CI
Cutaneous water loss	This study	WH67 Urodela	1.460	1.455	1.465	-0.035	-0.051	-0.018
Total resistance to water loss	This study	WH67 Urodela	0.698	0.694	0.702	-0.027	-0.038	-0.015

SUPPLEMENTAL MATERIALS – CHAPTER THREE

Table S1. Model comparisons for all linear models tested across the full dataset, and subsets based on 20% mass quantiles. Compared models are listed in order of support by mean squared error (MSE), with each set of models separated by a solid line. MSE values in bold represent the predictor that is the best unbiased estimator of the response. Bold pR^2 values represent the predictor that explains the most variance in the response. Bold beta weight (BW) values represent the predictor whose variation effects the greatest magnitude of change in the response. FDR values are false discover rate-corrected p-values across all 180 regressions.

Dataset	Response	Predictor	*F* value	*p*-value	FDR	MSE	R^2	pR^2	BW
full	Resp	BSI_2 res.	7.778	0.006	0.005	**1.485**	0.102	0.070	0.296
full	Resp	BSI_1	173.294	0.000	0.000	2.888	0.574	0.539	0.806
full	Resp	Mass	185.984	0.000	0.000	2.975	0.676	**0.638**	0.839
full	Resp	BSI_1 res.	157.731	0.000	0.000	3.575	0.477	0.474	**2.752**
full	Resp	BSI_2	97.429	0.000	0.000	11.645	0.427	0.395	0.727
full	sResp	BSI_1	21.904	0.000	0.000	**2.301**	0.223	0.173	-0.428
full	sResp	BSI_2 res.	0.258	0.613	0.180	2.962	0.054	0.004	0.064
full	sResp	BSI_1 res.	12.415	0.001	0.001	3.585	0.347	**0.331**	**-1.037**
full	sResp	Mass	22.921	0.000	0.000	5.563	0.247	0.196	-0.449
full	sResp	BSI_2	8.374	0.004	0.004	15.176	0.123	0.072	-0.276
full	EWL	BSI_2	72.276	0.000	0.000	**4.214**	0.681	0.189	0.432
full	EWL	Mass	224.389	0.000	0.000	13.948	0.836	0.327	0.553
full	EWL	BSI_2 res.	7.341	0.007	0.006	17.734	0.495	0.038	0.207
full	EWL	BSI_1 res.	74.786	0.000	0.000	18.120	0.519	**0.423**	**1.479**
full	EWL	BSI_1	104.613	0.000	0.000	50.593	0.774	0.248	0.476
full	sEWL	BSI_2	58.638	0.000	0.000	**2.833**	0.661	0.186	-0.468
full	sEWL	Mass	221.865	0.000	0.000	11.885	0.836	0.304	-0.571
full	sEWL	BSI_2 res.	0.161	0.689	0.190	13.817	0.540	0.002	-0.035
full	sEWL	BSI_1 res.	143.177	0.000	0.000	16.548	0.501	**0.448**	**-2.146**

full	sEWL	BSI_1	149.502	0.000	0.000	45.307	0.763	0.303	-0.609
full	CWL	BSI_2	8.040	0.007	0.006	**1.039**	0.738	0.024	-0.160
full	CWL	Mass	27.916	0.000	0.000	1.731	0.774	0.050	-0.236
full	CWL	BSI_2 res.	0.730	0.406	0.139	2.023	0.739	0.002	0.052
full	CWL	BSI_1 res.	18.507	0.000	0.000	2.594	0.574	**0.279**	**-0.831**
full	CWL	BSI_1	22.981	0.000	0.000	19.101	0.753	0.059	-0.255
full	*r*	Mass	25.609	0.000	0.000	**0.917**	0.343	0.126	0.378
full	*r*	BSI_2	6.499	0.015	0.011	1.021	0.262	0.052	0.241
full	*r*	BSI_1 res.	13.307	0.001	0.001	1.416	0.394	**0.337**	**1.158**
full	*r*	BSI_2 res.	0.876	0.363	0.130	1.493	0.233	0.008	-0.096
full	*r*	BSI_1	19.386	0.000	0.000	17.213	0.327	0.128	0.394
1 - 20%	Resp	BSI_1 res.	20.097	0.000	0.000	**1.107**	0.171	0.169	**2.488**
1 - 20%	Resp	Mass	26.190	0.000	0.000	2.159	0.284	**0.217**	0.481
1 - 20%	Resp	BSI_1	23.071	0.000	0.000	3.191	0.186	0.147	0.516
1 - 20%	Resp	BSI_2 res.	0.760	0.403	0.139	4.506	0.089	0.019	-0.150
1 - 20%	Resp	BSI_2	4.919	0.031	0.020	14.760	0.114	0.076	0.368
1 - 20%	sResp	Mass	0.193	0.662	0.187	**1.012**	0.080	0.002	-0.047
1 - 20%	sResp	BSI_2 res.	0.113	0.742	0.200	2.682	0.081	0.003	-0.061
1 - 20%	sResp	BSI_1 res.	0.244	0.657	0.187	3.108	0.083	**0.010**	**-0.104**
1 - 20%	sResp	BSI_1	0.358	0.552	0.168	4.261	0.085	0.005	-0.073
1 - 20%	sResp	BSI_2	0.279	0.602	0.178	12.978	0.086	0.006	-0.086
1 - 20%	EWL	BSI_2	9.593	0.003	0.003	**3.096**	0.731	**0.054**	**0.243**
1 - 20%	EWL	BSI_1 res.	0.047	0.832	0.211	12.161	0.798	0.000	-0.013
1 - 20%	EWL	BSI_2 res.	0.257	0.627	0.183	12.823	0.800	0.001	0.036
1 - 20%	EWL	Mass	13.819	0.001	0.001	17.745	0.835	0.050	0.175
1 - 20%	EWL	BSI_1	8.547	0.005	0.004	52.894	0.797	0.034	0.164
1 - 20%	sEWL	BSI_2	0.056	0.819	0.211	**4.560**	0.762	0.000	-0.018
1 - 20%	sEWL	BSI_1 res.	0.142	0.712	0.193	15.856	0.762	0.001	0.022
1 - 20%	sEWL	BSI_2 res.	1.969	0.194	0.084	16.631	0.769	0.012	0.098
1 - 20%	sEWL	Mass	36.669	0.000	0.000	22.268	0.840	0.077	-0.282
1 - 20%	sEWL	BSI_1	30.616	0.000	0.000	57.231	0.681	**0.082**	**-0.303**
1 - 20%	CWL	BSI_2	0.100	0.759	0.202	**0.558**	0.813	0.000	0.021
1 - 20%	CWL	BSI_1 res.	0.092	0.765	0.202	1.886	0.813	0.000	0.016
1 - 20%	CWL	BSI_2 res.	1.689	0.227	0.095	2.122	0.817	0.008	0.081
1 - 20%	CWL	Mass	8.632	0.005	0.004	4.344	0.831	**0.018**	**-0.141**

1 - 20%	CWL	BSI_1	3.250	0.078	0.042	25.716	0.821	0.009	-0.094
1 - 20%	*r*	BSI_1 res.	0.068	0.797	0.207	**0.640**	0.358	0.001	-0.026
1 - 20%	*r*	BSI_2 res.	1.474	0.261	0.105	0.804	0.377	0.020	-0.142
1 - 20%	*r*	BSI_2	0.285	0.607	0.179	1.272	0.361	0.004	-0.065
1 - 20%	*r*	Mass	4.839	0.033	0.021	2.299	0.396	**0.038**	**0.198**
1 - 20%	*r*	BSI_1	1.913	0.173	0.077	20.534	0.375	0.018	0.135
21 - 40%	Resp	BSI_2 res.	1.022	0.346	0.125	**2.462**	0.147	0.079	0.285
21 - 40%	Resp	Mass	2.136	0.150	0.071	2.601	0.093	0.012	0.143
21 - 40%	Resp	BSI_1 res.	0.086	0.786	0.205	2.810	0.084	0.011	0.089
21 - 40%	Resp	BSI_1	0.903	0.365	0.130	3.016	0.137	0.068	0.269
21 - 40%	Resp	BSI_2	2.026	0.190	0.083	13.129	0.198	**0.137**	**0.409**
21 - 40%	sResp	BSI_2 res.	1.752	0.227	0.095	**2.429**	0.182	**0.122**	**0.367**
21 - 40%	sResp	Mass	0.443	0.509	0.160	2.572	0.079	0.007	-0.066
21 - 40%	sResp	BSI_1 res.	0.103	0.766	0.202	2.804	0.079	0.013	0.096
21 - 40%	sResp	BSI_1	0.007	0.934	0.228	2.932	0.068	0.000	-0.024
21 - 40%	sResp	BSI_2	1.299	0.290	0.114	13.224	0.155	0.091	0.305
21 - 40%	EWL	BSI_2	0.661	0.464	0.151	**3.446**	0.758	0.005	-0.058
21 - 40%	EWL	BSI_1 res.	1.596	0.295	0.114	14.733	0.762	0.010	-0.086
21 - 40%	EWL	Mass	14.362	0.000	0.001	15.054	0.798	**0.045**	**0.213**
21 - 40%	EWL	BSI_2 res.	1.405	0.305	0.115	15.113	0.761	0.009	-0.083
21 - 40%	EWL	BSI_1	0.188	0.691	0.190	51.134	0.755	0.002	-0.031
21 - 40%	sEWL	BSI_2	0.302	0.613	0.180	**3.496**	0.787	0.002	-0.036
21 - 40%	sEWL	BSI_1 res.	0.746	0.451	0.148	14.840	0.788	**0.004**	-0.055
21 - 40%	sEWL	Mass	1.019	0.317	0.117	15.151	0.788	0.003	**0.058**
21 - 40%	sEWL	BSI_2 res.	0.420	0.554	0.168	15.223	0.787	0.003	-0.042
21 - 40%	sEWL	BSI_1	0.389	0.574	0.172	51.360	0.787	0.003	-0.041
21 - 40%	CWL	BSI_2	0.436	0.547	0.168	**0.801**	0.782	0.003	-0.044
21 - 40%	CWL	Mass	3.609	0.062	0.035	2.045	0.790	**0.012**	**0.109**
21 - 40%	CWL	BSI_1 res.	1.044	0.382	0.134	2.050	0.784	0.006	-0.065
21 - 40%	CWL	BSI_2 res.	0.724	0.445	0.148	2.111	0.783	0.005	-0.056
21 - 40%	CWL	BSI_1	0.338	0.598	0.178	21.777	0.781	0.003	-0.039
21 - 40%	*r*	BSI_2	0.234	0.655	0.187	**0.865**	0.250	0.005	0.060
21 - 40%	*r*	BSI_1 res.	0.540	0.515	0.161	1.323	0.254	0.010	0.089
21 - 40%	*r*	Mass	3.202	0.079	0.042	1.382	0.282	**0.039**	**-0.191**
21 - 40%	*r*	BSI_2 res.	0.443	0.544	0.168	1.391	0.253	0.009	0.082

21 - 40%	*r*	BSI_1	0.105	0.765	0.202	19.818	0.247	0.002	0.041
41 - 60%	Resp	BSI_1 res.	2.931	0.151	0.071	**1.138**	0.260	0.156	0.514
41 - 60%	Resp	BSI_2 res.	5.244	0.030	0.020	1.323	0.280	0.150	0.454
41 - 60%	Resp	Mass	19.766	0.000	0.000	2.488	0.247	0.074	0.367
41 - 60%	Resp	BSI_1	17.505	0.000	0.000	3.898	0.367	**0.227**	**0.578**
41 - 60%	Resp	BSI_2	12.699	0.001	0.001	10.920	0.347	0.208	0.538
41 - 60%	sResp	BSI_1 res.	1.786	0.244	0.100	**1.850**	0.244	**0.084**	**0.295**
41 - 60%	sResp	BSI_2 res.	1.957	0.178	0.078	2.117	0.243	0.069	0.252
41 - 60%	sResp	BSI_1	0.874	0.357	0.128	2.997	0.196	0.019	0.139
41 - 60%	sResp	Mass	0.069	0.795	0.207	3.721	0.163	0.000	0.024
41 - 60%	sResp	BSI_2	1.648	0.209	0.089	12.877	0.221	0.042	0.196
41 - 60%	EWL	BSI_2	0.664	0.436	0.145	**4.585**	0.821	0.001	0.050
41 - 60%	EWL	Mass	6.186	0.016	0.012	13.968	0.834	**0.019**	**0.126**
41 - 60%	EWL	BSI_2 res.	0.091	0.772	0.203	18.148	0.819	0.000	0.019
41 - 60%	EWL	BSI_1 res.	1.064	0.335	0.122	19.133	0.822	0.002	0.060
41 - 60%	EWL	BSI_1	4.132	0.061	0.034	54.539	0.831	0.012	0.115
41 - 60%	sEWL	BSI_2	0.404	0.540	0.168	**3.297**	0.819	0.004	-0.041
41 - 60%	sEWL	Mass	5.369	0.024	0.017	11.544	0.832	**0.004**	**-0.118**
41 - 60%	sEWL	BSI_2 res.	0.031	0.866	0.217	15.375	0.818	0.002	-0.011
41 - 60%	sEWL	BSI_1 res.	1.145	0.318	0.118	16.265	0.821	0.002	0.064
41 - 60%	sEWL	BSI_1	0.004	0.950	0.231	49.657	0.818	0.001	-0.004
41 - 60%	CWL	BSI_2	0.029	0.868	0.217	**0.723**	0.830	0.001	-0.010
41 - 60%	CWL	Mass	0.581	0.449	0.148	1.191	0.831	0.000	-0.039
41 - 60%	CWL	BSI_2 res.	0.000	0.993	0.239	2.481	0.830	0.001	-0.001
41 - 60%	CWL	BSI_1 res.	1.193	0.309	0.116	2.850	0.833	**0.002**	**0.061**
41 - 60%	CWL	BSI_1	0.357	0.560	0.169	21.687	0.831	0.002	0.034
41 - 60%	*r*	BSI_2	0.122	0.735	0.199	**0.655**	0.400	0.003	0.040
41 - 60%	*r*	Mass	0.785	0.380	0.134	0.764	0.403	0.002	0.085
41 - 60%	*r*	BSI_2 res.	0.031	0.866	0.217	1.924	0.399	0.002	0.020
41 - 60%	*r*	BSI_1 res.	0.842	0.388	0.136	2.289	0.405	**0.007**	**-0.099**
41 - 60%	*r*	BSI_1	0.162	0.693	0.190	20.429	0.399	0.003	-0.044
61 - 80%	Resp	BSI_1 res.	3.097	0.145	0.070	**0.710**	0.301	0.273	**0.719**
61 - 80%	Resp	BSI_2 res.	4.675	0.046	0.028	0.819	0.305	0.270	0.651
61 - 80%	Resp	BSI_1	9.243	0.005	0.004	3.163	0.277	0.240	0.583
61 - 80%	Resp	Mass	10.875	0.002	0.002	3.368	0.140	0.094	0.337

61 - 80%	Resp	BSI_2	8.666	0.007	0.006	10.012	0.342	**0.306**	0.684
61 - 80%	sResp	BSI_1	1.615	0.213	0.090	**1.162**	0.108	**0.062**	**-0.279**
61 - 80%	sResp	BSI_1 res.	0.044	0.845	0.214	2.690	0.055	0.007	-0.083
61 - 80%	sResp	BSI_2 res.	0.171	0.686	0.190	3.013	0.064	0.011	0.136
61 - 80%	sResp	Mass	2.742	0.105	0.052	7.426	0.085	0.033	-0.188
61 - 80%	sResp	BSI_2	0.099	0.755	0.202	15.905	0.059	0.008	-0.084
61 - 80%	EWL	BSI_2	8.880	0.167	0.075	**4.911**	0.792	0.071	0.273
61 - 80%	EWL	Mass	2.851	0.099	0.050	12.361	0.740	0.010	0.099
61 - 80%	EWL	BSI_2 res.	10.191	0.248	0.100	19.831	0.791	0.072	**0.277**
61 - 80%	EWL	BSI_1 res.	9.821	0.207	0.089	20.787	0.790	**0.075**	0.273
61 - 80%	EWL	BSI_1	6.636	0.059	0.033	50.794	0.784	0.058	0.238
61 - 80%	sEWL	BSI_2	5.543	0.025	0.017	**2.249**	0.693	0.079	-0.320
61 - 80%	sEWL	Mass	14.207	0.001	0.001	7.106	0.763	0.046	-0.215
61 - 80%	sEWL	BSI_2 res.	0.551	0.479	0.154	13.270	0.704	0.012	-0.123
61 - 80%	sEWL	BSI_1 res.	0.045	0.847	0.214	13.973	0.714	0.001	-0.033
61 - 80%	sEWL	BSI_1	9.697	0.004	0.003	40.479	0.698	**0.095**	**-0.351**
61 - 80%	CWL	Mass	4.034	0.052	0.031	**0.460**	0.752	0.013	-0.116
61 - 80%	CWL	BSI_2	0.749	0.399	0.138	1.099	0.724	0.010	-0.111
61 - 80%	CWL	BSI_2 res.	0.101	0.766	0.202	2.089	0.749	0.003	0.043
61 - 80%	CWL	BSI_1 res.	1.001	0.432	0.145	2.368	0.763	0.015	0.114
61 - 80%	CWL	BSI_1	1.752	0.199	0.086	16.885	0.723	**0.017**	**-0.144**
61 - 80%	*r*	Mass	3.698	0.062	0.035	**0.153**	0.271	0.033	0.192
61 - 80%	*r*	BSI_2	0.606	0.448	0.148	0.936	0.238	0.021	0.172
61 - 80%	*r*	BSI_2 res.	0.141	0.726	0.197	1.887	0.254	0.010	-0.087
61 - 80%	*r*	BSI_1 res.	1.264	0.394	0.137	2.306	0.298	**0.053**	-0.216
61 - 80%	*r*	BSI_1	1.492	0.235	0.097	15.992	0.249	0.038	**0.228**
81 - 100%	Resp	BSI_2 res.	0.021	0.903	0.222	**0.496**	0.078	0.000	0.037
81 - 100%	Resp	BSI_1 res.	0.005	0.977	0.237	0.716	0.078	0.000	0.027
81 - 100%	Resp	BSI_1	0.054	0.872	0.217	1.479	0.082	0.002	0.075
81 - 100%	Resp	Mass	0.422	0.526	0.164	4.665	0.091	**0.010**	**0.116**
81 - 100%	Resp	BSI_2	0.064	0.846	0.214	9.657	0.081	0.002	0.074
81 - 100%	sResp	BSI_1	4.467	0.099	0.050	**0.489**	0.302	**0.244**	**-0.533**
81 - 100%	sResp	BSI_2 res.	0.354	0.558	0.169	4.245	0.045	0.004	0.140
81 - 100%	sResp	BSI_1 res.	1.936	0.446	0.148	5.829	0.237	0.177	-0.441
81 - 100%	sResp	Mass	6.951	0.019	0.013	13.919	0.257	0.191	-0.444

81 - 100%	sResp	BSI_2	1.283	0.493	0.157	21.789	0.171	0.099	-0.295
81 - 100%	EWL	BSI_2	2.775	0.394	0.137	**5.320**	0.715	0.038	0.243
81 - 100%	EWL	Mass	7.674	0.016	0.012	10.515	0.724	0.054	0.267
81 - 100%	EWL	BSI_1 res.	1.497	0.697	0.191	20.948	0.701	0.036	0.244
81 - 100%	EWL	BSI_2 res.	1.304	0.423	0.142	22.037	0.686	0.008	0.162
81 - 100%	EWL	BSI_1	3.469	0.296	0.114	42.901	0.724	**0.062**	**0.295**
81 - 100%	sEWL	BSI_2	0.000	0.990	0.239	**0.728**	0.709	0.000	-0.003
81 - 100%	sEWL	Mass	0.948	0.349	0.126	3.016	0.719	**0.010**	**-0.094**
81 - 100%	sEWL	BSI_1 res.	0.000	0.993	0.239	9.222	0.709	0.000	0.005
81 - 100%	sEWL	BSI_2 res.	0.112	0.783	0.205	9.915	0.712	0.001	0.046
81 - 100%	sEWL	BSI_1	0.078	0.854	0.215	25.032	0.712	0.004	-0.048
81 - 100%	CWL	Mass	0.058	0.814	0.210	**0.398**	0.713	0.000	0.024
81 - 100%	CWL	BSI_1 res.	0.154	0.896	0.221	1.226	0.717	0.004	0.078
81 - 100%	CWL	BSI_2 res.	0.458	0.600	0.178	1.446	0.721	**0.005**	**0.090**
81 - 100%	CWL	BSI_2	0.295	0.701	0.191	1.949	0.719	0.004	0.080
81 - 100%	CWL	BSI_1	0.118	0.824	0.211	9.088	0.715	0.002	0.059
81 - 100%	*r*	Mass	0.047	0.832	0.211	**0.122**	0.165	0.001	-0.037
81 - 100%	*r*	BSI_1 res.	0.171	0.893	0.221	1.262	0.180	0.016	-0.141
81 - 100%	*r*	BSI_2 res.	0.535	0.576	0.172	1.490	0.188	**0.023**	**-0.166**
81 - 100%	*r*	BSI_2	0.331	0.688	0.190	1.496	0.182	0.017	-0.145
81 - 100%	*r*	BSI_1	0.122	0.822	0.211	9.538	0.172	0.008	-0.103

Note: Resp = gross respiration, sResp = specific respiration, EWL = gross evaporative water loss, sEWL = specific evaporative water loss, CWL = cutaneous water loss, *r* = total resistance, res. = residuals

Table S2. Model parameters for all evolutionary regressions. Null models test for only the effect of phylogeny (the model intercept), while alternative models additionally test for the effect of the predictor (the model slope). FDR values are false discovery rate-corrected p-values across all 18 regressions. Significant correlations are presented in bold.

Predictor	Response	Intercept	Slope ± SE	R^2	Null Log Likelihood	Alternative Log Likelihood	*p*-value	FDR
BSI_1	Resp	0.655	0.646 ± 0.170	0.630	-6.134	-2.158	0.005	**0.016**
BSI_1	sResp	-2.415	-0.240 ± 0.135	0.293	-1.247	0.134	0.096	0.134
BSI_1	EWL	5.724	0.538 ± 0.089	0.828	-3.548	3.311	0.000	**0.001**
BSI_1	sEWL	2.642	0.354 ± 0.098	0.631	-1.244	2.655	0.005	**0.016**
BSI_1	CWL	1.146	-0.075 ± 0.051	0.136	7.500	7.984	0.325	0.341
BSI_1	*r*	1.372	0.067 ± 0.046	0.208	7.670	8.578	0.178	0.229
BSI_2	Resp	-4.218	1.478 ± 0.641	0.431	-6.133	-3.936	0.036	0.065
BSI_2	sResp	-0.848	-0.542 ± 0.415	0.189	-1.247	-0.504	0.223	0.267
BSI_2	EWL	1.656	1.254 ± 0.406	0.563	-3.547	-0.326	0.011	**0.022**
BSI_2	sEWL	5.077	-0.726 ± 0.380	0.392	-1.244	0.519	0.060	0.091
BSI_2	CWL	1.531	-0.079 ± 0.150	0.157	7.616	8.070	0.341	0.341
BSI_2	*R*	0.925	0.105 ± 0.143	0.204	7.672	8.280	0.270	0.304
Mass	Resp	-1.573	0.731 ± 0.119	0.827	-8.075	0.668	0.000	**0.000**
Mass	sResp	-1.581	-0.271 ± 0.119	0.386	-1.247	0.695	0.049	0.080
Mass	EWL	3.879	0.562 ± 0.042	0.978	-29.934	10.639	0.000	**0.000**
Mass	sEWL	3.879	-0.435 ± 0.043	0.966	-13.249	10.743	0.000	**0.000**
Mass	CWL	1.369	-0.115 ± 0.041	0.662	7.616	10.994	0.009	**0.021**
Mass	*r*	1.123	0.111 ± 0.030	0.625	7.672	11.288	0.007	**0.018**

Note: Resp = gross respiration, sResp = specific respiration, EWL = gross evaporative water loss, sEWL = specific evaporative water loss, CWL = cutaneous water loss, *r* = total resistance, res. = residuals

Table S3. Estimated marginal means (EMMs) for mean squared errors (MSE), semi-partial R^2 (pR^2), and BW (BW) values compared between predictor variables. Values included in EMMs are estimated across all response variables, meaning EMMs represent a predictor's holistic performance in predicting all physiological responses (MSE), variability (pR2), or effect size (BW). p-values are corrected for multiple comparisons using Tukey honest significant differences. Significant values ($p<0.05$) are presented in bold, and represent differences in the performance of one predictor over another across all response phenotypes.

Dataset	Predictor 1	Predictor 2	MSE 1	MSE 2	MSE *t*-ratio	MSE *p*-value	pR^2 1	pR^2 2	pR^2 *t*-ratio	pR^2 *p*-value	BW 1	BW 2	BW *t*-ratio	BW *p*-value
full	BSI_1	BSI_2	22.90	5.99	2.666	0.088	0.242	0.153	1.102	0.804	0.064	0.083	-0.035	1.000
full	BSI_1	Mass	22.90	6.17	2.637	0.094	0.242	0.273	-0.395	0.995	0.064	0.086	-0.040	1.000
full	BSI_1	BSI_1 res.	22.90	7.64	2.405	0.147	0.242	0.382	-1.745	0.426	0.064	0.229	-0.307	0.998
full	BSI_1	BSI_2 res.	22.90	6.59	2.571	0.107	0.242	0.021	2.745	0.075	0.064	0.081	-0.032	1.000
full	BSI_2	Mass	5.99	6.17	-0.029	1.000	0.153	0.273	-1.497	0.574	0.083	0.086	-0.006	1.000
full	BSI_2	BSI_1 res.	5.99	7.64	-0.260	0.999	0.153	0.382	-2.847	0.061	0.083	0.229	-0.273	0.999
full	BSI_2	BSI_2 res.	5.99	6.59	-0.094	1.000	0.153	0.021	1.643	0.485	0.083	0.081	0.003	1.000
full	Mass	BSI_1 res.	6.17	7.64	-0.232	0.999	0.273	0.382	-1.350	0.664	0.086	0.229	-0.267	0.999
full	Mass	BSI_2 res.	6.17	6.59	-0.066	1.000	0.273	0.021	3.140	**0.032**	0.086	0.081	0.008	1.000
full	BSI_1 res.	BSI_2 res.	7.64	6.59	0.166	1.000	0.382	0.021	4.490	**0.001**	0.229	0.081	0.275	0.999
1 - 20 %	BSI_1	BSI_2	27.30	6.20	2.984	**0.045**	0.049	0.023	0.810	0.925	0.058	0.077	-0.067	1.000
1 - 20 %	BSI_1	Mass	27.30	8.30	2.687	0.085	0.049	0.067	-0.570	0.978	0.058	0.064	-0.022	1.000
1 - 20 %	BSI_1	BSI_1 res.	27.30	5.79	3.042	**0.040**	0.049	0.067	0.597	0.974	0.058	0.397	-1.175	0.765
1 - 20 %	BSI_1	BSI_2 res.	27.30	6.59	2.928	0.051	0.049	0.010	1.221	0.740	0.058	-0.023	0.280	0.999
1 - 20 %	BSI_2	Mass	6.20	8.30	-0.297	0.998	0.023	0.067	-1.380	0.645	0.077	0.064	0.045	1.000

1 - 20 %	BSI_2	BSI_1 res.	6.20	5.79	0.058	1.000	0.023	0.067	-0.213	1.000	0.077	0.397	-1.108	0.801
1 - 20 %	BSI_2	BSI_2 res.	6.20	6.59	-0.055	1.000	0.023	0.010	0.411	0.994	0.077	-0.023	0.347	0.997
1 - 20 %	Mass	BSI_1 res.	8.30	5.79	0.355	0.996	0.067	0.067	1.167	0.769	0.064	0.397	-1.153	0.777
1 - 20 %	Mass	BSI_2 res.	8.30	6.59	0.242	0.999	0.067	0.010	1.791	0.401	0.064	-0.023	0.302	0.998
1 - 20 %	BSI_1 res.	BSI_2 res.	5.79	6.59	-0.113	1.000	0.030	0.010	0.624	0.970	0.397	-0.023	1.455	0.600
21 - 40 %	BSI_1	BSI_2	25.01	5.83	2.928	0.051	0.013	0.041	-1.276	0.708	0.029	0.106	-0.856	0.910
21 - 40 %	BSI_1	Mass	25.01	6.47	2.830	0.063	0.013	0.020	-0.307	0.998	0.029	0.044	-0.168	1.000
21 - 40 %	BSI_1	BSI_1 res.	25.01	6.43	2.836	0.062	0.013	0.020	0.187	1.000	0.029	0.011	0.198	1.000
21 - 40 %	BSI_1	BSI_2 res.	25.01	6.45	2.832	0.063	0.013	0.038	-1.144	0.782	0.029	0.092	-0.701	0.954
21 - 40 %	BSI_2	Mass	5.83	6.47	-0.098	1.000	0.041	0.020	0.969	0.866	0.106	0.044	0.688	0.957
21 - 40 %	BSI_2	BSI_1 res.	5.83	6.43	-0.092	1.000	0.041	0.020	1.462	0.595	0.106	0.011	1.054	0.828
21 - 40 %	BSI_2	BSI_2 res.	5.83	6.45	-0.096	1.000	0.041	0.038	0.131	1.000	0.106	0.092	0.155	1.000
21 - 40 %	Mass	BSI_1 res.	6.47	6.43	0.006	1.000	0.020	0.020	0.493	0.987	0.044	0.011	0.366	0.996
21 - 40 %	Mass	BSI_2 res.	6.47	6.45	0.002	1.000	0.020	0.038	-0.838	0.916	0.044	0.092	-0.533	0.983
21 - 40 %	BSI_1 res.	BSI_2 res.	6.43	6.45	-0.004	1.000	0.009	0.038	-1.331	0.675	0.011	0.092	-0.899	0.895
41 - 60 %	BSI_1	BSI_2	25.53	5.51	2.989	**0.045**	0.044	0.043	0.020	1.000	0.136	0.129	0.063	1.000
41 - 60 %	BSI_1	Mass	25.53	5.61	2.973	**0.046**	0.044	0.017	0.690	0.957	0.136	0.074	0.524	0.984
41 - 60 %	BSI_1	BSI_1 res.	25.53	7.25	2.728	0.078	0.044	0.017	0.046	1.000	0.136	0.149	-0.108	1.000
41 - 60 %	BSI_1	BSI_2 res.	25.53	6.89	2.782	0.070	0.044	0.037	0.169	1.000	0.136	0.122	0.120	1.000
41 - 60 %	BSI_2	Mass	5.51	5.61	-0.015	1.000	0.043	0.017	0.670	0.961	0.129	0.074	0.461	0.990
41 - 60 %	BSI_2	BSI_1 res.	5.51	7.25	-0.260	0.999	0.043	0.017	0.026	1.000	0.129	0.149	-0.171	1.000
41 - 60 %	BSI_2	BSI_2 res.	5.51	6.89	-0.207	1.000	0.043	0.037	0.149	1.000	0.129	0.122	0.057	1.000
41 - 60 %	Mass	BSI_1 res.	5.61	7.25	-0.245	0.999	0.017	0.017	-0.644	0.966	0.074	0.149	-0.632	0.968
41 - 60 %	Mass	BSI_2 res.	5.61	6.89	-0.191	1.000	0.017	0.037	-0.522	0.984	0.074	0.122	-0.404	0.994
41 - 60 %	BSI_1 res.	BSI_2 res.	7.25	6.89	0.054	1.000	0.042	0.037	0.123	1.000	0.149	0.122	0.228	0.999

61 - 80 %	BSI_1	BSI_2	21.41	5.85	2.478	0.128	0.085	0.083	0.046	1.000	0.046	0.102	-0.308	0.998
61 - 80 %	BSI_1	Mass	21.41	5.15	2.590	0.103	0.085	0.038	0.886	0.900	0.046	0.018	0.151	1.000
61 - 80 %	BSI_1	BSI_1 res.	21.41	7.14	2.273	0.187	0.085	0.038	0.273	0.999	0.046	0.129	-0.456	0.991
61 - 80 %	BSI_1	BSI_2 res.	21.41	6.82	2.324	0.171	0.085	0.063	0.416	0.993	0.046	0.149	-0.565	0.979
61 - 80 %	BSI_2	Mass	5.85	5.15	0.113	1.000	0.083	0.038	0.840	0.916	0.102	0.018	0.459	0.990
61 - 80 %	BSI_2	BSI_1 res.	5.85	7.14	-0.205	1.000	0.083	0.038	0.227	0.999	0.102	0.129	-0.148	1.000
61 - 80 %	BSI_2	BSI_2 res.	5.85	6.82	-0.154	1.000	0.083	0.063	0.370	0.996	0.102	0.149	-0.257	0.999
61 - 80 %	Mass	BSI_1 res.	5.15	7.14	-0.317	0.998	0.038	0.038	-0.613	0.972	0.018	0.129	-0.606	0.973
61 - 80 %	Mass	BSI_2 res.	5.15	6.82	-0.266	0.999	0.038	0.063	-0.469	0.989	0.018	0.149	-0.716	0.951
61 - 80 %	BSI_1 res.	BSI_2 res.	7.14	6.82	0.051	1.000	0.071	0.063	0.144	1.000	0.129	0.149	-0.109	1.000
81 - 100 %	BSI_1	BSI_2	14.75	6.82	1.382	0.644	0.054	0.027	0.721	0.950	-0.043	-0.008	-0.279	0.999
81 - 100 %	BSI_1	Mass	14.75	5.44	1.624	0.497	0.054	0.044	0.251	0.999	-0.043	-0.028	-0.116	1.000
81 - 100 %	BSI_1	BSI_1 res.	14.75	6.53	1.433	0.613	0.054	0.039	0.400	0.994	-0.043	-0.038	-0.037	1.000
81 - 100 %	BSI_1	BSI_2 res.	14.75	6.60	1.421	0.621	0.054	0.007	1.255	0.720	-0.043	0.051	-0.748	0.943
81 - 100 %	BSI_2	Mass	6.82	5.44	0.241	0.999	0.027	0.044	-0.470	0.989	-0.008	-0.028	0.163	1.000
81 - 100 %	BSI_2	BSI_1 res.	6.82	6.53	0.050	1.000	0.027	0.039	-0.321	0.998	-0.008	-0.038	0.241	0.999
81 - 100 %	BSI_2	BSI_2 res.	6.82	6.60	0.038	1.000	0.027	0.007	0.534	0.983	-0.008	0.051	-0.469	0.990
81 - 100 %	Mass	BSI_1 res.	5.44	6.53	-0.191	1.000	0.044	0.039	0.149	1.000	-0.028	-0.038	0.078	1.000
81 - 100 %	Mass	BSI_2 res.	5.44	6.60	-0.203	1.000	0.044	0.007	1.004	0.851	-0.028	0.051	-0.632	0.968
81 - 100 %	BSI_1 res.	BSI_2 res.	6.53	6.60	-0.012	1.000	0.039	0.007	0.855	0.911	-0.038	0.051	-0.710	0.952

Note: res. = residuals

Table S4. Estimated marginal means (EMMs) for mean squared errors (MSE), semi-partial R^2 (pR^2), and beta weight (BW) values compared between mass quantiles. Values included in EMMs are estimated across all response variables, meaning EMMs represent a predictor's holistic performance in predicting all physiological responses (MSE), variability (pR^2), or effect size (BW). p-values are corrected for multiple comparisons using Tukey honest significant differences. Significant values ($p<0.05$) are presented in bold, and represent differences in the performance of the predictor in one mass quantile versus another.

Predictor	Dataset 1	Dataset 2	MSE 1	MSE 2	MSE *t*-ratio	MSE *p*-value	pR^2 1	pR^2 2	pR^2 *t*-ratio	pR^2 *p*-value	BW 1	BW 2	BW *t*-ratio	BW *p*-value
Mass	1 - 20 %	21 - 40 %	8.30	6.47	0.484	0.9882	0.067	0.020	1.567	0.531	0.064	0.044	0.159	1.000
Mass	1 - 20 %	41 - 60 %	8.30	5.61	0.709	0.9526	0.067	0.017	1.665	0.472	0.064	0.074	-0.081	1.000
Mass	1 - 20 %	61 - 80 %	8.30	5.15	0.832	0.9182	0.067	0.038	0.953	0.873	0.064	0.018	0.367	0.996
Mass	1 - 20 %	81 - 100 %	8.30	5.44	0.754	0.9411	0.067	0.044	0.746	0.943	0.064	-0.028	0.738	0.945
Mass	21 - 40 %	41 - 60 %	6.47	5.61	0.225	0.9994	0.020	0.017	0.098	1.000	0.044	0.074	-0.240	0.999
Mass	21 - 40 %	61 - 80 %	6.47	5.15	0.348	0.9966	0.020	0.038	-0.615	0.971	0.044	0.018	0.207	1.000
Mass	21 - 40 %	81 - 100 %	6.47	5.44	0.271	0.9987	0.020	0.044	-0.822	0.921	0.044	-0.028	0.579	0.977
Mass	41 - 60 %	61 - 80 %	5.61	5.15	0.123	0.9999	0.017	0.038	-0.712	0.952	0.074	0.018	0.448	0.991
Mass	41 - 60 %	81 - 100 %	5.61	5.44	0.046	1	0.017	0.044	-0.919	0.887	0.074	-0.028	0.819	0.922
Mass	61 - 80 %	81 - 100 %	5.15	5.44	-0.077	1	0.038	0.044	-0.207	1.000	0.018	-0.028	0.372	0.996
BSI_1	1 - 20 %	21 - 40 %	27.30	25.00	0.191	1.000	0.049	0.013	0.840	0.916	0.058	0.029	0.187	1.000
BSI_1	1 - 20 %	41 - 60 %	27.30	25.50	0.147	1.000	0.049	0.044	0.115	1.000	0.058	0.136	-0.511	0.986
BSI_1	1 - 20 %	61 - 80 %	27.30	21.40	0.489	0.988	0.049	0.085	-0.841	0.915	0.058	0.046	0.078	1.000
BSI_1	1 - 20 %	81 - 100 %	27.30	14.80	1.041	0.834	0.049	0.054	-0.114	1.000	0.058	-0.043	0.654	0.964
BSI_1	21 - 40 %	41 - 60 %	25.00	25.50	-0.044	1.000	0.013	0.044	-0.725	0.949	0.029	0.136	-0.698	0.955

BSI_1	21 - 40 %	61 - 80 %	25.00	21.40	0.298	0.998	0.013	0.085	-1.681	0.463	0.029	0.046	-0.109	1.000
BSI_1	21 - 40 %	81 - 100 %	25.00	14.80	0.851	0.912	0.013	0.054	-0.954	0.873	0.029	-0.043	0.467	0.990
BSI_1	41 - 60 %	61 - 80 %	25.50	21.40	0.342	0.997	0.044	0.085	-0.956	0.872	0.136	0.046	0.589	0.976
BSI_1	41 - 60 %	81 - 100 %	25.50	14.80	0.894	0.896	0.044	0.054	-0.229	0.999	0.136	-0.043	1.165	0.770
BSI_1	61 - 80 %	81 - 100 %	21.40	14.80	0.552	0.981	0.085	0.054	0.727	0.948	0.046	-0.043	0.576	0.977
BSI_2	1 - 20 %	21 - 40 %	6.20	5.83	0.104	1.000	0.023	0.041	-0.417	0.993	0.077	0.106	-0.211	1.000
BSI_2	1 - 20 %	41 - 60 %	6.20	5.51	0.191	1.000	0.023	0.043	-0.480	0.989	0.077	0.129	-0.376	0.996
BSI_2	1 - 20 %	61 - 80 %	6.20	5.85	0.097	1.000	0.023	0.083	-1.430	0.615	0.077	0.102	-0.183	1.000
BSI_2	1 - 20 %	81 - 100 %	6.20	6.82	-0.170	1.000	0.023	0.027	-0.083	1.000	0.077	-0.008	0.617	0.971
BSI_2	21 - 40 %	41 - 60 %	5.83	5.51	0.087	1.000	0.041	0.043	-0.063	1.000	0.106	0.129	-0.165	1.000
BSI_2	21 - 40 %	61 - 80 %	5.83	5.85	-0.007	1.000	0.041	0.083	-1.014	0.847	0.106	0.102	0.028	1.000
BSI_2	21 - 40 %	81 - 100 %	5.83	6.82	-0.274	0.999	0.041	0.027	0.334	0.997	0.106	-0.008	0.828	0.920
BSI_2	41 - 60 %	61 - 80 %	5.51	5.85	-0.094	1.000	0.043	0.083	-0.950	0.874	0.129	0.102	0.194	1.000
BSI_2	41 - 60 %	81 - 100 %	5.51	6.82	-0.361	0.996	0.043	0.027	0.397	0.994	0.129	-0.008	0.993	0.856
BSI_2	61 - 80 %	81 - 100 %	5.85	6.82	-0.267	0.999	0.083	0.027	1.348	0.665	0.102	-0.008	0.799	0.928
BSI_1 res.	1 - 20 %	21 - 40 %	5.79	6.43	-0.146	1.000	0.030	0.009	0.526	0.984	0.397	0.011	1.325	0.679
BSI_1 res.	1 - 20 %	41 - 60 %	5.79	7.25	-0.338	0.997	0.030	0.042	-0.301	0.998	0.397	0.149	0.852	0.912
BSI_1 res.	1 - 20 %	61 - 80 %	5.79	7.14	-0.311	0.998	0.030	0.071	-1.006	0.850	0.397	0.129	0.920	0.887
BSI_1 res.	1 - 20 %	81 - 100 %	5.79	6.53	-0.171	1.000	0.030	0.039	-0.217	1.000	0.397	-0.038	1.494	0.576
BSI_1 res.	21 - 40 %	41 - 60 %	6.43	7.25	-0.191	1.000	0.009	0.042	-0.827	0.920	0.011	0.149	-0.473	0.989
BSI_1 res.	21 - 40 %	61 - 80 %	6.43	7.14	-0.165	1.000	0.009	0.071	-1.533	0.552	0.011	0.129	-0.405	0.994
BSI_1 res.	21 - 40 %	81 - 100 %	6.43	6.53	-0.025	1.000	0.009	0.039	-0.743	0.944	0.011	-0.038	0.169	1.000
BSI_1 res.	41 - 60 %	61 - 80 %	7.25	7.14	0.027	1.000	0.042	0.071	-0.705	0.953	0.149	0.129	0.068	1.000
BSI_1 res.	41 - 60 %	81 - 100 %	7.25	6.53	0.167	1.000	0.042	0.039	0.084	1.000	0.149	-0.038	0.642	0.967
BSI_1 res.	61 - 80 %	81 - 100 %	7.14	6.53	0.140	1.000	0.071	0.039	0.789	0.931	0.129	-0.038	0.574	0.978

BSI_2 res.	1 - 20 %	21 - 40 %	6.59	6.45	0.032	1.000	0.010	0.038	-0.803	0.927	-0.023	0.092	-1.051	0.829
BSI_2 res.	1 - 20 %	41 - 60 %	6.59	6.89	-0.070	1.000	0.010	0.037	-0.790	0.931	-0.023	0.122	-1.323	0.680
BSI_2 res.	1 - 20 %	61 - 80 %	6.59	6.82	-0.052	1.000	0.010	0.063	-1.543	0.546	-0.023	0.149	-1.571	0.529
BSI_2 res.	1 - 20 %	81 - 100 %	6.59	6.60	-0.002	1.000	0.010	0.007	0.107	1.000	-0.023	0.052	-0.680	0.959
BSI_2 res.	21 - 40 %	41 - 60 %	6.45	6.89	-0.102	1.000	0.038	0.037	0.013	1.000	0.092	0.122	-0.272	0.999
BSI_2 res.	21 - 40 %	61 - 80 %	6.45	6.82	-0.084	1.000	0.038	0.063	-0.740	0.945	0.092	0.149	-0.520	0.985
BSI_2 res.	21 - 40 %	81 - 100 %	6.45	6.60	-0.035	1.000	0.038	0.007	0.910	0.890	0.092	0.052	0.371	0.996
BSI_2 res.	41 - 60 %	61 - 80 %	6.89	6.82	0.018	1.000	0.037	0.063	-0.753	0.942	0.122	0.149	-0.248	0.999
BSI_2 res.	41 - 60 %	81 - 100 %	6.89	6.60	0.067	1.000	0.037	0.007	0.897	0.895	0.122	0.052	0.644	0.966
BSI_2 res.	61 - 80 %	81 - 100 %	6.82	6.60	0.050	1.000	0.063	0.007	1.650	0.481	0.149	0.052	0.891	0.898

Note: res. = residuals

Table S5. Linear regressions testing predictor support across mass quantiles. Regressions are between mass quantile (the independent variable in all instances) and estimated marginal means of the support metric (the dependent variable) of a prior regressions between each predictor and response (see Table S1). FDR values are false discovery rate-corrected p-values across all 15 regressions for each response variable. Significant correlations are presented in bold.

Predictor	Response	Support Metric	Intercept	Slope	R^2	*F*-statistic	*p*-value	FDR
Mass	Resp	pR^2	0.147	-0.002	0.385	1.879	0.264	0.684
BSI_1	Resp	pR^2	0.160	-0.001	0.033	0.102	0.770	0.947
BSI_2	Resp	pR^2	0.141	0.000	0.001	0.003	0.962	0.962
BSI_1 res.	Resp	pR^2	0.137	0.000	0.011	0.033	0.867	0.947
BSI_2 res.	Resp	pR^2	0.073	0.001	0.048	0.153	0.722	0.947
Mass	Resp	BW	0.396	-0.003	0.298	1.271	0.342	0.684
BSI_1	Resp	BW	0.518	-0.003	0.160	0.573	0.504	0.840
BSI_2	Resp	BW	0.477	-0.002	0.048	0.150	0.725	0.947
BSI_1 res.	Resp	BW	1.626	-0.021	0.456	2.519	0.211	0.684
BSI_2 res.	Resp	BW	0.287	0.001	0.008	0.025	0.884	0.947
Mass	Resp	MSE	1.901	0.029	0.831	14.711	0.031	0.155
BSI_1	Resp	MSE	3.604	-0.016	0.339	1.536	0.303	0.684
BSI_2	Resp	MSE	14.360	-0.067	0.932	41.383	0.008	0.120
BSI_1 res.	Resp	MSE	1.873	-0.014	0.274	1.131	0.365	0.684
BSI_2 res.	Resp	MSE	3.853	-0.048	0.883	22.568	0.018	0.135
Mass	sResp	pR^2	-0.034	0.002	0.610	4.690	0.119	0.255
BSI_1	sResp	pR^2	-0.042	0.003	0.696	6.876	0.079	0.203
BSI_2	sResp	pR^2	0.029	0.001	0.134	0.463	0.545	0.680
BSI_1 res.	sResp	pR^2	-0.008	0.002	0.494	2.933	0.185	0.308
BSI_2 res.	sResp	pR^2	0.064	-0.001	0.108	0.364	0.589	0.680
Mass	sResp	BW	-0.029	0.005	0.690	6.691	0.081	0.203
BSI_1	sResp	BW	-0.026	0.006	0.824	14.081	0.033	0.165

BSI_2	sResp	BW	0.154	0.001	0.084	0.275	0.637	0.683
BSI_1 res.	sResp	BW	0.071	0.003	0.434	2.298	0.227	0.341
BSI_2 res.	sResp	BW	0.206	0.000	0.009	0.029	0.876	0.876
Mass	sResp	MSE	-0.404	0.153	0.886	23.222	0.017	0.128
BSI_1	sResp	MSE	4.231	-0.047	0.935	42.848	0.007	0.105
BSI_2	sResp	MSE	11.294	0.102	0.710	7.359	0.073	0.203
BSI_1 res.	sResp	MSE	2.191	0.027	0.310	1.351	0.329	0.449
BSI_2 res.	sResp	MSE	2.155	0.019	0.509	3.111	0.176	0.308
Mass	EWL	pR^2	0.041	0.000	0.046	0.144	0.729	0.795
BSI_1	EWL	pR^2	0.011	0.001	0.443	2.387	0.220	0.332
BSI_2	EWL	pR^2	0.027	0.000	0.033	0.104	0.769	0.795
BSI_1 res.	EWL	pR^2	-0.003	0.001	0.472	2.678	0.200	0.332
BSI_2 res.	EWL	pR^2	0.003	0.000	0.156	0.556	0.510	0.695
Mass	EWL	BW	0.162	0.000	0.026	0.081	0.795	0.795
BSI_1	EWL	BW	0.075	0.002	0.514	3.177	0.173	0.332
BSI_2	EWL	BW	0.130	0.001	0.096	0.319	0.611	0.764
BSI_1 res.	EWL	BW	0.006	0.003	0.780	10.651	0.047	0.141
BSI_2 res.	EWL	BW	0.026	0.002	0.442	2.376	0.221	0.332
Mass	EWL	MSE	17.359	-0.086	0.983	169.580	0.001	**0.008**
BSI_1	EWL	MSE	54.518	-0.102	0.515	3.182	0.172	0.332
BSI_2	EWL	MSE	3.089	0.030	0.953	60.455	0.004	**0.020**
BSI_1 res.	EWL	MSE	12.827	0.118	0.908	29.486	0.012	**0.045**
BSI_2 res.	EWL	MSE	12.961	0.116	0.993	406.945	0.000	**0.000**
Mass	sEWL	pR^2	0.046	0.000	0.199	0.747	0.451	0.770
BSI_1	sEWL	pR^2	0.050	0.000	0.046	0.144	0.730	0.811
BSI_2	sEWL	pR^2	0.002	0.000	0.121	0.415	0.565	0.770
BSI_1 res.	sEWL	pR^2	0.002	0.000	0.161	0.575	0.503	0.770
BSI_2 res.	sEWL	pR^2	0.008	0.000	0.132	0.457	0.547	0.770
Mass	sEWL	BW	0.197	-0.001	0.140	0.487	0.536	0.770
BSI_1	sEWL	BW	0.189	-0.001	0.037	0.115	0.757	0.811
BSI_2	sEWL	BW	0.033	0.001	0.091	0.300	0.622	0.778
BSI_1 res.	sEWL	BW	0.047	0.000	0.144	0.504	0.529	0.770

BSI_2 res.	sEWL	BW	0.069	0.000	0.007	0.020	0.896	0.896
Mass	sEWL	MSE	21.127	-0.233	0.985	192.180	0.001	**0.015**
BSI_1	sEWL	MSE	59.807	-0.376	0.899	26.610	0.014	0.070
BSI_2	sEWL	MSE	4.648	-0.045	0.945	51.367	0.006	**0.045**
BSI_1 res.	sEWL	MSE	16.858	-0.071	0.622	4.942	0.113	0.339
BSI_2 res.	sEWL	MSE	17.160	-0.077	0.861	18.572	0.023	0.086
Mass	CWL	pR^2	0.015	0.000	0.435	2.314	0.226	0.484
BSI_1	CWL	pR^2	0.006	0.000	0.001	0.003	0.960	0.966
BSI_2	CWL	pR^2	0.001	0.000	0.326	1.449	0.315	0.525
BSI_1 res.	CWL	pR^2	0.002	0.000	0.201	0.754	0.449	0.633
BSI_2 res.	CWL	pR^2	0.006	0.000	0.190	0.702	0.464	0.633
Mass	CWL	BW	0.131	-0.001	0.485	2.828	0.191	0.478
BSI_1	CWL	BW	0.067	0.000	0.015	0.044	0.847	0.966
BSI_2	CWL	BW	0.016	0.001	0.491	2.895	0.187	0.478
BSI_1 res.	CWL	BW	0.032	0.001	0.599	4.490	0.124	0.465
BSI_2 res.	CWL	BW	0.053	0.000	0.001	0.002	0.966	0.966
Mass	CWL	MSE	3.583	-0.047	0.847	16.638	0.027	0.203
BSI_1	CWL	MSE	26.660	-0.191	0.894	25.343	0.015	0.203
BSI_2	CWL	MSE	0.410	0.015	0.778	10.543	0.048	0.240
BSI_1 res.	CWL	MSE	2.277	-0.005	0.070	0.225	0.668	0.835
BSI_2 res.	CWL	MSE	2.325	-0.007	0.336	1.521	0.305	0.525
Mass	*r*	pR^2	0.039	0.000	0.425	2.221	0.233	0.441
BSI_1	*r*	pR^2	0.010	0.000	0.033	0.103	0.770	0.814
BSI_2	*r*	pR^2	0.002	0.000	0.640	5.340	0.104	0.390
BSI_1 res.	*r*	pR^2	0.002	0.000	0.319	1.404	0.321	0.535
BSI_2 res.	*r*	pR^2	0.011	0.000	0.022	0.067	0.812	0.814
Mass	*r*	BW	0.205	-0.002	0.462	2.573	0.207	0.441
BSI_1	*r*	BW	0.086	0.001	0.062	0.198	0.686	0.814
BSI_2	*r*	BW	0.042	0.001	0.545	3.593	0.154	0.441
BSI_1 res.	*r*	BW	0.042	0.002	0.646	5.471	0.101	0.390
BSI_2 res.	*r*	BW	0.089	0.000	0.022	0.066	0.814	0.814
Mass	*r*	MSE	2.061	-0.028	0.927	38.153	0.009	0.135

BSI_1	*r*	MSE	22.426	-0.129	0.753	9.138	0.057	0.390
BSI_2	*r*	MSE	0.941	0.003	0.060	0.191	0.691	0.814
BSI_1 res.	*r*	MSE	1.119	0.011	0.239	0.940	0.404	0.606
BSI_2 res.	*r*	MSE	1.126	0.009	0.423	2.195	0.235	0.441

Note: Resp = gross respiration, sResp = specific respiration, EWL = gross evaporative water loss, sEWL = specific evaporative water loss, CWL = cutaneous water loss, *r* = total resistance, res. = residuals, MSE = mean squared error, pR^2 = semi-partial R^2, BW = beta weight

SUPPLEMENTAL MATERIALS – CHAPTER FOUR

Supplementary Methods

Physiological constraint: Skin thicknesses

We estimated skin thicknesses using linear measurements of histological sections. Detailed histological methods are available in Forzán and Johnson (unpublished data). Briefly, we sectioned one euthanized individual from each of six species (*E. bislineata*, *E. longicauda*, *P. cinereus*, *P. glutinosus*, *P. larselli*, and *P. vehiculum*), obtaining 5μm-thick cross-sections at multiple locations along the body trunk by paraffin-embedding and staining with hematoxylin and eosin. Stained slides were digitized at 40x magnification by an external proprietary service (ResourcePath LLC, Sterling, VA, USA) to enable accurate measurement of skin thickness. To produce mean estimates that adequately capture variation in thickness across the primary respiratory surface of the body, we took the mean of multiple measurements per individual.

It is not known how heterogeneous gas exchange is across the body surface of lungless salamanders, but a generally thinner epidermis on the dorsum and trunk than on the ventrum and tail, respectively (Czopek 1961), suggests the dorsum anterior to the tail is the primary region of exchange. Similarly, cutaneous circulation in frogs is highest in the dorsum and flanks (Moalli et al. 1980), suggesting higher gas exchange in these regions. Accordingly, we measured thicknesses for each individual from two transverse sections located toward the anterior and posterior ends of the trunk (posterior to the forelimbs and anterior to the hindlimbs). We divided each section into six regions: the left and right dorsum, left and right ventrum, and left and right flank. From each of these regions we took measurements at two locations: the point along the

skin with the thinnest epidermis, and the point with the thinnest dermis (both approximated visually), excluding the collagen portion of the dermis. Focusing on these locations minimizes the chance of measuring the skin at sites that are artefactually "thickened" due to angled histological sectioning, and focuses our measurements on thin locations that best facilitate gas exchange across the body surface. We only measured at sites that appeared naturally thin, ignoring sites that appeared artificially thin due to tearing or other slide processing artefacts. At each of these 12 locations we measured the thickness of the epidermis, the cellular component of the dermis, and the collagen layer of the dermis perpendicular to the body surface using the line annotation tool in QuPath v0.2.3 (Bankhead et al. 2017). At each location, we used these three measurements to calculate the total thickness of the skin (epidermis + cellular dermis + collagen). From our epidermis measurements and total thickness calculations, we took the mean across all 24 measured locations to use as final representative values per species in downstream analyses. Because we lacked measurements of skin thicknesses for *P. dunni* and *P. vandykei*, we inferred these values using our empirical estimates in an ancestral character estimation across a phylogeny of our eight species (Johnson et al. 2021) using the 'anc.ML' function in the R package 'phytools' v0.7.90 (Revell 2012).

Physiological constraint: Diffusing capacities

We estimated diffusing capacities of the skin using a combination of our measured morphological variables and published physiological variables. We followed the morphometric approach of Piiper et al. (1976), in which the diffusing capacity per unit body mass (nmol min^{-1} $torr^{-1}$ g^{-1}) can be estimated as $\mathrm{D} = D \cdot \alpha \cdot \frac{\mathrm{F}}{\mathrm{x}}$ (1), where D is the diffusivity of CO_2 in amphibian connective tissue (cm^2 min^{-1}), α is the solubility of CO_2 in amphibian connective tissue (μmol

CO_2 L^{-1} $torr^{-1}$), x is the mean skin thickness (μm), and F is the specific functional respiratory surface area (cm^2 g^{-1}): the surface area of capillaries in the skin that is involved in gas exchange, per unit body mass. We calculated *D* and α values for CO_2 based on conversion factors between CO_2 and Freon 22 (Piiper et al. 1976), and substituted x with our species-mean estimates for skin and epidermal thickness. We used an allometric approach to estimate F. Czopek (1961) measured capillary densities and sizes in seven diverse plethodontid species across a wide range of body masses (0.51 - 13.60g; n=24), offering empirical estimates of capillary surface area that are generalizable to temperate Plethodontidae. We multiplied F measurements from Czopek (1961) by their corresponding mass measurements to produce a sample of whole-organism total functional surface areas (cm^2). We modeled covariance between mass and functional surface area for the Plethodontidae using an ordinary least squares regression between body mass and total F following natural log transformations of both variables. We used parameter estimates from this regression to model the allometry of total F in our sample of lungless salamanders, converting our final total F estimates to mm^2 for consistency with units in other variables examined in this study. We then estimated the whole-organism diffusing capacity for all of our experimental salamanders following Equation (1), lastly applying unit conversions (10^{-3} L cm^{-3} * 10^{-2} cm^2 mm^{-2} * 10^4 μm cm^{-1} * 10^3 nmol μmol^{-1} * 60 min h^{-1}) for more intuitive interpretation of estimates as the molar quantity of CO_2 diffused across the path length (either skin or epidermis) per hour per torr of CO_2 partial pressure gradient between capillaries and air surrounding the body (nmol CO_2 h^{-1} $torr^{-1}$).

mtDNA library preparation and sequencing

Following physiological experiments, we sampled liver and tail tissues from euthanized salamanders for preservation in 95% molecular grade ethanol. We extracted whole genomic DNA from preserved tissues using the Omega Bio-tek E.Z.D.N.A Tissue DNA Kit (Omega Bio-tek Inc., Norcross, GA, USA) following manual instructions. We downloaded plethodontid whole-mitochondrial genome sequences from Genbank (Clark et al. 2016) (accession AY728212- AY728235; Mueller et al. 2004) and aligned sequences using MUSCLE in Geneious Prime v2019.2 (Biomatters Inc., San Diego, CA, USA). From this alignment we identified a 74-bp conserved region located in the 16S large ribosomal subunit RNA locus. We designed adjacent, outward-facing long-range PCR primers within this region to amplify whole mitochondrial genomes in our eight species (Table S11). We amplified undiluted DNA extractions in 10 µl PCR reactions using 1 µl DNA template, 2 µl 5X LongAmp Taq Reaction Buffer (New England Biolabs (NEB), Ipswich, MA), 0.5 µl LongAmp Hot Start *Taq* DNA polymerase (NEB), 0.3 µl 10mM dNTP, and 0.2 µl 10 uM forward and reverse primers. PCR reactions included 32 cycles of DNA denaturation at 95°C (40 s), annealing at 56°C (45 s), and extension at 65°C (16.5 min), followed by a final 65°C extension (10 min). We visualized PCR products on a 0.8% agarose gel in 1X TAE buffer using KB-plus ladder (New England Biolabs [NEB], Ipswich, MA, USA).

PCR amplification was highly variable both within and among species. Long-range PCRs successfully amplified whole mitogenomes from a subset of individuals in all eight of our species, however within species multiple individuals either failed to amplify, or amplified only a portion of the mitochondrial genome. To ensure higher PCR specificity, we sequenced 11 successfully amplified PCR amplicons (2 *P. cinereus*, 1 *P. glutinosus*, 2 *P. vandykei*, 3 *P.*

vehiculum, 1 *E. bislineata*, 1 *E. longicauda*) for species-specific primer design. We sheared PCR templates with dsDNA fragmentase (NEB) in 10 µl reactions using 1 µl fragmentase, 1 µl fragmentase buffer, 5µl water, and 3µl PCR template. Fragmentase reactions were amplified for 17 min at 37°C before the addition of 10µl 100 mM EDTA and 18 µl Ampure XP beads (Beckman-Coulter Inc., Indianapolis, IN, USA). The beads were bound to a plate magnet to remove the reaction solution, followed by two rounds of a 70% ethanol wash and brief air drying. We resuspended the beads and bound DNA product in 20 µl 0.5x AE buffer.

To prepare fragments for Illumina sequencing, we end-polished fragmented DNA by creating and phosphorylating blunt ends. To each of our 20 µl fragmented samples we added 0.4 µl T4 DNA polymerase (NEB) and 0.4 µl T4 polynucleotide kinase (NEB), plus 0.7 µl 10 mM dNTP, 3 µl 10 mM ATP, 2.4 µl water, and 3 µl NEB 2 buffer. We cycled end-polish reactions for 30 min at 25°C and 20 min at 75°C. Blunt end samples were adenylated by adding a solution of 1.3 µl water, 0.2 µl NEB 2 buffer, and 0.5 µl NEB OneTaq DNA polymerase at 72°C for 20 min before adapter ligation with 1 µl of T4 ligase (NEB) and 1 µl of 25 mM NEB +A adapter at room temperature for 2 h. We PCR amplified ligated samples in 20 µl reactions using a master mix of 12.7 µl water, 4 µl 5X standard *Taq* reaction buffer (NEB, 0.4 µl 10 mM dNTP, and 0.1 µl Hot Start *Taq* polymerase (NEB). Each sample included 2 µl ligated DNA template and 0.4 µl each of sample-specific 10 uM i5 and i7 NEBNext multiplex oligos for Illumina sequencing (NEB). PCR reactions included 20 cycles of denaturation at 95°C (40 s), annealing at 62°C (45 s), and extension at 68°C (30 s) followed by a 5 min extension at 68°C. We visualized PCR products on a 0.8% agarose gel, keeping all samples with any sign of amplification. Final libraries were pooled onto an Illumina MiSeq sequencer (Illumina Inc., San Diego, CA, USA)

alongside unrelated samples at the Cornell University Institute of Biotechnology, using single-end, 150 bp reads.

mtDNA read processing and assembly

We trimmed raw reads using Trimmomatic v0.39 (Bolger et al. 2014). We cropped the first 12 bp from each read, plus all Illumina adapter sequences using default settings. We further removed all nucleotides from the ends of reads below a Phred quality threshold of 20, as well as all sequences beyond a 5 bp sliding window with average quality below 20. After all these steps, we only kept reads that were at least 40 bp long. We assessed read quality using FastQC v0.11.8 before proceeding to assembly. We assembled mitogenomes de novo using SPAdes v3.14.1 (Bankevich et al. 2012) by iterating up k-mer sizes of 21, 33, 55, and 77 bp and using the –isolate setting as suggested by the SPAdes manual for high-coverage data. From this first set of 10 assemblies, we designed a second set of general primers for the genus *Plethodon* within the 12S short ribosomal locus, plus species-specific primers for each species of *Plethodon* within the nad4 locus (Table S11). For *Eurycea*, we designed genus-level primers within both 16S and nad4. We re-ran PCRs on all remaining unsequenced samples using these primers and the same protocols for amplification, library preparation, sequencing, and assembly as described above.

Assembly processing and locus alignments

We cleaned each assembly following Douglass et al. (2019) by visualizing coverage depth versus length of all contigs. After visual inspection, we assigned threshold values for both coverage and length, filtering out reads that fell below both thresholds using a custom R script. We then queried all remaining contigs against the National Center for Biotechnology

Information (NCBI) nonredundant (nr/nt) nucleotide database using BLASTN with an e-value cutoff of $1e^{-10}$ and kept only reads whose highest bit score matched a vertebrate mitochondrial sequence. Using this final set of contigs, we annotated each individual assembly using the MITOS2 web server (Donath et al. 2019). We extracted all protein-coding sequences from our assemblies, grouping all sequences for each of the 13 mtDNA OXPHOS loci. Each group was aligned using the L-INS-i method in MAFFT v7.453 (Katoh and Standley 2013) and poorly aligned positions were removed using Gblocks v0.91b (Castresana 2000) using the codons setting (t=c) with a maximum of seven contiguous nonconserved regions (b3=7), a minimum block length of six (b4=6), and allowing gap positions in up to half of all sequences (b5=h).

RNA sequencing and transcriptome assembly

To test for selection on the nuclear genome associated with physiological constraint, we assembled nuclear transcriptomes for three focal species (*P. cinereus*, *P. glutinosus*, and *P. vandykei*). We selected these three species as representative of morphological and nucleotypic extremes: *P. cinereus* is small-bodied (mean 0.73 g in our sample), whereas *P. glutinosus* is much larger (mean 5.12 g), but both have comparable genome sizes (19.17 and 24.21 pg, respectively). *P. vandykei* is intermediate in size (mean 1.99 g), but with an exceptionally large genome (49.77 pg) (Johnson et al., unpublished data). In combination, these taxa should enable us to identify selective regimes associated with constraints on body and genome size. RNA was extracted from 10 RNALater-preserved tissues from each species using an in-house phenol protocol at the Cornell University Transcriptional Regulation & Expression (TREx) facility. RNA libraries were prepared at TREx using the NEB Ultra II directional library prep kit. Libraries were sequenced in 2x150 bp paired-end reads on a single lane of an S4 flowcell of an

Illumina Novaseq sequencer. We assessed read quality using FastQC and trimmed raw reads using fastp v0.20.0 (Chen et al. 2018). We cropped the first 15 bp from each read before removing remaining Illumina adapter sequences and set our Phred quality filter at 20, dropping sequences with >30% of base pairs under 20. We discarded all unpaired reads and assembled *de novo* transcriptomes from trimmed paired reads for each individual using Trinity v2.8.4 (Grabherr et al. 2013) with default parameters.

Assembly optimization and quality assessment

To identify coding regions in our transcripts, we filtered our transcriptome assemblies using TransDecoder v5.4.0. We identified long open reading frames (ORFs, minimum length 100 amino acids) in each species assembly. To maximize sensitivity to capture ORFs of functional significance, we scanned all ORFs for homology to known proteins in the nr/nt database using BLASTP with an e-value cutoff of $1e\text{-}^{10}$. We reduced redundancy among our consensus ORF transcripts using CD-HIT v4.6.8 (Fu et al. 2012) by clustering ORFs with a sequence identity threshold of 1.00. To remove contaminant sequences from our transcriptomes, we queried each assembly against the nr/nt database using BLASTP with an e-value cutoff of $1e^{-10}$ in DIAMOND v2.0.7 (Buchfink et al. 2021) and removed all non-chordate transcripts using a custom Python script. We assessed completeness of our optimized assemblies by comparing them against a set of highly conserved single-copy orthologous genes using BUSCO v3.1.0 (Sima et al. 2015) to search each transcriptome against the OrthoDB v10.1 database (Kriventseva et al. 2019) to determine the number of complete, duplicated, fragmented, and missing orthologs within each of our *de novo* assemblies.

Orthologous loci and functional groups

We identified groups of orthologous sequences shared between our individual assemblies using Orthofinder v2.5.2 (Emms and Kelly 2019), using DIAMOND for alignment and an inflation parameter of I=5. To test hypotheses about evolution across mitonuclear loci, we divided orthogroups from Orthofinder into three functional groups: 1) loci with known function in oxidative phosphorylation ("nuOX"), 2) loci whose mitochondrial proteins are not involved in OXPHOS ("mitochondrially-targeted proteins" or "MTPs"), and 3) loci with no known mitochondrial function or interaction ("background loci"). We assigned orthogroups to their respective categories by comparing each to the MitoCarta v3.0 *Mus musculus* mitochondrial proteome (Rath et al. 2021). We queried each individual assembly against custom local blast databases of all MitoCarta OXPHOS and MTP loci using BLASTP with an e-value cutoff of $1e^{-6}$, using successful blast hits to categorize sequences as either nuOX or MTP loci. Sequences without blast hits to either database were classified as background loci.

We saved all orthogroups that were represented by all 30 sequenced individuals. From this set, we randomly sampled 1000 MTP and 1000 background orthogroups. 146 orthogroups were fully represented, and we additionally retained 52 nuOX orthogroups that were represented by at least five individuals in each species. We retained only the longest isoform per individual in each orthogroup using a custom Python script before aligning orthogroups using MAFFT L-INS-i and converting alignments to DNA format using PAL2NAL v14 (Suyama et al. 2006). We eliminated poorly aligned positions from our alignments with Gblocks, using the same settings as our mitochondrial alignments above.

Selection on functional groups

We used locus-wide estimates of d_N/d_S to test for differences in selection strength between species and loci of different functional categories. We ran all models twice to ensure consistency of model estimates. We compared all duplicate runs using Deming regressions (Linnet 1993), comparing estimates of ω between repeated runs. We visually examined residuals from Deming regressions to identify outliers from a 1:1 regression and removed all models with inconsistent estimates from downstream analyses. For all remaining models, we kept the model run with the higher likelihood score. From this set of models, we removed all runs with extremely high ω estimates ($\omega > 20$), suggesting poor convergence of the model run.

Selection across phylogeny

To test our 12 phylogenetic hypotheses, we used an unrooted phylogeny of three species (as recommended by the PAML documentation), with individuals within each species related as a polytomy clade. For each species, we used likelihood ratio tests (LRT) to test for signals of episodic positive selection on the branch leading to the clade (LRT 1: H_{P1}-H_{P3}), long-term positive selection across all branches of the clade (LRT 2: H_{P4}-H_{P6}), episodic changes in selection along the branch leading to the clade (LRT 3: H_{P7}-H_{P9}), and long-term changes in selection across the entire clade (LRT 4: H_{P10}-H_{P12}).

To test for episodic positive selection (LRT 1) we compared constrained and unconstrained forms of branch-site model A (Zhang et al. 2005). This model permits selection intensity to vary both among codon sites and branches in the phylogeny. Episodic selection is identified by specifying unique selection along a specific foreground (FG) branch (ω_{FG}) for a portion of sites within the gene of interest (p_{FG}). For each hypothesis test, we fit a null model

constraining the FG branch to neutral evolution ($\omega_{FG} = 1$) and an alternative model without this constraint ($\omega_{FG} > 1$), and compared models using an LRT. This LRT thus explicitly tests for an episode of positive selection, with a significant result suggesting increased positive selection on the FG branch relative to all other branches in the phylogeny.

We applied LRT 1 under three episodic hypotheses, testing for positive selection on the branch leading to *P. cinereus* (H_{P1}), to *P. glutinosus* (H_{P2}), and to *P. vandykei* (H_{P3}). For each individual hypothesis test, we assessed LRT significance by comparing the test statistic to a chi squared distribution with one degree of freedom. Using this framework allows us to test *a priori* hypotheses about positive selection operating during the evolution of each target species due to their respective physiological constraints. Specifically, we tested for evidence of positive selection during the evolution of *P. cinereus* due to physiological constraints associated with the evolution of small body size (H_{P1}), during the evolution of *P. glutinosus* due to physiological constraints associated with the evolution of large body size (H_{P2}), and during the evolution of *P. vandykei* due to physiological constraints associated with the evolution of large genome size (H_{P3}).

We tested for a long-term shift in positive selection (LRT 2) by comparing clade model C (Bielawski and Yang 2004) to the "relaxed" form of sites model 2a (Weadick and Chang 2012). Clade model C allows selection to vary among codon sites and entire clades, identifying a shift in the strength of positive selection between background and foreground clades at some sites ($\omega_{FG} \neq \omega_{BG}$). The relaxed model 2a serves as the null hypothesis to model C by constraining ω across clades ($\omega_{FG} = \omega_{FG}$). We compared these models using an LRT with a chi squared distribution with one degree of freedom, testing for shifts in selection across *P. cinereus* (H_{P4}), *P. glutinosus* (H_{P5}), and *P. vandykei* clades (H_{P6}). These models test the hypotheses that positive

selection acts on *P. cinereus* due to physiological constraints associated with small body size, on *P. glutinosus* due to physiological constraints associated with large body size, and on *P. vandykei* due to physiological constraints associated with large genome size. We interpreted significant results as evidence of positive selection promoting adaptation to each species' respective physiological constraints.

We tested for episodic changes in selection intensity (LRT 3) by comparing branch-site model B (Yang and Nielsen 2002) to sites model 3 (Yang et al. 2000). Model B is conceptually similar to model A by allowing episodic changes in selection across both sites and branches, however this model tests for any directional change in selection intensity ($\omega_{FG} \neq 1$), and is not constrained to positive selection as in model A ($\omega_{FG} > 1$). Model 3 serves as a null hypothesis to model B by allowing selection to vary among sites, but not among branches (i.e., there is no proportion of sites on the foreground branch undergoing a shift in selection: $p_{FG} = 0$). We set the number of site categories (k) in model 3 as k = 2 and compared these models using an LRT and chi-squared distribution with two degrees of freedom to test for changes in natural selection during the evolution of *P. cinereus* (H_{P7}), *P. glutinosus* (H_{P8}), and *P. vandykei* (H_{P9}), interpreting significant results as evidence of molecular adaptation during the evolution of small body size, large body size, and large genome size, respectively.

We tested for long-term shifts in selection intensity (LRT 4) by comparing clade model D (Bielawski and Yang 2004) to sites model 3 (Yang et al. 2000). Clade model D operates similarly to model C, but allows for any directional shift in selection across a clade ($\omega_{FG} \neq 1$), rather than purifying selection specifically ($\omega_{FG} > 1$). This alternative model expands upon model 3 as a null by allowing for a fraction of sites to differ in selection among clades ($p_{FG} > 0$). We set k = 2 in model 3 and compared models using an LRT with a chi-squared distribution with three

degrees of freedom to test for changes in selection across *P. cinereus* (H_{P10}), *P. glutinosus* (H_{P11}), and *P. vandykei* (H_{P12}) attributable to their respective physiological constraints, interpreting significant results as evidence for molecular adaptation to these constraints.

We ran all CODEML models twice to ensure consistency of model estimates. We compared estimates of ω at neutral sites (ω_0) and foreground sites (ω_{FG}) (or analogous background sites in null models) using Deming regressions between repeated runs, and removed all models with inconsistent estimates from downstream analyses. For all remaining models, we kept the model run with the higher likelihood score and removed poorly converged runs with extreme ω_{FG} estimates ($\omega_{FG} > 20$), suggesting poor convergence of the model run. From this final set of models, for each evolutionary hypothesis (H_{P1}-H_{P12}) we corrected for multiple tests across all tested loci by using an FDR correction (Storey 2002), using an FDR cutoff of $q<0.05$ as evidence for a change in selection intensity in foreground sites relative to background sites.

SUPPLEMENTARY REFERENCES

Bankevich, A., S. Nurk, D. Antipov, A. A. Gurevich, M. Dvorkin, A. S. Kulikov, V. M. Lesin, S. I. Nikolenko, S. Pham, A. D. Prjibelski, A. V Pyshkin, A. V Sirotkin, N. Vyahhi, G. Tesler, M. A. Alekseyev, and P. A. Pevzner. 2012. SPAdes: A new genome assembly algorithm and its applications to single-cell sequencing. J. Comput. Biol. 19:455–477.

Bankhead, P., M. B. Loughrey, J. A. Fernández, Y. Dombrowski, D. G. Mcart, P. D. Dunne, S. McQuaid, R. T. Gray, L. J. Murray, H. G. Coleman, J. A. James, M. Salto-Tellez, and P. W. Hamilton. 2017. QuPath: Open source software for digital pathology image analysis. Sci. Rep. 7:16878.

Bielawski, J. P., and Z. Yang. 2004. A maximum likelihood method for detecting functional divergence at individual codon sites, with application to gene family evolution. J. Mol. Evol. 59:121–132.

Bolger, A. M., M. Lohse, and B. Usade. 2014. Trimmomatic: A flexible trimmer for Illumina sequence data. Bioinformatics 30:2114–2120.

Buchfink, B., K. Reuter, and H. Drost. 2021. Sensitive protein alignments at tree-of-life scale using DIAMOND. Nat. Methods 18:366–368.

Castresana, J. 2000. Selection of conserved blocks from multiple alignments for their use in phylogenetic analysis. Mol. Biol. Evol. 17:540–552.

Chen, S., Y. Zhou, Y. Chen, and J. Gu. 2018. fastp: An ultra-fast all-in-one FASTQ preprocessor. Bioinformatics 34:i884–i890.

Clark, K., I. Karsch-Mizrachi, D. J. Lipman, J. Ostell, and E. W. Sayers. 2016. Genbank. Nucleic Acids Res. 4:D67–D72.

Czopek, J. 1961. Vascularization of respiratory surfaces in some Plethodontidae. Zool. Pol. 11:131–148.

Donath, A., F. Juhling, M. Al-Arab, S. H. Bernhart, F. Reinhardt, P. F. Stadler, M. Middendorf, and M. Bernt. 2019. Improved annotation of protein-coding genes boundaries in metazoan mitochondrial genomes. Nucleic Acids Res. 47:10543–10552.

Douglass, A. P., C. E. O'Brien, B. Offei, A. Y. Coughlan, R. A. Ortiz-Merino, G. Butler, K. P. Byrne, and K. H. Wolfe. 2019. Coverage-versus-length plots, a simple quality control step for de novo yeast genome sequence assemblies. G3 Genes|Genomes|Genetics 9:879–887.

Emms, D. M., and S. Kelly. 2019. OrthoFinder: pPhylogenetic orthology inference for comparative genomics. Genome Biol. 20:1–14.

Forzán, M. D., and B. B. Johnson. Histologic morphology of the skin of six species of lungless salamanders, Family Plethodontidae. Unpublished data in preparation for J. Am. Assoc. Lab. Animal Sci.

Fu, L., B. Niu, Z. Zhu, S. Wu, and W. Li. 2012. CD-HIT: Accelerated for clustering the next-generation sequencing data. Bioinformatics 28:3150–3152.

Grabherr, M. G., B. J. Haas, M. Yassour, J. Z. Levin, D. A. Thompson, I. Amit, X. Adiconis, L. Fan, R. Raychowdhury, Q. Zeng, Z. Chen, E. Mauceli, N. Hacohen, A. Gnirke, N. Rhind, F. di Palma, B. W. Birren, C. Nusbaum, K. Lidbland-Toh, N. Friedman, and A. Regev. 2013. Trinity: Reconstructing a full-length transcriptome without a genome from RNA-Seq data. Nat. Biotechnol. 29:644–652.

Johnson, B. B., J. B. Searle, and J. P. Sparks. 2021. Genome size influences adaptive plasticity of water loss, but not metabolic rates, in lungless salamanders. J. Exp. Biol. 224:jeb242196.

Katoh, K., and D. M. Standley. 2013. MAFFT multiple sequence alignment software version 7: Improvements in performance and usability. Mol. Biol. Evol. 30:772–780.

Kriventseva, E. V, D. Kuznetsov, F. Tegenfeldt, M. Manni, R. Dias, F. A. Simao, and E. M. Zdobnov. 2019. OrthoDB v10: Sampling the diversity of animal, plant, fungal, protist, bacterial and viral genomes for evolutionary and functional annotations of orthologs. Nucleic Acids Res. 47:D807–D811.

Linnet, K. 1993. Evaluation of regression procedures for methods comparison studies. Clin. Chem. 39:424–432.

Moalli, R., R. S. Meyers, D. C. Jackson, and R. W. Millard. 1980. Skin circulation of the frog, *Rana catesbeiana*: distribution and dynamics. Respir. Physiol. 40:137–148.

Mueller, R. L., J. R. Macey, M. Jaekel, D. B. Wake, and J. L. Boore. 2004. Morphological homoplasy, life history evolution, and historical biogeography of plethodontid salamanders inferred from complete mitochondrial genomes. Proc. Natl. Acad. Sci. U. S. A. 101:13820–13825.

Piiper, J., R. N. Gatz, and E. C. Crawford Jr. 1976. Gas transport characteristics in an exclusively skin-breathing salamander, *Desmognathus fuscus* (Plethodontidae). Pp. 339–356 *in* G. M. Hughes, ed. Respiration of Amphibious Vertebrates. Academic Press.

Rath, S., R. Sharma, R. Gupta, T. Ast, C. Chan, T. J. Durham, R. P. Goodman, Z. Grabarek, M. E. Haas, W. H. W. Hung, P. R. Joshi, A. A. Jourdain, S. H. Kim, A. V Kotrys, S. S. Lam, J. G. Mccoy, J. D. Meisel, M. Miranda, A. Panda, A. Patgiri, R. Rogers, S. Sadre, H. Shah, O. S. Skinner, T.-L. To, M. A. Walker, H. Wang, P. S. Ward, J. Wengrod, C.-C. Yuan, S. E. Calvo, and V. K. Mootha. 2021. MitoCarta3.0: An updated mitochondrial proteome now with sub-organelle localization and pathway annotations. Nucleic Acids Res. 49:D1541–D1547.

Revell, L. J. 2012. phytools: An R package for phylogenetic comparative biology (and other things). Methods Ecol. Evol. 3:217–223.

Sima, F. A., R. M. Waterhouse, P. Ioannidis, E. V Kriventseva, and E. M. Zdobnov. 2015. BUSCO: Assessing genome assembly and annotation completeness with single-copy orthologs. Bioinformatics 31:3210–3212.

Storey, J. D. 2002. A direct approach to false discovery rates. J. R. Stat. Soc. B 64:479–498.

Suyama, M., D. Torrents, and P. Bork. 2006. PAL2NAL: Robust conversion of protein sequence alignments into the corresponding codon alignments. Nucleic Acids Res. 34:W609–W612.

Weadick, C. J., and B. S. W. Chang. 2012. An improved likelihood ratio test for detecting site-specific functional divergence among clades of protein-coding genes. Mol. Biol. Evol. 29:1297–1300.

Yang, Z., and R. Nielsen. 2002. Codon-substitution models for detecting molecular adaptation at individual sites along specific lineages. Mol. Biol. Evol. 19:908–917.

Yang, Z., R. Nielsen, N. Goldman, and A.-M. K. Pedersen. 2000. Codon-substitution models for heterogeneous selection pressure at amino acid sites. Genetics 155:431–449.

Zhang, J., R. Nielsen, and Z. Yang. 2005. Evaluation of an improved branch-site likelihood method for detecting positive selection at the molecular level. Mol. Biol. Evol. 22:2472–2479.

Table S1. Species sampling and variation in physical constraints. Phenotype values are species means. Units: mass (g), C-value (pg), biological size (g pg^{-1}), surface area-to-volume ratio (SA:V; mm^2 mm^{-3}), epidermal thickness (μm), skin thickness (μm), epidermal diffusing capacity for CO_2 (D_{CO2}; nmol CO_2 h^{-1} $torr^{-1}$), skin diffusing capacity for CO_2 (DCO_2; nmol CO_2 h^{-1} $torr^{-1}$).

Species	**N**	**Mass**	**C-value**	**Bio. size**	**SA:V**	**Epi. thickness**	**Skin thickness**	**Epi. D_{CO2}**	**Skin D_{CO2}**
Eurycea bislineata	18	0.79	20.08	0.040	1.331	19.28	74.84	1534.50	395.28
Eurycea longicauda	7	2.46	26.90	0.093	0.893	23.21	132.98	3105.58	541.94
Plethodon cinereus	24	0.71	19.17	0.038	1.374	15.72	77.18	1739.29	354.32
Plethodon dunni	12	3.41	35.53	0.097	0.823	19.94	75.55	4606.27	1215.88
Plethodon glutinosus	20	5.03	24.21	0.211	0.701	26.71	137.14	4733.47	922.01
Plethodon larselli	12	1.32	38.28	0.035	1.114	15.17	61.76	2907.90	714.41
Plethodon vandykei	19	1.97	49.77	0.040	0.980	17.02	69.09	3524.56	868.39
Plethodon vehiculum	14	1.21	37.57	0.032	1.151	20.74	74.32	1972.24	550.30

Table S2. Functional constraints on metabolic rates across all individuals from eight plethodontid species. Constraint on a given response is characterized by model support (MSE) and performance (beta weights, pR2) in significant regressions between the predictor and response. FDR: false discovery rate-corrected *P* value for the regression, MSE: mean squared error, BW: beta weight, R^2: portion of variation in the response explained by the model (including environmental and random effects), pR^2: portion of variation in the response explained by the predictor.

Predictor	**Response**	***P* value**	**FDR**	**MSE**	**BW**	**R^2**	**pR^2**
SA:V	Gross respiration	0.000	**0.000**	**2.310**	**-0.839**	0.676	**0.638**
Biological size	Gross respiration	0.000	**0.000**	2.888	0.806	0.574	0.539
Epidermis thickness	Gross respiration	0.016	**0.021**	17.856	0.665	0.423	0.386
Skin thickness	Gross respiration	0.053	0.064	32.128	0.534	0.287	0.249
Epidermis diffusing capacity	Gross respiration	0.000	**0.000**	83.134	0.700	0.502	0.462
Skin diffusing capacity	Gross respiration	0.000	**0.000**	58.529	0.688	0.443	0.406
SA:V	Specific respiration	0.000	**0.000**	3.067	**0.449**	0.247	**0.196**
Biological size	Specific respiration	0.000	**0.000**	**2.301**	-0.428	0.223	0.173
Epidermis thickness	Specific respiration	0.845	0.845	21.839	-0.056	0.051	0.004
Skin thickness	Specific respiration	0.737	0.804	37.622	-0.088	0.055	0.008
Epidermis diffusing capacity	Specific respiration	0.000	**0.000**	92.530	-0.397	0.226	0.169
Skin diffusing capacity	Specific respiration	0.000	**0.000**	66.675	-0.386	0.211	0.156

Table S3. Evolutionary correlations between constraint phenotypes and metabolic rates across eight plethodontid species, per phylogenetic least squares regressions using an Ornstein-Uhlenbeck (OU) model. Constraint across evolutionary history is characterized by model support (MSE) and performance (R^2), and degree of evolutionary influence of the predictor over the response (α) in significant models. FDR: false discovery rate-corrected *P* value for the regression, α: the OU-modeled selective pull toward an adaptive optimum response value exerted by the predictor, MSE: mean squared error, R2: portion of variation in the response explained by the model

Predictor	**Response**	***P* value**	**FDR**	**α**	**MSE**	**R^2**
SA:V	Gross respiration	0.001	**0.012**	11.149	**1.791**	**0.796**
Biological size	Gross respiration	0.015	**0.045**	**37.118**	2.956	0.596
Epi. thickness	Gross respiration	0.012	**0.045**	10.313	16.765	0.586
Skin thickness	Gross respiration	0.003	**0.018**	0.001	28.783	0.581
Epi. diffusing capacity	Gross respiration	0.023	0.052	38.181	82.276	0.538
Skin diffusing capacity	Gross respiration	0.059	0.089	10.099	57.612	0.321
SA:V	Specific respiration	0.083	0.102	11.339	2.860	0.303
Biological size	Specific respiration	0.085	0.102	4.802	2.073	0.131
Epidermis thickness	Specific respiration	0.800	0.800	31.464	21.576	-0.150
Skin thickness	Specific respiration	0.589	0.643	8.158	37.390	-0.193
Epi. diffusing capacity	Specific respiration	0.026	0.052	8.441	92.440	0.487
Skin diffusing capacity	Specific respiration	0.049	0.084	7.923	66.397	0.372

Table S4. Pairwise comparisons between dN/dS in different genomic functional groups. Mann-Whitney U tests compared all locus-wide dN/dS estimates for each pair of groups within each given subset, using either mitochondrial (mtDNA) loci or the combination of mtDNA and nuclear genomic loci, depending on the dataset. Median dN/dS values are provided for reference. FDR: false disovery rate-corrected *P* values corrected across all pairwise tests.

Dataset	Loci	Subset	Group 1	Group 2	Median 1	Median 2	*P* value	FDR
3 species	mtDNA + nuclear	all	MTP	Background	0.106	0.130	0.002	**0.013**
3 species	mtDNA + nuclear	all	MTP	nuOX	0.106	0.122	0.717	0.747
3 species	mtDNA + nuclear	all	MTP	mtOX	0.106	0.105	0.820	0.818
3 species	mtDNA + nuclear	all	Background	nuOX	0.130	0.122	0.215	0.423
3 species	mtDNA + nuclear	all	Background	mtOX	0.130	0.105	0.744	0.753
3 species	mtDNA + nuclear	all	nuOX	mtOX	0.122	0.105	0.945	0.893
3 species	mtDNA + nuclear	*P. cinereus*	MTP	Background	0.113	0.127	0.415	0.634
3 species	mtDNA + nuclear	*P. cinereus*	MTP	nuOX	0.113	0.127	0.668	0.742
3 species	mtDNA + nuclear	*P. cinereus*	MTP	mtOX	0.113	0.088	0.668	0.742
3 species	mtDNA + nuclear	*P. cinereus*	Background	nuOX	0.127	0.127	0.986	0.893
3 species	mtDNA + nuclear	*P. cinereus*	Background	mtOX	0.127	0.088	0.568	0.711
3 species	mtDNA + nuclear	*P. cinereus*	nuOX	mtOX	0.127	0.088	0.545	0.695
3 species	mtDNA + nuclear	*P. glutinosus*	MTP	Background	0.012	0.042	0.312	0.524
3 species	mtDNA + nuclear	*P. glutinosus*	MTP	nuOX	0.012	0.000	0.241	0.461
3 species	mtDNA + nuclear	*P. glutinosus*	MTP	mtOX	0.012	0.000	0.624	0.728
3 species	mtDNA + nuclear	*P. glutinosus*	Background	nuOX	0.042	0.000	0.098	0.257
3 species	mtDNA + nuclear	*P. glutinosus*	Background	mtOX	0.042	0.000	0.716	0.747
3 species	mtDNA + nuclear	*P. glutinosus*	nuOX	mtOX	0.000	0.000	0.441	0.659

3 species	mtDNA + nuclear	*P. vandykei*	MTP	Background	0.150	0.185	0.001	**0.007**
3 species	mtDNA + nuclear	*P. vandykei*	MTP	nuOX	0.150	0.216	0.192	0.401
3 species	mtDNA + nuclear	*P. vandykei*	MTP	mtOX	0.150	0.119	0.975	0.893
3 species	mtDNA + nuclear	*P. vandykei*	Background	nuOX	0.185	0.216	0.690	0.747
3 species	mtDNA + nuclear	*P. vandykei*	Background	mtOX	0.185	0.119	0.484	0.666
3 species	mtDNA + nuclear	*P. vandykei*	nuOX	mtOX	0.216	0.119	0.605	0.728
3 species	mtDNA + nuclear	MTP	*P. cinereus*	*P. glutinosus*	0.113	0.012	0.000	**0.000**
3 species	mtDNA + nuclear	MTP	*P. cinereus*	*P. vandykei*	0.113	0.150	0.097	0.257
3 species	mtDNA + nuclear	MTP	*P. glutinosus*	*P. vandykei*	0.012	0.150	0.000	**0.000**
3 species	mtDNA + nuclear	Background	*P. cinereus*	*P. glutinosus*	0.127	0.042	0.000	**0.000**
3 species	mtDNA + nuclear	Background	*P. cinereus*	*P. vandykei*	0.127	0.185	0.000	**0.000**
3 species	mtDNA + nuclear	Background	*P. glutinosus*	*P. vandykei*	0.042	0.185	0.000	**0.000**
3 species	mtDNA + nuclear	nuOX	*P. cinereus*	*P. glutinosus*	0.127	0.000	0.001	**0.005**
3 species	mtDNA + nuclear	nuOX	*P. cinereus*	*P. vandykei*	0.127	0.216	0.165	0.366
3 species	mtDNA + nuclear	nuOX	*P. glutinosus*	*P. vandykei*	0.000	0.216	0.000	**0.000**
3 species	mtDNA + nuclear	nuOX	complex I	complex II	0.137	0.112	0.977	0.893
3 species	mtDNA + nuclear	nuOX	complex I	complex III	0.137	0.004	0.066	0.206
3 species	mtDNA + nuclear	nuOX	complex I	complex IV	0.137	0.236	0.046	0.174
3 species	mtDNA + nuclear	nuOX	complex I	complex V	0.137	0.042	0.064	0.206
3 species	mtDNA + nuclear	nuOX	complex II	complex III	0.112	0.004	0.355	0.555
3 species	mtDNA + nuclear	nuOX	complex II	complex IV	0.112	0.236	0.462	0.666
3 species	mtDNA + nuclear	nuOX	complex II	complex V	0.112	0.042	0.312	0.524
3 species	mtDNA + nuclear	nuOX	complex III	complex IV	0.004	0.236	0.004	**0.020**
3 species	mtDNA + nuclear	nuOX	complex III	complex V	0.004	0.042	0.929	0.893
3 species	mtDNA + nuclear	nuOX	complex IV	complex V	0.236	0.042	0.004	**0.020**
8 species	mtDNA only	all	*P. cinereus*	*P. glutinosus*	0.088	0.000	0.839	0.825
8 species	mtDNA only	all	*P. cinereus*	*P. dunni*	0.088	0.000	0.130	0.310
8 species	mtDNA only	all	*P. cinereus*	*P. vehiculum*	0.088	0.000	0.171	0.368

8 species	mtDNA only	all	*P. cinereus*	*P. vandykei*	0.088	0.119	0.532	0.695
8 species	mtDNA only	all	*P. cinereus*	*P. larselli*	0.088	0.000	0.002	**0.010**
8 species	mtDNA only	all	*P. cinereus*	*E. bislineata*	0.088	0.073	0.727	0.747
8 species	mtDNA only	all	*P. cinereus*	*E. longicauda*	0.088	0.035	0.264	0.492
8 species	mtDNA only	all	*P. glutinosus*	*P. dunni*	0.000	0.000	0.590	0.725
8 species	mtDNA only	all	*P. glutinosus*	*P. vehiculum*	0.000	0.000	0.482	0.666
8 species	mtDNA only	all	*P. glutinosus*	*P. vandykei*	0.000	0.119	0.543	0.695
8 species	mtDNA only	all	*P. glutinosus*	*P. larselli*	0.000	0.000	0.060	0.206
8 species	mtDNA only	all	*P. glutinosus*	*E. bislineata*	0.000	0.073	0.969	0.893
8 species	mtDNA only	all	*P. glutinosus*	*E. longicauda*	0.000	0.035	0.719	0.747
8 species	mtDNA only	all	*P. dunni*	*P. vehiculum*	0.000	0.000	1.000	0.894
8 species	mtDNA only	all	*P. dunni*	*P. vandykei*	0.000	0.119	0.047	0.174
8 species	mtDNA only	all	*P. dunni*	*P. larselli*	0.000	0.000	0.098	0.257
8 species	mtDNA only	all	*P. dunni*	*E. bislineata*	0.000	0.073	0.303	0.524
8 species	mtDNA only	all	*P. dunni*	*E. longicauda*	0.000	0.035	0.101	0.257
8 species	mtDNA only	all	*P. vehiculum*	*P. vandykei*	0.000	0.119	0.048	0.174
8 species	mtDNA only	all	*P. vehiculum*	*P. larselli*	0.000	0.000	0.120	0.296
8 species	mtDNA only	all	*P. vehiculum*	*E. bislineata*	0.000	0.073	0.339	0.544
8 species	mtDNA only	all	*P. vehiculum*	*E. longicauda*	0.000	0.035	0.205	0.415
8 species	mtDNA only	all	*P. vandykei*	*P. larselli*	0.119	0.000	0.000	**0.003**
8 species	mtDNA only	all	*P. vandykei*	*E. bislineata*	0.119	0.073	0.340	0.544
8 species	mtDNA only	all	*P. vandykei*	*E. longicauda*	0.119	0.035	0.020	0.088
8 species	mtDNA only	all	*P. larselli*	*E. bislineata*	0.000	0.073	0.006	**0.029**
8 species	mtDNA only	all	*P. larselli*	*E. longicauda*	0.000	0.035	0.001	**0.006**
8 species	mtDNA only	all	*E. bislineata*	*E. longicauda*	0.073	0.035	0.622	0.728
8 species	mtDNA only	all	complex I	complex III	0.058	0.037	0.522	0.695
8 species	mtDNA only	all	complex I	complex IV	0.058	0.011	0.096	0.257
8 species	mtDNA only	all	complex I	complex V	0.058	0.122	0.466	0.666

8 species	mtDNA only	all	complex III	complex IV	0.037	0.011	0.634	0.728
8 species	mtDNA only	all	complex III	complex V	0.037	0.122	0.305	0.524
8 species	mtDNA only	all	complex IV	complex V	0.011	0.122	0.139	0.320

Table S5. Evolutionary correlations between selection strength (ω) on mitochondrial OXPHOS genes (mtOX) and metabolic rates per phylogenetic least squares regressions using an Ornstein-Uhlenbeck model. FDR: false discovery rate-corrected *P* values corrected across all four regressions. Because no regressions are significant, we did not estimate model support.

Dataset	**Predictor**	**Response**	***P* value**	**FDR**
8 species	median mtOX ω	Gross respiration	0.543	0.543
8 species	median mtOX ω	Specific respiration	0.127	0.254
3 species	median nuOX ω	Gross respiration	0.342	0.455
3 species	median nuOX ω	Specific respiration	0.092	0.254

Table S6. Evolutionary correlations between physical constraints and selection strength (ω) on mitochondrial OXPHOS genes (mtOX) in eight plethodontid species per phylogenetic least squares regressions using an Ornstein-Uhlenbeck model. FDR: false discovery rate-corrected *P* values corrected across all four regressions. Because no regressions are significant, we did not estimate model support.

Predictor	**Response**	***P* value**	**FDR**
SA:V	median mtOX ω	0.225	0.537
Biological size	median mtOX ω	0.336	0.537
Epi. thickness	median mtOX ω	0.358	0.537
Skin thickness	median mtOX ω	0.843	0.947
Epi. diffusing capacity	median mtOX ω	0.248	0.537
Skin diffusing capacity	median mtOX ω	0.133	0.537

Table S7. Evolutionary correlations between physical constraints and selection strength (ω) on nuclear functional groups in three plethodontid species per phylogenetic least squares regressions using an Ornstein-Uhlenbeck model. FDR: false discovery rate-corrected *P* values corrected across all four regressions. Because no regressions are significant, we did not estimate model support.

Functional Group	Predictor	Response	*P* value	FDR
nuOX	SA:V	median ω	0.519	0.630
nuOX	Biological size	median ω	0.250	0.594
nuOX	Epi. thickness	median ω	0.297	0.594
nuOX	Skin thickness	median ω	0.189	0.594
nuOX	Epi. diffusing capacity	median ω	0.525	0.630
nuOX	Skin diffusing capacity	median ω	0.668	0.668
MTP	SA:V	median ω	0.417	0.630
MTP	Biological size	median ω	0.148	0.594
MTP	Epi. thickness	median ω	0.195	0.594
MTP	Skin thickness	median ω	0.087	0.594
MTP	Epi. diffusing capacity	median ω	0.423	0.630
MTP	Skin diffusing capacity	median ω	0.566	0.637
Background	SA:V	median ω	0.512	0.630
Background	Biological size	median ω	0.242	0.594
Background	Epi. thickness	median ω	0.290	0.594

Background	Skin thickness	median ω	0.181	0.594
Background	Epi. diffusing capacity	median ω	0.518	0.630
Background	Skin diffusing capacity	median ω	0.661	0.668

Table S8. Differences in selection strength (dN/dS) between genomic functional groups in three plethodontid species. The magnitude of difference in median dN/dS estimates between two groups and the percent overlap in their distributions act as estimates of differing selective constraints between the two, with low overlap and large differences between mitochondrial OXPHOS loci (mtOX) and nuclear OXPHOS loci (nuOX) suggestive of nuclear compensation from mtOX mutations.

Species	Group 1	Group 2	Median 1	Median 2	| Difference |	Overlap
all	mtOX	MTP	0.1051	0.1060	0.0009	0.505
all	mtOX	Background	0.1051	0.1302	0.0251	0.570
all	mtOX	nuOX	0.1051	0.1216	0.0165	0.755
all	MTP	Background	0.1060	0.1302	0.0241	0.744
all	MTP	nuOX	0.1060	0.1216	0.0155	0.572
all	Background	nuOX	0.1302	0.1216	0.0086	0.660
P. cinereus	mtOX	MTP	0.0883	0.1126	0.0242	0.295
P. cinereus	mtOX	Background	0.0883	0.1273	0.0390	0.239
P. cinereus	mtOX	nuOX	0.0883	0.1271	0.0387	0.468
P. cinereus	MTP	Background	0.1126	0.1273	0.0148	0.690
P. cinereus	MTP	nuOX	0.1126	0.1271	0.0145	0.581
P. cinereus	Background	nuOX	0.1273	0.1271	0.0003	0.465
P. glutinosus	mtOX	MTP	0.0001	0.0120	0.0119	0.615
P. glutinosus	mtOX	Background	0.0001	0.0001	0.0000	0.370
P. glutinosus	mtOX	nuOX	0.0001	0.0120	0.0119	0.608
P. glutinosus	MTP	Background	0.0120	0.0001	0.0119	0.282
P. glutinosus	MTP	nuOX	0.0120	0.0120	0.0000	0.504
P. glutinosus	Background	nuOX	0.0001	0.0120	0.0119	0.449
P. vandykei	mtOX	MTP	0.1186	0.1496	0.0310	0.189
P. vandykei	mtOX	Background	0.1186	0.1846	0.0659	0.212
P. vandykei	mtOX	nuOX	0.1186	0.2161	0.0975	0.257

P. vandykei	MTP	Background	0.1496	0.1846	0.0350	0.695
P. vandykei	MTP	nuOX	0.1496	0.2161	0.0665	0.564
P. vandykei	Background	nuOX	0.1846	0.2161	0.0315	0.709

Table S9. Evolutionary correlations between physical constraints and differences in selection strength (dN/dS) between genomic functional groups in three plethodontid species, per phylogenetic least squares regressions using an Ornstein-Uhlenbeck model. The magnitude of difference in median dN/dS estimates between two groups and the percent overlap in their distributions act as estimates of of differing selective constraints between the two, with low overlap and large differences between mitochondrial OXPHOS loci (mtOX) and nuclear OXPHOS loci (nuOX) suggestive of nuclear compensation from mtOX mutations.FDR: false discovery rate-corrected *P* values corrected across all regressions.

Group 1	Group 2	Predictor	Response	*P* value	FDR
mtOX	nuOX	SA:V	median ω1 - median ω2	0.312	0.435
mtOX	nuOX	Biological size	median ω1 - median ω2	0.046	0.222
mtOX	nuOX	Epidermis thickness	median ω1 - median ω2	0.092	0.335
mtOX	nuOX	Skin thickness	median ω1 - median ω2	0.013	0.187
mtOX	nuOX	Epidermis diffusing capacity	median ω1 - median ω2	0.317	0.435
mtOX	nuOX	Skin diffusing capacity	median ω1 - median ω2	0.463	0.472
mtOX	nuOX	SA:V	overlap(ω1,ω2)	0.423	0.472
mtOX	nuOX	Biological size	overlap(ω1,ω2)	0.689	0.512
mtOX	nuOX	Epidermis thickness	overlap(ω1,ω2)	0.643	0.511
mtOX	nuOX	Skin thickness	overlap(ω1,ω2)	0.748	0.512
mtOX	nuOX	Epidermis diffusing capacity	overlap(ω1,ω2)	0.417	0.472
mtOX	nuOX	Skin diffusing capacity	overlap(ω1,ω2)	0.271	0.435
mtOX	MTP	SA:V	median ω1 - median ω2	0.284	0.435
mtOX	MTP	Biological size	median ω1 - median ω2	0.018	0.187
mtOX	MTP	Epidermis thickness	median ω1 - median ω2	0.064	0.282
mtOX	MTP	Skin thickness	median ω1 - median ω2	0.041	0.222
mtOX	MTP	Epidermis diffusing capacity	median ω1 - median ω2	0.290	0.435

mtOX	MTP	Skin diffusing capacity	median ω1 - median ω2	0.435	0.472
mtOX	MTP	SA:V	overlap(ω1,ω2)	0.172	0.435
mtOX	MTP	Biological size	overlap(ω1,ω2)	0.438	0.472
mtOX	MTP	Epidermis thickness	overlap(ω1,ω2)	0.392	0.472
mtOX	MTP	Skin thickness	overlap(ω1,ω2)	0.497	0.473
mtOX	MTP	Epidermis diffusing capacity	overlap(ω1,ω2)	0.167	0.435
mtOX	MTP	Skin diffusing capacity	overlap(ω1,ω2)	0.021	0.187
mtOX	Background	SA:V	median ω1 - median ω2	0.296	0.435
mtOX	Background	Biological size	median ω1 - median ω2	0.030	0.187
mtOX	Background	Epidermis thickness	median ω1 - median ω2	0.076	0.303
mtOX	Background	Skin thickness	median ω1 - median ω2	0.029	0.187
mtOX	Background	Epidermis diffusing capacity	median ω1 - median ω2	0.302	0.435
mtOX	Background	Skin diffusing capacity	median ω1 - median ω2	0.447	0.472
mtOX	Background	SA:V	overlap(ω1,ω2)	0.018	0.187
mtOX	Background	Biological size	overlap(ω1,ω2)	0.248	0.435
mtOX	Background	Epidermis thickness	overlap(ω1,ω2)	0.202	0.435
mtOX	Background	Skin thickness	overlap(ω1,ω2)	0.307	0.435
mtOX	Background	Epidermis diffusing capacity	overlap(ω1,ω2)	0.024	0.187
mtOX	Background	Skin diffusing capacity	overlap(ω1,ω2)	0.169	0.435
nuOX	MTP	SA:V	median ω1 - median ω2	0.719	0.512
nuOX	MTP	Biological size	median ω1 - median ω2	0.453	0.472
nuOX	MTP	Epidermis thickness	median ω1 - median ω2	0.499	0.473
nuOX	MTP	Skin thickness	median ω1 - median ω2	0.394	0.472
nuOX	MTP	Epidermis diffusing capacity	median ω1 - median ω2	0.725	0.512
nuOX	MTP	Skin diffusing capacity	median ω1 - median ω2	0.870	0.570
nuOX	MTP	SA:V	overlap(ω1,ω2)	0.433	0.472
nuOX	MTP	Biological size	overlap(ω1,ω2)	0.699	0.512
nuOX	MTP	Epidermis thickness	overlap(ω1,ω2)	0.653	0.511
nuOX	MTP	Skin thickness	overlap(ω1,ω2)	0.758	0.512
nuOX	MTP	Epidermis diffusing capacity	overlap(ω1,ω2)	0.427	0.472
nuOX	MTP	Skin diffusing capacity	overlap(ω1,ω2)	0.282	0.435

nuOX	Background	SA:V	median ω1 - median ω2	0.522	0.473
nuOX	Background	Biological size	median ω1 - median ω2	0.256	0.435
nuOX	Background	Epidermis thickness	median ω1 - median ω2	0.302	0.435
nuOX	Background	Skin thickness	median ω1 - median ω2	0.197	0.435
nuOX	Background	Epidermis diffusing capacity	median ω1 - median ω2	0.528	0.473
nuOX	Background	Skin diffusing capacity	median ω1 - median ω2	0.673	0.512
nuOX	Background	SA:V	overlap(ω1,ω2)	0.631	0.511
nuOX	Background	Biological size	overlap(ω1,ω2)	0.898	0.579
nuOX	Background	Epidermis thickness	overlap(ω1,ω2)	0.851	0.566
nuOX	Background	Skin thickness	overlap(ω1,ω2)	0.956	0.597
nuOX	Background	Epidermis diffusing capacity	overlap(ω1,ω2)	0.626	0.511
nuOX	Background	Skin diffusing capacity	overlap(ω1,ω2)	0.480	0.473
MTP	Background	SA:V	median ω1 - median ω2	0.309	0.435
MTP	Background	Biological size	median ω1 - median ω2	0.575	0.505
MTP	Background	Epidermis thickness	median ω1 - median ω2	0.529	0.473
MTP	Background	Skin thickness	median ω1 - median ω2	0.634	0.511
MTP	Background	Epidermis diffusing capacity	median ω1 - median ω2	0.303	0.435
MTP	Background	Skin diffusing capacity	median ω1 - median ω2	0.158	0.435
MTP	Background	SA:V	overlap(ω1,ω2)	0.754	0.512
MTP	Background	Biological size	overlap(ω1,ω2)	0.980	0.597
MTP	Background	Epidermis thickness	overlap(ω1,ω2)	0.974	0.597
MTP	Background	Skin thickness	overlap(ω1,ω2)	0.921	0.586
MTP	Background	Epidermis diffusing capacity	overlap(ω1,ω2)	0.748	0.512
MTP	Background	Skin diffusing capacity	overlap(ω1,ω2)	0.603	0.511

Table S10. CODEML codon models employed across a phylogeny of three species. All models were tested on all sequenced nuclear and mitochondrial loci. For a given hypothesis test on a given locus, a significant difference between the null and alternative models suggests selection acting on a subset of codon sites across the evolutionary history of the target (either the branch leading to the species, or the clade of all individuals in the species).

Hypothesis	Null model	Alternative model	Selection	Target	Foreground Species
H_{P1}	A (constrained)	A (relaxed)	positive	branch	*P. cinereus*
H_{P2}	A (constrained)	A (relaxed)	positive	branch	*P. glutinosus*
H_{P3}	A (constrained)	A (relaxed)	positive	branch	*P. vandykei*
H_{P4}	2A (relaxed)	C	positive	clade	*P. cinereus*
H_{P5}	2A (relaxed)	C	positive	clade	*P. glutinosus*
H_{P6}	2A (relaxed)	C	positive	clade	*P. vandykei*
H_{P7}	3	B	change	branch	*P. cinereus*
H_{P8}	3	B	change	branch	*P. glutinosus*
H_{P9}	3	B	change	branch	*P. vandykei*
H_{P10}	3	D	change	clade	*P. cinereus*
H_{P11}	3	D	change	clade	*P. glutinosus*
H_{P12}	3	D	change	clade	*P. vandykei*

Table S11. General and taxon-specific PCR primer sequences used to amplify either whole or partial mitochondrial genomes.

Primer	Sequence
Eurycea_ND4_F	CCCTCATYCAAACACCATGAAGCTTCACAGG
Eurycea_ND4_R	GARGARAYAAGTCCATGTGAAATTATTAAAATAATTGCTCC
Eurycea_16S_F	CCTTAAGCAGAAGTTATAAGAGGTACTGCCTGCCCAG
Eurycea_16S_R	GCTACCTTTGCACGGTCATAATACCGCGG
Pleth_16S_F	CTGAGTTCAGACCGGAGHAATCCAGGTCAGTTTCTATC
Pleth_16S_R	GATCACGTAGGRCTTTAATCGTTGAACAAACGAACC
Pleth_12S_F	GTGCCAGCCACCGCGGTTATACG
Pleth_12S_R	TGACGGGCGGTGTGTGCGTG
Pcin_ND4_R	ATTATTGGTAATAGGTGTATTGTTAGAAGACAGTGTTCTCGGG
Pglut_ND4_R	GAGCAGATGTATTGTTAGAAGGCAGTGCTCTCGGG
Plars_ND4_R	GGTGTTAAGTGTAAAAAAATTAGGCAGTGCTCTCGGG
Pvand_ND4_R	GCGAGGTGTAAGGAAATTAGACAGTGCTCTCGGG
Pvehic_ND4_R	GAAGTATTGGGGCTAAATGTATTATTATTAAACAGTGTTCTCGGG
Pdunn_ND4_R	GTATCGGGGTTAGGTGTATTAATATTAAACAATGTTCTCGAG
Pcin_ND4_F	ATTTAACATGGCCCTCCCTCCAACCCC
Pglut_ND4_F	CTATCTAACCTATTTAATATAGCCCTCCCTCCTACCCC
Plars_ND4_F	GATTATTATTAAACTTATTTAATATAGCACTACCCCCAACCCC
Pvand_ND4_F	TTCAAGCCTGTTTAATATAGCTCTACCCCCAACCCC
Pvehic_ND4_F	GATTATTATCAAATTTATTTAATATAGCCCTACCTCCAACCCC
Pdunn_ND4_F	GATTATTATCAAACCTATTTAATATAGCCCTACCCCCAACTCC